Electromagnetic microsystem for the detection of magnetic nanoparticles in a microfluidic structure for immunoassays

Amine Rabehi

University Pierre et Marie Curie

Rheinisch-Westfälische Technische Hochschule (RWTH) Aachen University

Doctoral school ED 391 Ecole Doctorale Science Mécanique Acoustique Electronique et Robotique (SMAER)

Laboratory of electronics and electromagnetism (L2E)

Thesis title

Electromagnetic microsystem for the detection of magnetic nanoparticles in a microfluidic structure for immunoassays

Par **Amine Rabehi**

Thèse de doctorat d'électronique

Dirigée par Prof Hamid KOKABI et Prof Andreas OFFENHAUSSER

Présenté et soutenue publiquement le: XX. 01.2018

Devant un Jury composé de:

M. Pierre-Yves JOUBERT	Professeur, Université Paris-Sud	Rapporteur
M. Uwe Schnakenberg	Professeur, Université RWTH Aachen	Rapporteur
M. Hans-Joachim KRAUSE	Professeur, Institute of Bioelectronics, Peter Grünberg Institute (PGI-8), Juelich, Germany	Examinateur
M. Andreas OFFENHÄUSSER	Professeur RWTH University, Aachen, Germany	Co-directeur de thèse
M. Stéphane HOLE	Professor, Université UPMC	Examinator
M. Hamid KOKABI	Professor, Université UPMC	Directeur de thèse

Acknowledgment

There are many people I would like to thank for their help, support and encouragement during my PhD work. I would like first to thank my supervisors, Hamid Kokabi, Hans-Joachim Krause and Kieu Ngo. Each of them helped me in numerous aspects of the thesis work whether it was in the field of electromagnetics or microfluidic. I would also like to thank professor Offenhäusser for his helping with my joint PHD thesis ("thèse de doctorat en cotutelle) between RWTH Aachen and UPMC.

My work in this project started with my final Master internship at the Institute for Bioelectronics at Forschungszentrums **Jülich (FZJ)** in Germany under the joint supervision of H.-J. Krause and H. Kokabi in the framework of a UPMC-FZJ French-German PHC collaboration ("Partenariat Hubert Curien") called PROCOPE.I had a very good experience and learned a lot through my interactions with all the members of the research team from whom I cite Mr. La Chen, Mr. Alexander Krings and Mr. Dieter Lamparski and the support from L2E laboratory at UPMC and PHENIX laboratory for advises and different magnetic nanoparticles elaboration and characterizations.

Following my master thesis, we started working on the miniaturization of the pathogen sensing device at L2E laboratory in Paris. There, I had the chance to meet many valuable colleagues. This includes all the PhD students as well as the teachers and other members from which I especially thank Chloé Hamel-Dellenbach and Yves Chatelon for their support in many issues.

Also, this multidisciplinary work would not have been possible without our various partner laboratories at UPMC. I therefore thank Mrs. Sophie Neveu, Jérôme Fresnais and Jean-Michel Siaugue (PHENIX, UPMC,) for all their help concerning the nanoparticles and biofunctionalization aspects. I also thank Nour Yakdi, Damien Bricault (LISE, UPMC) and Stephanie Graff-Dubois (CIMI, UPMC) for their help on the microfluidics and immunoassays respectively.

Personally, I'm very grateful to god for the family and friends that I have as well as for the way things turned out. At first, I would like to thank my parents for their continuous care of my wellbeing and my siblings for their support. Moreover, my uncles, aunts and cousins were/are always a source of joy and love for me. During my thesis, my family expanded with my recent marriage to my wonderful wife. I'm grateful for all her support, patience, love and kindness. On top of that, my stepfamily also supported me and made my life better through our numerous encounters. Next to my family, there are my old friends Mounir Teniou, Lydia Hettak and Badreddine Ratni with whom I shared many memories for more than 7 continuous years. I wish you all the best in life. I also thank my friend Ahmed Abudabbousa for his wise advices.

Finally, I dedicate this work to my beloved classmate, roommate and friend Houssam RETIMA.

Amine RABEHI

Abstract

The detection and quantification of a biological agent or entity has become paramount to anticipate a possible health threat (epidemic or pandemic) or environmental threat or to combat other contextual threats (bioterrorism, chemical and biological weapons, drugs). Consequently, developing a portable cost effective device that could detect and quantify such threats is the research focus of the joint project between RWTH Aachen and Université Pierre et Marie Curie (UPMC). The design and fabrication of such systems is very challenging because it involves interdisciplinary knowledge ranging from electromagnetic modeling, multiphysics simulations and fine measurement techniques, microfluidics design, simulation and fabrication, physics and chemistry of magnetic particle synthesis, characterization and functionalization, and finally immunological validation aspects.

In the framework of this project, we studied the multidisciplinary aspects of an electromagnetic microsystem for immunologic detection based on magnetic nanoparticles (MNP) in a microfluidic lab-on-chip (LoC). A comprehensive summary of the state of the art of the various aspects of lab-on-chip components and corresponding challenges is given with an emphasis on detection.

Because of their extractability and sortability, magnetic nanoparticles are adapted for examination of biological samples, serving as markers for biochemical reactions. So far, the final detection step is mostly achieved by well-known immunochemical or fluorescence-based techniques. Optical detection has a limited dynamic range and requires transparent, non-fluorescent media. Standard enzymatic detection as used in ELISA exhibits a limited sensitivity and is time-consuming. Because of regulations for radiation protection, radioactive markers are also problematic. Therefore, magnetic immunoassays detecting the analyte by means of magnetic markers constitute a promising alternative. MNP covered with biocompatible surface coating can be specifically bound to analytes, cells, viruses or bacteria. They can also be used for separation and for concentration enhancement.

The novel frequency mixing magnetic detection method allows quantifying magnetic nanoparticles with a very large dynamic measurement range. By observation of amplitudes and phases of higher order frequency mixing components, specific non-linear signatures of different types of magnetic nanoparticles can be discriminated. In this thesis, emphasis is put on the miniaturized implementation of this detection scheme.

Following the development using analytical and multiphysics simulations tools for optimization of both excitation frequencies and detection planar coils, a first multilayered printed circuit board (PCB) prototype integrating all three different coils along with an adapted microfluidic chip has been

designed and realized. The prototype structures have been tested and characterized with respect to their performance for limit of detection (LOD) of MNP, linear response and validation of theoretical concepts. Using the frequency mixing magnetic detection technique, a LOD of 15ng/mL of 20 nm core sized MNP has been achieved without any shielding with a sample volume of 14 µL corresponding to a drop of blood.

For biosensing, the microfluidic chip has been functionalized with specific antibodies using an appropriate surface functionalization method. For immunoassay validation and assessment tests, C-reactive protein (CRP) has been chosen for proof of concept validation as it plays an important role in inflammatory reactions, and serves as a biological marker for these. This first realized magnetic immunodetection system along with the developed analytical and simulations tools will serve as groundwork for a further improved fully integrated device for the detection of other relevant infectious disease biomarkers such as Procalcitonin (PCT) for immunoassays.

Zusammenfassung

Die Detektion und Quantifizierung biologischer Substanzen oder Strukturen ist von zunehmender Wichtigkeit zur Bekämpfung potentieller epidemischer oder sogar pandemischer Gesundheitsgefahren, zur Vermeidung von Umweltschädenund zur Bekämpfung anderer Groß-Gefährdungslagendurch Bioterrorismus, chemische und biologische Waffen sowieDrogen. Aus diesem Grunde ist es das Ziel eines Kooperationsprojekts zwischen RWTH Aachen und UPMC Paris, ein einfaches tragbares und kostengünstiges Gerät zur Detektion und Quantifizierung solcher Bedrohungen zu entwickeln. Design und Entwicklung derartiger Systeme ist sehr anspruchsvoll, da sie interdisziplinäre Kenntnisse aus den Bereichen elektromagnetischer Modellierung, Multiphysik-Simulation, empfindlicher Messtechnik, Mikrofluidik-Design, -Simulation und -Herstellung, Physik und Chemie der Magnetpartikel-Synthese, -Charakterisierung und –Funktionalisierung sowie immunologischer Validation erfordert.

Im Rahmen dieses Projektes wurden die multidisziplinären Aspekte eines elektromagnetischen Mikrosystemszur immunologischen Detektion auf Basis magnetischer Nanopartikelaufeinem mikrofluidischen Lab-on-Chip untersucht. Die Arbeit beinhaltet eine umfassende Darstellung des Stands der Technik der verschiedenen Aspekte von Lab-on-Chip-Komponenten und die damit verbundenen Herausforderungen insbesondere hinsichtlich empfindlicher Detektion biologischer Substanzen.

Magnetische Nanopartikel sind wegen ihrer Extrahierbarkeit und Sortierbarkeit besonders geeignet für die Untersuchung biologischer Proben, da sie als Marker für biochemische Reaktionen dienen können. Bislang wird der finale Detektionsschritt meistens durch etablierte immunochemische oder fluoreszenzbasierte Techniken durchgeführt. Optische Detektionsmethoden haben einen begrenzten dynamischen Bereich und erfordern transparente, nicht-fluoreszierende Medien. Die gewöhnlich bei ELISA verwendete enzymatische Detektion weist eine begrenzte Empfindlichkeit auf und ist zeitaufwändig. Radioaktive Marker sind aufgrund strenger Regeln zum Strahlenschutz problematisch. Magnetische Immunoassays, die den Analyten mit magnetischen Markern detektieren, bieten eine vielversprechende Alternative. MNP mit biokompatibler Oberflächenbeschichtung können spezifisch an verschiedene Analyte, Zellen, Viren oder Bakterien gebunden werden. Außerdem können sie zur Separation und zur Aufkonzentrierung von Substanzen verwendet werden.

Die neuartige Frequenzmischungs-Magnetdetektions-Technik erlaubt eine Quantifizierung magnetischer Nanopartikel mit einem sehr großen dynamischen Messbereich. Durch Beobachtung der Amplituden und Phasen von Mischkomponenten höherer Ordnung können spezifische nichtlineareSignaturen verschiedener Arten magnetischer Nanopartikel unterschieden werden. In dieser Arbeit liegt der Schwerpunkt auf der Realisierung einer miniaturisierten Version dieses Detektionsprinzips.

Zusammenfassung

In der Folge der Entwicklung analytischer und Multiphysik-Simulations-Tools zur Optimierung der Planarspulen sowohl für die Erzeugung beider Anregungsmagnetfelder als auch für die Detektionsspulen wurde eine Multilagen-Leiterplatten-Spuleals Prototyp zur Integration aller drei verschiedenen Spulen zusammen mit einem adaptierten mikrofluidischen Chip entworfen und realisiert. Die Prototyp-Strukturen wurden hinsichtlich ihrer Leistungsfähigkeit in Bezug auf das Detektionslimit für magnetische Nanopartikel, die Linearität ihres Antwortsignals und zur Validierung der theoretischen Konzepte getestet und charakterisiert. Mit der magnetischen Frequenzmischungs-Detektion wurde ohne äußere Abschirmung ein Detektionslimit von 15ng/mL im Falle magnetischer Nanopartikel der Kerngröße 20 nm erreicht.

Um als empfindlicher und selektiver Biosensor zu wirken, wurde der mikrofluidische Chip mit spezifischen Antikörpern unter Verwendung einer geeigneten Oberflächenchemie funktionalisiert. Zur Erprobung und Validation eines beispielhaften Immunoassays wurde C-reaktives Protein (CRP) als Modellsystem gewählt, da eseine wichtige Rolle als Biomarker bei Entzündungsprozessen spielt. Dieses erste magnetische Immundetektions-System soll zusammen mit den neuentwickelten analytischen und Simulations-Tools als Basis für weiter verbesserte vollintegrierte Systeme zur Detektion anderer Biomarker für Infektionskrankheiten wie zum Beispiel Procalcitonin (PCT) dienen.

Content

Content

Content

General introduction

The ever increasing number of traveling people leads to faster spreading of diseases worldwide. More than 3 billion travel each year, which is equivalent to 100 passengers per second. Consequently, the detection and quantification of a biological agent or entity has become paramount to anticipate a possible health threat (epidemic or pandemic), environmental threat or to combat other contextual threats (bioterrorism, biological weapons, and drugs). In many diseases, early detection of pathogen enhances substantially the chances of recovery (e.g. food poisoning and early stage cancer…etc.). In this context, it is important to develop a rapid and sensitive low-cost system for pathogen detection.

To this end, Lab on Chip (LoC) technologies offer promising solutions. They allow miniaturizing most of the constituting components of a typical diagnostic system (sorting, amplification, mixing, incubation, detection…etc.). Also, LoC systems benefit from various advantages such as using low sample and reagent volumes as well as rapid detection. Moreover, technological advances in fabrication push the limits of different types of devices which can be created. For all these reasons, LoC systems have been subject of extensive research in the past few years.

In this context, we propose the development of an electromagnetic microsystem for the detection of magnetic nanoparticles in a LoC structure for immunoassays. In addition to LoC benefits, the chosen approach takes advantage of magnetic nanoparticles' performance and integration possibilities as well as the specificity and sensitivity of immunoassays.

The detection of these magnetic particles is operated through the use of the frequency mixing technique. In a previous work at the Bioelectronics institute of Research Center Juelich, first macroscopic readout electronics as well as a measurement head were realized and tested [1]. This technique has demonstrated its ability for sensitive detection of various pathogens and biological entities (Francisella tularensis [2], CRP [3], Yersinia pestis [4], H1N1, H3N2 [5]).

In this report, we studied the possibilities of integration of this method for the development of the envisioned LoC system. The developed device can be used in the following applications:

- Field biological analysis by practitioners in disaster areas especially in underdeveloped countries.
- Epidemiological control at airports.

- Autonomous biological analysis (autonomous elderly people, sailors, hikers and frequent travelers ...).
- Biological analysis for the protection of the environment.

The research objectives of this project can be organized into short and long term targets. Our ultimate long term objective is the development of a completely integrated and automated LoC pathogen sensing system. For this, several challenges must be addressed:

1. **LoC pathogen sensing system relying on magnetic immunoassays:** By using the mixing frequency technique in order to have sensitive, specific detection of analytes. The challenge here is to miniaturize the existing system while achieving similar or better performance.
2. **Highly biofunctionalized stable surface/volume:** By choosing the right functionalization method that allows high density antibody immobilization, good functionality and low nonspecific binding.
3. **Single step external interaction of the user:** By designing an appropriate microfluidic circuit allowing adequate automatic flow control, mixing, washing, incubation and detection.
4. **Fast assay time:** By optimizing the microfluidic channel's shape and dimensions along with a fast enough flow velocity.
5. **Low cost disposable chip:** because such systems are intended for Point-Of-Care POC diagnosis, the trend is to achieve low cost per assay. This can be done by choosing an appropriate design of the microfluidic chip.
6. **Multiassays:** By designing appropriate microfluidic multi reservoir circuitry and/or improving the mixing frequency detection technique selectivity through differentiation of nonlinear behavior, a multiassay parallel scheme could be performed.

Keeping these objectives in mind, we decided to focus on the first most important objective: the miniaturization of the detection system. Short term objectives that constitute this Ph.D. thesis work allow for preliminary important contributions to the project. They can be summarized as follows:

1. **State of the art review of the major aspects of LoC pathogen sensing systems:**

The compilation of information about all the major studied aspects of LoC systems ranging from material choice to biofunctionalization methods allow to plan the completely integrated system with as little potential drawback as possible. All the mentioned aspects of LoC systems must be planned before subsequent optimization. We must keep the final goal in mind.

2. **Design of analytical and simulation tools:** These tools will allow to design and optimize the completely integrated structure without the high cost of multiple clean room prototyping.
3. **Conception and realization of a first magnetic sensing prototype:** In order to validate the concept of the detection structure, we have developed a first prototype structure that relies on planar coils with microfluidic chip. This will allow optimizing the developed tools accuracy, to validate the miniaturization of the detection system and to optimize the various parameters (type of nanoparticle to use, best flow rate, magnetic system optimization…etc.)

Finally, this report is structured around these contributions as follows:

Chapter 1- State of the art of pathogen sensing techniques: In this chapter, an extended state of the art of the different immunoassay methods and multiple aspects regarding LoC pathogen sensing are presented. Key concepts are described concerning both the pathogen sensing and the microfluidic aspects. They allow understanding better the multiple interdependent and complex parameters and multidisciplinary aspects of our research project.

Chapter 2- Magnetic sensing: Theoretical background about magnetic detection and magnetic nanoparticle's basic theory are presented. We then explain our chosen magnetic detection scheme based on the magnetic mixing frequency technique [1].Following that, a first prototype for the structure miniaturization will be explained.

Chapter 3- Optimization of the detection structure through analytical and multiphysics simulation: This chapter describes the first developed tools for the optimization and miniaturization of the detection structure. They consist of analytical calculations and multiphysics simulations (electromagnetic, thermal and microfluidic). The last part of this chapter presents first designed and realized prototypes for validation of the optimization procedure. They constitute primary approach toward complete miniaturization. Design and realization of all constituting excitation and detection coils as well as microfluidic reservoir

are explained in this chapter.

Chapter 4- Experiments and preliminary work on biosensing: In this chapter, preliminary results concerning magnetic sensing are given. A test bench with appropriate electronics, instrumentation and LABVIEW data acquisition software is developed. Additionally, the biosensing aspect is discussed and first preliminary work is provided. These results will serve as a ground basis for further optimization.

The work is concluded with a summary of the most important findings and results. An outlook to future work towards the final goal of a rapid and sensitive low-cost system for pathogen detection is given.

Chapter 1. State of the art of pathogen sensing techniques

1.1 Introduction

For several years, researcher's focus shifted from benchtop pathogen sensing techniques to the design of completely integrated portable systems. The design and fabrication of such systems is often challenging because it involves interdisciplinary knowledge from fluid handling to detection schemes (microfabrication, microelectronics, microfluidics, chemistry, material science and biology)

The detection part is the most important component of LoC systems. For that, the main focus of this chapter is on reviewing most common detection schemes and studying critical aspects of such methods. The detection is usually done using a biosensor; as the main building block of the pathogen detection system. As a general context, a brief description will be given followed by main applications.

Afterwards, we will describe in more detail the pathogen sensing systems. These systems will be mainly organized by type of the transducer such as optical and electrochemical methods. Theses detection methods are illustrated by a miniaturized system from recent literature. Additionally, we will present general aspects of immunoassays as it is our chosen bioreceptor type of detection scheme.

For efficient miniaturizing of existing benchtop devices, critical aspects need to be taken into account, such as, fluid handling, fabrication method and biofunctionalization techniques. Ideal composition and criteria for a LoC system will be presented with some comparison tables.

Finally, following these major aspects, a synthetic summary table about different miniaturized detection schemes will be given with some critical notes.

1.2 Biosensors and applications

Simply put, biosensors are analytical devices that convert a biological response into an electrical signal. They are used in various applications such as biomedicine, industry and defence.

The first biosensor was invented by Clark and Lyons (1962) to measure glucose in biological samples with an electrochemical detection of oxygen or hydrogen peroxide using immobilized glucose oxidase electrode [6].

Any biosensor is composed of three major parts:

1. **Biorecognition site (bioreceptor):**
   It is composed of biomolecules selected due to their high specificity to the target analyte and are immobilised onto a transducer to form a functional sensor. In viral sensing, the major bioreceptors are whole cells, antibodies, peptides, nucleic acids and aptamers.
2. **Biotransducer :**
   They convert the biological response into a measureable signal. Examples of transducers include electrodes, piezoelectric elements, photo-detectors or coils.
3. **Electronic system:**
   The electronic circuit following the transducer is responsible for the signal conditioning and treatment.

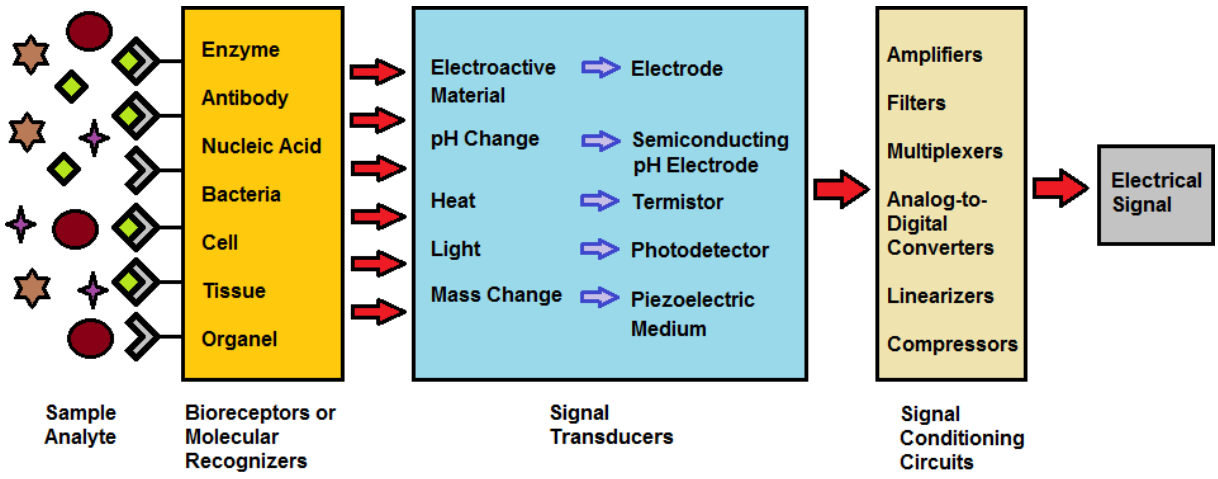

Figure 1-1: Most common types of bioreceptors, biotransducers and signal processing circuits [7].

The biosensor type thus mainly depends on the type of bioreceptor and biotransducer to be used. Figure 1-1 illustrates the most common type of bioreceptors and biotransducers. Some of the biosensor techniques included in the diagram will be explained in the context of pathogen sensing applications (see section 1.3).

It has to be noted that biosensors could also be divided into two other categories: labelled and label-free biosensors. Label-free biosensors detect the physical response of bio-entities and

do not need the use of labels like fluorescent markers, nanoparticles, radiolabels…etc [6]. On the other hand, label-based sensors allow indirect detection of the target through binding or interaction with the label.

The materials used in biosensors including bioreceptors and reagents used to reveal the reaction can be categorized into three groups depending on their mechanism (interaction): (i) bioaffinity group such as antibodies and nucleic acid, (ii) biocatalytic group comprising enzymes, and microbe based group (iii) that contain microorganisms. The first enzyme-based sensor was reported by Updike and Hicks in 1967 to measure the concentration of glucose in biological solutions [8].

Biosensors are very attractive because they take advantage of the sensitivity and specificity of biology in conjunction with the physiochemical transducers in order to perform complex bioanalytical measurements in a simple-to-use format. However, the fabrication of such devices requires interdisciplinary knowledge in chemistry, biology and engineering [8].

Ideally, the fabricated biosensor should be highly specific, reusable and independent of environmental physical parameters such as temperature and pH change. Due to their usage in environmental and biomedical applications, biosensors should also be simple andas sensitive as required by the application.

Biosensors can be used for various applications. The applications can be divided into clinical and nonclinical applications.

On one hand, clinical applications are concerned with the immediate observation, examination and treatment of patients. For example, potentiometric biosensors for monitoring gases and other liquids dissolved in blood. As another example, we can cite glucose sensors. Blood-glucose biosensors for home usage account for 85% of the gigantic current biosensors world market. Due to high demand, both portable and laboratory systems are widely spread.

On the other hand, non-clinical applications represent any other indirect or not related applications to medical treatment. Examples of this type of applications are environmental monitoring, plant biology, food monitoring and pharmaceutical application (drug development, manufacturing…etc.). More detail can be found in [8].

Although the technique presented hereafter can be used in other fields such as biodefense and environmental monitoring, in the context of this project we focus on the application of biosensors in pathogen sensing methods. In fact, biosensors are being used extensively in the medical field to diagnose infectious diseases. In consequence, a great amount of research is oriented toward the improvement of such systems.

1.3 Pathogen sensing methods

Substances that can initiate a disease are called pathogens. Generally, this term is used to

describe an infectious agent such as a virus, a bacterium, a fungus, or another living micro-organism. Pathogen sensing methods aim at detecting the presence of these agents and quantifying them. These techniques achieve their objective by: detecting/measuring the whole pathogen, its genetic material, or proteins specific to the target pathogen, or the metabolites released or consumed [9].

One of the oldest techniques used to detect pathogens such as bacteria is the plate culture method [9], [10]. This method is widely used and dates back to the end of the 19th century and introduced by Robert Koch. It is a method of multiplying microbial organisms by providing them with a convenient media and adequate conditions for rapid controlled growth. After a controlled amount of time, the number of growing colonies will be counted. It is then possible to distinguish individual colonies using a range of dilutions. Thus, one can establish the initial concentration present in the original sample.

Although this method is very effective, it suffers major drawbacks: it is tedious, uses a great amount of material, labor intensive and may take weeks in order to provide results. Moreover, the process is more complicated for multibacteria detection, as it will mean using different selective media and specialized trained staff. In order to provide a more efficient system and to tackle these drawbacks, other pathogen sensing systems have been developed. As with biosensors in general, these techniques could be divided according to either the bio-receptor type or the transducer type.

1.3.1 Bioreceptors

In most detection systems, bioreceptors can be either bioaffinity-based or biocalatylic-based. Other bioreceptors including microorganism are not used as widely. Bioaffinity receptors can be either nucleic acids like DNA (deoxyribonucleic acid) and RNA (Ribonucleic acid) or proteins like antibodies. On the other hands, biocatalytic receptors mainly include enzymes.

In the case of DNA biosensors, the main ability is that a single-strand nucleic acid molecule is able to recognize and bind to its complementary strand. This formation is done by stable hydrogen bonds between the two strands [8]. Nucleic acid-based sensing systems are generally more sensitive than antibody-based detection methods as they provide gene-based specificity.

Antibodies (abbreviated Ig for Immunoglobulin) constitute a good example of a widely used protein receptor. They are Y-shaped proteins (Figure 1-2) produced by plasma cells. Antibodies are naturally used by the immune system in order to neutralize pathogens. Each antibody is unique in that it contains a variable region (Fab) in the tip of the ‘Y’ shape. This latter holds a “paratope” that is specific to a characterized region on an antigen (virus or bacteria) called “epitope”. These specific regions allow the antibody to bind exclusively to its antigen counterpart (Figure 1-2).

Systems using antibodies exhibit a high degree of precision, specificity and low false positive results. In general, peptide and protein biosensors are easily manufactured through synthetic

chemistry. On the other hand, the price of antibodies is usually higher than that of enzymes. Another disadvantage is the irreversibility of the reaction, so that the detection area should be used only once (disposable chip). Indeed, very harsh conditions need to be used in order to reverse the reaction or to clean the surface.

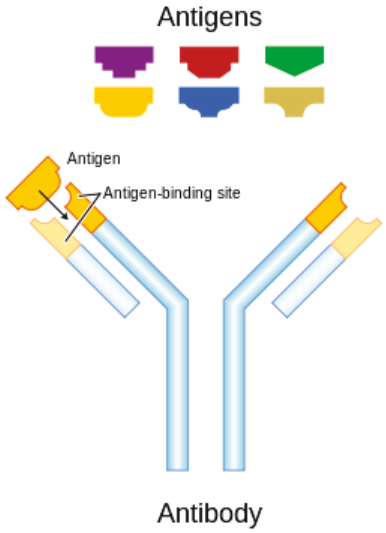

Figure 1-2: Antibody representation and antibody-antigen binding sites.

The other major bioreceptor is the enzyme. Enzymes are macromolecular protein catalysts. Their main role is to accelerate chemical reactions. Biosensor systems using enzymes rely on the following principle: The detectable signal, generated from the reaction of the analyte with a substrate catalyzed by the enzyme, can result in a change in proton concentration, release or uptake of gases, such as ammonia or oxygen, light emission, absorption or reflectance, heat emission, and so forth, brought about by the reaction catalyzed by the enzyme. The transducer then converts the resultant signal into a measurable response. That means that optical, potentiometric, amperometric and thermistor sensors can be used. These sensors rely on the specificity and catalytic nature of enzymes [11]. As an example: amperometric biosensors rely on the measurement of the current resulting from the oxidation or reduction of an electroactive biological element using enzymes in order to provide specific analytical information. In this case, redox enzymes will be used ([12], [13]).

Concerning the drawbacks of such systems: the enzymes are expensive to produce due to the cost of source, extraction, isolation and purification [14]. Moreover, the reaction is not always stable in terms of results and the relation between analyte concentration and products of enzymatic based reaction might be logarithmic. In addition, non-specific effects, such as thermal effects could happen. Moreover, fouling agents and interference from chemicals present in the sample matrix constitute another big issue [15]. Finally, some environmental and pathological conditions could modify some fluid parameters like chemical composition or pH, influencing the activities of the enzyme and, consequently, the biosensor performance [16].

Despite of these disadvantages, techniques exist in order to prevent or reduce the effect of

these issues. Enzyme-related pathogen-sensing systems are still widely used. Enzymes are also used in food industry, defense and environmental monitoring.

1.3.2 Biotransducers

Pathogen sensing system could also be organized in terms of biotransducers. Transducers convert the physical signal generated from or because of the receptor into an understandable one. Different types of transducers exist.

Electrochemical transducers dominate the distribute diagnostics (potable systems like glucose monitors), while optical techniques have found their use primarily in R&D [17].

1.3.2.1 Optical methods

Optical detection methods utilize optical properties of reactions, reagents and analyte physical characteristics in order to detect the analyte. They include a light source and other optical components to generate a light beam. The light/color property change resulting from the presence of the analyte is detected using a specific sensing head. The signal is then transformed to an understandable quantity using a conditioning signal circuit.

Two types of optical methods exist: on one hand, there are direct detection methods that monitor the light properties such as fluorescence, absorbance and luminescence. On the other hand, indirect methods such as the Surface Plasmon Resonance (SPR) technique uses the modulation properties of light. The latter type also includes interferometry, evanescent waves, Raman spectrometry, fiber optics and optical waveguides [18].

Optical detection methods are very convenient for real-time detection because they are simple, rapid, highly sensitive, and easy to be integrated with microfluidic chip. Furthermore, detection can be multiplexed and cost effective. In fact, many products are already available in the market [19], each product having its own advantage and characteristics. However, these techniques still suffer from some drawbacks like difficulty of integration, background interference and need for pretreatment (e.g blood is difficult to use with colorimetric methods directly). In the next section, we will describe the most common optical detection techniques: colorimetric, fluorescent, bio- or chemiluminescence, and Surface Plasmon Resonance (SPR).

Colorimetric sensors

Colorimetric biosensors involve the generation of colored compounds which can be measured and correlated with the concentration of analytes. These methods are very simple to implement and the result, if a sufficient concentration of analyte is present, can be assessed with the naked eye. Its simplicity and low cost aspects allow these methods to be widely preferred in the diagnostic market.

The most common colorimetric method is the Lateral Flow Assay (LFA) colorimetric method [20], with which most pregnancy tests are made. This method can also be found under the name lateral flow immunochromatographic assay or dip-stick assay.

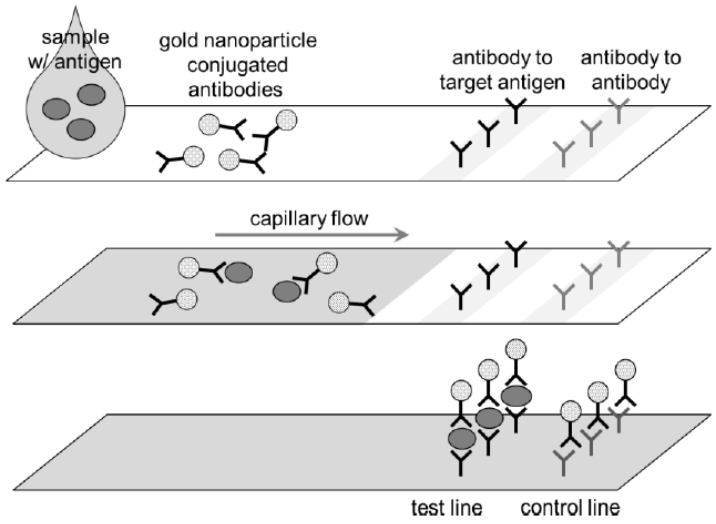

Figure 1-3: Schematic representation of the LFA method ([20]).

In the case of the pregnancy test, a urine sample is introduced into the device using a strip or putting the sample in a sample area. Due to the membrane capillarity, the liquid flows to the reaction area. Nitrocellulose membrane is the most common one; the pore size varies between 0.05 to 12 μm. This material could be changed in the case of highly viscous fluids, or media with fat globules (milk) [21].

As can be seen in Figure 1-3, two lines exist in this set up, one for the test and the other to control the antibody to antibody immobilization. The two are preloaded with different antibodies (anti-IgG and anti-antigen). Therefore, if the person is pregnant, i.e. the analyte is present in the sample, the control and test lines are both colored and can be seen by the eye (two pink lines usually). If not, only the control line is colored. If no color is present in the control line, it means that the test failed (probably due to lack of sample quantity or malfunctioning of the membrane flow).

The color comes from either gold nanoparticles (<50 nm [22]) or colored latex particles (100-900nm [23]). Gold nanoparticles absorb green light and an amount of blue light, consequently the test line looks pink.

Although the LFA comes mostly in a sandwich form (see section 1.3.3), the test can be performed in a competitive format in the case of the antigen having just one epitope (binding site). Also, nucleic acids could be used instead of antibodies but this is less popular due to the need of signal amplification through Polymerase Chain Reaction (PCR) [21].

These techniques are very advantageous in a sense that they are inexpensive, easy to use and the test strip can be disposable. However, the main drawback is its lack of sensitivity and reproducibility, thus rendering it usable only for qualitative tests in a yes/no fashion. Efforts are made to address these weaknesses like using cellphone cameras and reflectometers to make the test quantitative and more sensitive [24].

Fluorescent methods

Fluorescent biosensors are small structures onto which fluorescent probes are mounted (chemically, enzymatically and genetically) through a receptor. The role of the receptor is to identify the target analyte and consequently transduces a fluorescent signal to be detected and measured by adequate equipment. Thus, the fluorescent sensing technique is based on the measurement of fluorescence intensity which is proportional to the concentration of the target analyte.

These sensors can probe protein biomarkers and various metabolites with good sensitivity. Furthermore, it is also possible to observe the presence, status and activity of the target. They can indicate cardiovascular, inflammatory and cardiovascular diseases as well as viral infection and cancer [8].

Along with colorimetric methods, fluorescent-based methods constitute the most widely used optical pathogen sensing techniques. They most commonly involve the use of an excitation light source and a photodetector (CCD camera or photomultiplier). Fluorescent ImmunoAssays (FIA) are one of the most common pathogen detection assays. They rely on sandwich immunoassay procedures (see section 1.3.3) and use fluorochrome molecules to label secondary antibodies (receptors).

As depicted in Figure 1-4,when the fluorescent label is excited by the light source at a certain wavelength (in that case 635 nm), the label responds by emitting a longer wavelength (fluorescence at 647 nm) that is detected by a CCD camera [25]. The concentration of the analyte is directly related to the intensity of the fluorescence.

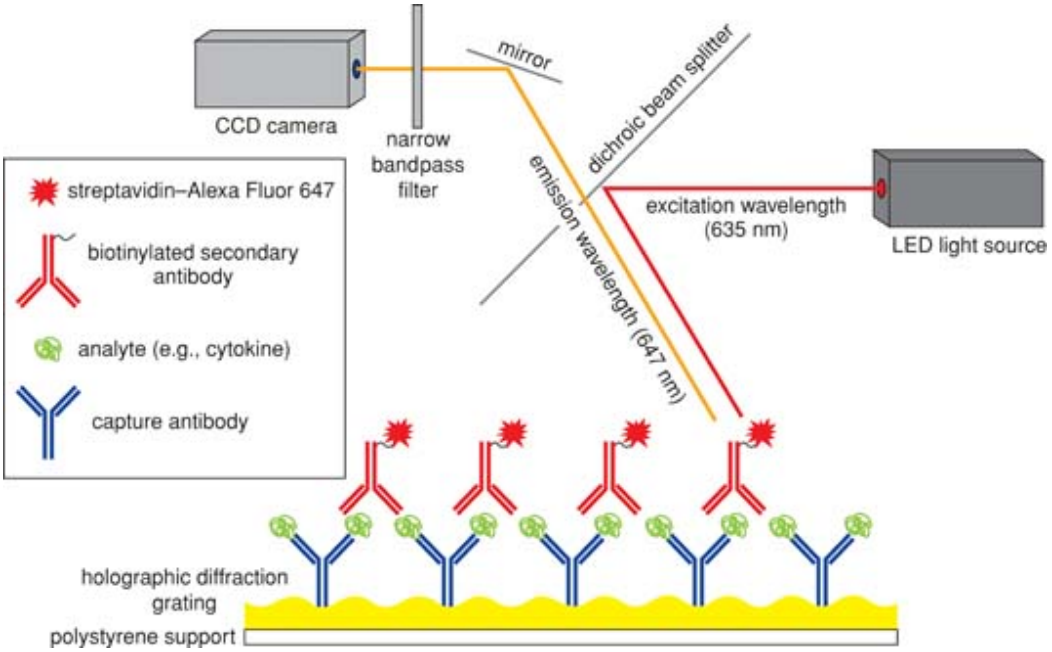

Figure 1-4: Example of Fluorescent ImmunoAssay method (FIA) [25].In this case the fluorescent label is Alexa Fluor 647.

Advantages of fluorescent sensors include their high sensitivity that can reach single molecule detection [26], high selectivity and ease of integration of the fluorescent markers. Another major advantage of this technique is the possibility of multiplex detection using different fluorescent markers [27]. However, current fluorescence sensors still require a long assay time, external lenses, and a large and complex detector. These issues limit their practical use as a POC device [19]. Also, high cost, extensive calibration and lack of appropriate fluorophores constitute additional drawbacks.

Extended research is conducted for the full integration of the fluorescent detection methods, where one solution is to use optical waveguides in order to integrate the light source and to eliminate the background noise [12], [28].

An example is illustrated in Figure 1-5, where the researchers used a single mode planar optical waveguides comprised of thin (~120 nm) high refractive index dielectric materials deposited on a substrate with a much lower index. Due to diffraction gratings that are etched into the substrate, a small portion of light (evanescent field) that was contained into the waveguide passes through the medium where the sample is present. The intensity of the field is big enough to excite the fluorescent molecules and small enough so that its amplitude is almost zero within half the wavelength (~300nm), i.e. the rest of the media. This latter property allows the reduction of background noise by eliminating the excitation possibility of the non-desired fluorescent constituents present in the sample.

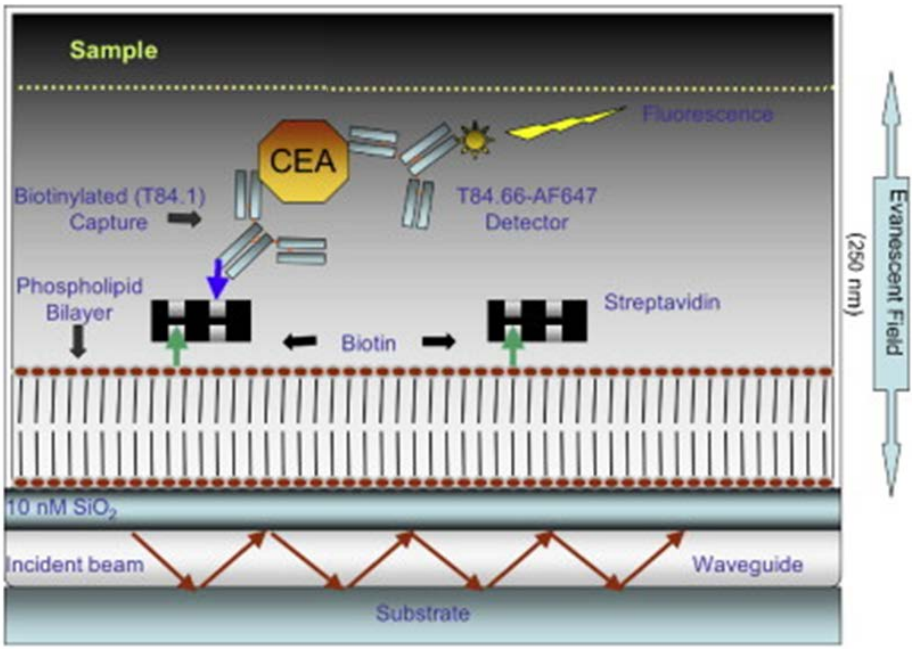

Figure 1-5: A schematic representation of the sandwich immunoassay on the waveguide-based biosensor [12], [28].

Surface plasmon resonance (SPR)

When total internal reflection of the incident light occurs, an evanescent wave is set up that

exerts a field outside of the prism. This can only occur when the film is very thin (50nm).The delocalised electrons within the metal cause a surface plasmon to be established at the metal–ambient interface [13]. Consequently, a wave propagates along the surface and reduces the intensity of the reflected light (Figure 1-6).The angle of incidence of this occurrence is called the SPR angle. This angle depends, among other parameters, on the refractive index, η, that is determined by the medium itself. In consequence, if an analyte immobilizes on the bioreceptor, it leads to the SPR angle change.

SPR techniques are fast, reliable and sensitive. However, in general SPR equipment is expensive. Several companies have developed instruments in the mid-range price bracket of tens of thousands of US dollars. SPR devices could also be used in the case of array-based sensing with the introduction of SPR imaging which permits multiple assay spots to be monitored simultaneously [17].

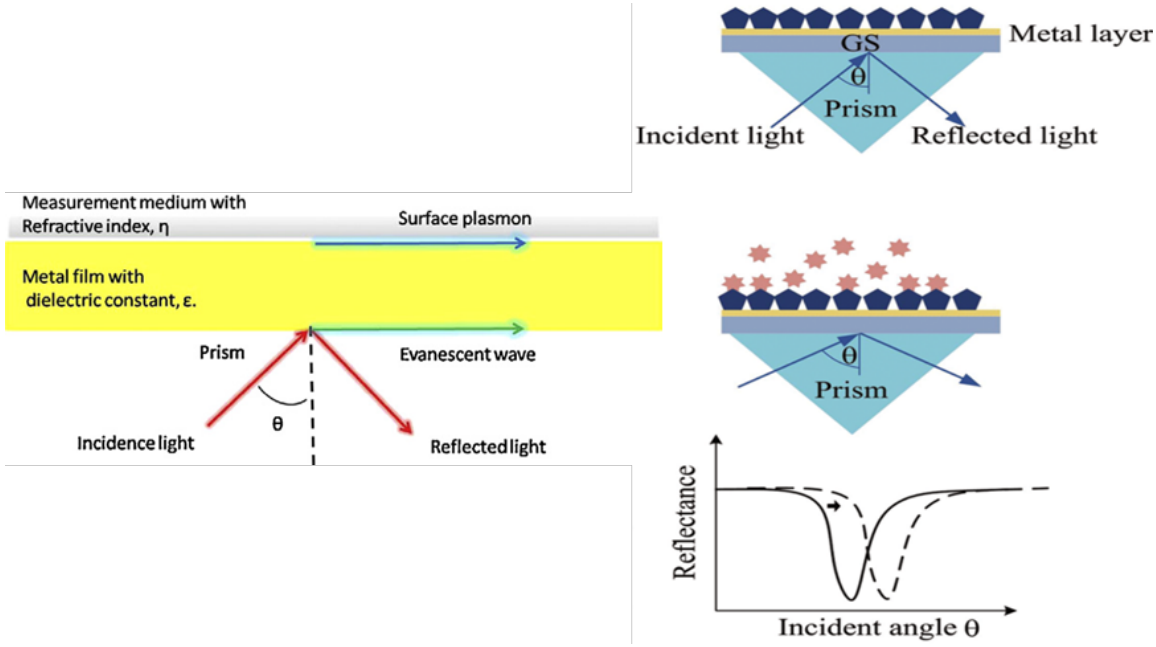

Figure 1-6: Surface Plasmon resonance technique illustration. left: Physical phenomenon [13].Right:change of SPR angle before and after analyte(pathogen)immobilization [18].

Luminescence

Bioluminescence

Some living organisms react to the presence of some analyte or chemical compound by emitting a luminescence or change of luminescence (Figure 1-7). This property can be used for the detection of specific analytes (like microbes). In this case of living organism luminescence the detection is termed bioluminescence.

The class of enzymes that catalyse the reaction leading to the release of luminescence in cells are called “luciferease”. The lux gene, encoding luciferase in microorganisms, is the most popular reporter gene in bioluminescent microbial biosensors. These bioluminescent

organisms can be used in either a constitutive or an inducible manner [29]. In the constitutive way, the lux gene is always active and the luminescence changes with the addition of the chemical sample to be detected. These techniques find applications in the detection of heavy metal contamination and common environmental pollutants [29].

On the other hand, the inductive manner can be used to have a more specific detection. Here, the lux gene in fused with a promoter gene that is regulated by the existence of the targeted analyte. For example, the detection of E.coli could be done by the use of the lux gene with pgi promoter [30]. In this case, the presence of E.coli provokes a reaction that leads to the luminescence of the lux gene coded luciferase.

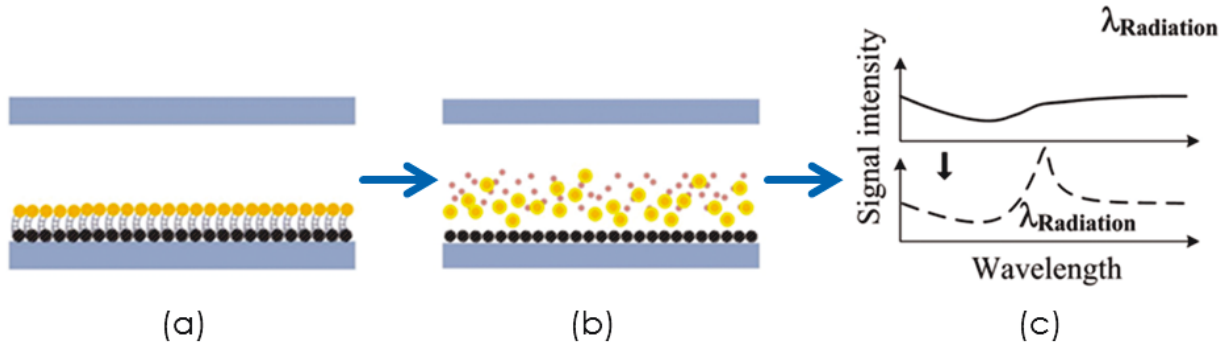

Figure 1-7: Luminescence detection. (a) Before test. (b) During test light is emitted due to biological/chemical stimulus. (c) Detected signal intensity before and after test [18].

Chemiluminescence

Chemiluminescence in another form of luminescence. Basically, it is the emission of light as the results of a chemical reaction. In contrary to bioluminescence, a chemiluminescent substrate should be added for the detection (Figure 1-8).

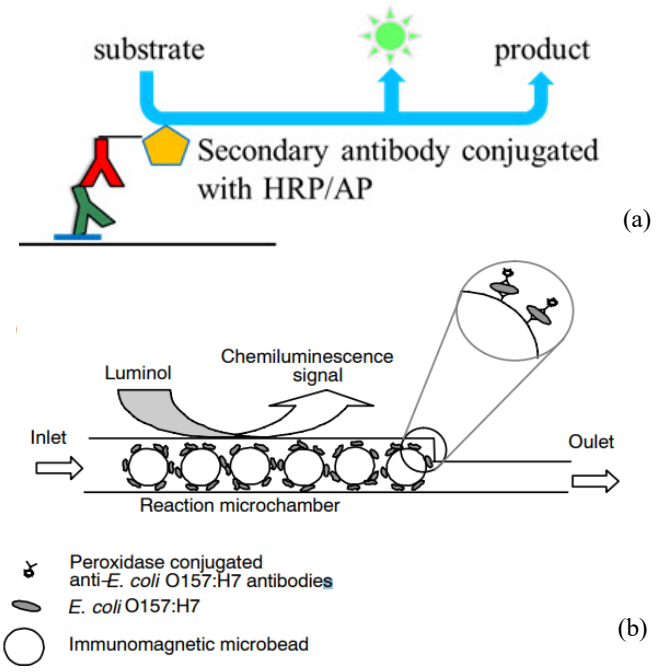

Figure 1-8: (a) Chemiluminescence detection principle of protein on membrane [31]. (b) Detection of E.coli O157:H7 using immunomagnetic beads and generation of chemiluminescence signal inside microfluidic chamber [32].

As an example, the detection of E.coli O157:H7 can be achieved using chemiluminescence and a sandwich immunoassay [32] in a microfluidic channel. The immune-complex is composed of a first magnetic bead coated antibody and secondary anti-E.coli O157:H7 peroxidase (HRP) labeled antibodies. After the sandwich formation, the user adds luminol substrate; luminol is a chemiluminescent substrate of HRP. In the presence of peroxide, HRP oxidizes luminol to an excited product called 3-aminophthalate that emits light at 425 nm. The emission continues till 3-aminophthalate decays and enters the ground state. The emitted light can be captured by CCD camera (Figure 1-8.b).

Comparatively to fluorescence, chemiluminescence methods eliminate the need of external light sources, which leads to better integration and simplicity in the case of Lab-On-Chip systems. However, luminescence methods are restricted to certain chemiluminescent agents and to cells that produce the luminescence.

1.3.2.2 Electrochemical methods

Electrochemical biosensors rely on the fact that in aqueous solutions, the electrical charge can be carried by ions. When we put two electrodes in the solution, an electrical current from one electrode to the other can build up. The electrical properties can then be modulated by the presence of certain analytes that undergo redox reactions [18]. Depending on the electrical property under study, electrochemical methods can be divided into four major categories: amperometric [33], [34], [35], potentiometric [36], conductometric [37] and impedance-based measurements [13].

Optical and electrochemical biosensors constitute the most used type of sensors. The adaptation of screen printing for the production of enzyme electrodes, along with the use of proprietary mediators and capillary-fill designs, machine fabrication of enzyme electrodes enabled the market dominance change from optical (reflectance photometry) to the electrochemical devices [17].

At first, these sensors were used to detect small analytes like urea, lactate or glucose amperometrically ([38], [39], [13]) and were mainly focused on the detection of electroactive species. The first electrochemical sensor was a glucose sensor [6]. In this case, an enzyme, glucose oxidase (GOx), was immobilized on an electrode. These enzyme catalyses the reaction between glucose and oxygen into gluconic acid and hydrogen peroxide. Hydrogen peroxide works as a mediator between the enzyme and the electrode. This means that following the catalytic reaction, hydrogen peroxides undergoes an oxidation at the surface of the electrode, thus releasing electrons into it (Figure 1-9). When we apply a fixed voltage, the amount of current is directly related to the concentration of glucose. The selectivity in this case comes from the use of specific glucose enzyme.

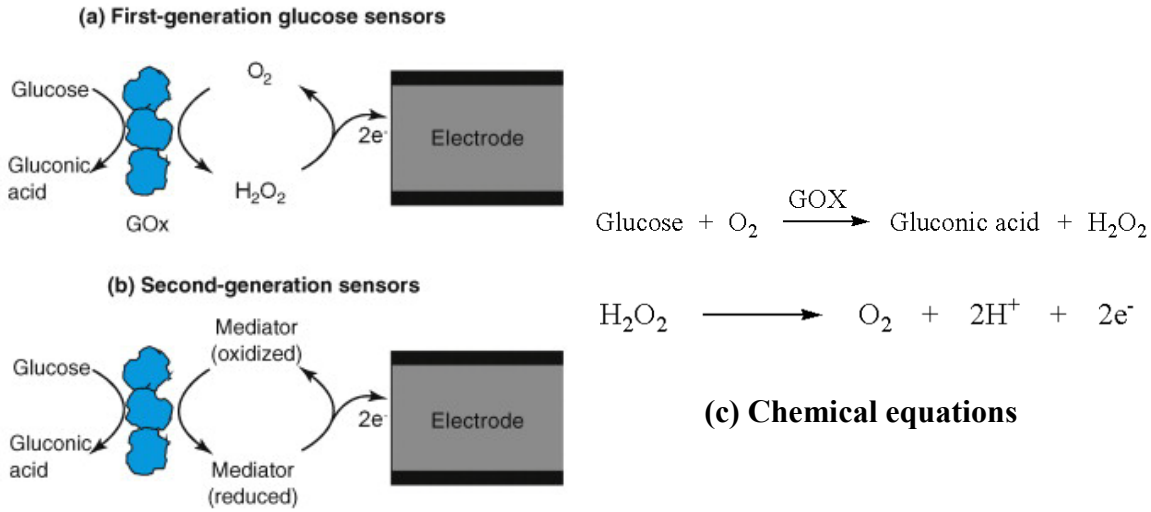

Figure 1-9: Electrochemical glucose sensor. (a) and (b): Schematic description of the first and second generation glucose sensors. (c) Redox reaction of glucose due to Glucose Oxidase (GOx) and accompanying half equation of hydrogen peroxide oxidation [40].

These glucose sensors were later improved using other types of mediators [40]to enhance selectivity (Figure 1-9.b).

Later on, electrochemical sensors were used to detect bigger analytes like pathogens and various proteins. In this case, the detection of the binding of the analyte itself to other components (bioreceptors) using electrochemical transduction has been widely used [41], [42], [43].

In these cases, the surface of the electrode (carbon or metal) is modified in order to immobilize various biomaterials, such as enzymes, antibodies or DNA [6], [44]. Gold is one of the most frequently used metals [45] because it is inert and compatible with biomolecules

and cell structures. Although metals do not allow immobilization of biomolecules, many solutions exist in order to modify the surface properties. One of them is the use of self-assembled monolayers (SAMs) [46], [47].

The basic principle of electrochemical immunoassays is illustrated in Figure 1-10**.** In this case, the antibodies were immobilized to the SAMs surface by means of protein A. Antibodies' amine group covalently bond to the aldehyde group on protein A (see section 0for more detail). This pretreatment step is done on the working electrode. Additionally, counter and references electrodes are also needed in order to form the electrochemical system.

In this example and after these pretreatment steps, a sample solution containing salmonella is introduced, followed by secondary labeled antibodies with enzymes as markers. Finally a substrate is introduced that will react due to enzymes. As products of this reaction, electroactive species emit analytical response signals for the immunosensor.

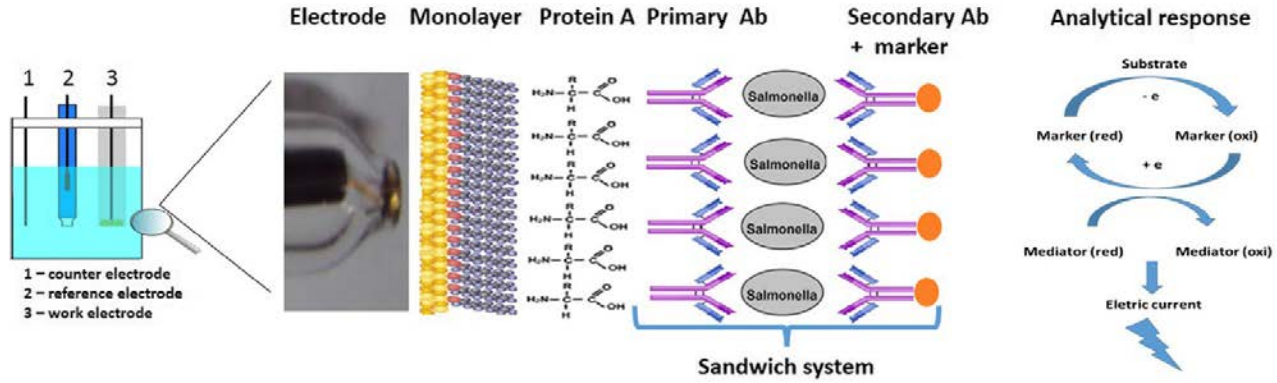

Figure 1-10: Schematic diagram of the electrochemical immunosensor and the analyte response [47].

Nowadays, electrochemical biosensors are the most widely used sensors in industry. This is mainly due their many advantages; they are low-cost, robust and have a low power consumption. These devices can also be simple to operate [12], [13], they can be used together with either electrophoresis or capillary fluid actuation methods in order to integrate the flow control [18]. Thus, with the advance of electronics and microfabrication, electrochemical systems are more suitable than their optical counterparts for integration in a miniaturized lab-on-chip system.

Despite all this advantages, electrochemical biosensors suffer from some drawbacks. For instance, the current accompanying the aforementioned miniaturization goal requires improved electronics/shielding in order to keep good sensitivity. Also, a stable reference electrode is required [12]. In addition, the surface must have appropriate electrochemical characteristics and compatibility to the chosen immobilization method [47]. Furthermore, particles other than the target may get deposited or adhere non-specifically to the surfaces being monitored, thereby yielding false positive results. Finally, diffusion time has to be taken into account so that the performance of the system is not degraded [9].

In the next sections, the four major electrochemical methods: amperometric, impedance-

based, potentiometric or voltammetry and conductometric measurements will be described.

Amperometric sensors

Most of these sensors are based on the use of enzyme related systems that generate electroactive products. In this case, the potential is fixed and the resulting current is the electrical parameter of interest [12]. The altered current flow is then measured and the magnitude of the current is proportional to the substrate concentration, thus indirectly proportional to the analyte of interest.

Amperometric techniques are the most popular electrochemical method. In fact, this detection format has several advantages, including the capacity to fabricate disposable and customised screen-printed electrodes, low fabrication costs and robustness. The selectivity can be improved by using well-chosen mediators like ferrocenedicarboxylic acid (FEDC) or iodine [48].

In one example, amperometric detection of Salmonella in milk was achieved using magnetic beads coated with specific antibodies for an immunomagnetic separation step. Using magnetic beads and immunoreactions, the bacteria are captured and preconcentrated from milk samples. A second antibody labeled with peroxidase (HRP) is used for the electrochemical detection [49]. Moreover, the magnetic beads allow concentrating the bacteria in the area of detection (electrode). The HRP enzyme then boosts the redox reaction and a resulting amperometric unit allows the detection (Figure 1-11).

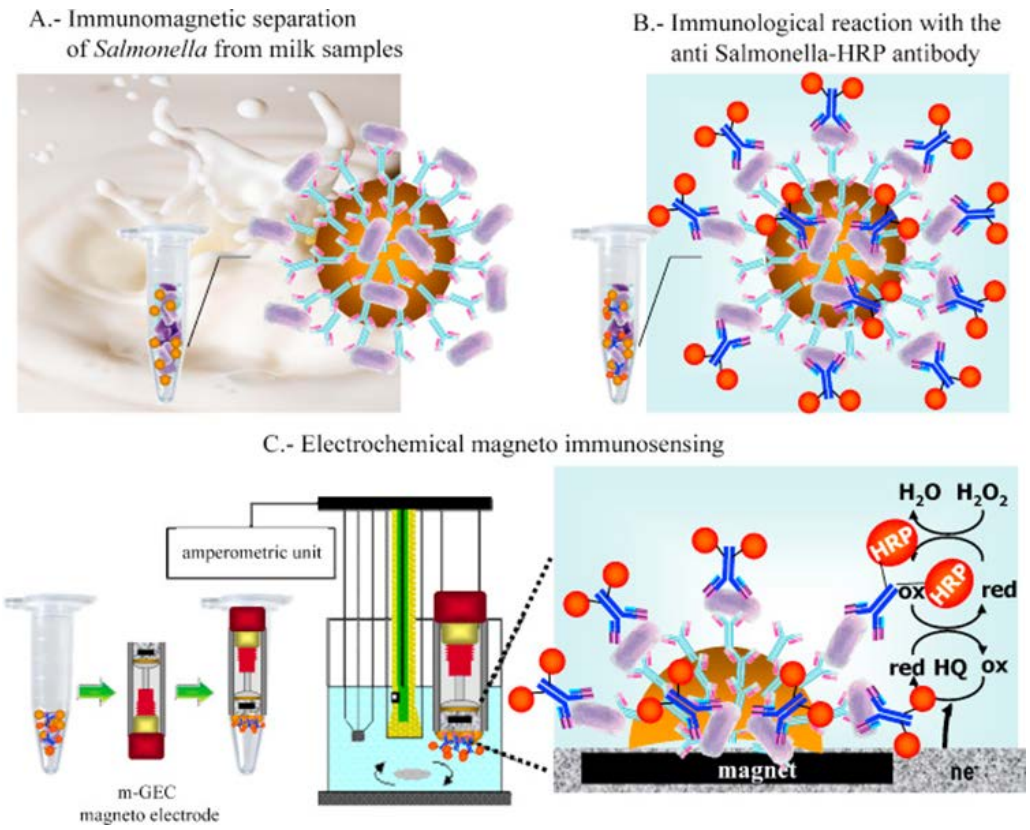

Figure 1-11: Schematic representation of the 'IMS/m-GEC electrochemical immunosensing' approach: (A) immunomagnetic separation (IMS) from milk samples; (B) immunological reaction with the anti-Salmonella-HRP antibody; (C) electrochemical detection [49].

The approach showed a limit of detection of 5 × 103 and 7.5 × 103 CFU (Colony Forming Unit) mL^{-1}. The main problems faced with these types of sensors are the sensitivity to pH changes and non-specific binding of molecules, leading to false positive detection [13].

Impedance based sensors

Upon the binding of the bioreceptor with the antigen, there is a measurable response in conductivity across the electrode surface. This response can be translated in terms of impedance/capacitance change. The advantage in this case is that no reference electrode is needed [13], thus making the detection easier and fabrication simpler.

Early issues involved low sensitivity and non-specific binding. To address these common problems, a blocking protein, such as BSA (Bovin Serum Albumin), can be used. Also, in order to amplify the signal, a secondary set of antibodies or gold nanoparticles can be added at the expense of maxing the measurement more complex and time consuming. This technique has been used to detect multiple viruses, such as influenza [50], rabies [51], dengue [52] and HIV viruses [53].

In the case of LoC systems, the method usually relies on an array of interdigitated microelectrodes (IME) combined with an immunoassay procedure [20]. Antibodies are immobilized on the IME. The detection scheme stays the same and the change of signal

properties is analyzed using an impedance analyzer electronic system (Figure 1-12.a).

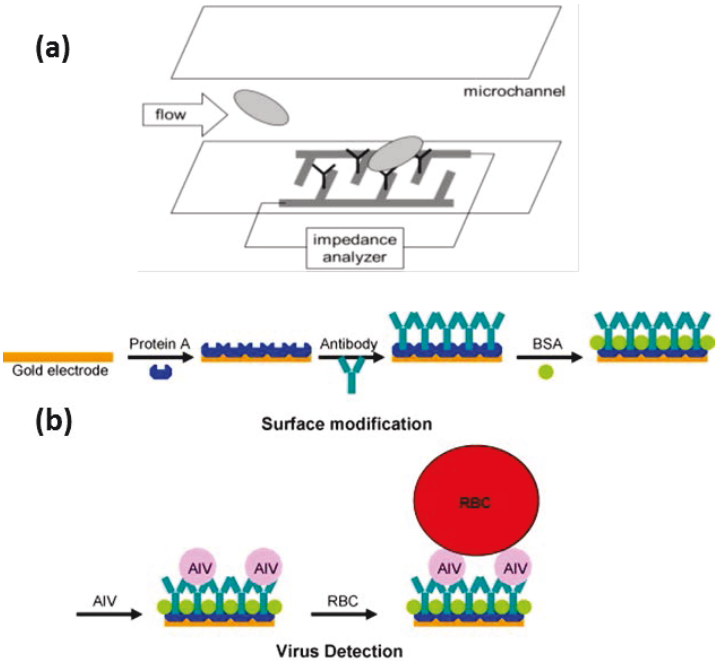

Figure 1-12: (a) IME (interdigitated microelectrode) immunoassay lab-on-a-chip [20]. (b) Practical example from [54]: IME for the detection of avian influenza virus (AIV). RBC: Red Blood Cell, BSA: Bovin Serum Albumin.

A practical example of the use of IME is reported in ([54]), where both antibodies and BSA blocker protein were immobilized on the gold electrodes through the use of protein A (Figure 1-12). In this case, an amplification step was added in order to have better signal to noise ratio by adding red blood cells that have binding sites with influenza-type viruses. The experiment showed low nonspecific results but the procedure is time consuming (2h).

Impedance-based techniques are still in their infancy. Improvement is still needed in terms of sensitivity, stability, selectivity and speed of response as well as the ability to monitor real time dynamic fluctuations [13]. Finally, because the results are not adequately reproducible, commercialization will remain an issue. However, efforts to address these issues are being made with respect to improving the detection protocol and the surface chemistry of the electrodes.

Potentiometric based sensors

In this case, analyte detection is realized by measuring the potential of an ion-selective electrode (usually a membrane) versus a reference electrode. This method is also called voltammetry. When these later ions pass through the electrode and equilibrium is locally established at the sensing interface, the consequent charge separation induces a potential difference between the working electrode and the reference electrode [18]. This potential is related in relation to the species type and concentration of the targeted entity.

Voltammetry has a comparative advantage to other electrochemical technique in that the

signal-to-noise ratio improves when the electrodes are reduced (low micrometer range). In the case of common millimeter diameter electrodes, the diffusion of electroactive species is planar whereas in microelectrodes, the diffusion becomes nonplanar (e.g. hemispherical). This change in diffusion aspect causes an improvement of the collection efficiency of electroactive species which leads to an increased signal-to-noise ratio and thus a lower detection limit [12].

As an illustration, a bead-based immunoassay procedure with microelectrode detection was demonstrated [55]. Here, the analyte of interest was mouse IgG antibody labeled with alkaline phosphatase enzyme (AP) and p-aminophenyl phosphate (PAPP) as the enzyme substrate. Results showed that the microelectrodes allowed monitoring the chemical reactions in real time. A detection limit of 10 ng/mL was achieved. This system served as validation of the usability of microelectrodes for immunoassays.

Conductometric sensors

The principle of conductometric detection is that the conductivity of a zone is affected by the charged species in that zone. Different types of species have their specific conductivity response which also varies with different concentration [18]. The detection involves measuring the conductivity at a series of frequencies. This method can, in principle, deal with all charged species of interest.

This technique is usually coupled with electrophoresis in order to allow both actuation and detection of the analyte of interest. In [37], the authors experimented the use of potential gradient detection using a capacitively coupled contactless conductivity detection method. This method uses two electrodes for actuation and two electrodes for the detection of the potential change that is proportional to the conductivity change of the medium, indicating the presence of the analyte. The detection method was tested for potassium ions with a detection limit of 15 μM.

This technique is also usable for the detection of pathogens, conventional techniques uses conductive polymers in order to convert the biological signal to a change in conductivity. Examples of conductive polymers include polyacetylene, polypyrrole or polyaniline [56]. For instance, a conductimetric biosensor incorporating a polyclonal antibody-based sandwich assay format in which the detection antibody was labelled with polyaniline was developed [57]. This sensor could detect approximately 79 CFU/mL and 83 CFU/mL of E. coli O157:H7 and Salmonella spp, respectively (Figure 1-13).

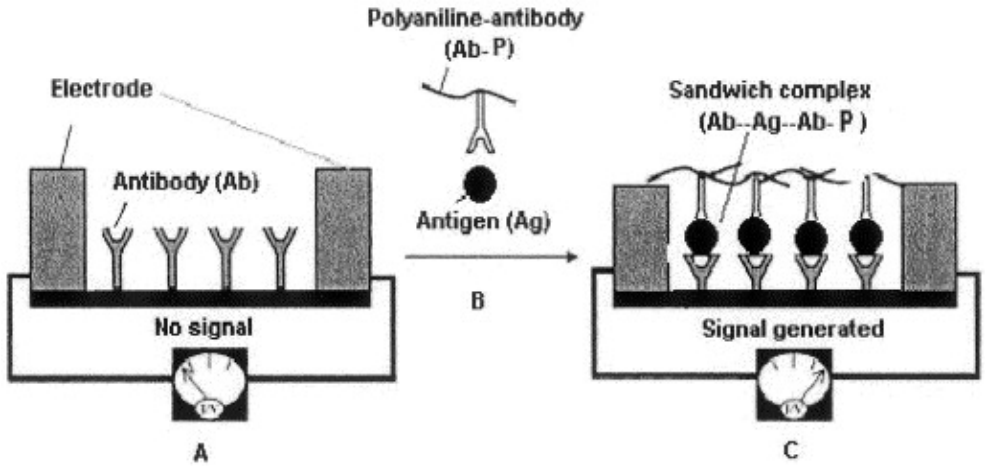

Figure 1-13: Cross-section of a capture membrane before (A) and after (C) analyte application [57].

Furthermore, a modern method for E.coli detection was demonstrated using magnetic nanoparticles (MNP) coated with streptavidine and selective antibodies [58]. The MNP were immobilized to the conductimetric electrode surface using glutaraldehyde. Biotinylated antibodies were used in order to attach to nanoparticles and allow forming an immunocomplex with E.coli. The incorporation of nanoparticles facilitated an increase in conductivity, enabling 0.5 CFU/mL to be detected. A small amount of non-specific signal was detected when S. epidermis cells were assayed in parallel. This was attributed to the use of a polyclonal capture antibody. The authors concluded that in some assay formats, monoclonal or recombinant antibodies may be more suitable.

Concerning the advantages of conductance based technique: first, they require low drive voltage and thus low power consumption. Second, there is no need to use a reference electrode, which simplifies the system.

Despite these comparative advantages, practical application and commercialization of such techniques are hindered by some difficulties, such as the need of adequate experimental conditions (e.g., buffer concentrations and dissolution of ingredients in solution) in order to avoid reduction in signal to noise ratio and low specificity [47].

Nanomaterial based electrochemical sensors

In recent years, nanomaterials have been used extensively in order to revolutionize biosensors in general and electrochemical biosensors in particular. Nanomaterials range from gold, silver, silicon, and copper nanoparticles, carbon-based materials, such as graphite, graphene, and carbon nanotubes [59], [6]. Nanoparticle-based materials are widely used because they provide great sensitivity and specificity for developing electrochemical biosensors.

In this context, carbon nanotubes (CNT) based immunoassays show the most promising results in terms of sensitivity, low drive voltage, integration in LoC device and rapid electrode kinetics. Most of CNT surface area is accessible to both electrochemistry and functionalization with biomolecules [20].

In one case, a multi-wall carbon nanotube (MWCNT) based electrochemical sensor was developed in order to detect Salmonella bacteria with a detection limit of $10^3 CFU/mL$. Carbon nanotubes were functionalized with multiple layers of enzyme Tyrosinase and avidin [60]. These CNT were then dropped on a screen-printed electrode surface. Catechol substrate was then used in order to assess the sensitivity and rapidity of the system. Typical reported response times were around 2s.

The main drawback of CNT is that these structures cannot serve as transducers; they must be fixed to an electrode. Another drawback is that these systems are not yet made for long term reliable usage [6]. A reliable LoC ELISA like CNT based immunosensor is yet to be developed by taking advantage of the advance of NEMS (nano-electro mechanical system) techniques [20].

1.3.2.3 Mechanical methods

Mechanical methods can also be called mass-based methods. That is, the intrinsic property of pathogens exploited in this case is “mass”. Moreover, each solid rigid object has its own resonant frequency that shifts when an additional mass is applied on it [61]. That additional mass could be the pathogens themselves. One can then relate the mass or resonance frequency change into a qualitative and quantitative measurement of the analyte presence. In general, mechanical detection methods have the comparative advantages of very low detection limit and label-free detection. If these sensors are intended for pathogen sensing, usually a bioreceptor should be immobilized on the transducer surface. That can be either antibody, antigen, DNA…etc. From this principle of detection, two main types of mechanical methods exist; either they are quasistatic surface-stress sensors or dynamic-mode sensors [62].

Surface stress sensors

Surface stress sensors are mainly fabricated using cantilevers. They are beams that are fixed at one end and free at the other. Weight and external forces causes the beam to bend. Cantilevers are typically made of silicon, crystalline or in some cases polymer materials [9].

In the case of immunosensors, pathogens bind to antibodies immobilized on the cantilever surface (Figure 1-14.a). If the cantilevers are used in a static way, the conventional detection method involves the use of laser light (Figure 1-14.b). The light is applied to the sensor surface and the deflection of the light changes when the pathogen is immobilized [62]. Another way to detect the bending is by using piezoelectric materials; in this case the mechanical stress provokes an electrical signal due to the piezoelectric properties. The latter method has the advantage of being able to be integrated on a lab on chip device and is generally less cumbersome. Reported sensitivities range from 100pM to several nM range [63].

The main drawbacks are parasitic factors that follow their exposure to the sample aliquot. Indeed, changes of refraction index, temperature and fluidic disturbance result in nonspecific additional deflections [62]. One solution in this case is to use a differential mode

measurement by using a reference cantilever.

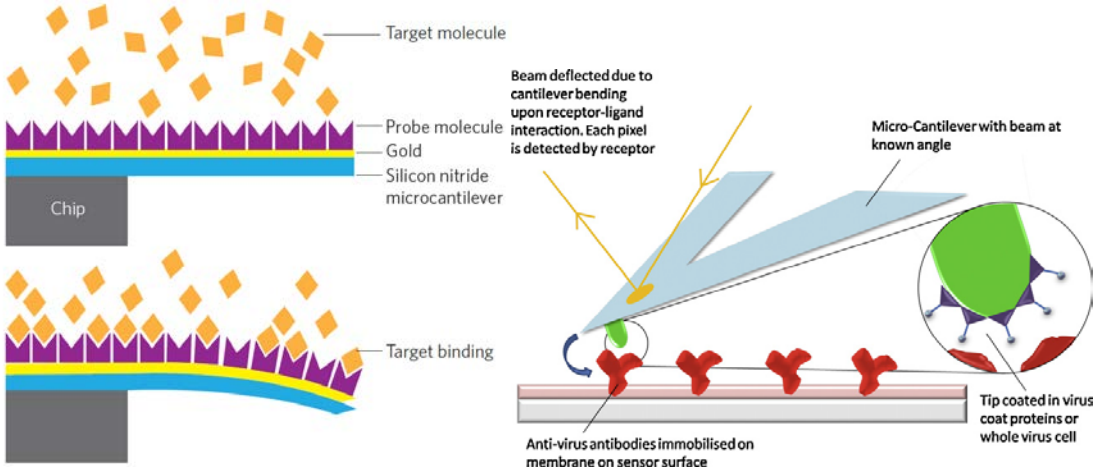

Figure 1-14 (Left) Schematic of static-mode surface-stress sensing MEMS device. Binding of target molecules generates a surface stress, which leads to a quasistatic deflection of the cantilever (bottom) [64]. (Right)Microcantilever detection based onAFM topping mode. A laser is angled to reflect off the micro-cantilever as it passes over the sensor surface. Upon virus–antibody interaction, the micro-cantilever bends and causes the angle of the reflected beam to change [13].

Dynamic mode sensors

These systems can be divided into two major groups: micocantilever (or microcantilever arrays) based methods and quartz crystal based methods. Usually, both of them are made using piezoelectric materials and they are operated in a dynamic manner using their resonance properties.

Cantilevers:

In this case, another property of the cantilever can be used. In fact, after the beam bends, its elasticity attempts to restore it to its original shape, thus leading the system to have a characteristic natural frequency of vibration (principal resonance frequency) [9]. This value depends on the effective mass and the spring constant of the beam. Consequently, the positive change in the mass results in a decrease of the resonance frequency [65].

Microcantilever-based techniques are derived from Atomic Force Microscopy (AFM) [13]. AFM utilizes a sharp tipped oscillating cantilever to characterize the surface of a sensor. A laser is focused onto the cantilever in a way that the position of the reflected beam is detected by a CCD chip. Tip deflection can then be followed. For this, the lever is set to oscillate at a frequency close to that of the surface [13]. When characterizing an antibody immobilized surface of an immunosensor, a corresponding pathogen is attached to the tip of the cantilever. This causes the tip to bend when it encounters the antibody (Figure 1-14.b). The cantilever's movement is constant because it is mediated by a piezoactuator and the sensor can be characterized by observing the amplitude, phase and resonance frequency of the cantilever. The signal is extrapolated to give a 3D image of the surface with a spatial resolution down to 1 nm. AFM is highly sensitive and can detect atomic bonding and van der Waals forces. In

medical diagnosis, AFM constitutes a useful tool in order to confirm the presence of pathogens in laboratory based studies. However, due to its extreme vibration sensitivity, AFM is not suitable for field use.

Microcantilevers fill the need to have a more portable system that is less complex. In this case, the cantilevers are not used for sensor characterization but rather for pathogen sensing. After immobilizing specific antibodies to the cantilevers' surface, the cantilevers can detect any specific pathogen. The resonance frequency change is directly correlated to the amount of pathogen. Traditionally, a washing step is added in order to remove adherence of non-related particles. Also, the detection limit can be improved by using sandwich assay format or labels that allow the increase of the mass and consequently lowering the detection limit.

Apart from the previously mentioned issues, cantilever based methods suffer from 'striction' problems, which means that fluid can remain stuck underneath the cantilever due to surface tension. In this case, special techniques like critical point drying and freeze drying are used to prevent striction [9], thus making the procedure more complex.

Moreover, the adaptation of such system to multiple detection is complicated, since, in principle, multiple microcantilevers should be each coated with different antibodies. Because it involves multiple surface treatment steps, this procedure is very complicated, rendering the use of cantilevers for multiplex detection not yet feasible.

Quartz Crystal Microbalance (QCM):

QCM methods are also based on the use of piezoelectric materials. The quartz crystal microbalance (QCM) is an instrument that utilizes a piezoelectric quartz crystal that can vibrate at high frequencies with an electrical current to perform frequency-based measurement of pathogen mass (Figure 1-15.3) [61]. The quartz surface usually has a thin gold or other metal layer deposited onto it that allows bio-functionalization of the surface. After affixing bioreceptors to the surface of the sensor, the pathogen binding can be monitored by measuring the frequency decrease caused by the additional mass on the chip via the Sauerbrey equation [66]. Like cantilevers, an additional washing step with fast flow rate is necessary in order to remove non-specific binding.

As an example, the QCM can be used for the detection of DNA by using a DNA probe and measure the subsequent hybridization to the target DNA. Hybridization is a phenomenon in which single-stranded deoxyribonucleic acid (ssDNA) or ribonucleic acid (RNA) molecules bind to complementary DNA. This will result in a mass change (Figure 1-15.1).

The mass change can be amplified by using gold nanoparticles (AuNP). This is done by first immobilizing DNA-specific strands to the nanoparticle surface. Then the detection scheme is similar to the conventional method, except that an additional step is required at the end. In fact, after DNA hybridization, functionalized AuNP should be added. The resulting mass amplification yields significant signal amplification. In this case, AuNP can also serve to reduce nonspecific detection since they work like a sandwich assay (Figure 1-15.2). In [67]

and [68], the authors reported the use of this method in order to detect E.coli and Dengue virus respectively. The later method uses two layers of AuNP in order to increase the amplification. The reported limit of detection was 1.2 10^2 CFU/ml of E. coli O157:H7 and 2 PFU (plaque forming unit) / ml.

As with other piezoelectric methods, QCM methods are advantageous as they are label-free, sensitive, simple to construct, low power demanding and allow quick analysis. However, with the exception of some cases [61], QCM technique is limited by the difficulty of incorporating multiplexed detection of multiple samples. Moreover, these methods need dry conditions, meaning that after hybridization, the QCM must be dried for accurate measurements. This is because the liquid medium imposes significant damping of the vibration. Therefore, this technology is not yet suitable for in-field use but it is very convenient in laboratories when combined with other methods (like Polymerase Chain Reaction (PCR) for amplification, SPR detection…etc.). QCM can also be used for characterizing immunosensor chip fabrication. In this case, it is usually used with electrochemical techniques for the observation of the sensor construction at each stage [13].

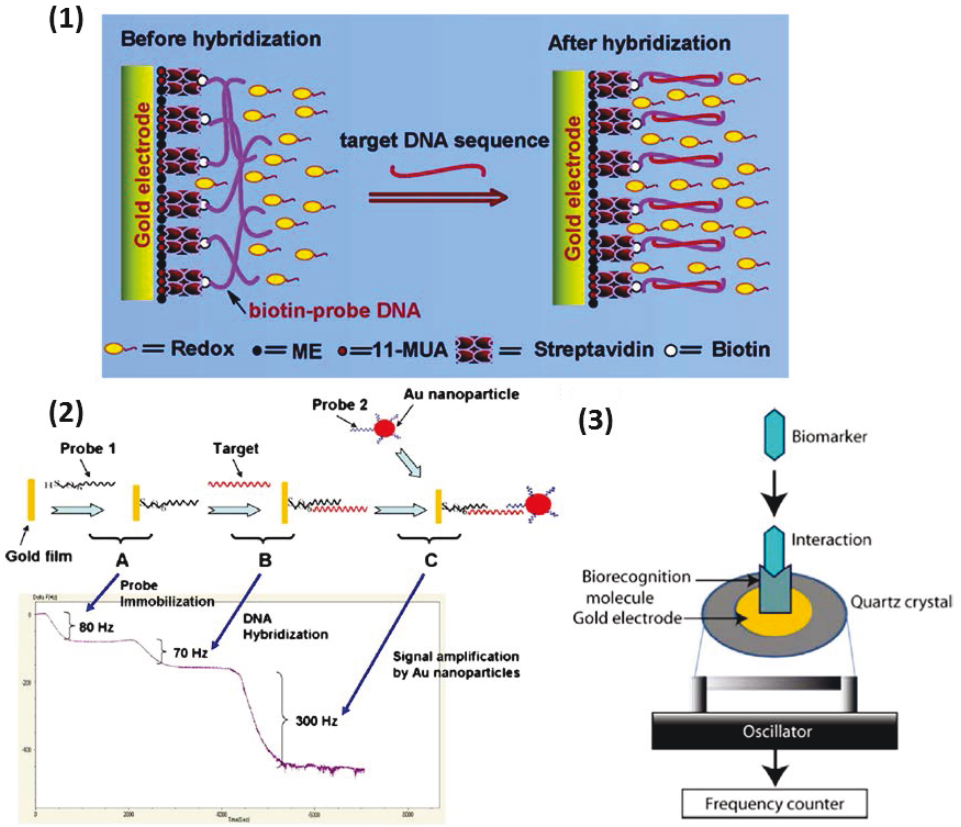

Figure 1-15: **1:**Schematic illustration of DNA probe immobilization through avidin-biotin chemistry and the hybridization of target DNA on a self-assembled monolayer (SAM)-modified Au electrode [69].**2:** Time-dependent frequency changes of the QCM sensor. (A) Addition of DNA Probe 1 self-assembly immobilized on the surface of the QCM sensor. (B) The complementary target oligonucleotides were subsequently introduced for DNA hybridization. (C) Additional treatment of the DNA hybridized QCM with Probe 2-capped Au nanoparticles. The sequences of Probe 1 and Probe 2 are complementary to the two ends of the analyte DNA (i.e., target sequences) [67].
3: Transduction systems in QCM based sensors [70].

Other mechanical methods

Other mechanical methods exist that can deal with some of the aforementioned issues. For liquid phase detection, some reported the use of higher working frequencies in order to prevent the damping caused by viscous liquids. This is achieved by reducing the dimension of the device or by operating with higher order vibration modes [71], [72]. Another technique uses Suspended Microchannel Resonators (SMR) which constrains the fluid to channels embedded in the mechanical resonator itself [62].

Finally, Surface Acoustic Wave (SAW) sensors constitute another major reported technique [70]. They rely on the generation of acoustic waves caused by an electric signal. This results in a consequent wave that is transformed into an electrical signal. The mass change of the device is related to the frequency shift of the output signal [73]. This technique has been used for the detection of breast cancer markers like HER2 (human epidermal growth factor receptor-2) with a detection limit of 2 ng/mL [74].

In conclusion, mechanical methods have great potential for their use in medical diagnosis. An extensive research is done in order to have multiplexed and automated LoC systems that allow the detection of multiple different pathogens down to the single cell limit of detection. However, the main issues consist in the biofunctionalization of the multiple cantilevers, the electrical handling of multiplexed signals without interference and the background biological noise [62].

1.3.2.4 Magnetic methods

Major detection techniques were discussed in the previous sections. Electrochemical and optical based sensors are preferred to all other types of sensors. Thus, a wide body of research has been done and many commercial devices use these technologies in order to develop Point of Care (POC) pathogen sensing devices and biosensors in general. In these recent years, however, magnetic detection techniques have become increasingly popular.

Magnetic biosensors mostly detect the value or change of magnetic properties like the magnetic field. For the case of LoC systems, miniaturized magnetic detection methods usually rely on the detection of magnetic beads present in microfluidic channels [8]. The magnetic beads are used as markers and an indirect detection of the pathogen is done through affinity binding of the functionalized magnetic beads.

The increasing interest toward magnetic detection methods is mainly due to the advances in microfabrication and nanomaterial technologies. The introduction of well controlled magnetic nanoparticles (MNP) and all their advantages increased the interest of researchers on magnetic detection and actuation techniques.

The unique advantages of MNP can be summarized in the following points [75]:

- **High affinity binding flexibility:** their structure allows them to be functionalized by a variety of affinity ligands on their surface. Because many binding sites can be

created on a single MNP, high binding efficiency can be achieved.

- **Easy and selective actuation of MNP**: due to their unique magnetic properties, they can easily be manipulated inside the biological sample using a magnetic field gradient [76]. This enables manipulation and sorting of biological targets.
- **High contrast:** this is because the biological background naturally contains almost no magnetic materials; this allows having a high SNR.
- **Can serve as amplifier:** In the case of nuclear magnetic resonance (NMR) tests, MNP influence the relaxation of surrounding water molecules and consequently amplify the NMR signal.
- **Low influence of sample properties:** indeed, properties like pH and salinity to not perturb the magnetic properties of MNP [77].

In addition to these unique benefits, MNP are physically and chemically stable, can easily be made biocompatible [78] and are available at relatively low cost. It is the multi-functionality of MNP that makes them an attractive candidate for LoC applications. Furthermore, using standard silicon integrated circuit technology, magnetic fields can be applied and tuned either externally or internally in a complete integrated solution [79], [76]. Consequently, both sensor and MNP can be scaled down to the micro- or nanometer scale.

All the above advantages make magnetic detection methods that use MNP quite appropriate candidates for their use in a completely integrated diagnostic system. Since MNP constitute a key component; some theoretical background about MNP properties will be given in Chapter 2.

Besides, magnetic pathogen sensing techniques can be classified by the detection format; homogeneous or heterogeneous. In the homogeneous format we find techniques such as nuclear magnetic resonance (NMR), magnetic relaxation switches (MRsws) and remanence detection techniques like AC susceptometry. On the other hand, surface-based methods include magnetoresistive sensors and Hall sensors. Moreover, magnetic sensors can also be divided by the physical parameters [78] like magnetic permeability, remanence …etc.

Next, we will present some major magnetic pathogen sensing techniques with an emphasis on recent miniaturized detection methods like magnetoresistive (MR), micro Hall based sensors and micro NMR sensors. In this project, we have chosen another effective detection method developed at Juelich [1] and called “the frequency mixing technique”. This method has several advantages as linearity, simplicity and large dynamic range. It is also implementable in a miniaturized LoC. Details of this adopted technique will be given in the following chapter.

Magnetic permeability sensors

One of the most basic parameters to be measured by magnetic sensors is the change in permeability. This can be assessed either by measuring the resulting change in inductance (L) or by relating it to the change in resonant frequency [78].

In the former case, an early demonstration was done by using a typical cylindrical coil and a core made of magnetic material [80]. When the magnetic material is introduced into the coil, the value of the relative permeability changes (μ_r), resulting in a change of the coil inductance.

$L = \frac{\mu_r \mu_0 A}{l} N$ where N, A and l denote the number of turns, the cross section and the length of the coil, respectively. μ_0 represents the permeability of vacuum.

The coil was put in a Maxwell-Wien bridge configuration (Figure 1-16). Change of inductance results in an unbalance of the bridge and a detectable voltage difference appears. Reported magnetic sensitivity was $21 \pm 4\mu V/(\mu g\ Fe/mL)$.

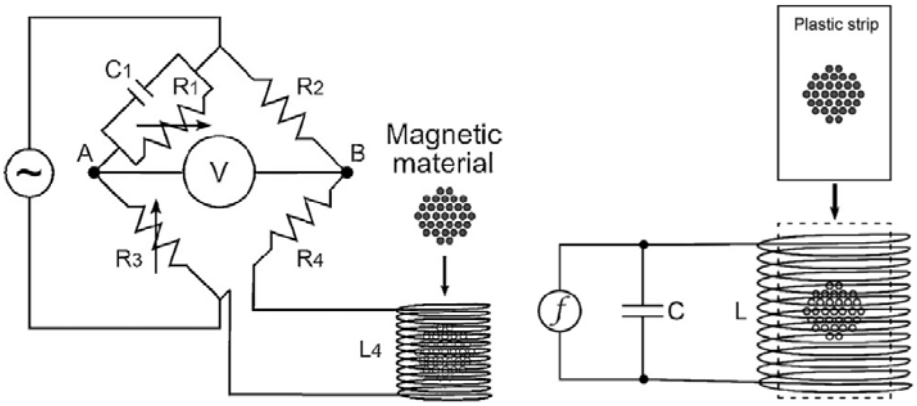

Figure 1-16: Measurement of permeability using: (left) Maxwell bridge. (right) resonance LC circuit [78].

Permeability can also be detected by means of resonance using an LC circuit and measuring the resonance frequency shift [81]. Indeed, when the permeability changes, the inductance changes and thus the resonance frequency changes (Figure 1-16). When a test strip is placed inside the measuring coil (connected in parallel with a capacitor), the presence of the particles causes the resonant frequency of the coil to decrease proportionally with the number of magnetic particles on the strip. This later technique was used using flat spiral coils and reported a sensitivity of Troponin 1 of about $0.5\ ng/ml$.

Magnetic relaxation based sensors

These techniques rely on the dynamic response of the magnetic nanoparticles relative to a certain magnetic field. In this case, it is the relaxation of the magnetic moment within the MNP that is the basis parameter for these detection methods. This relaxation is measured in two ways; by measuring the susceptibility or by measuring the decay in remanent magnetization using a superconducting quantum interference device (SQUID).

MNPs relaxation is driven by two relaxation processes: Brownian relaxation (τ_B) due to the thermal rotation of MNP and Néel relaxation (τ_N) related to the magnetic core inner magnetization decay.

AC susceptometers use the fact that when MNP bind to their target analyte, a change in the total hydrodynamic volume of the MNP occurs (complex MNP + analyte). The hydrodynamic size is positively related to the Brownian relaxation time, so that when the size is bigger the Brownian relaxation is slower. Typical relaxation times for 20 nm MNP are tens of microsecond and seconds for the Brownian and Néel relaxation respectively (Figure 1-18.a). The frequency dependent magnetic susceptibility (χ) of MNP is affected by the change of the Brownian relaxation. In fact, the imaginary part of the susceptibility has its peak at the frequency $f = 1/\tau_B$. The principle of the detection is then to measure the shift in this peak frequency. These measurements are usually done by inductive coils [82].

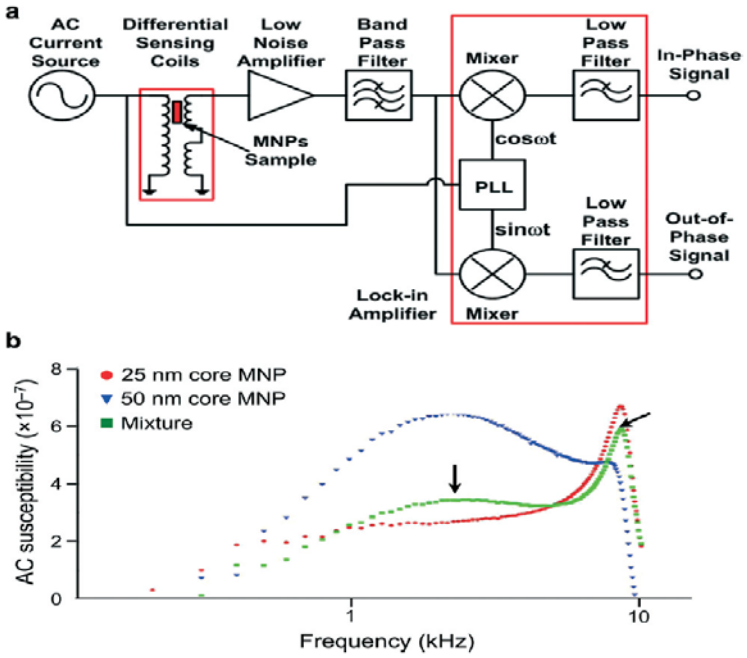

Figure 1-17: Multiplexed Brownian detection of 25 nm core (red) and 50 nm core (blue) MNPs. (a) Alternating current (AC) magnetic susceptibility is measured using a quadrature detector. The signals both in-phase and 90 degree out-of phase with respect to the AC source are measured, which correspond to the real and imaginary components of magnetic susceptibility, respectively. (b) The out-of-phase (imaginary) component of the susceptibility has its maximum when the excitation frequency is close to the Brownian relaxation time of the particle [83].

AC susceptometry which has the advantages of being a volumetric test, does not need any washing step and it can be multiplexed. Figure 1-17 shows an example of the simultaneous measurement of two different types of MNP [83]. In this experiment, the measurement setup could even discriminate a mixture of two MNP with 25 and 50 nm diameters. Despite these advantages, AC susceptometry still lacks appropriate sensitivity and discrimination of more than two types of MNP. Also, in order to apply this technique, it has to be made sure that Néel relaxation is slower than Brownian relaxation.

There are other methods that detect the Néel relaxation instead of the Brownian relaxation change [84]. This method is called magnetorelaxomety. When the MNP bind to the target, the Brownian relaxation is inhibited (Figure 1-18 b, c). However, the Néel relaxation only

depends on the magnetic core of the complex and it is thus unchanged. After external magnetization, unbound nanoparticles have then a total relaxation time of micro- or milliseconds and bound MNP have a total relaxation time of almost a second. Using a SQUID with a time measurement range between 1 ms and 1 s, one can detect only bound MNP and thus quantify their presence while discriminating them from unbound MNP (Figure 1-18 b, c). In [85] , this technique could detect 1.1 10^5 bacteria in a 20 µL sample volume.

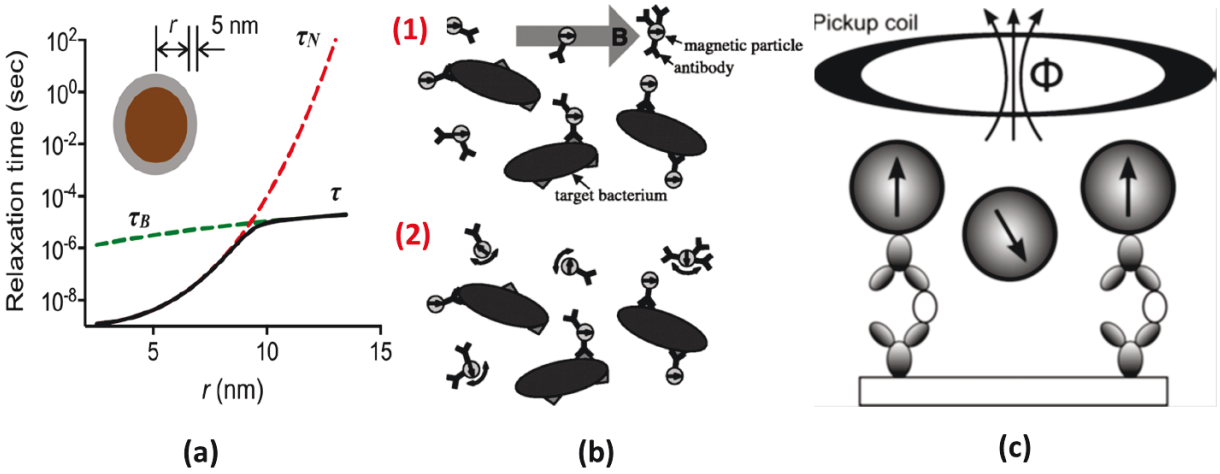

Figure 1-18: (a) Brownian and Néel relaxation with respect to the size of the MNP [75]. (b) Example of homogeneous detection by means of magnetorelaxometry. b.1: When subjected to a magnetic field pulse, all the MNP are oriented. b.2: After the end of the pulse, the unbound MNP moment relaxes faster due to Brownian relaxation whereas the bound MNP relaxation is restricted due to the new hydrodynamic size [84]. (c) Example of heterogeneous detection of bound MNP using a SQUID that relies on a superconducting pickup coil. The SQUID measures the decay of the remanent magnetization of bound MNPs that do not have any Brownian motion. On the other hand, nanoparticles that are unbound relax very rapidly by Brownian rotation and do not contribute to the overall signal [78].

This type of technique needs a much shorter measurement time and has the potential of an even higher sensitivity at the expense of a considerably increased technological effort (requirement for cooling the SQUID sensor to about -196° C in case of high-T_c SQUIDs and extensive magnetic shielding). Thus relaxometry is not yet suited for miniaturization and integration.

Hall effect sensors

The Hall effect appears when a magnetic field is applied perpendicular to a current-carrying conductor (Figure 1-19.a). Charge carriers are pushed to one side by the transverse force (Lorentz force) building up to generate an electrical field that results in a voltage difference (Hall voltage) perpendicular to both the current and the magnetic field [78]. This voltage is given by the equation:

$$V_H = \frac{IH}{t} R_H$$

Here, I denotes the current and H the magnetic field strength. R_H and t represent the Hall coefficient and the thickness of the Hall effect region. Hall-based sensors are advantageous because when the sensor is miniaturized, its sensitivity improves because t is much smaller and thus the detected voltage V_H is higher for the same magnetic field value. This is a unique advantage.

Hall sensors can be integrated using standard IC processes allowing *μHall* sensors to be fabricated. In an interesting example, a μHall sensor array was used to detect levels of epithelial cell adhesion molecules [86]. In this experiment, the microHall sensors had 8x8 μm² size and an array of 2x4 Hall sensors was used. The targeted cells were labeled with MNP. When the cells are moving on top of the array, an AC signal is detected by the Hall array that allows cell counting. The advantage of the AC detection scheme is that the signal is not affected by the magnetizing DC field. Results were compared to flow cytometry measurements for validation (Figure 1-19).

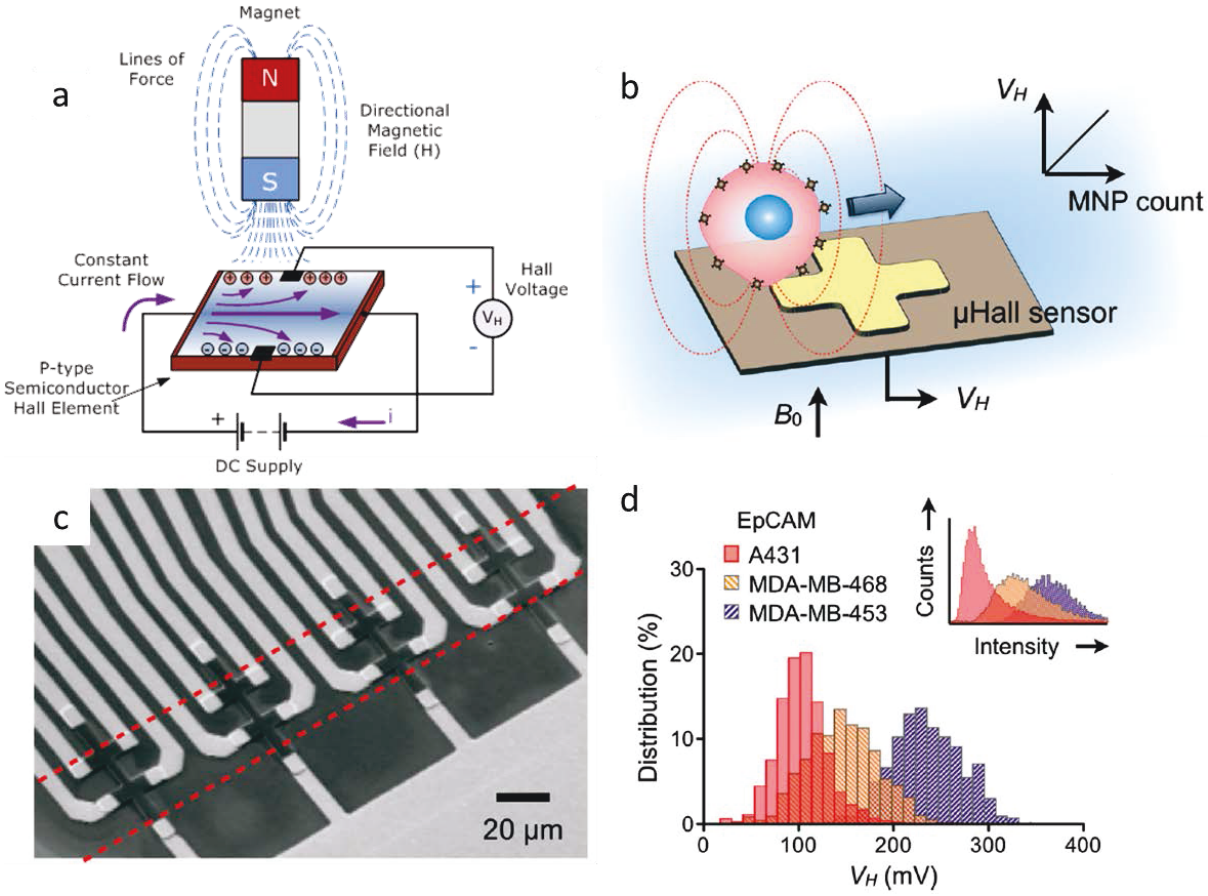

Figure 1-19: The basic concept of the Hall cross sensor. b, c and d: microHall sensor for cell detection [86]. (b) Each cell, targeted with MNPs, generates magnetic fields that are detected by the μHall sensor. The Hall voltage (VH) is proportional to the MNP counts. B0, external magnetic field. (c) The sensing area has a 2 × 4 array of μHall elements. The dotted lines indicate the location of fluidic channels. The sensors are arranged into an overlapping array across the fluidic channel width. (d) The μHall system accurately measured the expression levels of epithelial cell adhesion molecule (EpCAM) in different cell lines; the inset shows the same measurements by flow cytometry.

In summary, Hall based sensors have a lower sensitivity than magnetoresistive techniques but exhibit a better linearity with respect to the amount of MNP. This linearity is maintained even at very high magnetic fields (>2T). Furthermore, since the sensor fabrication is compatible with CMOS processing, these techniques are more convenient for easy integration and mass manufacturing.

Magnetoresistance based sensors

Magnetoresistance (MR) was first reported in 1857 by William Thomson [87]. When a magnetic field is applied to a material, its electrical resistance changes, thus the MR effect. At first, this change did account for just 0.033% [87], [78]. This effect was used over a century later for designing magnetic field sensors. This is due to the progress of modern microelectronics and thin-film technology that allowed to obtain more important change in resistance. Now, it is one of the main widely used magnetic detection method.

The basic principle of operation is as follows; the application of a magnetic field to a region that contains moving electrons will cause change in their trajectories due to Lorentz force. This change yields a change in effective resistance of the medium containing the electrons [76]. If the material layer is very thin, the change of resistance is considerable. The main figure of merit that allows comparison of different MR sensors is the MR ratio:

$$MR_{Ratio}\% = \frac{R_{H=H_{sat}} - R_{H=0}}{R_{H=0}} \cdot 100\%$$

It's the change of resistance divided by the minimum resistance. It indicates directly the maximum signal that can be obtained from the sensor. This effect was used to make recording tapes and disk recordings [88], [78]. MR based sensors are advantageous because they can detect very weak magnetic fields (nT) at room temperature.

MR sensors can be classified by effect into giant magnetoresistor sensors (GMR) and tunneling magnetoresistance sensors (TMR). GMR can further be divided to GMR multilayer sensors and spin valves sensors.

GMR multilayers are basically composed of a pair of ferromagnetic (FM) thin film layers separated by a non-magnetic conducting layer (Figure 1-20). In the absence of a magnetic field, the magnetic moments of the layers are antiparallel; this is done by careful design and fabrication of the nonmagnetic layer [76]. When we apply a magnetic field, the alignment becomes parallel and the electrical resistance of the multilayers decreases due to the reduction in the spin dependent electron scattering within the structure. Figure 1-20.b is an illustration of the change of resistance according to the applied external magnetic field (H_{ext}).

The other method that is based on GMR is the spin valve (SV) method. Here, tuning the coercivity (i.e. resistance to change of magnetization) of one of the ferromagnetic (FM) layer to a high value allows this change. The structure is composed of a pinned FM layer with a fixed alignment and a free FM layer that changes its alignment with the applied magnetic

field (

Figure 1-21.a). FM layers are separated by a conducting layer and the pinned FM layer alignment is fixed through the use of an antiferromagnetic layer (AF) [76].

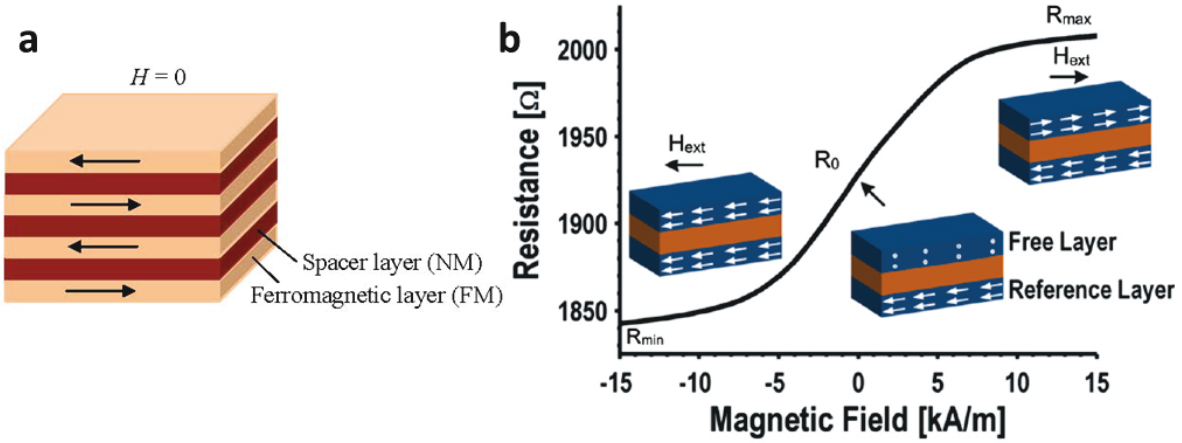

Figure 1-20: (a) Structure of a multilayer GMR sensor [76]. (b) Change of resistance relative to the external magnetic field [82].

We know that in a magnetic layer, the free electrons align their spins to the orientation of the magnetic field in the layer. The polarized electrons retain their spin as they move through the structure due to the potential that is applied. When the electrons encounter opposite magnetization, they need to flip spins to find an empty energy state in the new material thus requiring more energy. More effort to pass through the material means more resistance overall. The inverse also happens [76], [89]. Consequently, the final result is similar to that of the conventional GMRs.

Recently, a hybrid system was implemented that combines two chips, one containing an array of 256 GMR SV sensors, and the other was a processing CMOS based IC chip [90]. The device could monitor real time kinetics and detect concentrations of an ovarian cancer marker as low as 10 fM (

Figure 1-21.b).

Finally, one of the most sensitive MR sensor is a TMR sensor. It is based on the use of magnetic tunnel junction (MTJ) structure consisting of two ferromagnetic layers separated by a very thin insulating layer. It is based on a quantum mechanical phenomenon. Simply put, if the insulating layer is thin enough, the electrons can tunnel quantum-mechanically through the insulating layer. This tunneling is highly probable for parallel alignment, thus small resistance. For antiparallel alignment, the probability is much lower and thus it's like there is no current leading to high resistance. Based on this principle, MTJ function as switches between low and high states ([76], [89]). MTJ have a better sensitivity compared to other MR sensors and their MR ratio can be more than 50% ([91], [92]).

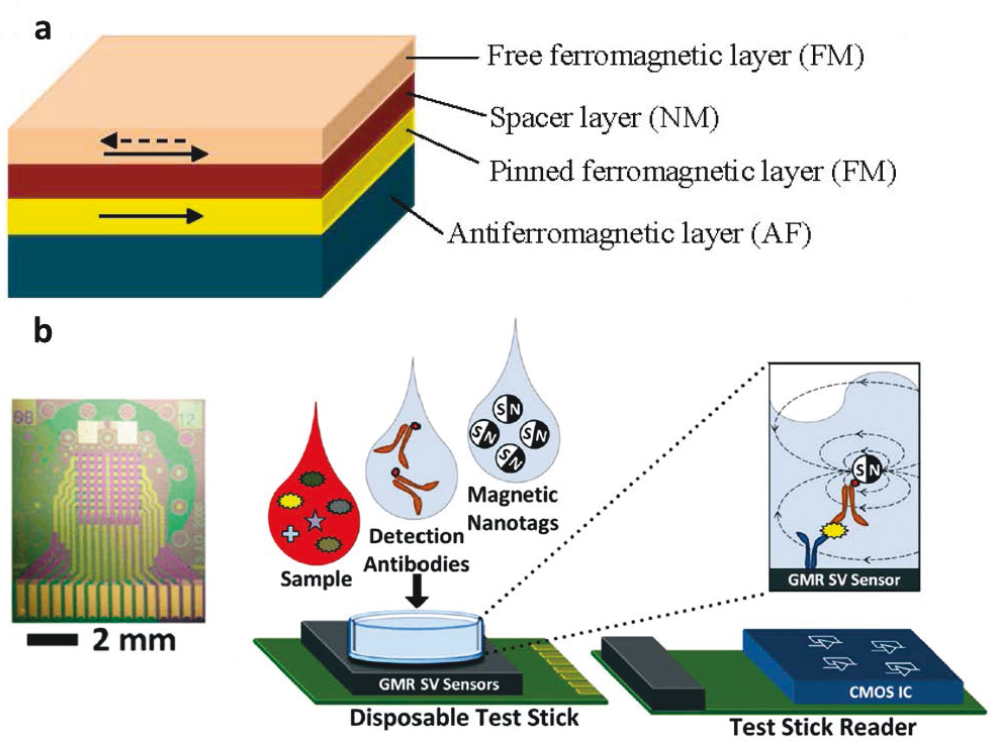

Figure 1-21: (a) basic structure of spin valve sensor [76]. (b) array of 256 GMR sensors (left) and schematic representation of the detection device (right) [90].

Diagnostic magnetic resonance methods (DMR)

Diagnostic magnetic resonance methods are techniques that use the magnetic resonance effect of MNP in order to detect them. This is an indirect detection since it detects the effect on the surrounding environment. The main principle is that the MNP are used to modulate the spin-spin relaxation time of neighboring water molecules [93]. Traditionally, this relaxation time is quantified using magnetic resonance imaging (MRI). However, new benchtop and miniaturized techniques emerged so that this principle can be used for LoC applications.

T2 relaxation is the process by which the transverse components of magnetization (M_{xy}) decay or dephase after application of a vertical magnetization field. The time "T_2" is the time required for 37% decay from its initial value. When the MNP are subjected to external magnetic field, they produce a large magnetic dipole. This dipole generates a magnetic field gradient that affects the relaxation time of neighboring water protons. This change is detected by either the NMR or MRI devices.

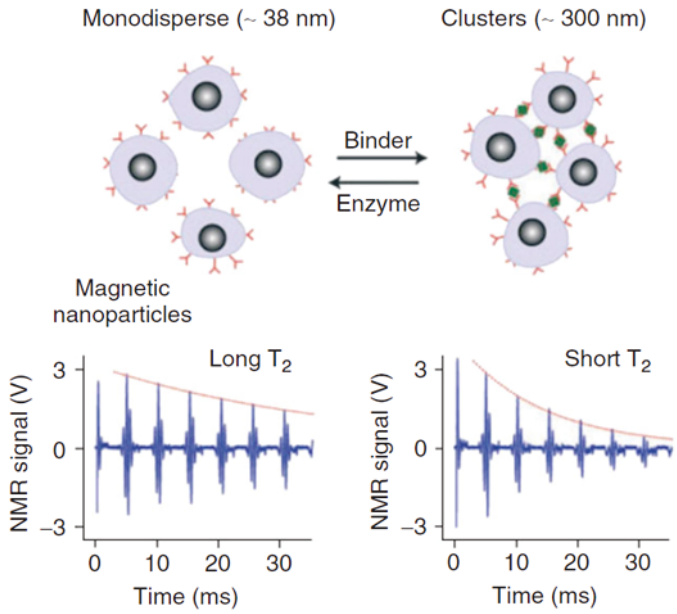

Figure 1-22: Magnetic Relaxation Switches (MRSws) assay illustration. (a) Typical assays involve the assembly of magnetic nanoparticle clusters using a target biomarker as a cross-linking bridge, or disassembly of preformed clusters using anenzyme or competitive binding. Clustering magnetic nanoparticles causes them to more efficiently dephase the nuclear spins of neighboring water molecules, shortening the transverse relaxation time (T_2). Likewise, disassembly of clusters increases T_2 relaxation time [94].

Moreover, when MNP are used in a way that they aggregate when they bind to the target analyte, the aggregate MNP cluster generates more important local inhomogeneity. This difference in impact (decreased T_2) is used to detect the amount of bound from unbound MNP and thus quantify the presence of analyte (Figure 1-22). This technique is termed “Magnetic Relaxation Switches” (MRSws) [84] and it is advantageous as it can be performed in volumetric configuration without being affected by nonspecific binding. Limits of detection are about "aM “range [78], [95]. MRSws can also work in a reversed way by monitoring the dispersion caused by enzymes or other biomolecules (Figure 1-22).

Early DMR systems were bulky and could not be used for point of care (PoC) applications. In this last decade, researchers miniaturized this detection scheme. An elegant solution was developed in [94]. A micro NMR system (µNMR) was developed to perform multiplexed magnetic resonance measurements in small sample volumes ($5 - 10\mu L$). The system consists of microcoils for both radio frequency excitation and NMR detection with accompanying electronics. Also, the strong required magnetic field was provided using a portable magnet that allowed enough homogeneity for the NMR detection. This was possible due to the small test area. Finally, a microfluidic chip was designed in order to mix and handle the reagents (Figure 1-23). The µNMR system could detect few bacteria withabout pM sensitivity being able to quantify a single mammalian cell [94].

The advantages of such a system are its relative sensitivity, multidetection possibility, easy handling, and homogeneous detection. The major drawback of NMR techniques is the drift of

the resonance frequency with temperature variations.

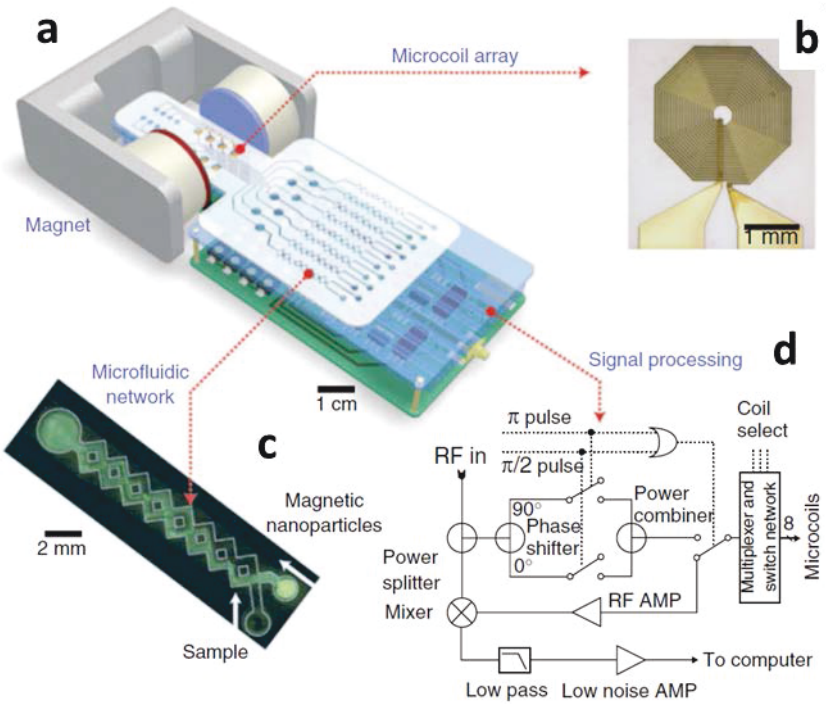

Figure 1-23: (a) Miniaturized NMR system including:an array of planar microcoils for NMR measurements, microfluidic networks for sample handling and mixing, miniaturized NMR electronics, and a portable magnet for polarizing magnetic field generation. (b) Planar microcoil. (c) Microfluidic mixing network. (d) Schematic of the NMR electronics [94].

1.3.3 Immunoassays

An immunoassay is a biochemical analysis technique that aims at measuring the presence or concentration of a specific analyte by means of using the reaction of the analyte (antigen) with an antibody. When these immunoanalytical reagents are mixed and incubated, the analyte is bound to the antibody, forming an immune complex.

The detected antigen that is referred to as the "Analyte", is by definition any substance that causes an immune system to produce antibodies against it. It can be a pathogen, a toxin, a metabolite, a cancer marker or other.

In the immunocomplex, antibodies (Abs) constitute the key component. They are proteins produced in animals and human bodies by immunological responses to the presence of antigens (Ags). Each Ab has a unique structure recognized by a corresponding Ag in a lock-and-key mechanism [96]. Antibodies can be generated by vaccinating animals with the analyte of interest. This process is described as immunization.

Immunoassays derive their unique specificity, sensitivity, and flexibility from three important properties of antibodies [97]:

1. Their ability to bind to an extremely wide range of natural and man-made chemicals, biomolecules, cells and viruses.

2. Exceptional specificity for the substance to which each antibody binds.

3. The strength of the binding between an antibody and its target.

These antibodies can be either polyclonal or monoclonal. However, for the majority of immunoassay applications, monoclonal antibodies are more advantageous than polyclonal ones. This is attributed to their higher degree of affinity and specificity towards the analyte [98] .

The principle of detection is shown in Figure 1-24. The immunocomplex is detected and quantified by adding a label to the antibody. Different types of labels can be used, we can cite radioisotopes (radioimmunoassays), enzymes (Enzyme immunoassays), fluorophores (Fluoroimmunoassay) and magnetic particles (magnetic immunoassays)...etc [98].

In order to detect the labels, the appropriate transduction mechanism should be used (see section 1.3.2).

Finally, the estimation of the analyte (antigen) concentration from the generated signal is usually done using a standard curve. This curve is obtained by measuring the signal of a series of appropriate dilutions of the measured sample analyte. The user can then estimate the unknown concentration of the analyte by referring to the curve. It has to be noted that, in commercial assay kits, dilution samples (calibrators) are given with the kit for the user to generate the calibration curvehimself [97].

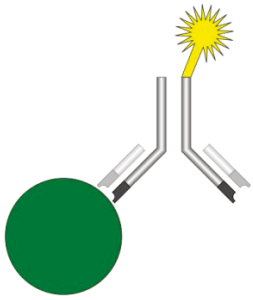

Figure 1-24: Basic components of an immunoassay: antigen (analyte) in green, antibody (grey) and label (yellow) [99].

Immunoassays are used for numerous applications. They allow the quantification and monitoring of small molecules, such as drugs and metabolites, large proteins, nucleic acids, and even whole pathogens [96]. Thus, they have been used in medical diagnosis, food safety, environmental monitoring, pharmaceutical analysis [98].

The main advantages of immunoassays are simplicity, sensitivity, specificity, and high throughput [98]. Therefore, the immunoassays are unarguably the most extensively utilized quantitative pathogen detection platform.

1.3.3.1 Classification of immunoassay methods

Immunoassays can be classified by two patterns: the assay format homogeneity, i.e. solid or liquid phase assays, and the competitive aspect of the assay procedure (competition or non between labeled reagents).

In **competitive** assays, the analyte (antigen from sample) competes in proportion to its concentration with labeled analyte for a limited number of antibody binding sites (Figure 1-25.a). As the amount of unlabeled antigens in a sample increases, the amount of labeled antigens bound to the Abs decreases, resulting in a decrease in the detection signal of the "Ab-bound Ag" complex. Thus, the generated signal is inversely dependent to the antigen concentration. Sometimes, if the labeled free (unbound) Ags are the ones to be detected, an increase in the signal related to the concentration of the measured antigen is expected.

This mode is particularly important for small antigens with limited numbers of epitopes (analyte's binding sites). The weight of these antigens is usually less than 1000 Da (Dalton).

For larger analytes, the **noncompetitive** assay format is preferred. These are also referred to as "sandwich" immunoassays (Figure 1-25.b). In this case, antibodies immobilized onto a surface (such as a well in a microtiter® plate) capture the test analyte from the sample. Besides a different antibody (secondary), specific for another part of the analyte molecule, is used as the basis of the signal generation system. This antibody is "labeled," e.g., with a fluorescent isotope. After an incubation step, the "sandwich" immunocomplex is formed [100]. Afterwards, unbound labeled antibodies are washed away. The final stage of the assay involves measurement of the level of signal, which is fluorescence in this example [97].

Contrary to competitive assays, the signal level in this type of assay is increasing with the analyte concentration in the sample.

From the sandwich complex, we can deduce that for the assay to be successful, the analyte should have at least two binding regions (recognition epitopes). That is why this assay format is only possible with large enough analytes ($> 1000\ Da$).

Alternatively, the fixed component could be the antigen instead of the analyte. This is used for example to detect previous exposure to a specific infectious disease [97]. The labeled secondary antibody that is raised in animals against the constant region of human antibodies can be used [97].

Immunoassays can also be divided into **heterogeneous and homogeneous** format assays.

In **heterogeneous** format, the antibody (or antigen) that plays the role of a "bait" is immobilized on a solid substrate (support). When coupled with sandwich format assay, the advantage of this technique is the good specificity obtained due to two separate recognition steps provided by the two antibodies that are generally selected to recognize two different epitopes on the antigen. This is usually the preferred assay format (heterogeneous sandwich assay) when the application demands the highest degree of sensitivity and selectivity. Also, this solid phase assay allows to easily remove unbound antibodies and antigens through washing with high enough flow rate. However, this format has some limitations; for example, the assay format depends heavily on the surface area/volume ratio and thus the test is limited by the number of binding sites. In addition, this test requires the addition of an immobilization and a washing step into the fabrication and assay procedures respectively. This immobilization step should be designed carefully in order to avoid nonspecific bindings into the solid phase.

Opposite to heterogeneous assays, there is the **homogeneous** format, where the conjugation takes place in the solution phase (Figure 1-25.c). In this case, the bound and unbound antibodies are discriminated based on physical [101], [102] or chemical [103] changes arising from the binding event [100]. They are commonly used for detecting therapeutic drugs that have a relatively high concentration in blood. The advantages here are that the assay is very simple, doesn't involve any immobilization or washing step and there is no issue of non-specific binding. These assays also take advantage of the multiplexing and very fast electrophoretic separation made possible by the microchip format [98]. However, these assays are more effective in partially purified samples, since matrices such as blood, environmental water samples and food can contain interferences that reduce the sensitivity of the assay. Thus, extensive preconcentration steps are usually required. These assays have generally poorer detection limits and selectivity than heterogeneous assays.

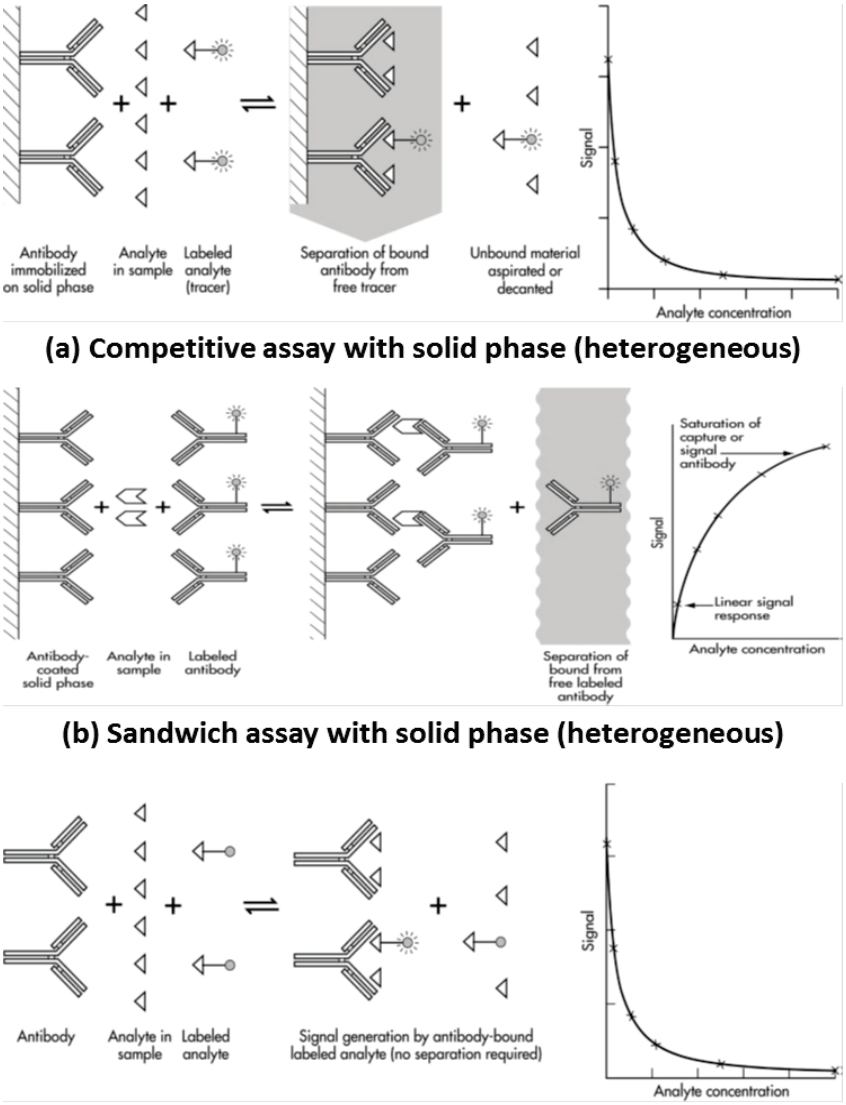

Figure 1-25: Classification of immunoassays [97].

1.3.3.2 Typical example: ELISA (enzyme-linked immunosorbent assay)

The most common enzyme based pathogen sensing system is the enzyme-linked immunosorbent assay (ELISA) which combines the advantages of enzymes and antibodies. It has become a standard fundamental immunoassay technique.

The starting material for an enzyme-catalyzed reaction is called a substrate. Enzyme labels, with the appropriate substrate, can be used to generate a color, or to create fluorescent or other end products (e.g. luminescence). This later can be measured by optical and electronic equipment [97]. Figure 1-26 shows the standard process. Enzymes have an amplification property so that a single one of them can convert many molecules of substrate. This property allows having a sensitive signal generation system [98].

There are several different ELISA types, including direct, competitive, and sandwich formats.

The sandwich ELISA will likely be one of the most immunoassay platforms employed on-chip. This is due to its good sensitivity and specificity traits, along with favorable kinetics [9].

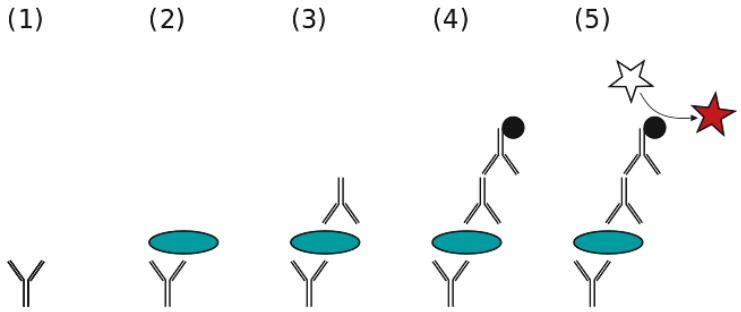

Figure 1-26: (1) Plate is coated with a capture antibody; (2) sample is added, and any antigen present binds to capture antibody; (3) detecting antibody is added, and binds to antigen; (4) enzyme-linked secondary antibody is added, and binds to detecting antibody; (5) substrate is added, and is converted by enzyme to detectable form (color, fluorescence).

ELISA is performed on a multi-well plate and it is static, which means that transport of the target molecule to the surface-coated molecule is only done by means of diffusion. This process is being both labor and time consuming, with assay times ranging from at least a few hours to a few days. These drawbacks led to the development of microfluidic (Lab-On-Chip) based ELISA methods.

The wells are replaced with a microchannel where the target solution continuously flows through the microchannel. The antibodies are immobilized onto the inner surface, at a specific location of a microchannel (Figure 1-27). The continuous flow‘s characteristics make the rinsing very effective. In fact, the flow itself should remove any excess molecules from the inner surface of a microchannel without the need of any stirring. If fluorescent label are used [20], light is irradiated to the location where the antibodies are immobilized. Then a light sensor reads the signal from the other side of a microchannel (Figure 1-27).

Guan et al. [104] demonstrated the use of ELISA with a microfluidic platform in order to detect E.coli O157:H7 using a bioluminescence detection method. Their limit of detection (LOD) was close to ELISA with a value of $3.2 \cdot 10^1\ CFU/mL$ and an assay time of 20 min.

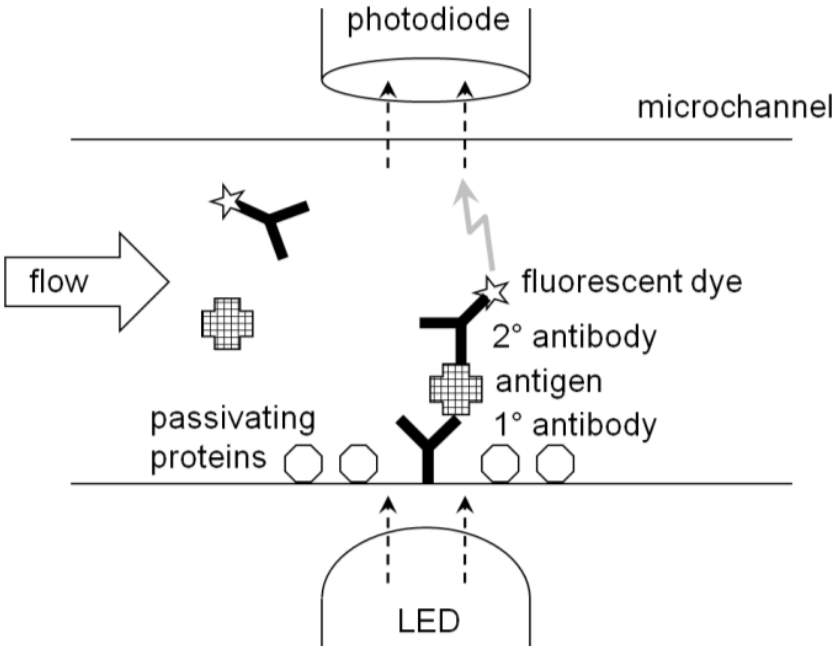

Figure 1-27: Lab-On-Chip ELISA with fluorescent detection [20].

1.4 Lab-On-Chip (LoC) systems

A lab on chip (LoC) system is a device that embeds several laboratory functions onto a small platform. The size of the platform does not exceed a few centimeters in general. Because of this miniaturization, the LoC system usually involves the handling of very small volumes of fluids, thus microfluidics play a key role in the design, improvement and fabrication of such systems [20]. Research on microfluidic systems involves the study of the behavior, manipulation and control of small volumes of liquid in small scale channels (sub-millimeter).

LoC development and improvement is driven by two main factors: technological advances in fabrication push the limits of different types of devices which can be created and the ever-increasing demand for sensitive, efficient, automated, and fast analytical systems [12], [105], [106].

The potential advantages and disadvantages of such devices are:

Advantages:

- Ease of use.
- Decreased analysis time due to reduced diffusion distances [12].
- Low sample and reagent consumption
- High reproducibility due to standardization and automation.
- Portability of complete integrated device including all analytical steps.
- Possibility of simultaneous multi-analyte assays.
- Cost reduction.
- Possible disposable of the entire system.

- Possibility for extra laboratory applications (Point Of Care or self-tests) removing the need of professional manipulation.

Disadvantages:

- Non-representative sampling.
- Possible sensitivity limitation compared to laboratory performance.
- Human interface prone to more errors.
- Possibly higher cost per test.

The fabrication of such small devices that include all these aspects is very challenging and requires multidisciplinary technical expertise in several areas.

The next sections describe the requirements of an ideal LoC system, the constituent parts and important aspects of typical LoC devices with their corresponding challenges, as well as a comparison of some LoC pathogen sensing methods.

1.4.1 Ideal LoC system requirements

Typical Lab-on-Chip systems should have these fundamental functionalities:

- Sample handling and pretreatment.
- Fluid actuation.
- Mixing and incubation.
- Detection of one or multiple analytes.

From these set of functional aspects, we can derive ideal requirements that any LoC system development should aim at providing [20]:

1. Automated liquid handling (mixing, transport, and separation if necessary).
2. Minimal sample pre-treatment.
3. Fast analysis time.
4. Fully integrated miniaturized system.
5. Battery-powered.
6. No required storage (refrigerator).
7. Very sensitive.
8. High precision and reproducibility (minimal intra- and inter-assay variation).
9. Specific detection (low false positives and good discrimination between different analytes).
10. High volume - low cost manufacturing possibility.
11. Low cost per test.
12. Multiple analyte detection possibility.

To this date, no system includes all of the mentioned specifications. Each of the developed LoC systems and ongoing research work aims at improving one or more of these aspects.

1.4.2 Components of LoC systems and challenges

The proposed ideal Lab-on-Chip device aimed at pathogen sensing is illustrated in the following schematic figure with its main components [97]. All these components are necessary for the aforementioned functionalities. The most important aspects being; material

choice, fabrication method, microfluidic design, bioreceptor immobilization strategy and appropriate detection method and format (homogeneous, heterogeneous…etc.).

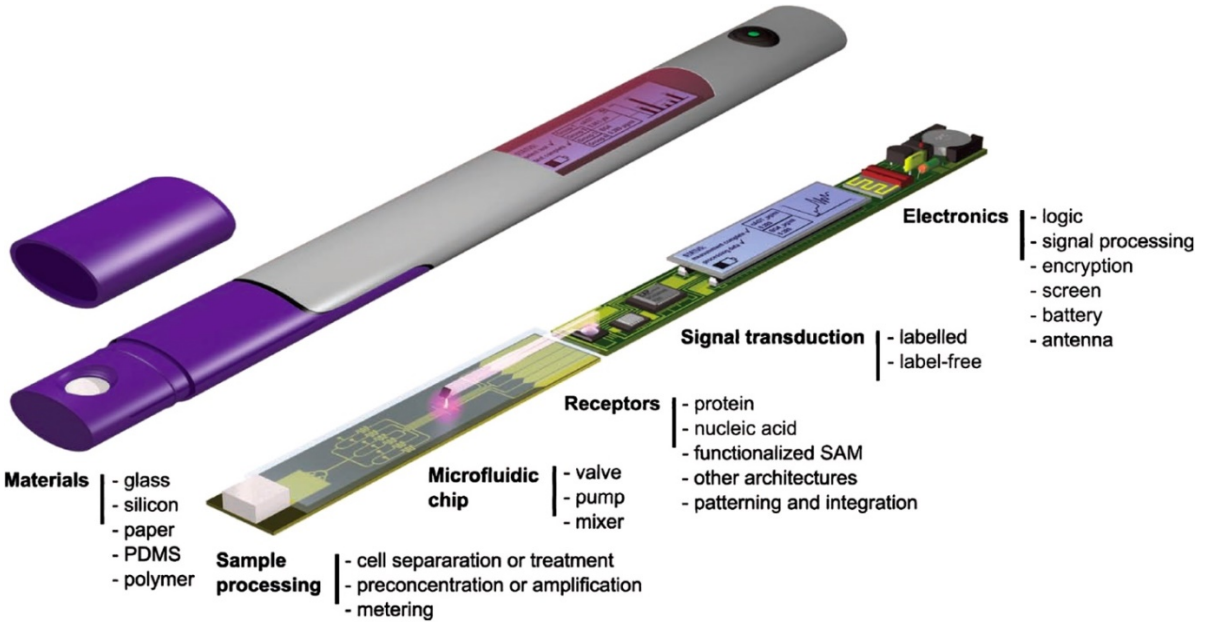

Figure 1-28: Schematic components of an idea LoC diagnostic system [97]

1.4.2.1 Materials

Along with practical considerations for fabrication, the materials used for microfluidic surfaces are of high importance due to the large surface area to volume ratio. The surface is then exploited for immobilization of various molecules.

The vast majority of systems are constructed out of glass, silica or polymers [12]. It has to be noted that other materials, like paper, constitute cheap alternatives.

Glass substrates have outstanding optical properties throughout the visible spectrum, and can be used to transport fluids electrokinetically. In addition, washing of the microfluidic glass with acids and other strong solutions is made possible due to its highly resistant characteristic. Also, a vast majority of clean room fabrication techniques are adapted to be used with glass, such as etching, electrodeposition and metal deposition. These properties allow the use of glass along with a variety of detection and actuation techniques, such as electrochemical, optical detection and electrophoresis. However, glass-based techniques have some important drawbacks; they are more fragile than other substrates (silicon), their fabrication and prototyping is confined to clean rooms and is thus expensive and difficult to access. They are also incompatible with CMOS technologies.

Along with glass, **silicon** is the most used material for microfabrication. It is mechanically stronger than glass and allows the fabrication of nanometer scale features. Moreover, as with glass, its surface has been studied extensively in order to immobilize biomolecules (e.g. antibodies). This is a key property that impacts directly the performance of the sensing method. However, silicon has conductive properties that prevent it from being used along

with electrophoresis or other electrode based techniques. Additionally, silicon is not optically transparent in the wavelength range of optical detection techniques.

Regarding immobilization features, different solutions exist, such as adding a silanization step [107]. Like for the glass, fabrication depends on clean room apparatus, therefore automatization and high reproducibility of silicon-based systems may become difficult.

With the increasing demand for better material solutions, researchers switched their interest from glass and silicon to biocompatible polymers. There are many possible polymers with interesting properties that include optical, surface and mechanical characteristics as well as solvent resistance [108], [109]. These polymers and plastic materials are simple to fabricate, inexpensive and also can be mass produced. The main drawback (especially for PDMS) is that reagents may adsorb nonspecifically to the surface of the polymer, leading to a reduced performance of the LoC device [110]. Nonetheless, many techniques have been devised in order to change the surface chemistry of the polymers [107].

The most commonly used polymer for prototyping is PDMS (polydimethylsiloxane). PDMS is a transparent, elastomeric polymer that can be fabricated with features of sub-μm scale. Furthermore, this fabrication process can be done under normal conditions. The subsequent PDMS structure can be sealed to other hard materials like glass by means of plasma treatment. Like other polymers, PDMS has a hydrophobic surface, thus it allows biomolecules to adsorb to its surface, and encourages the formation of bubbles due to its poor wettability. Fortunately, as can be seen later in section 0, extensive research has been done in order to change the PDMS surface chemistry in order to prevent or reduce these undesired effects.

Finally, compared to other polymers, PDMS is not very durable and cannot be mass produced. Thus, it is only convenient for prototyping. For more durable materials, polystyrene, polymethyl methacrylate (PMMA) and polycarbonate (PC) constitute better choices [96].

A summary of the three major materials properties is given in Table 1-1 [96].

Table 1-1 Comparison of the properties of main materials used for micorfluidic structures [96].

	Silicon	**Glass**	**Polymers**
Thermal conductivity	Good	Good	Poor
Endurance to high temperatures	Good	Good	Poor
Optical transparency	No	Yes	Yes
Electrical conductivity	Yes	No	No
Cost	High	Medium	Low
Mass production	Yes	Yes	Yes to some

1.4.2.2 Fabrication methods

Concerning the fabrication methods, there was a transition between conventional integrated circuits (ICs) and silicon based MEMs processes to more glass and/or polymer based processes. Conventional methods included photolithography, thin film metallization and chemical etching [18]. This transition is driven by the fact that polymers are in sum more advantageous to glass and silicon based devices. Nevertheless, glass has remained interesting due to its biocompatibility and surface properties. A compromise is the use of a mixed microfluidic structure including glass on one side and a polymer on the other. Along with polymer-only devices, these devices yield low fabrication cost, high volume production capability, good reproducibility and versatility in design for a wide spectrum of specific applications.

Polymer-based microfluidic fabrication methods can be divided, according to the application, into two main categories: prototyping and direct fabrication methods.

Prototyping methods are cheaper and are widely used for both research and commercial production. Prototyping involves the use of a master mold made from glass, silicon, metals, photoresists, or other. This master is then used to transfer a specific pattern to the polymer (Figure 1-29).

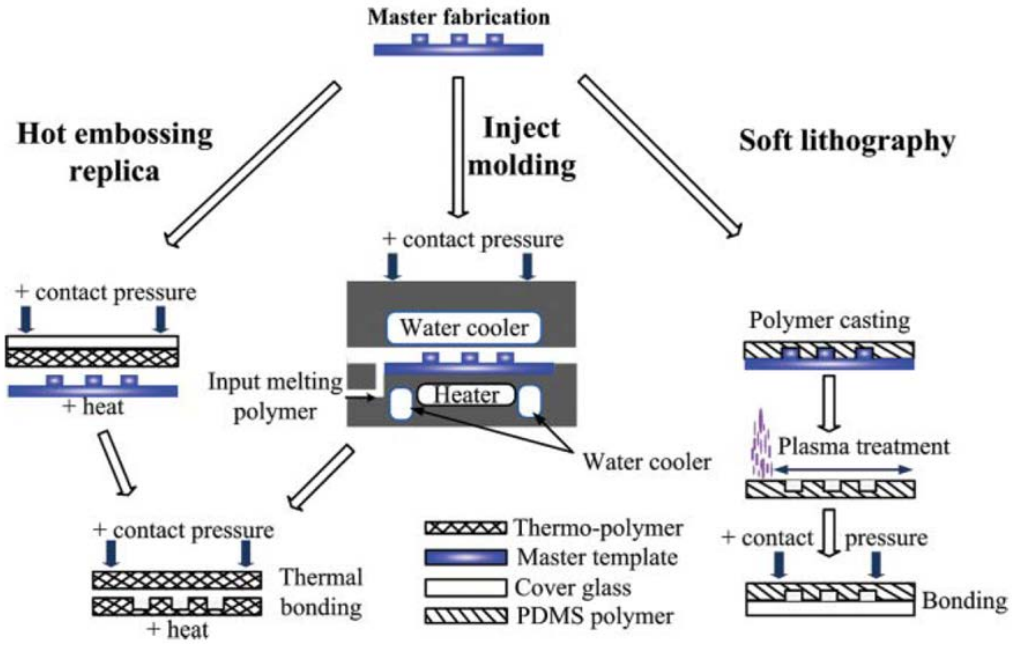

Figure 1-29: Typical fabrication procedures for the prototyping techniques [18].

Three main prototyping techniques exist and are represented in Figure 1-29. First, soft lithography (casting) is the easiest, cheapest and mostly used technique in the academic world and involves the pouring of the polymer over the master mold, curing and peeling the replicate. The main drawback is that this technique cannot be used for mass production. Hot embossing is the second simple procedure which involves polymer heating a little above its

glass transition temperature (from hard to soft rubbery material), then applying it to the master with contact pressure under vacuum conditions. Although this process is quick and inexpensive, it cannot be fully automated [61]. For commercial mass production, there is a third well-knowns technique called injection molding. In this technique, heated polymer small particles (pellets) are injected at high pressure into the mold for replication. This process is quick and can produce high volumes but is not convenient for academic purposes.

For more versatility and choice of customization, direct fabrication techniques are preferred (Figure 1-30). These techniques are more expensive but offer also more choice of fabrication patterns [61]. They can be further divided into three techniques: laser photoablation, photolithography and x-ray lithography. Photolithography and x-ray lithography work in basically the same way. The main difference is that the former uses UV light and the latter uses an x-ray exposure. This results in better resolution but higher cost for x-ray exposure. On the other hand, laser photoablation works by using a pulsed laser to remove polymer fragments to form clean cut surface (see Figure 1-30). However, the laser may induce unwanted surface modifications [61].

To conclude, Table -2 reproduced partly from [18], presents the key advantages and disadvantages of the fabrication procedures. Ultimately, the choice of the method depends on the required resolution, the choice of the polymer and on the desired application.

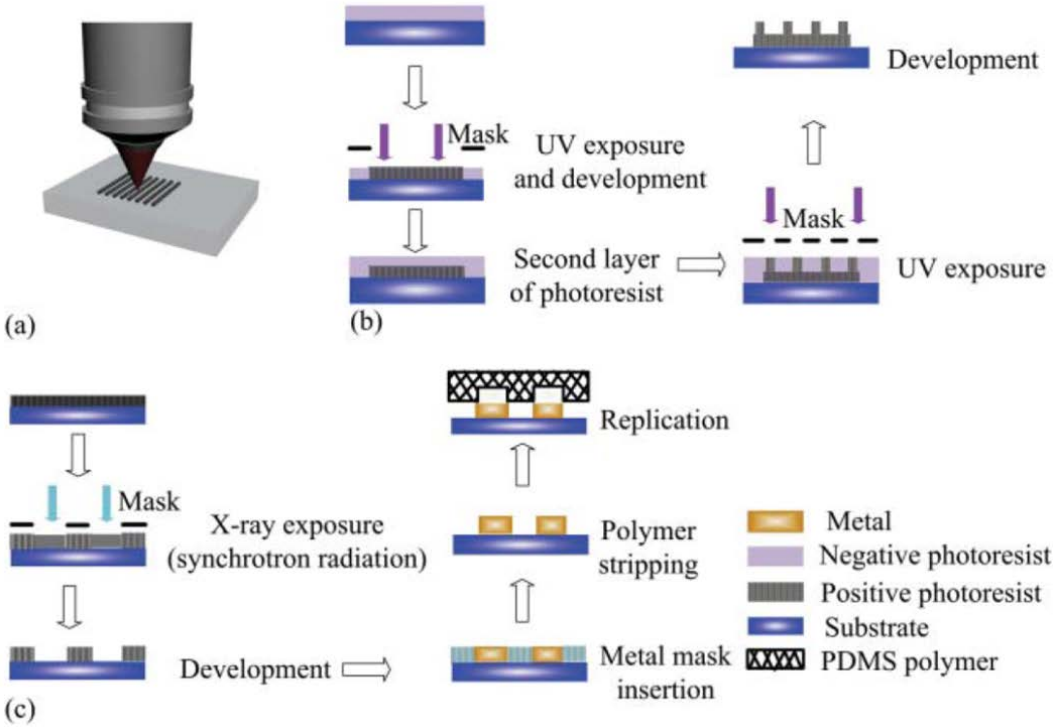

Figure 1-30: Main direct fabrication techniques: (a) laser photoablation, (b) photolitography and (c) x-ray lithography [18].

Table 1-2: Microfluidic fabrication techniques with information partially extracted from [18].

Fabrication technique	Advantages	Disadvantages	Ref.
Soft lithography	Cost effective, 3D geometries possible, high resolution	Pattern deformation, vulnerable to defect, cannot be mass produced	[111]
Hot embossing	Cost effective, precise, fast, semi-automated mass production	Restricted to thermoplastics, not suited for 3D structures, not fully automated for mass production	[112]
Injection molding	Easy to use, 3D structures possible, mass production, fully automated	Thermoplastics only, high cost mold, issues with large geometries	[113]
Photolithography	High wafer throughput, well controlled technique for microscale structures	Requires flat surface, needs chemical post treatment	[114]
X-ray lithography	Very high resolution (nm), produces straight smooth walls	Difficult for master fabrication, time consuming, high cost	[115]
Laser photoablation	Rapid, large format production	Multiple treatment sessions, limited range of possible materials, unwanted surface modifications	[116]

1.4.2.3 Microfluidic design

A strategy must be elaborated in order to interface the macroscale laboratory procedures to the microscale world of LoC devices. In sensitive detection systems, the fluid handling must be done with appropriate care. The issues like bubbles formation must be prevented as they can negatively affect or block sample flow, resulting in poor detection properties. Since it is a key aspect of LoC devices, extensive research has been done for fluid handling.

Fluid handling can be done primarily using three main components: pumps, mixers and valves. These components can be controlled by one of the three major fluid handling forces: electric, pressure and passive forces. Other emerging techniques include piezoelectric [117] and thermopneumatic [118] based approaches. General objectives of fluid control systems include precision, automation, ease of fabrication, low power consumption and low dead volume.

Electrical fluid handling:

Electrical fluid handling methods can be categorized in two main techniques; electrokinetic and electrowetting force techniques. In electrokinetics, the flow is generated by either electrophoretic or electroosmotic interactions due to an applied field and the presence of ionic species in the controlled fluid [100]. Basically, in electrophoresis, charged molecules move by means of electrostatic forces. Electroosmosic flow, on the other hand, results from the longitudinal electrical field applied along the solution double layer [119]. For example with silicon, cations built along the wall of the substrate (silicon) because of the natural negatively

charged surface, creat the “double layer”. When applying an electrical field along the flow, the bulk positively charged double layer moves with the solution.

Electrokinetic techniques could be applied for fluid transport, separation and sample stacking [100]. The advantage of such techniques is a better reaction kinetics as compared to pressure-based techniques. The main drawback is the requirement for specific buffers and reagents, thus limiting its use with fluids like blood and urine.

Electrowetting force or more generally digital microfluidics (DMF) allows the control of droplets instead of a continuous fluid [120]. Here, AC and DC electric potentials are applied to an array of electrodes in order to split, move, merge and dispense the droplets by means of electrostatic and dielectrophoresic forces (Figure 1-31).

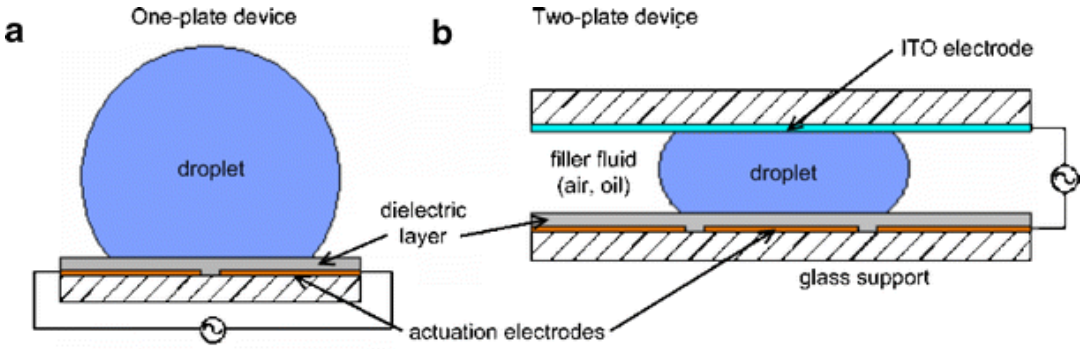

Figure 1-31: Digital microfluidic devices. (a) single-plate format: Both ground and actuation electrodes are in the same plate (droplets move in the plane of the page). (b) Two-plate format, the top plate is used as a ground plate. It allows two-dimensional, reconfigurable movement of the droplet [120].

Pressure driven fluid actuation

This is the most popular fluid handling technique. It is widely used in immunoassays and other well-known pathogen detection techniques. A pressure driven flow can be created with either: (1) a vacuum pump by applying vacuum at the outlet and opening the inlet to the atmosphere or the inverse (2) that consists in a positive pressure application at the inlet and an atmospheric pressure at the outlet. Other inventive techniques include chemical reactions and thumb actuation means of flow control ([121], [122]). The main advantage here is the compatibility with almost all the materials and solvent compositions. However, the parabolic flow profile induces sample plug dispersion and peak broadening which leads to poor separation abilities [100]. Two main categories of pressure driven flow are cited in the literature ([123], [124]) because of their attractivity and wide use; pneumatic valves and centrifugal based microfluidics.

Integrated pneumatic valves are very popular due to their integration and ease of automation. A good example is shown in Figure 1-32. Here, the micro pneumatic pump is composed of a flexible PDMS membrane, a liquid flow microchannel and an air chamber. The later allows deflecting the membrane by introduction of compressed air. This resulting peristaltic effect can be driven by sequencing of several PDMS membranes that allow the fluid to be moved in

one direction, forming a micropump. Also, a mixing component can be formed by placing several pneumatic valves in a circular loop [125]. Consequently, valves, mixers and pumps can be integrated by this simple technology. A more complete experiment allowed the detection of clenbuterol, a substance used to treat people with asthma and other breathing disorders [123]. The researchers included the entire fluid control component in the microfluidic chip using a multilayers system of channel layer, PDMS membrane and a pneumatic layers (Figure 1-32).

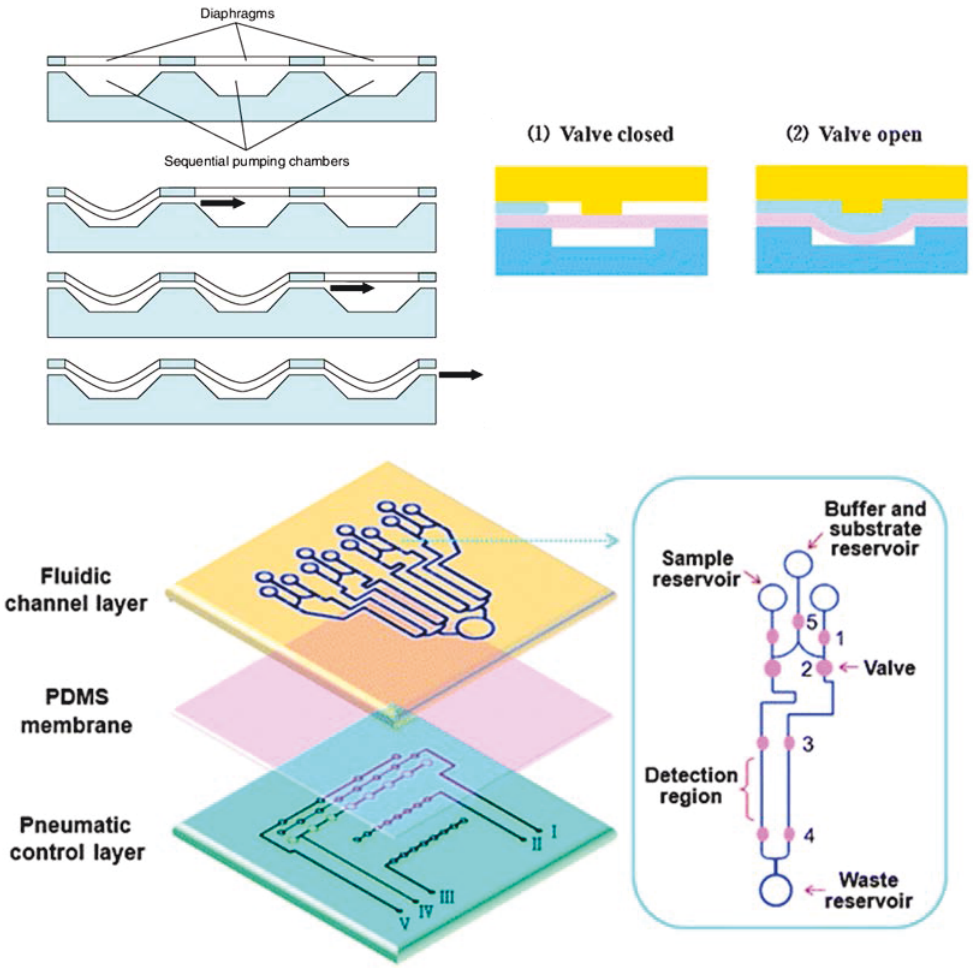

Figure 1-32: (Top) Structure and operation of a peristaltic micropump and valves [126]. (Bottom) Schematic of pneumatic driven integrated microfluidic device for surface based immunoassays [123].

Centrifugal force handling is a promising alternative to pneumatic systems. These systems have been mainly applied with compact discs shaped microfluidics (CDs) and a rotation system causing the centrifugal force. Fluid movement is related to the spin velocity, and the control of the fluid movement's directions is done either by hydrophobic or capillary valves. Indeed, when the disc spins at a certain velocity, the centrifugal force overcomes the capillary or surface forces of these valves. Consequently, the fluid flows from the center of the disc outwards [100]. Centrifugal based microfluidic systems can perform valving, sample splitting, mixing, calibration, decanting and blood separation [124], [127]. This way, CD based ELISA could be implemented where all the steps are performed as in a traditional ELISA procedure

(Figure 1-33).

Centrifugal force technique is also not sensitive to pH, chemical compositions or other factors that otherwise impact electrical handling systems.

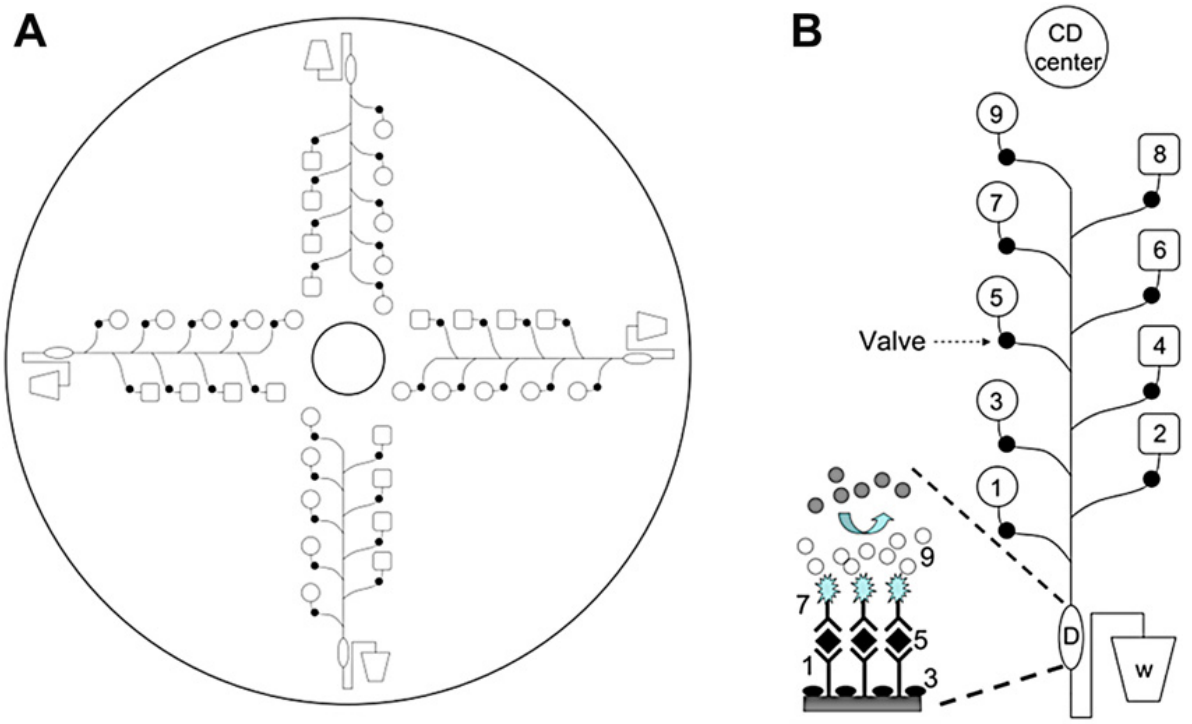

Figure 1-33: Schematic description of ELISA in a lab-on-a-CD. (a) CD-ELISA design with 4 arrays. (b) Description of a single assay. Washing buffers are loaded in 2, 4, 6 and 8, whereas chambers W, D, 1, 3, 5, 7, 9 are used for waste, detection, first antibody, blocking solution, sample, second antibody and substrate respectively. The rotation of the CD allows the solutions in all 9 chambers to flow out in sequential manner to accomplish the ELISA procedure. This sequential flow is due to the decreasing centrifugal force [96].

Passive fluid actuation

This approach is privileged while seeking the benefits of low power consumption, completely integrated system and low dead volume. Passive fluid handling is mainly done through the use of capillary forces. A very interesting example was developed by Gervais et al. [128]. Capillary forces were used to develop a one step, simple to use microfluidic immunoassay. The chip is composed of a sample collector, delay valves, flow resistors, a detection antibody deposition zone, a reaction chamber with the immobilized capture antibody and a capillary pump (Figure 1-34). The complex structure of the capillary pump, sample collector, delay valves and flow resistors influence the flow rate that is directly correlated to the total capillary pressure and flow resistance [129]. Additionally, the blood filter membrane allows reducing the inferences from red and white blood cells and letting only plasma flow through the capillaries. The flow resistor allows having enough time for the binding of detection Abs with the antigen. It is also used to store overflow quantities of detection antibodies (dAbs)

immobilized in the deposition zone and to prevent them from reaching the serum collector or the reaction chamber. As with lateral flow assays, there is a control and detection chamber that allow to validate the assay. This structure was able to detect C-reactive protein with a limit of detection of 10 ng/mL in a few minutes (3 mn). Finally, previously mentioned lateral flow devices also use capillary forces to produce qualitative or semi quantitative results (see section 0).

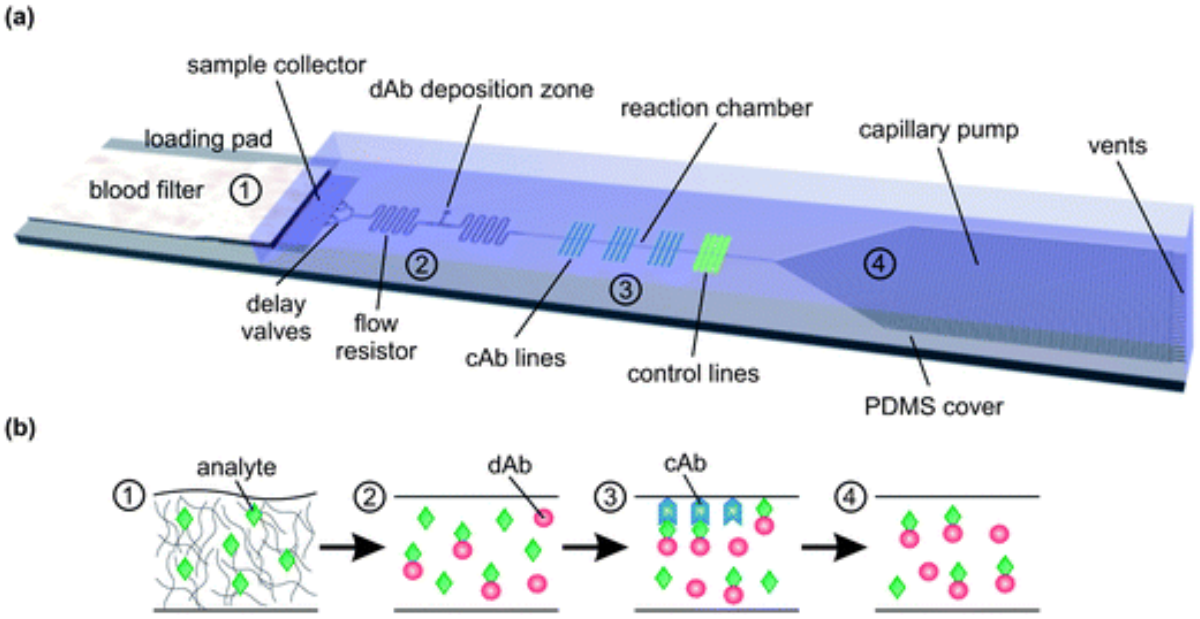

Figure 1-34: Concept of a capillary-driven microfluidic chip for one step immunoassays. (a) The ship is composed of various functional microfluidic elements for performing immunoassays. (b) The position and interaction between the analyte, dAbs and cAbs are illustrated along different parts of the chip. The PDMS is patterned with control lines including cAbs and antigens [128].

Comparison of major fluid handling strategies

The choice of the fluid handling strategy depends on the desired application and the most important resulting criteria. For example, when we consider choosing a type of valve, performance criteria include: size, dead volume, channel dimensions, actuation pressure, power consumption and scalability [130]. Most of these criteria apply to pumps too. When we want to design or choose a mixing system, we should consider: degree of mixing, fluid volume, ease of fabrication, power consumption and feasibility [61].

To conclude, a summary of the aforementioned handling strategies is depicted in Table 1-3. Important aspects like full integration possibility, flow rate and complexity of the assay should be considered.

Table 1-3: Comparison of different characteristics of microfluidic propulsion techniques [96], [124].

Mechanism /Criteria	Electroosmosis	Electrowetting	Micropumps	Centrifugal force	Capillary
Materials	Glass, Polymers	Glass, Polymers	Polymers	Polymers	Polymers, paper.
Flow rate /velocity	nL/s to µL/s	0.01 to 0.1 m/s	10 nL/s to 10 µL/s	nL/s to 10 µL/s	nL/s
External power source	Electrical voltage	Electrical voltage	Air pump or battery	Rotary motor	Not necessary
Valve integration	Yes	No, liquid stopped by removing applied voltage	Yes	Yes	Yes
Influence on flow	pH, ionic strength	pH, ionic strength	Nothing particular	Viscosity, density	Capillary pressure, flow resistance
Additional remarks	Cannot use blood or urine. Can handle complex procedures	Droplets, not continuous fluid handling. Better for separation. Complex procedure.	Preferred for sequential procedure. Not good for separation.	Allow multiplexing, easy but not fully embedded.	Adequate for simple sequential procedures only.
Ref.	[119], [131]	[132]	[133]	[124]	[134]

1.5 Comparison of LoC pathogen sensing methods

1.5.1 Criteria of comparison

In the last section of this chapter, we review the most common detection schemes. In this section, the aim is to have a comparative table that sums up all the advantages and challenges/disadvantages of the mentioned techniques. For this, we should first define the most important comparison criteria for LoC detection systems. They serve for comparison, reference and optimization of the developed structure.

From various reviews ([18], [19]), we define the following criteria:

1. **Sensitivity:** When assessing the detection part of a LoC system, sensitivity is the primary and most important feature. It is the main performance that all researchers seek to optimize. However, most papers only give the sensitivity without reporting the statistical data. Many conventional sensitivity variables are defined in the literature. Of them, we can cite the limit of detection (LOD),the limit of quantification (LOQ) and the functional sensitivity.
   a. LOD is the lowest analyte concentration likely to be reliably distinguished from the limit of blank (LOB) and at which detection is feasible. LOB is defined in [97] as the highest apparent analyte concentration expected to be found when replicates of a blank sample containing no analyte are tested. It is the most frequently reported value, especially by exploratory research articles. However, it is often estimated from a low number of assays and is used to assess the performance of a new system. Furthermore, the chosen assay (bioreceptor, incubation times…etc.) strongly influences the LOD and therefore direct comparison between techniques is not accurate.
   b. LOQ, on the other hand is often used for medical assessment and it is the lowest analyte concentration that can be quantified with a certain precision (less than 30%) and bias requirements. The test is more rigorous that for LOD determination and is thus more trusted for final validation of medical diagnostic systems. LOQ can be almost equal to the LOD if the response curve is linear.
   c. Functional sensitivity is similar to the LOQ. It is determined from the imprecision of very low concentration samples, either within or between assays [97]. The concentration that has a coefficient of variation (CV) of less than 20 % is usually defined as the functional sensitivity.
2. **Specificity:** It describes the ability of a bioreceptor to produce a measurable response only for the analyte of interest. Cross-reactivity is a measurement of bioreceptor response to substances other than the analyte. Measurement of specificity are often done when evaluating chosen antibodies for immunoassays. Polyclonal antibodies, for example, are known for poor specificity.
3. **Precision:** It describes the repeatability of an analytical technique. Its inverse is imprecision; it is an estimate of the error in an analytical technique, expressed as the percent coefficient of variation (%CV) or, less often, as the standard deviation (SD) at a particular analyte level.

4. **Accuracy:** It can be defined by the closeness of the average measured value and the true value. The difference between these two values is called **bias** and represents the degree of inaccuracy [97].
5. **Cost:** Depending on the end application, the cost of the system and of each test can be the deciding factor.
6. **Linearity:** It is the ability of the assay to return values that are directly proportional to the concentration of the target pathogen or analyte in the sample. For some cases, the nonlinear response of the signal to the analyte concentration makes the subsequent retrieval of the accurate analyte concentration very difficult.
7. **Dynamic range:** It is the detectable range of concentrations of analyte between the low and high limits of quantification. Within the assay range, linearity, accuracy and precision are all within the acceptable defined values.
8. **Complexity of system:** The less complex the system is, the easier it usually is for mass production, to assess and to optimize.
9. **Number of steps:** Reducing the required steps to one initial step is the aim of LoC systems. It will allow self-testing to be possible and can even reduce potential errors that cumulate with each step due to manipulation errors.
10. **Time to result:** It is the time from the beginning of the measurement until the result is displayed.
11. **Portability and integration:** The goal here is to see if the detection method can be fully embedded in a portable LoC platform. This means that all the components for signal detection and conditioning should be miniaturized.

1.5.2 Comparison table

Almost all research article provide some but not all of the before mentioned criteria. It's due to the fact that doing the required experiments in order to have all these data is very time consuming and not necessary for early stage development. Full characterization of diagnostic systems is only done for commercial or near to commercialization products.

The Table 1-4 presents most of mentioned detection techniques with comments relative to these criteria. It has to be noted that the mentioned notes are only there to get an idea about the "usual" performance of the corresponding technique and are not representative of the best possible results that could be found in literature.

Table 1-4: Comparison of important characteristics for different pathogen sensing methods.

Method		Sensitivity	Dynamic Range	Assay time	Portability	Simplicity	Cost	Comments	Refs[2]
Optical ([18], [19]) [1]	Colorimetric (e.g LFA)	*	*	Rapid (minutes)	****	Very simple	$	Difficult for multiplexing. Must use preconcentration step for quantitative measurements	[23], [21], [24]
	Fluorescence	*****	***	Rapid to long (10 mins to > hour)	*	Complex	$$$	Very versatile (allows observing activity of target). Multiplexing possible. Extensive research is done to integrate the method	[26], [27]
	Plasmonic (SPR and SEPR)	****	***	Relatively fast to slow (minutes-hours)	*	Complex	$$$	Multiplexing possible. Label free.	[135]
	Luminescence	***	***	Average time (> hour)	***	Simple	$$	Can be used to detect chemicals like heavy metals or for specific bacterial detection. Restricted detection to certain antigens.	[30], [32]
Electrochemical[1] [45], [47], [136]	Amperometry	***	***	Relatively rapid (dozens mins)	****	Simple	$	Sensitive to environment (pH) possible nonspecific binding. Need for reference electrode.	[49]
	Voltammetry	***	**	Real time monitoring	***	Moderate	$/$$	Need of reference electrode, better performance when miniaturized	[55]
	Conductometry	**	**	Rapid (minutes)	****	Simple	$/$$	Good coupling with electrophoresis actuation. Low power consumption. Issue of low specificity and low SNR.	[37]
	Impedance based (e.g IME)	**	NA	Moderate time	****	Moderate	$/$$	No need for reference electrode. Issues are nonspecific binding, reproducibility.	[54]

Comparison of important characteristics for different pathogen sensing methods **(continued)**

Method		Sensitivity	Dynamic Range	Assay time	Portability	Simplicity	Cost	Comments	Refs
Mechanical [62][1]	Microcantiliver	***	NM	> 10 mins	***	Moderate	$$	Can be label free, can be coupled with optical detection. Issue with striction, multiplexing is very difficult.	[65]
	QCM	***	NM	> 10 mins	***	Simple	$$	Can be label free, low power consumption. Can be used to validate immunosensors fabrication steps. Difficult multiplexing and need of dry environment.	[67], [68]
Magnetic [75][1]	Relaxation based	** to****	****	Dozens of minutes	**	Simple to complex	$/$$$$	Difficult to multiplex, not much integration attempts. Low background noise.	[82], [83], [85]
	Magnetoresistance based	****	***	minutes	****	Moderate to complex	$$/$$$	Possibility to multiplex. Extensive research for miniaturization. Requires clean room work. Issues with linearity.	[89]
	Hall effect sensors	****	****	minutes	****	Moderate	$/$$	Better when miniaturized, detection is localized. Compatible with CMOS technology	[86]
	Magnetic resonance	***	***	Minutes	**	Moderate	$$	Volumetric testing possible. Issues with temperature drift. Needs high magnetic field.	[94]
	Frequency mixing technique	****	****	minutes	***	Simple	$/$$	Can be optimized for qualitative and quantitative multiassay, compatible with miniaturization technologies but not yet miniaturized. Possibility to multiplex.	[1], [2], [3]

Notes:

1. General reviews that study specifically one or many aspects of optical microfluidic sensors are given whenever possible.
2. References include examples and review articles that discuss methods characteristics.

Chapter summary

In this chapter, we reviewed the state of the art of different pathogen sensing techniques and especially for LoC systems. It is only by studying the key concepts of such systems that we can plan, design and realize a completely integrated and automated pathogens sensing microsystem. The detection method is the most important aspect of a LoC system. The principles of operation as well as the advantages and disadvantages of each method were discussed.

A LoC system can be realized by choosing the adequate set of microfluidics circuit, sensing method as well as the biofunctionalization technique. All these aspects are interdependent and cannot be considered separately. Consequently, we presented common choices regarding each aspect ranging from the material choice to the fluid handling.

Finally, we discussed the criteria of an ideal LoC system. These criteria constitute a basis of comparison of the potential LoC pathogen sensing systems. A comparison table was then presented to summarize the important characteristics such as sensitivity, dynamic range, assay time, multiplexing, simplicity, cost, miniaturization possibility and portability for potential LoC realization for different pathogen sensing methods.

Due to its prospective advantages in term of simplicity of miniaturization, sensitivity, cost and rapidity of analysis, we have chosen the frequency mixing technique for our miniaturized magnetic detection system. In fact, this technique benefits also from the particular properties of magnetic nanoparticles as well as the fact that the biological samples do not present any considerable magnetic background.

Chapter 2. Magnetic sensing

In this chapter, we describe the magnetic detection method that has been chosen to miniaturize into a LoC pathogen sensing technique. As a top-down approach, we will first describe fundamentals of magnetism and then. Then we will describe the basic phenomena that affect the magnetic behavior and what leads to superparamagnetism. Since our main focus is on superparamagnetic nanoparticles (SPN), their properties, applications and general requirements are explained in more detail.

Due to SPN benefits (see section 1.3.2.4), we illustrate the use of their properties in our chosen detection method; "magnetic frequency mixing technique". In this case, theory along with previous experimental results will be presented (section 2.3).

Finally, based on this detection method and LoC systems requirements, a first prototype concept structure towards complete miniaturization is proposed (section 2.4).

2.1 Fundamentals of magnetism

2.1.1 Basics

The origin of magnetism is in the electron's behavior; (i) their orbital (around nucleus), (ii) their spin motion (around itself) motions and the interaction between each other (Figure 2-1.a and b) [137]. These movements cause each electron to have a proper tiny magnetic moment. So, in principle, all matter is somewhat magnetic. However, in many cases these magnetic moments cancel each other and the bulk effect on a material is 'non-magnetic' (Pauli's exclusion principle).

There are two representations of basic magnetism; fictitious magnetic dipoles and current sources model. The latter is the most common representation nowadays. It states that a loop of magnetic current generates a magnetic dipole field (Figure 2-1.c). This is equivalent to the field generated by an arrangement of numerous very small two pole fictitious magnet (Figure 2-1.d). We will only use SI unit based equations.

The magnetic field generated by the current loop is termed as H.

$$H = \frac{i}{2r}[\text{A/m}] \qquad 2\text{-}1$$

Here, i and r denote the current magnitude and the loop radius, respectively.

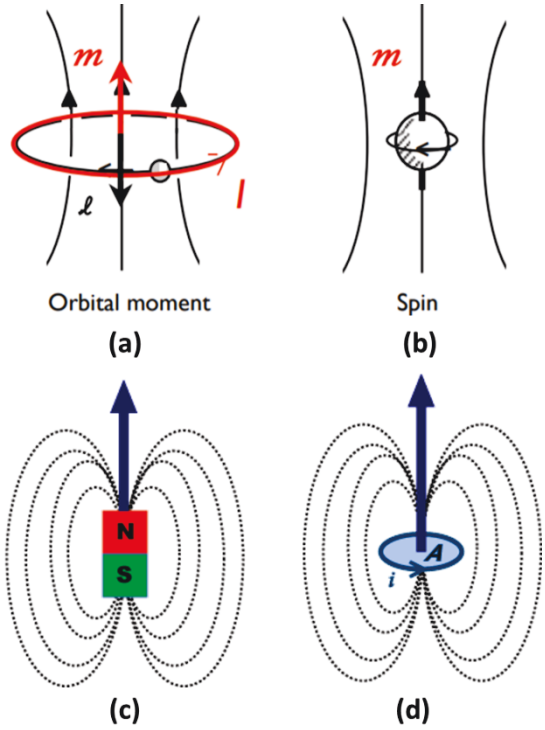

Figure 2-1: Magnetization from electrons: (a) magnetic orbital moment and (b) Spin. Two Magneto-static representations: (c) magnetic poles, (d) magnetic dipole from current loop. Sources: [138], [139].

The current loop also generates what is called a magnetic moment, represented by 'm' or 'μ'.

$$\boldsymbol{m} = i * \boldsymbol{A}\ [Am^2] \qquad 2\text{-}2$$

where A is the area of the loop. Note that this loop could as well represent the total magnetic moment of an atom.

For each unit volume 'v' in space, there is an intensity of magnetization (or simply magnetization):

$$\boldsymbol{M} = \frac{\boldsymbol{m}}{\boldsymbol{v}}\ [\boldsymbol{A/m}] \qquad 2\text{-}3$$

This intensity can also be expressed per unit mass, "σ": $\sigma = \frac{m}{mass}\ [Am^2/kg]$.

For a given bulk material, the total magnetization effect depends on the density of magnetic moments, on their orientations and on their magnitudes.

Moreover, the magnetic field and the magnetization (M) induce a magnetic flux density termed "B" that sums the total magnetic effect:

$$\boldsymbol{B} = \mu_0(\boldsymbol{H} + \boldsymbol{M})\ [T] \qquad 2\text{-}4$$

where μ_0 is the permeability of the free space that is equal to $4\pi \cdot 10^{-7}$ [Henry/meter]. This is the main equation that links the three basic quantities of magnetism.

However, other quantities are used to relate B, H and M. Permeability (μ) for example denotes the ratio B/H. Susceptibility 'χ, on the other hand, represents the ratio of M over H:

$$\chi = \frac{M}{H}[dimensionless] \qquad 2\text{-}5$$

Finally, the last basic quantity represents the effect of an applied magnetic field (H or B) to a magnetic moment (m). In fact, when the field and the moment do not align, a torque is created that forces the moment to align with the magnetic field lines (Figure 2-2).

$$Torque = \boldsymbol{m} \times \boldsymbol{B} \qquad 2\text{-}6$$

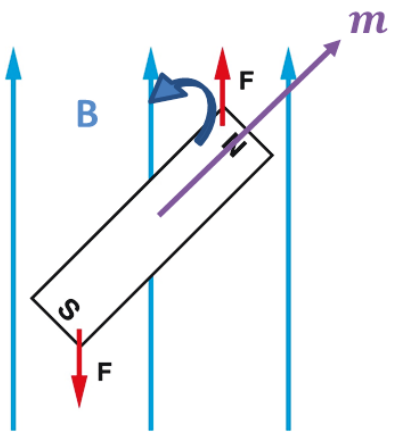

Figure 2-2: Torque caused by an applied magnetic field.

This last phenomenon is used to understand the behavior of different types of magnetic materials.

2.1.2 Magnetic materials

Different types of magnetism are usually described by the behavior of different materials in response to a magnetic field.

The magnetic behavior of materials can be classified into five major categories:

1. Diamagnetism
2. Paramagnetism
3. Ferromagnetism
4. Antiferromagnetism
5. Ferrimagnetism

Diamagnetic and paramagnetic materials are considered 'nonmagnetic' because they exhibit no collective magnetic effect among their atoms. If the material exhibits one of the three last behaviors, it is termed to be magnetic. In this case, there is a strong collective magnetic contribution. A good example is iron.Iron has unpaired electrons that are aligned in parallel, and this is the main cause of the magnetism of iron. Moreover, magnetic materials exhibit significant values of susceptibility 'χ' while nonmagnetic materials have very low values of χ. A basic way to characterize the material's behavior is to use their magnetization curve and its dependence on temperature.

Diamagnetic materials

These are the materials that are composed of atoms that have no net magnetic moment (because all electrons are paired and the orbital shells are all filled). Also, unlike other materials, the susceptibility is negative and does not depend on the temperature (Figure 2-3). A common example of diamagnetic material is water ($\chi = -0.9\ 10^{-6}$).

Paramagnetic materials

In this case, atoms do have a net magnetic moment (due to unpaired electrons) but as a whole, the individual magnetic moments do not interact magnetically. So the sum is still zero when no magnetic field is present. Contrary to diamagnetic materials, paramagnetic ones exhibit a positive higher susceptibility (around 2-3 orders higher) and when they are subjected to a magnetic field, there is partial alignment of the atomic moments (Figure 2-3). Moreover,

paramagnetic materials are affected by temperature (Curie Law).

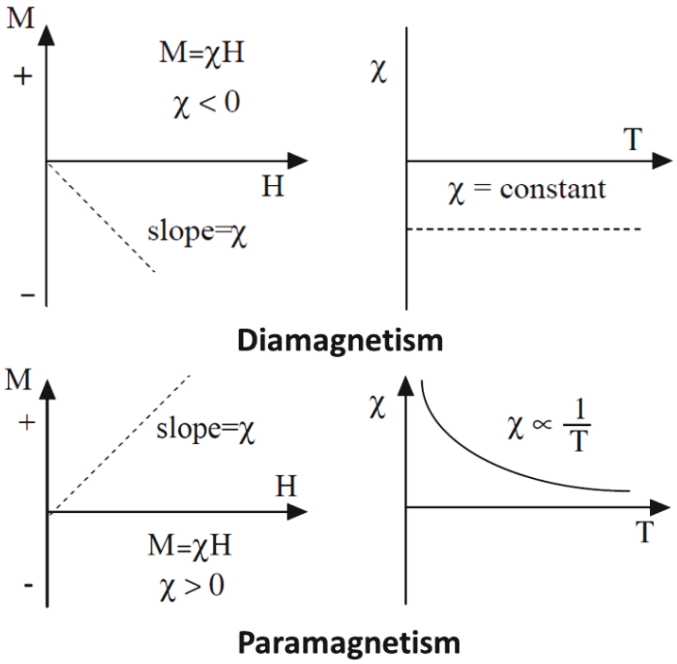

Figure 2-3: Diamagnetic and paramagnetic behaviors [137].

Ferromagnetism

In this case, the material has individual atomic moments and a strong magnetic interaction between them. These interactions are caused by electronic exchange forces and result in either parallel (ferromagnetism) or antiparallel (antiferromagnetism) alignment of atomic moments. The exchange force is a quantum mechanical phenomenon.

Due to these strong magnetic interactions, ferromagnetic materials exhibit a net magnetic moment without any external applied magnetic field. Additionally, their susceptibility is very high and there is a hysteresis effect in the magnetization curve (Figure 2-4.b). Hysteresis is translated to a retained memory of the applied field after it is removed. When the field is switched off, the magnetization that remains is called magnetic remanence (M_r). The magnetic memory also shows up as hysteresis in the magnetization curve. Magnetization is different depending on the direction of change of the externally applied magnetic field. The shape of the hysteresis curve is dependent on size, on mechanical stress, on the domain state and on temperature. Thus it is not an intrinsic property of the material.

Finally, although the exchange forces are very strong, if the temperature is high enough, the

moment's orientations will be subject to randomization, leading to paramagnetic behavior after a certain threshold (Curie temperature) (Figure 2-4.c). However, this temperature is usually very high (575°C for magnetite). Typical ferromagnetic compounds are iron (Fe), cobalt (Co) and Nickel (Ni).

Ferrimagnetism and antiferromagnetic materials

In antiferromagnetic materials, the electronic exchange forces favor the antiparallel alignment of atomic moments, opposite to the case of ferromagnetic materials. Some compounds like oxides have crystal structures that lead to a more complex form of magnetic ordering of moments. This lattice crystal structure is usually subdivided into two sublattices (A and B). A and B have antiparallel alignment (Figure 2-5). On one hand, if the magnetic moments of A and B are exactly equal in magnitude, the material is called antiferromagnetic. Features of this type of material are; zero remanence, no hysteresis, positive susceptibility (small) and effect of temperature on magnetic susceptibility.

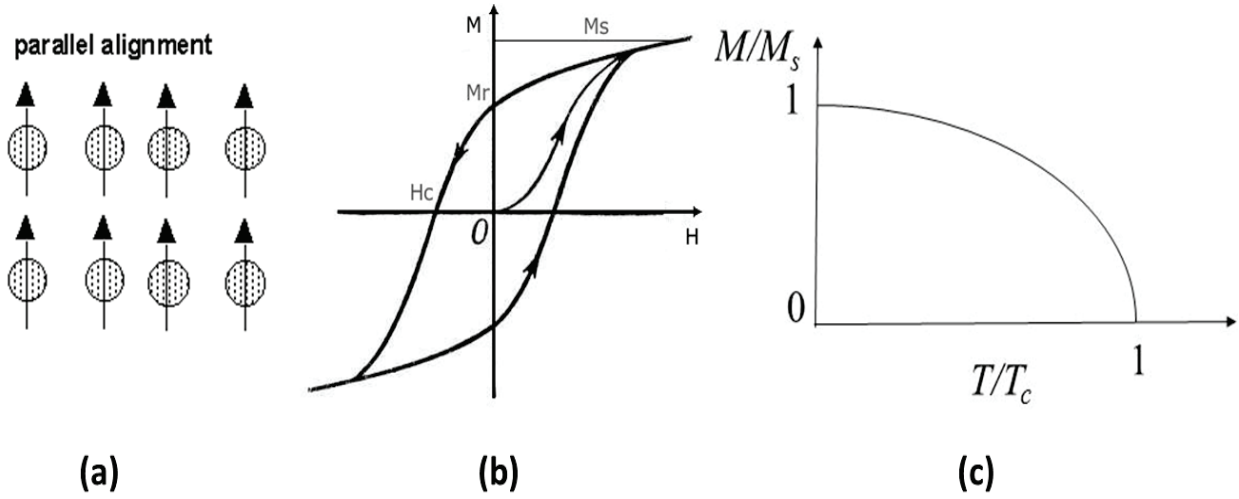

Figure 2-4: Ferromagnetism properties. (a) Atomic moment's alignment. (b) Typical magnetization curve with hysteresis loop showing magnetic remanence (Mr) and coercivity (Hc). (c) Effect of temperature on magnetization, when the temperature is above the Curie limit (Tc) the material becomes paramagnetic.

On the other hand, if the magnetic moments are not equal, this will result in a net magnetic moment and the material is called ferrimagnetic (Figure 2-5). The resulting effects are very similar to that of ferromagnetism. However, the cause of these effects is different now. For example, the exchange forces in magnetite are mediated through the oxygen anions

(superexchange).

2.1.3 Magnetic behavior of blood

The magnetic behavior of blood is very important since the magnetism-based methods use magnetic nanoparticles and mix them with whole blood to enable targeting and subsequent detection.

The blood has basically two magnetic responses; diamagnetic and paramagnetic [140]. The diamagnetic response comes, for example, from intra-vessel proteins and other chemicals that comprise carbon, hydrogen, oxygen and nitrogen atoms. The paramagnetic response comes from hemoglobin molecules. They are the iron-containing oxygen-transport metalloproteins in the red blood cells.

This latter very small paramagnetic response of the blood constitutes the only source of magnetic noise. This explains why magnetic detection methods have potential for high selectivity and signal to noise ratio.

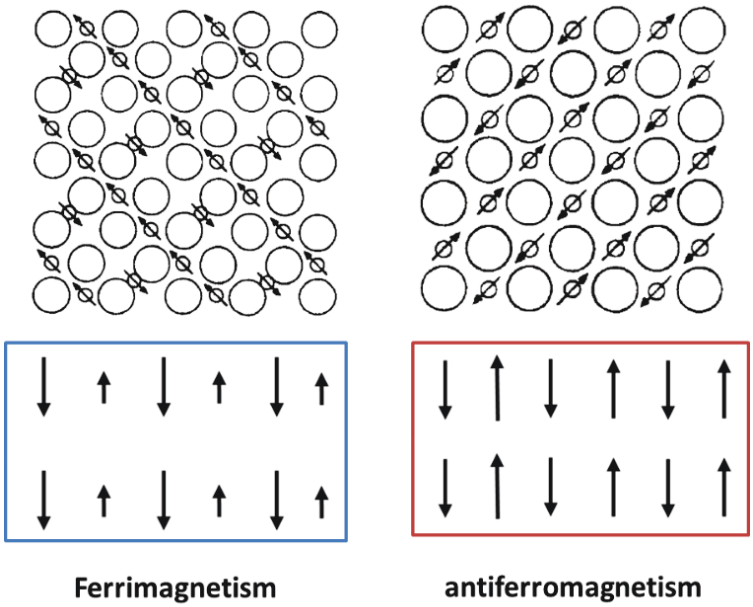

Figure 2-5: Ferrimagnetic and antiferromagnetic behavior. Structure simplified representation (Up) and corresponding moment's alignment and magnitude (Lower figure) [137].

2.1.4 Magnetic anisotropy

Magnetic anisotropy means the dependence of magnetic properties on a preferred direction. This is a very important phenomenon that strongly affects the shape of the hysteresis loop and

corresponding remanence and coercivity.

Magnetic anisotropy results from three causes:

1. Crystal structure (magnetocrystalline anisotropy)
2. Grain shape (shape anisotropy)
3. Applied or residual stress (stress anisotropy)

The first two factors are the most influential; magnetocrystalline anisotropy is the energy necessary to turn the magnetic moment from its preferred direction to the hard direction. In some structures, like hexagonal crystals, it is very difficult to reach saturation magnetization because of this effect (one needs more than 2 Tesla). This effect is usually important in relatively big grains or particles (more than $100\mu m$).

The other determinant factor is the shape of the unit grain; the magnetized body produces magnetic poles on the surface, this surface change causes a demagnetization field to appear that acts opposite to the applied field. The preferred direction here is the direction where the demagnetization field is lower. Shape anisotropy is very important in case of small particles. Practically, magnetite particles smaller than $20\mu m$ are much more influenced by shape anisotropy than magnetocrystalline anisotropy [137].

2.1.5 Magnetic domains and the effect of size

Relatively big ferromagnetic and ferrimagnetic materials are actually composed of small regions which are usually magnetized to saturation but in different directions (Figure 2-6.a). Magnetic domains simply exist because they are energy efficient. They allow to reduce the magnetostatic energy associated to the shape anisotropy mentioned earlier. Because the preferred direction of magnetization of each domain is somewhat random, the net total magnetization is near zero. Domain sizes are small on a macroscopic scale ($1 - 100\mu m$).

Figure 2-6illustrates this phenomenon. The magnetization of single domain material will produce a north pole and a south pole. These poles produce in turn a magnetic field opposite to the initial magnetization (demagnetization field, blue line), this demagnetization field depends on the specimen. When the material is composed of two anti-symetric domains (Figure 2-6.c), the magnetostatic energy is reduced by half (blue line). Each time we divide into more subdomains, the magnetostatic energy becomes less and less. A closure domain

structure could then make the magnetostatic energy zero (Figure 2-6.d).

However, the creation and maintaining of the walls (interface) between domains also requires energy. This is because the transition between domains means that the individual magnetization of atoms must change direction from one domain to another (Figure 2-6.e). This requires energy. The domain width is determined by a compromise between the magnitude of the exchange forces and the magnetocrystalline anisotropy; exchange forces favor smooth transitions (wide walls) and the structure anisotropy favors abrupt transitions (thin walls). Depending on the material, the wall width is around the order of $100\ nm$.

Ultimately, the number of domains is dictated by the smallest energy demanding number. That is the compromise between magnetostatic energy (demagnetization field) and domain wall formation energy.

From these explanations, we deduce that the formation of domains is size-dependent. Hence, depending on a size, the magnetic behavior of the same material may change. A material can either favor multidomain (MD) or single domain formation (SD). For a given material, when the particle is smaller than the domain wall itself, it will only exhibit a single domain (SD). On the other hand, if the particle is bigger than the order of the wall size, multiple domains can exist (Figure 2-7).

The change in material behavior due to size change can be followed by a change of the hysteresis loop shape.

If we take d_0 as the middle point between MD and SD states, when the particle diameter is bigger thand_0, the magnetization is changed through the process of wall translation. The walls move in order to give more area to the domains favoring the applied field direction. The more domains there are (bigger sizes), the easier the transition is, and thus, the particle exhibits a sharp hysteresis loop (small H_c).

When $d = d_0$, there is only one domain and thus there is uniform magnetization along the easy axis. Magnetic anisotropy allows this and it can be approximated by:

$$\Delta E = KV \qquad 2\text{-}7$$

where K and V are the anisotropy constant and the particle volume, respectively.

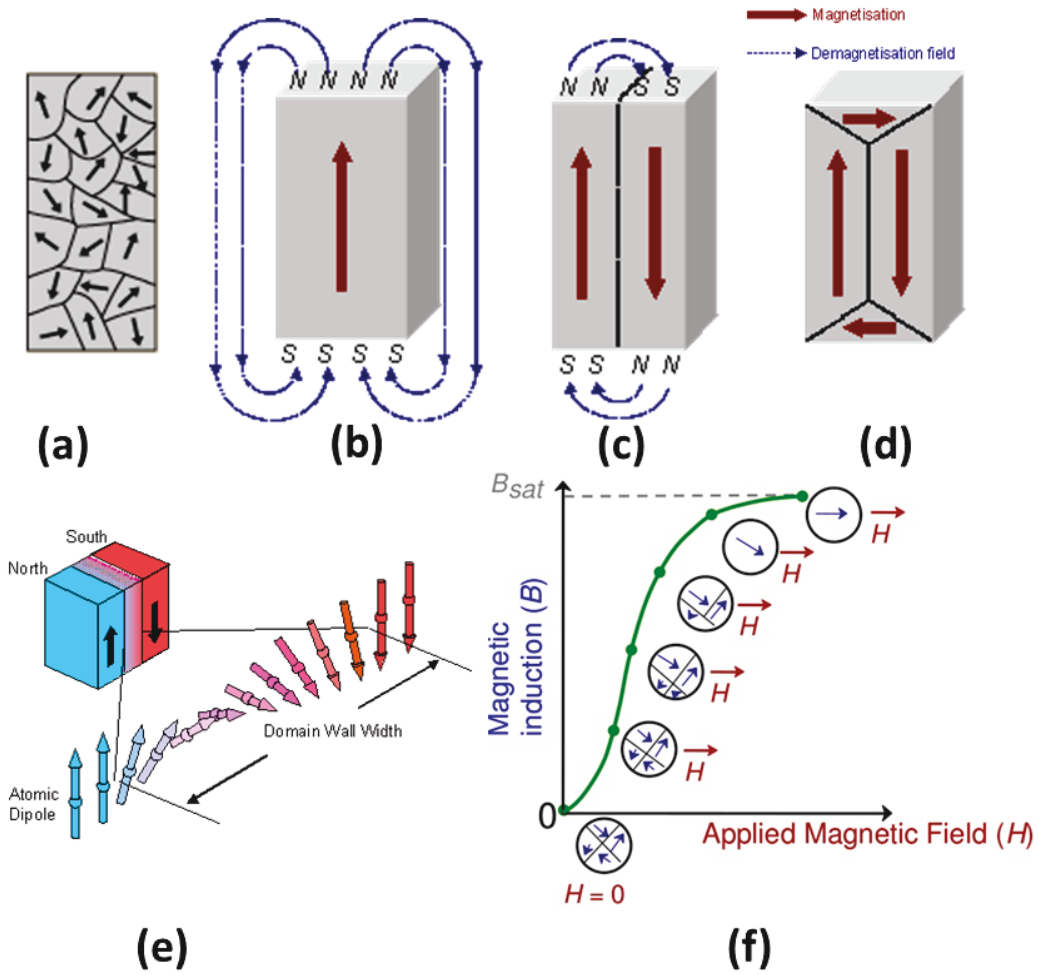

Figure 2-6: Origin of magnetic domains. (a) Magnetic material is divided into many subdomains. (b) and (c) domain exist to reduce effect of shape anisotropy that creates the demagnetization field (blue lines). (d) Case where the total effect of domains is zero magnetostatic energy (closure domain). (e) Domain walls representation in the case of a 180° flip [141].(f) B-H behavior of a ferromagnetic material in the initial magnetization [142].

In this case, H_c is high and thus, the hysteresis loop is wide (Figure 2-7).

When $d_s < d < d_0$, the thermal fluctuation becomes non-negligible. Here, because ΔE becomes increasingly smaller as the volume is smaller (small d), the thermal energy starts randomizing this orientation, thus H_c becomes smaller and the hysteresis loop thinner and thinner (MD). Thermal energy is expressed by:

$$E_{thermal} = k \cdot T \qquad 2\text{-}8$$

where *k* and *T* are Boltzmann constant and absolute temperature, respectively.

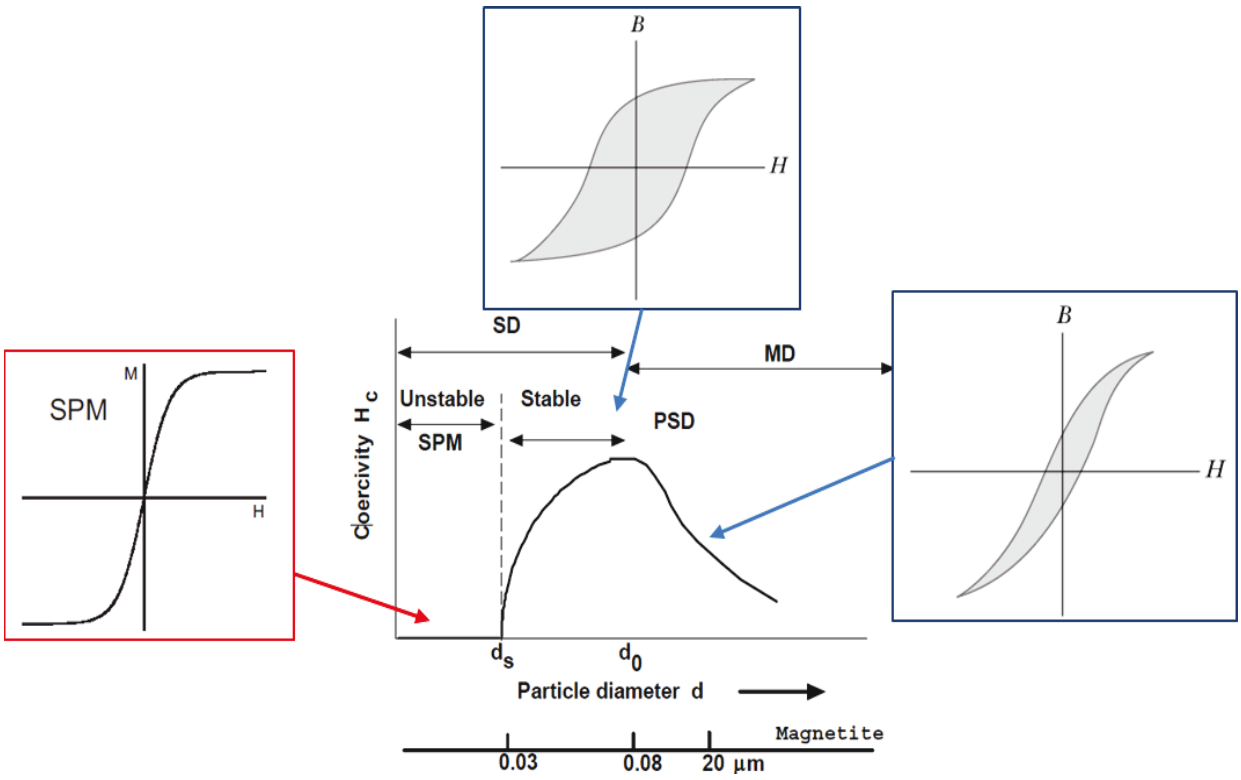

Figure 2-7: Particle size magnetic properties (room temperature) and example of characteristic diameters for magnetite. SD: single domain, MD: multidomain, PSD: pseudosingle domain, SPM: superparmagnetism [143].

When the diameter is below a certain threshold ($d \leq d_s$), thermal energy is in the same order of anisotropy energy. The magnetic moment is then free to fluctuate in response to thermal energy [140]. This leads to a non-hysteresic (anhysteretic) loop (Figure 2-7 SPM).

In this particular state, the particle is called '**superparamagnetic**'.

2.2 Superparamagnetic nanoparticles (SPN)

As mentioned above, if the magnetic particle is small enough (order of tens of nanometers), it will exhibit superparamagnetic behavior. It is a paramagnetic behavior of ferromagnetic or ferrimagnetic materials with a much higher susceptibility than normal paramagnetic ones. It has a paramagnetic behavior because: (i) when no magnetic field is applied, the resulting magnetization is zero and (ii) when a field is applied, there is a net statistical alignment of magnetic moments. Now the magnetization comes from entire SD particles consisting of around 10^5 atoms instead of magnetization coming from moments of single randomized atoms (thus the term "super"). However, the magnetic energy of a superparamagnetic grain is smaller than the thermal energy, therefore superparamagnets lose their magnetism when the external magnetic field is switched off. Thus, superparamagnetism is ferromagnetism at small spatial scales. Finally, the superparamagnetic threshold diameter (d_s) depends on the material properties and can be illustrated in Figure 2-8.

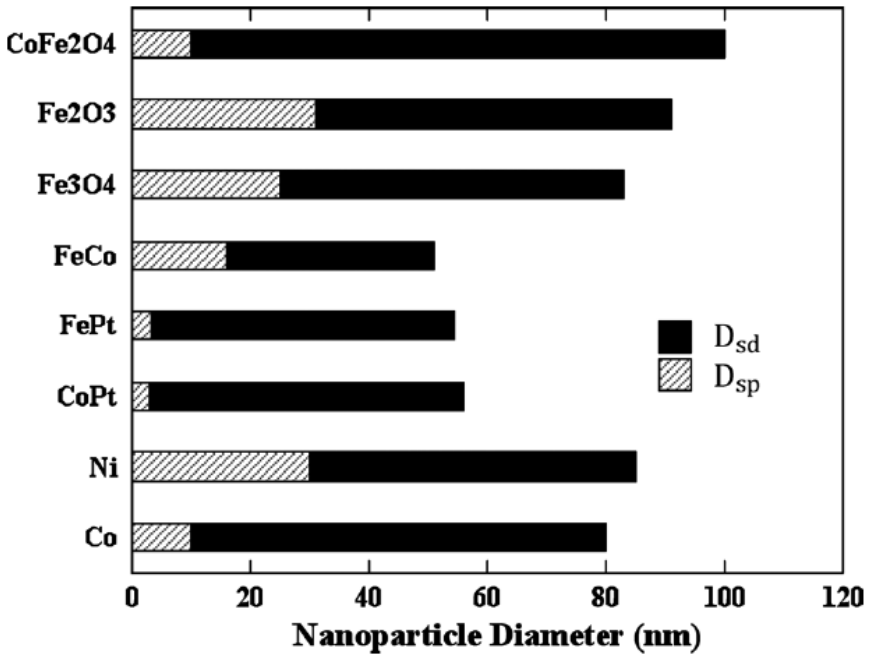

Figure 2-8: Variation in nanoparticle's single domain and SPM behavior diameters depending on the material. D_{sp}: superparamagnetic diameter, D_{sd}: single domain diameter [144].

2.2.1 Magnetic properties of SPN

There are two main properties of the SPN: the relaxation time and the magnetization curve.

2.2.1.1 SPN relaxation times

The basic relaxation time illustrates the competition between the randomizing effect of temperature and the anisotropy. The average time for the magnetic moment to flip is called "Néel relaxation" and is expressed by:

$$\tau_N = \tau_0 exp(\frac{\Delta E}{kT}) \quad 2\text{-}9$$

where τ_0 is characteristic time depending on the material and is order of magnitude around$10^{-9} - 10^{-12}\ s$.

If the magnetization of SPN particles is measured, there can be two states: the superparamagnetic state and the blocked state. Two dependent factors influence this observation, the measurement time (τ_m) and the temperature (T). If the measurement time is fixed, then:

If the temperature is so high that thermal energy is dominant, then$\tau_m \gg \tau_N$, average flipping time is smaller than the measurement. We observe a fluctuating state where magnetic moments randomly flip and the net magnetization over the measurement time is zero. This is termed the superparamagnetic state.

If the temperature is very small and thus$\tau_m \ll \tau_N$, the measurement time is much shorter than the average flip time, so the magnetic moments are still fixed in one direction. This state is termed the blocked state.

Consequently, for any given measurement time, there is a temperature that allows the transition between the blocked state and the SPM state. This temperature is called the "blocking" temperature (T_B):

$$T_B = \frac{\Delta E}{k_B \ln(\frac{\tau_m}{\tau_0})} \quad 2\text{-}10$$

This temperature threshold is very important because if the measurement is done under the blocked state, the particle will no longer behave as a SPN. It will behave as a SD particle and hysteresis will appear again as the temperature is lowered even more (or the frequency of measurement increased).

When the particle is in suspension in a solution, there is an additional relaxation that can happen to the nanoparticle. It is due to the Brownian motion and thus termed "Brownian relaxation" (see section **Erreur ! Source du renvoi introuvable.**). The cause is their collision with the fast-moving atoms or molecules in gas or liquid. For a particle with a given hydrodynamic volumeV_H:

$$\tau_B = \frac{3\eta V_H}{k_B T} \qquad 2\text{-}11$$

where η is the viscosity of the solution.

It expresses the 'physical' rotation of the particle. It is thus a function of the hydrodynamic size (not magnetic content only), temperature and viscosity of the medium.

The sum effect of Brownian and Néel relaxations is calculated using the following equation:

$$\tau_t = \frac{\tau_N \tau_B}{\tau_N + \tau_B} \qquad 2\text{-}12$$

Depending on the size of the particle (Figure 2-9), one of the relaxations is dominant and the other is negligible. For small particles, it is the Brownian motion that is of significance whereas for large particle, the Néel relaxation dominates.

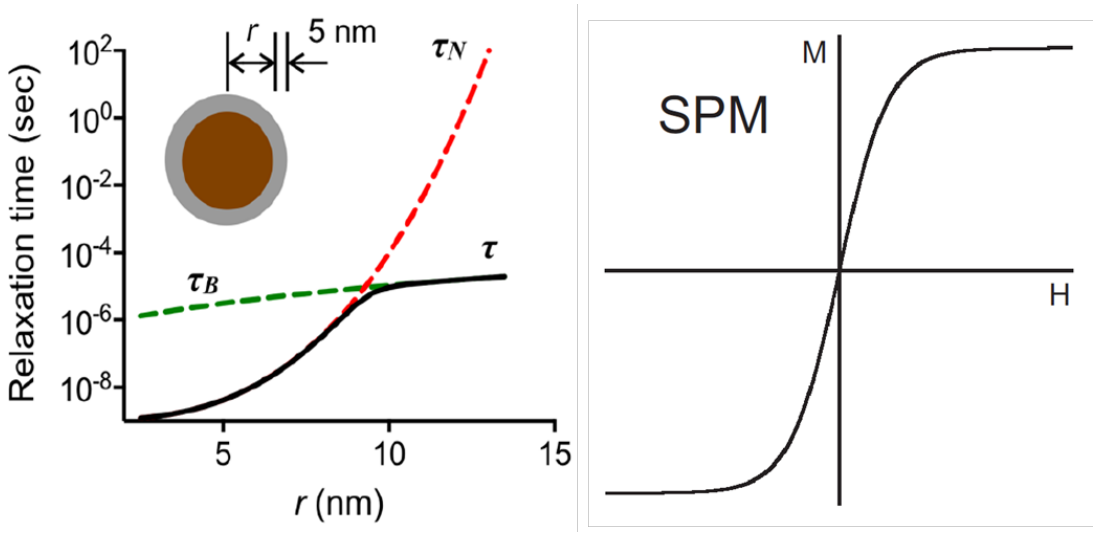

Figure 2-9: (Left) The Néel (τ_N) and the Brownian (τ_B) relaxation times calculated for Fe_3O_4MNPs with 5 nm surface coating (nonmagnetic). The effective relaxation time (τ) is shown in a black line [75]. (Right) magnetization curve of superparamagnetic particles.

2.2.1.2 Magnetization curve:

A typical magnetization curve of SPN is shown in Figure 2-9.b. The magnetization curve has three main properties:

1. No hysteresis.
2. Nonlinear.
3. Saturation effect.

When thermal energy is superior to anisotropy (usually the case), the magnetization curve follows a Langevin function:

$$M(\mu_0 H) = M_s L(\frac{\mu_0 Hm}{k_B T}) \ \ with\, M_s = nm \qquad 2\text{-}13$$

where:

- L: Langevin function $L(x) = \frac{1}{\tanh(x)} - \frac{1}{x}$
- M_s: Saturation magnetization.
- n : Density of particles in the sample.
- m: Individual magnetic moment of each particle.

2.2.2 Chemical properties

Magnetic particles are usually composed of a magnetic core and an external surface coating. The surface coating allows primarily to make the functionalization of SPN with biological molecules possible. It also allows the particle to be biocompatible.

In the literature, four main types of nanoparticles based on the composition of the core are distinguished [77], [82]:

a. Iron oxide core nanoparticles:

They are mainly composed of magnetite (Fe_2O_3) or maghemite (Fe_3O_4) cores. The most common example is the cross-linked iron oxide particles (CLIO) with magnetite core. They constitute one of the first widely used NP. They are biocompatible, stable and allow functionalization through binding with amine groups, but their magnetic properties were quickly considered inefficient. This is because they have a magnetic core of about 5 nm

with a coating of about 10nm in thickness. In consequence, there is a big dead volume.

b. Core/shell NP:

They have iron (only) core nanoparticles with thin shells to prevent oxidation of the core. Because of higher iron content, they allows improvement of magnetization. However, some strategies use thick nonmagnetic protective shells that also constitute a magnetic dead volume.

c. Doped metal oxide NP:

The iron oxide core is doped with magnetic compounds like Manganese Mn (example: $MnFe_2O_4$) or Co. In this way, the saturation magnetization is improved. However, biocompatibility may be compromised because the heavy metals are usually toxic.

d. Multicore large MP:

Composed of multiple small SPN attached to each other by means of using polymer or other compounds (silica). This alternative approach allows to increase the individual magnetization of nanoparticles when the core size cannot be increased further (SPM size limitation). Furthermore, these particles allow functionalization with more binding sites and are thus very suitable for biomedical applications.

2.2.3 Applications of magnetic particles and general requirements

Magnetic particles are used in a variety of applications:

1. Magnetic separation of cells: used for selectively removing tumor cells, for cell counting and as an amplification of the target when used with optical detection methods.
2. Drug delivery: they may allow the drug to be delivered directly to the area of the body in need. This may help reduce drastically the undesired side effects of the drug.
3. Hyperthermia: after the magnetic particles are directed to tumor cells, they can be heated under certain conditions (selected frequency and magnitude of the ambient magnetic field). When this procedure is well controlled, the tumor cells can be selectively destroyed by local heating while leaving neighboring healthy cells unharmed [140].
4. As an MRI contract agent: they amplify the relaxation time of water molecules (see section **Erreur ! Source du renvoi introuvable.**).

For the aforementioned biomedical applications, magnetic nanoparticles should be optimized regarding the following preferred criteria:

a. **Zero remanence:** This is a prime requirement for magnetic nanoparticles that are used as labels. The remanence can lead to natural clustering caused by the residual magnetic remanence [78]. Consequently, it will deteriorate the efficiency of the labeling, raising the nonspecific signals. It also makes the actuation of magnetic particles more difficult. The ability of the NP to remain not clustered in the fluid when no magnetic field is applied is also termed (**colloidal stability**)
b. **High magnetic moment:** The larger the magnetic response of magnetic particle (MP) the better it is for any given application. For example, when used as detection labels, the larger the magnetic moment, the better the signal and the more sensitive the measurements. The magnetization depends on: core material content, magnetic volume, percentage of dead volume because of functionalizing layer (dextran…etc.) and the shape of the particle (cubic nanoparticles have proven better magnetization [145])
c. **Monodisperse:** Nanoparticles with too much dispersity in size are difficult to control and to operate with some detection techniques that rely on the relaxation times (susceptometry).

When optimized, SPN offer the best compromise for all major applications. From our literature review, we think that the best compromise seems to be a large bead composed of multiple SPN embedded inside it. However, for sizes larger than 100 nm, some issues may arise like optimal binding and stability.

Additionally, each embedded SPN should not be too small in order to prevent surface effects. In fact, the surface layer of SPN has a different magnetization that the SPN core and thus the total magnetization depends on an "effective radius" expressed as $r_{ef} = r - d$, where r is the actual radius of the SPN and d the thickness of the magnetically frustrated layer (surface layer with different magnetization property). d is usually constant for a given material ($\sim 0.9\ nm$ for magnetite), so the solution is to reduce the surface/volume ratio by just increasing the size of the SPN core (**Erreur ! Source du renvoi introuvable.**).

Finally, a compromise between these different criteria should be found in order to choose the

best SPN for any given application.

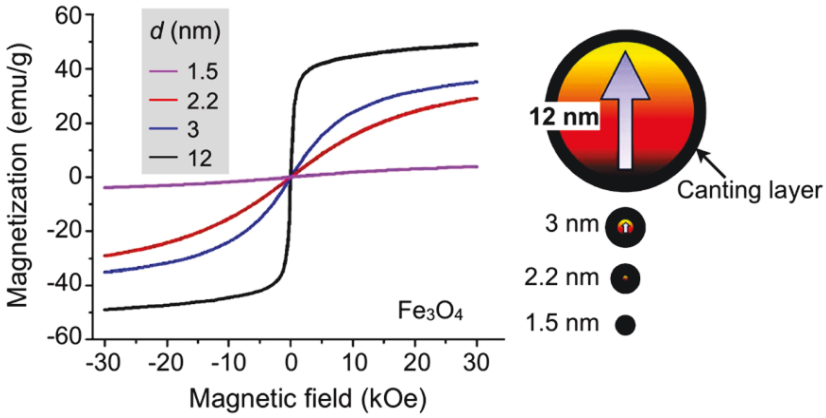

Figure 2-10: Canting effect (surface effect) on the magnetization moment. As the particle size is increased the canting effect becomes less influential [146].

2.3 Frequency mixing detection technique

In this project, we chose to exploit the magnetic frequency mixing technique in order to detect and quantify the presence of SPN [1]. This technique can be later used for pathogen sensing application. The method is advantageous in that, it is simple to implement and sensitive. It also takes the advantages of both magnetic sensing and SPN; such as high signal response, very low biological noise and low interference.

The basic concept and theory of this technique are firstly explained. Afterwards, we will give some previous work results as proof of practical validation of the efficiency of the method.

2.3.1 Theoretical aspects

The frequency mixing technique takes advantage of the properties of the SPN to be detected; they are nonlinear and have a saturation value. By measuring the specific response of this nonlinear curve, we can detect and quantify the presence of SPN included in a biological sample. As we have seen earlier, the magnetic response of blood is very small and linear. This makes nonlinear characterization a very sensitive method for discrimination and quantification. Furthermore, if we take into account the relaxation, the technique can be used in order to discriminate different types of nanoparticles in terms of size and material composition.

The Figure 2-11 shows the principle of the technique. SPN are exposed to an external magnetic field composed of two frequencies: f_1 (high frequency) and f_2 (low frequency). Both signals can be generated using normal coils (Figure 2-11a). The low frequency signal helps the SPN reach the nonlinear magnetization area (drive signal) whereas the high frequency signal probes this nonlinearity and contributes to a resulting induction signal. The resulting magnetization of nanoparticles is then nonlinear (Figure 2-11c). A coil used for detection can then detect the resulting total magnetic flux density: $B = \mu(H + M)$.

If we examine the spectral composition of the detected signal, we notice that additionally to the two initial frequencies (f_1 and f_2), the nonlinear response results in other emerging frequency peaks (Figure 2-11d). They can be expressed as: $f_i = m \cdot f_1 + n \cdot f_2$. If no offset field is used, the symmetry of the magnetization curve is shown in Figure 2-11b (uneven function) results in uneven additional terms. For example, we get $3f_1, 3f_2, f_1 + 2f_2, f_1 - 4f_2, 2f_1 + f_2$...etc.

If we use the same technique and there is no SPN in the sample being tested, the magnetic response is just composed of the initial two frequencies and there are 'no mixed terms' (Figure 2-11d). Thus, this makes the detection of these mixing terms highly specific to the presence of magnetic particles with this nonlinear response. Quantification of the amount of SPN can be achieved by measuring the amplitude of any significant mixed term (usually the one with the highest amplitude, such as $f_1 + 2f_2$).

The mathematical derivation behind these responses is as follow:

For general purpose study, we suppose that the exciting magnetic field is composed of an offset magnetic field and two distinct frequencies f_1 and f_2 ($f_1 > f_2$), H can be expressed by:

$$\mu_0 H(t) = B_0[A_0 + A_1 \sin(2\pi f_1 t) + A_2 \sin(2\pi f_2 t)] \qquad 2\text{-}14$$

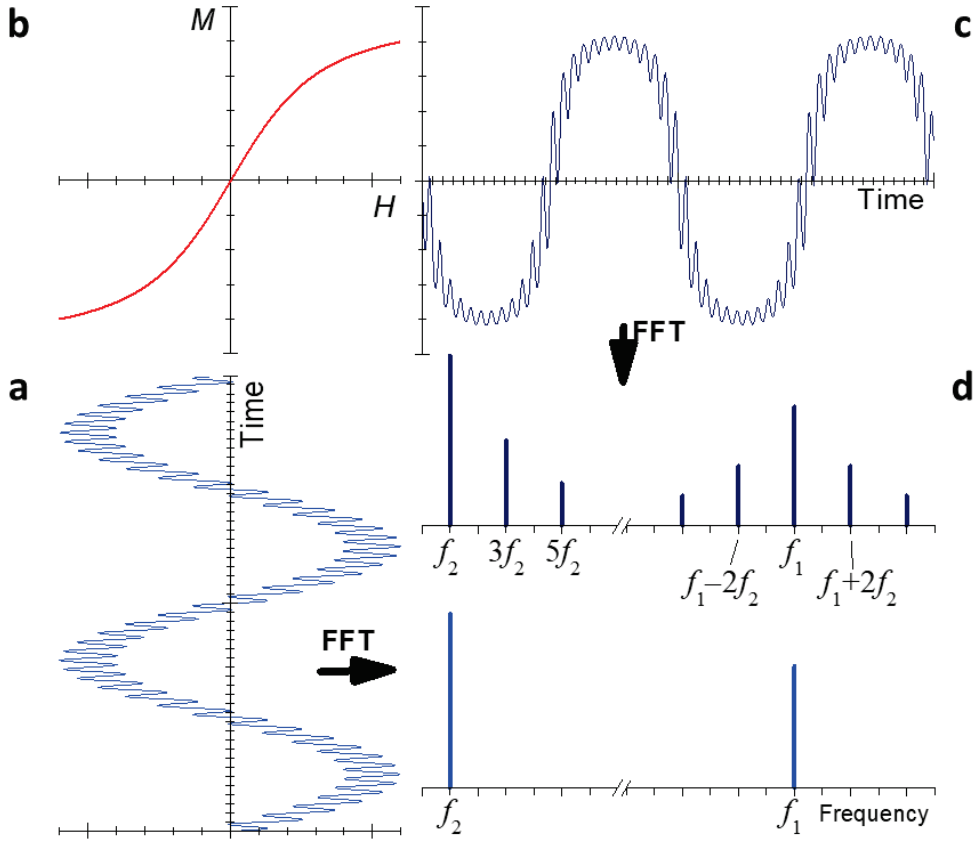

Figure 2-11: Principle of the "frequency mixing technique" (a) excitation signal composed of two sinusoids A magnetic field consisting of two spectral components. (b) The frequency spectrum of excitation field. (c) The nonlinear magnetization curve of superparamagnetic particles. (d) The resulting time-dependent magnetization curve. (e) The Fourier transform of magnetization response. Figure reported from [1].

The SPN responds to this excitation field with a magnetization, *M*, expressed by:

$$M(H) = \mathrm{M_s} \cdot L(x) \qquad 2\text{-}15$$

with M_s the saturation magnetization and *L*, the Langevin function expressed by:

$$L(x) = \coth(x) - \frac{1}{x} \ , \qquad \text{With } x = \frac{m_0 * \mu_0 * H}{k_b * T} \qquad 2\text{-}16$$

If we use the Taylor expansion on this function we get:

$$L(x) = L(x_0) + \frac{dL}{dx}|_{x=x_0}(x - x_0) + \frac{1}{2}\frac{d^2L}{dx^2}|_{x=x_0}(x - x_0)^2 + \frac{1}{6}\frac{d^3L}{dx^3}|_{x=x_0}(x - x_0)^3 + \cdots \qquad 2\text{-}17$$

The first three derivatives are shown in Figure 2-12, they have the following formulas:

$$\frac{dL}{dx}(x) = 1 - \coth^2(x) - \frac{1}{x^2}$$

$$\frac{d^2L}{dx^2} = -2\coth(x)\,(1 - \coth^2(x)) - \frac{2}{x^3} \qquad 2\text{-}18$$

$$\frac{d^3L}{dx^3} = -2(1 - \coth^2(x))^2 + 4\coth^2(x)\,(1 - \coth^2(x)) + \frac{6}{x^4}$$

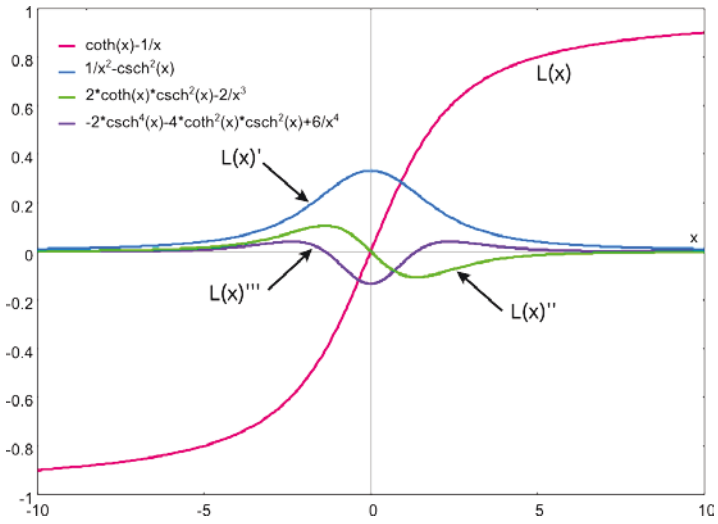

Figure 2-12: Langevin function and its derivatives.

We know that 'x' is directly proportional to H (other terms being constant) and thus has the same curve of variation. When we replace each value of x in the Taylor terms, we get mixed terms coming from powers of 'x'.

For example, in the second term, there is an x^2 term that can be replaced by:

$$x^2 = [A_0 + A_1\,sin(2\pi f_1 t) + A_2 sin(2\pi f_2 t)]^2 =$$
$$A_0^2 + 2A_1A_0\sin(2\pi f_1 t) + +A_1^2\sin(2\pi f_1 t)^2 + A_2^2\sin(2\pi f_2 t)^2 + \qquad 2\text{-}19$$
$$2A_2A_0\sin(2\pi f_2 t) + 2A_1A_2\sin(2\pi f_1 t)\sin(2\pi f_2 t)$$

In this, the term "$\sin(2\pi f_1 t)^2$"is equal to '$[1 - \cos(2\pi \mathbf{2} f_1 t)]/2$', which leads to a contribution to the mixed term '$2f_2$'.

Similarly, a mixed signal of frequency '$f_1 + f_2$' emerges from the product '$\sin(2\pi f_1 t)\sin(2\pi f_2 t)$'.

In the same manner, we get from the third term of $(x - x_0)^3$ the uneven sum frequency

term$f_1 + 2f_2$. If $A_0 = 0$ (representing static field) the second derivative is at zero and the third derivative of the Langevin function is at its maximum (Figure 2-12), thus making the uneven term dominant. Because the derivative of an even function is uneven and the derivative of an uneven function is even, the reasoning holds for all even and uneven mixed terms. The presence or absence of the static field favors the even or uneven terms, respectively.

When $A_0 = 0$, the magnetization mixed term$f_1 + 2f_2$ is at its maximum, which can be expressed by:

$$M_3 = \frac{M_s A_1 A_2^2}{2} \cdot L'''(x) \cdot \cos[2\pi(f_1 + f_2)t] \qquad 2\text{-}20$$

It has to be noted that the magnitude of the mixing frequency ($f_1 + 2f_2$) scales quadratically with the low frequency magnitude (A_2) and linearly with the magnitude of the high frequency field (A_1).This makes the amplitude of the low frequency very important for efficient magnetization.

Similarly, when $x = A_0 = 1.372$, the even term $f_1 + f_2$ is at its maximum:

$$M_3 = \frac{M_s A_1 A_2^2}{8} \cdot L''(x) \cdot \cos[2\pi(f_1 + 2f_2)t] \qquad 2\text{-}21$$

These are the most two dominant terms. These approximations in the calculations hold only if the excitation fields are considered small ($A_1 \text{and} A_2 \ll 1$). Other mixed terms can be used for qualitative detection but provide lower sensitivity for quantitative measurements. However, these terms may help discriminate different types of nanoparticles.

These approximations were validated in [1], using numerical calculations and experimental measurements (Figure 2-13).

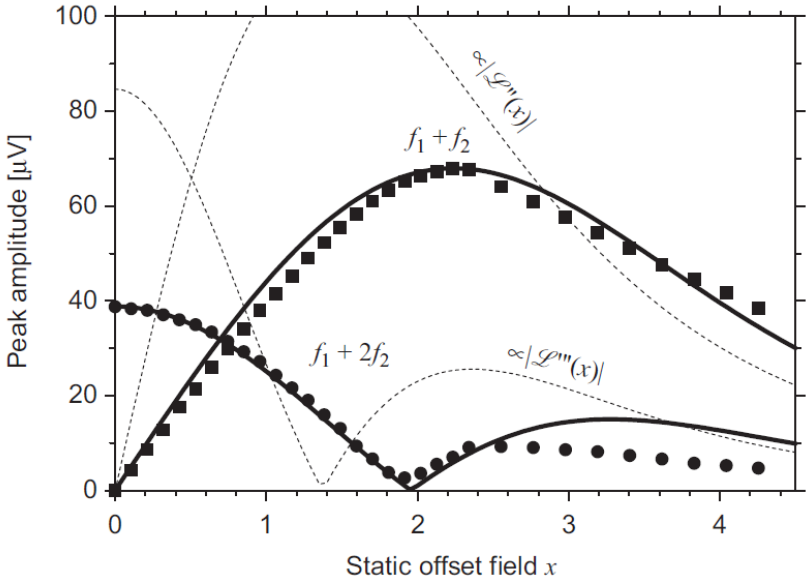

Figure 2-13: Measured and calculated mixed terms. Thin dashed lines represent the Taylor approximation. The thick solid lines represent the numerical calculation. Measurements are represented by discreet point (circles and squares). Parameters of the experiment are: $B_0 = 1.9\ mT$, $A_1 = 0.8 \cdot B_0\ and\ A_2 = 2.4 \cdot B_0$. Figure reported from [1].

There is a little shift between real and approximated values. This shift does not affect the optimization of the uneven term amplitude but affects the optimum point for the even term amplitude.

The detection method can be very sensitive but there is a key consideration with this method. There must be no ferromagnetic or ferrimagnetic material in close vicinity of the sample of the detection coil. For example, iron-cored coils could not be used in order to enhance the magnetic field amplitude. This is the main restriction of this detection technique.

2.3.2 Experimental setup and previous work

The mixing frequency technique was used to detect various antigens such as Francisella tularensis [2],CRP [3] and Yersinia pestis [4].

An illustration of one of the first developed magnetic reader (bioelectronics laboratory, Juelich research center) and a schematic representation are shown in Figure 2-14.

The system is composed of a measurement head and readout electronics with a display. Concerning the measurement head, it is composed of excitation coils and pick-up coils. The excitation coils are composed of two coaxial solenoid coils (red and blue) that generate the

low frequency and high frequency magnetic fields ($f_1$and f_2). The measurement head (yellow) detects the resulting magnetization. In order to enhance the SNR and reduce the noise, the detection coils are wound in a gradiometric (balanced) way so that the resulting signal is the difference between the upper and lower coils. If no sample is put in the upper pick-up coil and if the lower coil is exactly similar to the upper one, the detected signal is equivalent to the noise. This method helps to reduce the effect of external interfering signals (external noise) and is suitable for relatively low operating frequencies [147]. Furthermore, the gradiometric configuration also prevents saturation of the first stage preamplifier. Finally, the system is shielded with few millimeters thick aluminum shielding.

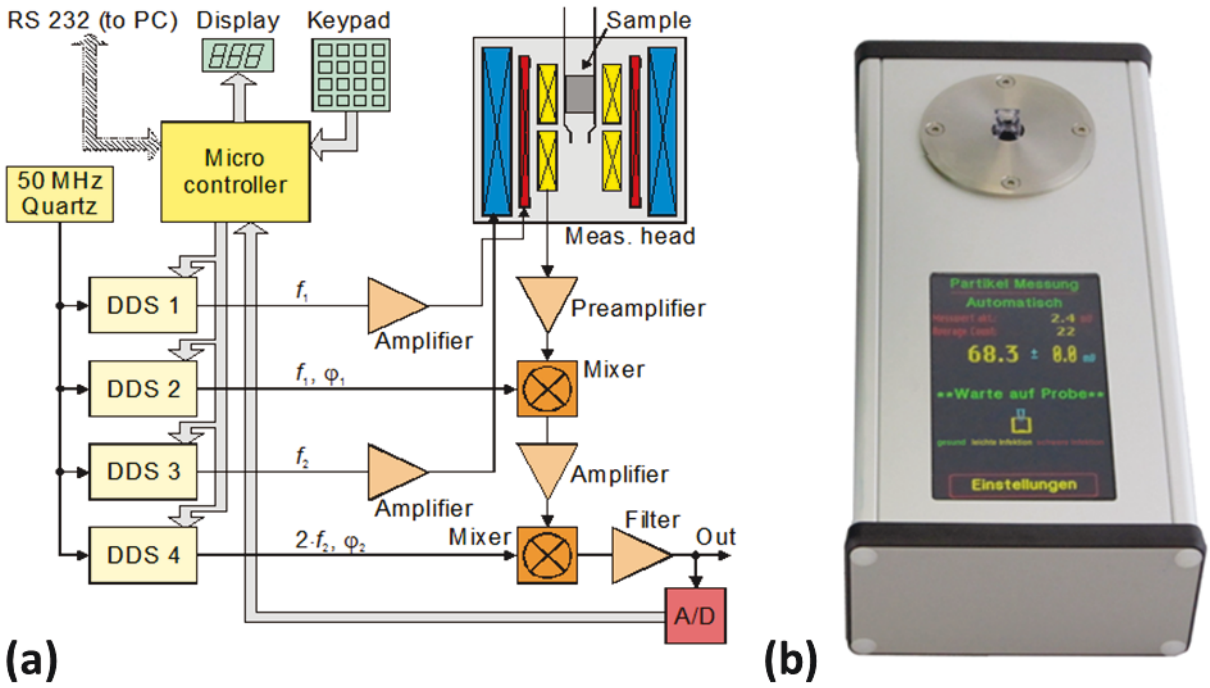

Figure 2-14: Schematic of readout electronics (a) and magnetic reader (b).

Regarding the readout instrumentation, it is used to generate the excitation electrical signal and to demodulate the detected signal at the chosen mixed frequency ($f_1 + 2f_2$). In this example, direct digital synthesizers (DDS) are used to generate the appropriate frequencies from a 50 MHz main signal. Signal are amplified and fed to the measurement head. On the detection side, the signal is firstly pre-amplified using a low noise amplifier and then demodulated at the first and second mixed term frequencies (here f_1 and $2f_2$). The resulting demodulated signal is then converted to a digital signal that transforms the signal into a

readable value (Figure 2-14.a).

Concerning the biosensing aspect, when used for the detection of a certain analyte, the system relies on magnetic sandwich immunoassays (see section 1.3.3), which means that there is a sandwich immunoassay configuration (immunometric, Figure 2-15) used with a magnetic label (SPN). In this macroscopic test, tubes with column filters made of polyethylene are precoated with primary antibodies that bind specifically to the targeted antigen. The experimenter first puts in the biological sample containing the antigen, the antigen fixes to the surface. A second set of biotinylated antibodies is then put in order to bind to the antigen and be a receptor for the label. The labels in this case are SPN; they are coated with a streptavidin layer. Streptavidin has a very high affinity to biotin and binds almost instantly. Washing steps are added in order to prevent nonspecific binding and thus unrelated signal. Finally, the test sample can be put in the reader and the detection proceeds as explained.

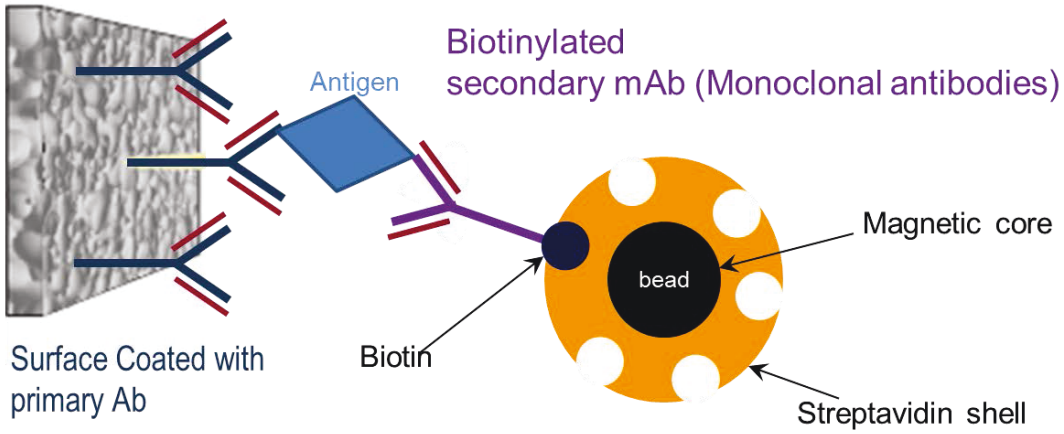

Figure 2-15: Principle of sandwich magnetic immunoassay.

For each assay of analyte, we have to use a curve fit of known concentrations of the antigen so that we can quantify the amount of analyte in a real test. This calibration is necessary in all immunoassays.

As a practical example of the method efficiency, a comparison was made between the ELISA and the proposed method for the detection of the grapevine fanleaf virus (FGLV) [148] . The frequency mixing method has been proved to be more sensitive due to its lower detection limit (6 ng/ml compared to 106 ng/ml for ELISA) with a good coefficient of determination.

Reported detection time is about 30 mins including all washing steps and the volume of sample holder was about 0.4 mL [148].

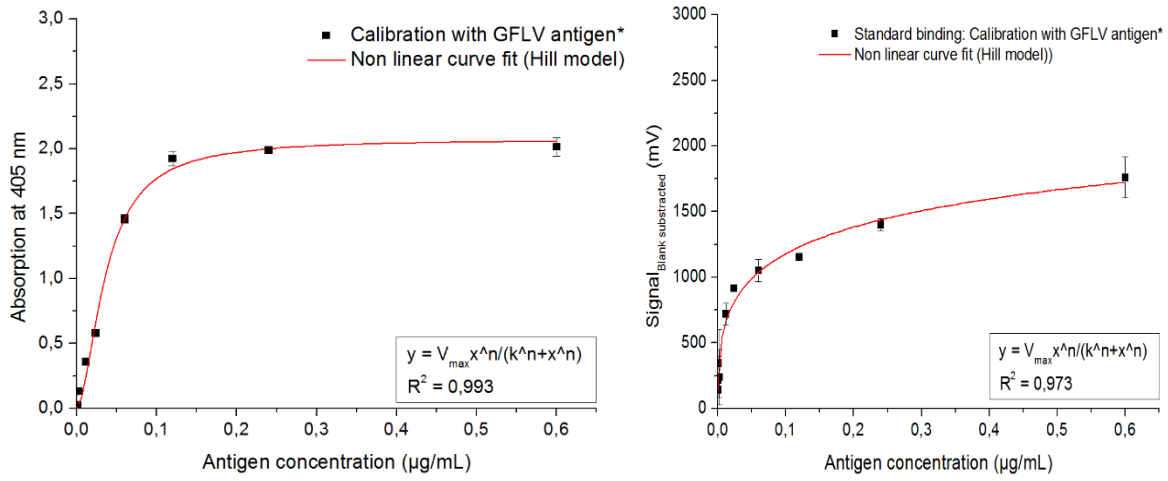

Figure 2-16: Comparison between the ELISA (a) and the frequency mixing method (b) [148].

2.4 Toward miniaturization, prototype concept

The magnetic immunoassays using this frequency mixing technique proved to be very sensitive and robust. That is why it is our method of interest for developing a completely integrated Lab-On-Chip (LoC) pathogen sensing device.

Our main objective in this project is miniaturizing this detection technique because of these comparative advantages:

1. **Faster analysis:** this stems from the shorter reaction time due to microfluidic properties (shorter diffusion distances). This results in minutes of total analysis time (compared to dozens of minutes for the macroscopic system).
2. **Low reagent consumption**: because of very small volumes, LoC systems theoretically consume smaller amounts of reagents, leading to a cost decrease per assay.
3. **Better potential sensitivity**: Because the excitation and detection coils will be put much closer to the sample, better excitation and detection performances are expected.
4. **Better portability**
5. **Possibility for parallel testing (multipathogens):** Because each reservoir will be

miniaturized, the same quantity of analyte in a macrosystem can be divided into multiple micro reservoirs for parallel testing of multiple antigens. The state-of-the-art is well advanced in electronic and microfluidic channels multiplexing, so this multiplexing could theoretically be done without major difficulties.

All these advantages added to the initial advantages of the magnetic detection technique makes the envisioned system a good potential competitor to other major detection techniques (optical and electrochemical). However, as we have seen earlier, miniaturizing a whole system is challenging and requires optimization of each aspect (actuation, detection, flow control, biofunctionalization…etc.).

Therefore, in this early stage of the project, we focus on the miniaturization of the detection system only. It is indeed the main important aspect of a pathogen sensing LoC system. For magnetic frequency mixing detection of magnetic nanoparticles in a microfluidic structure, the detection coils should be adapted to and integrated with the microfluidic chip.

Figure 2-17 shows a possible layout for a first integrated detection system prototype. It comprises embedded excitation and detection coils. We chose flat spiral coils as a first test prototype because flat structures are much easier to miniaturize and fabricate using MEMS and clean room techniques. In order to provide balancing, the system is doubled with a reference side.

Additionally, the sample reservoir is between the coil systems. It must be pre-coated with primary antibodies before using it for immunoassays.

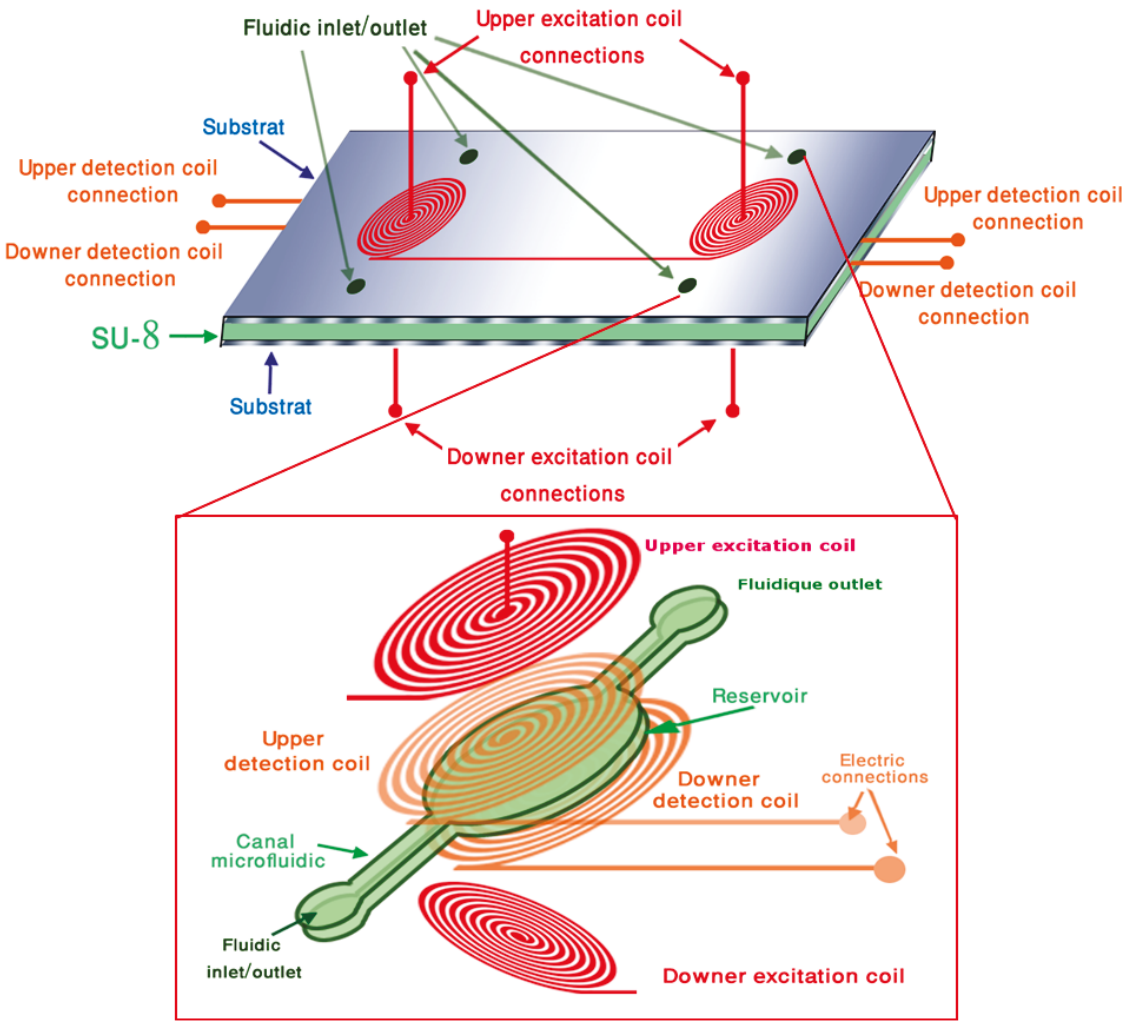

Figure 2-17: Envisioned detection structure. (Top) representation of the sandwich system. (Bottom) Exploded view of the detection side showing detection coils, excitation coils and sample reservoir.

As a first step for miniaturization, we only miniaturized the detection coils using multilayer PCBs. A new measurement head with planar detection coils for planar samples was designed and set up [149] (Figure 2-18, left). As excitation coils, multilayer solenoid coils (macroscopic in size) with several hundred turns were used. The dimensions and number of turns were chosen such that the excitation field is strong enough at the sample location. The measurement coils were realized as planar PCB printed coils with 8 layers of 28 windings each (Figure 2-18, right).

Calculations revealed that the magnetic moment sensitivity of the planar measurement head is $1.69 * 10^{-13}\ A.m^2/\sqrt{Hz}$.This is close to the sensitivity of $4 * 10^{-14}\ A.m^2/\sqrt{Hz}$of the coaxial standard head with 8 mm sample bore [4]. Practical measurements were in good

agreement with these results.

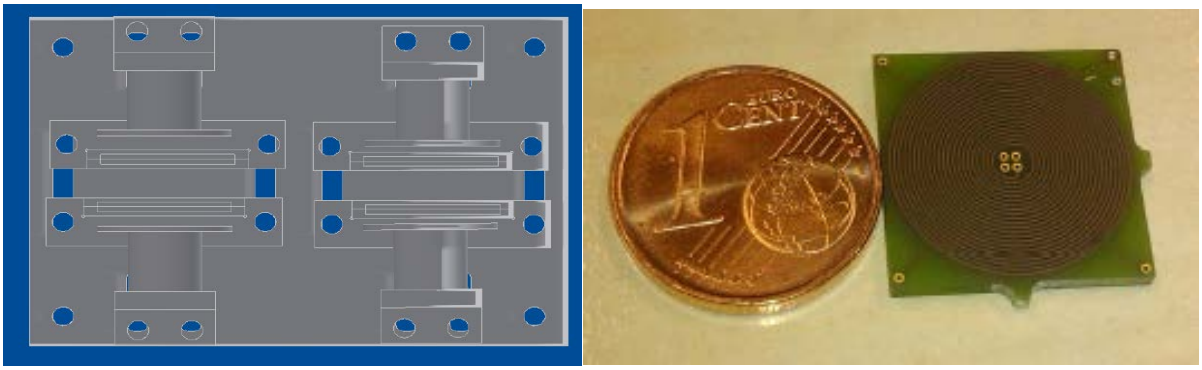

Figure 2-18: Left: cross-sectional scheme of the measurement head for planar samples; right: planar detection coil [149].

We used 20 nm nanoparticles because they yielded stronger signals. These MNPs were manufactured in the PHENIX Lab at UPMC. First measurement results are shown in Figure 2-19. The detection limit was found to be about threefold higher than the minimum quantity of 12 ng of nanoparticles determined with the previous coaxial measurement head [1]. These novel magnetic nanoparticles with 20 nm diameter allow the magnetic immunoquantification to be more precise.

This structure also allowed us to evaluate the accuracy of our analytical calculations about the magnetic excitation field in the case of “pancake” multilayer spiral coil.

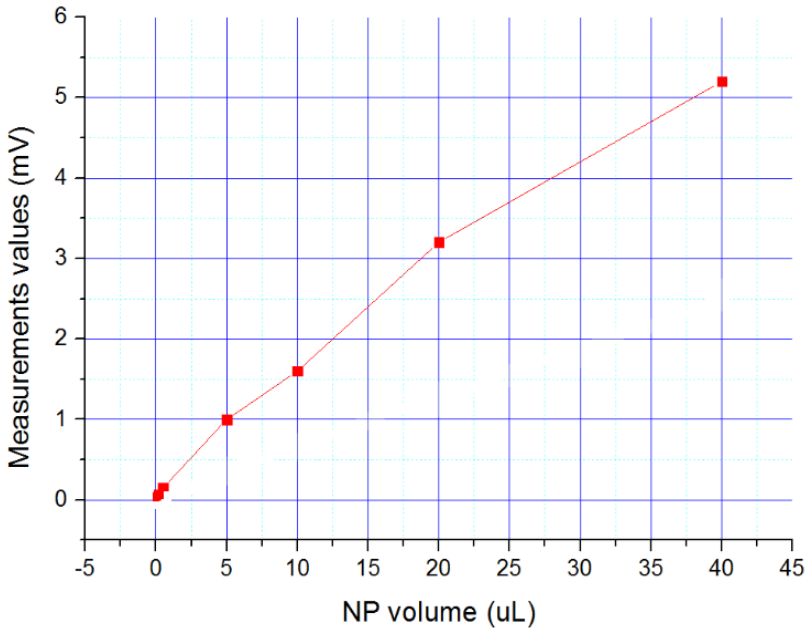

Figure 2-19: Measured frequency mixing signal as a function of the nanoparticle (NP) concentration.

Using both the state-of–the-art and these first validation tests. We identified the following major aspects to be considered for the miniaturization of the magnetic detection system:

a. **Optimization of dimensions and positions of the coils:** Excitation and detection coils could be optimized separately, but the positioning of the coils can only be done through a compromise. The most important coils are the low frequency and the detection coils. Low frequency coils ensure good magnetic response of the SPN and the vicinity of the detection coils ensures good detection sensitivity.
b. **Efficient biofunctionalization:** This is the second most important aspect, even if the magnetic detection system is sensitive. If the biofunctionalization method of the reservoir with antibodies is not chosen wisely, that could lead to false positive results, low sensitivity, and high assay variability. This aspect will be further discussed in the results chapter (chapter 4).
c. **Heat consideration:** Because of relatively high excitation currents and due to the close vicinity of the coils to the reservoir, heat dissipation must be considered. If the reservoir warms too much, that could destroy either the antibodies or the reagent itself; making the quantification much less sensitive.
d. **Homogeneous sample diffusion:** If the sample reservoir is not designed properly, optimal diffusion cannot occur and dead spaces can emerge where no antigen could

possibly reach antibodies within the analysis time. That may be due to big gradient between inlet/outlet and the diameter of the reservoir.

2.5 Chapter summary

In this chapter we described basic concepts of magnetic sensing and explained the theory behind our chosen method of frequency mixing detection. We showed that SPN derive their properties mainly from their size. The blood contains mainly paramagnetic or diamagnetic materials, consequently making the SPN the only 'magnetic' material usable inside the blood sample which makes the background noise very low.

Afterwards, we covered theoretical concepts and experimental aspects of the mixing frequency technique. Its main advantage is that it detects the specific nonlinearity of SPN magnetization response, thus making the technique very specific.

Consequently, the combination of SPN, the mixing frequency technique and the immunoassay advantages provides a very sensitive, easy to use and versatile detection technique.

These performances can be further improved by developing a completely integrated LoC system (analysis time, sensitivity…etc). If all the corresponding aspects are optimized, that could lead to an extremely efficient miniaturized detection system. However, realizing such LoC systems requires multidisciplinary work and there are many challenges to overcome.

In order to tackle these first considerations, we decided to perform both analytical and multiphysics simulations which will be presented in the following chapter. They will allow to optimize and to miniaturize the detection system. The analytical and multiphysics simulations will then be validated using a first realized prototype.

Chapter 3. Optimization of the detection structure through analytical and multiphysics simulations

This chapter discusses the optimization, design and realization of the first prototype of the LoC. In order to design this prototype, we developed a set of tools that allow us to optimize the structure dimensions. The structure is composed of two main parts, the electromagnetic parts with excitation and detection coils and the microfluidic part with microchannels.

In the first part of this chapter, we focus on the magnetic detection part. As stated in chapter 2, two magnetic excitation signals with distinct frequencies are used and the amplitude of the mixing frequency terms ($f_1 + 2f_2$) is measured to detect and quantify the amount of SPN [1].

For sensitive magnetic field detection, the detection system is optimized by taking into account the pick-up (detection) and excitation coils optimization for sensitive detection and efficient magnetization. Furthermore, practical aspects like heating effects have been considered as they can cause substantial damage to the biological samples and endanger the detection. Heating can also cause both a decrease and fluctuation in the detected signal since the magnetization of the SPN is dependent on the temperature. Consequently, compromises have to be made in order to get a sensitive miniaturized detection system.

Here, we propose to use simple planar coils for precise detection of magnetic nanoparticles in a miniaturized system. We lay out a magnetic sensing miniaturization scheme comprised of analytical calculations and simulations.

In the second part of this chapter, we validate the analytical calculations with a realized prototype based on planar multilayer excitation and detection coils in a Printed Circuit Board (PCB) on both sides of a PDMS microfluidic structure. We describe the details about the design and realization of the structure and our chosen dimensions for both the electromagnetic and microfluidic parts. . Additionally, we will present the characterization results and the comparison between calculated and measured properties.

3.1 Analytical calculations

The goal of these analytical calculations is to optimize the dimensions of the different coils. Especially, good sensitivity and appropriate magnetization of the SPN constitute our prime interest. For these calculations, flat spiral air cored coils are used.

Air cored pick up coils are used in many applications, including industrial, geophysical and biomedical applications. Their size range is between millimeters and hundreds of meters [150]. Recent advances in microelectromechanical systems (MEMS) design and microfabrication allow the design of miniaturized micro-coils. However, finding the optimal dimensions of a miniaturized coil is still challenging; the fabrication method, the practical distance from coil to sample and the area of detection are different factors that give an upper and lower dimension limit of the desired coil.

In the case of clean room fabrication, we are mostly restricted to 3D coils consisting of stacked planar coils. Thus, our calculations are restricted to planar spiral coils. These shapes are chosen due to their symmetry and the fact that they are relatively easy to calculate. Other shapes do not offer notably advantageous performance.

3.1.1 Electrical parameters calculations

An air cored inductance coil might be modeled using the RLC equivalent electrical circuit representation illustrated in Figure 3-1:

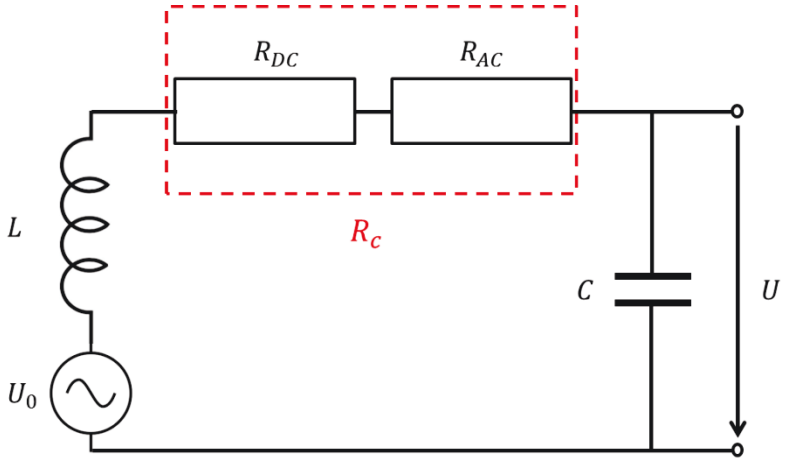

Figure 3-1: Equivalent electrical circuit diagram of an air cored inductance coil.

An ideal coil is only composed of the inductance L. However, in the real case, other effects

are represented by the presence of a resistance (losses) and a parasitic capacitance.

Resistance:

The resistance, R_c, represents the total loss. It can be divided into two parts: the direct current (DC) and alternating current (AC) resistances:

$$R_C = R_{DC} + R_{Skin} + R_{proximity} \cong R_{DC} \qquad 3\text{-}1$$

The skin and proximity effects represent the causes of the AC resistance. Skin effect represents the tendency of the current density to be larger near the surface of the conductor and decreases inside the conductor (more depth). So the current flows mainly in the skin depth of the conductor. Skin depth increases with the frequency and can be calculated by:

$$\delta = \sqrt{\frac{\rho}{\pi f \mu}} \qquad 3\text{-}2$$

In this project, our maximum operating frequency is around 200 kHz; the skin depth is then approximately 150 µm in case of copper. In the case of a miniaturized coil, the wire cross sectional diameter is smaller than 100 µm so the skin effect is negligible. Proximity effects represent the tendency of a current to flow in other directions. When a current flows into one wire it generates a proximity magnetic field that disturbs the current flowing in adjacent wires by causing circulating currents. The result is that the current is more located in areas far from nearby conductors carrying same direction currents. Hence, the resistance is increased. Proximity resistance increases with the frequency and is related to the skin depth.

Literature shows that proximity effects are negligible if the radius of the conductor is smaller or of the same order of the skin depth [151]. After measurement in the laboratory on PCB coils it was found that AC effects account for less than 20% of the resistance for frequencies below 100 kHz.

Only the DC resistance is taken into account for the next calculations. However, if accuracy is needed, the AC effects have to be taken into account, especially for operating frequencies above 100 kHz (see [152] for more complete formula).

R_{DC} can be approximated by the following common formula:

$$R_{DC} = \frac{\rho l}{A} \quad 3\text{-}3$$

where ρ is the material resistivity, $l\ and\ A$ are the length and cross section area of the wire, respectively. The geometry of a spiral coil can be approximated by a sum of multiple semi circles of increasing radii following an arithmetical sequence. The total length of a one layer spiral coil with equal wire width and inter-turn spacing is:

$$l = 2\pi N(R_{in} + W(N-1)) \quad 3\text{-}4$$

where R_{in} is the inner diameter, $W\ is$ the wire width and inter wire spacing and N is the number of turns per layer.

Inductance:

In order to approximate the value of inductance, we used the methodology given in [153]. The inductance of a multilayer spiral coil can be approximated by first calculating first the single layer inductance:

$$L_s = \frac{\mu_0 N^2 D_{Avg} C_1}{2}\left(\ln\left(\frac{C_2}{F_r}\right) + C_3 F_r + C_4 F_r^2\right) \quad 3\text{-}5$$

with F_r is the filling factor, C_1, C_2, C_3 are factors depending on the layout and D_{Avg} is the average diameter:

$$D_{Avg} = \frac{D_{out} + D_{in}}{2} \quad 3\text{-}6$$

In the case of a spiral layout, the coefficients are:

$$C_1 = 1, C_2 = 2.46, C_3 = 0, C_4 = 0.2$$

Next, we have to calculate the coupling factor between each two layers:

$$K_{C_i} = \frac{N^2}{(AX^3 + BX^2 + CX + D) * (1.67N^2 - 5.84N + 65) * 0.64} \quad 3\text{-}7$$

where X_i is the distance between the corresponding layers in millimiter. The distance between

two adjacent layers is called Δh. Consequently $X_i = i * \Delta h$

A, B, C, D are geometry dependent coefficients, for the case of spiral coils their value is :*A*=0.184, *B*=-0.525, *C*=1.038, *D*=1.001.

Since the layers are all the same and the distance between layers is equal,the total inductance is then approximated using this formula (here for an 8-layer coil):

$$L_{Tot} = 8L_s + 2(7K_{c1} + 6K_{c2} + 5K_{c3} + 4K_{c4} + 3K_{c5} + 2K_{c6} + K_{c7}) \qquad 3\text{-}8$$

Practical measurements of an existing 8-layer spiral coil (depicted in Figure 2-18) were made to test the accuracy of the formula. Table 3-1depicts these values.

8-layers spiral coils	**Calculated inductance (μH)**	**Measured inductance (μH)**	**Error**
16 mm sensor	152	160	**5%**
20 mm sensor	330	350	**5.7%**

Table 3-1: Validation of the inductance formula for two different diameters of 8-layers spiral coils

We can see that the difference between the calculated and the measured values does not exceed 6 %, which is an acceptable value for our optimization measurements.

Capacitance:

The lumped capacitance represents the capacitance between adjacent turns and between layers. It stems from the gradient potential between these areas. The capacitance causes an unwanted self-resonance of the coil and is directly related to the dielectric losses. The goal is then to minimize this capacitance. Calculating the value of the capacitance is very complex. However there are a few techniques that could help to have an expected reduction in the capacitance. In our case of multilayer spiral coils, we could use two suggested strategies from [154]; first we can reduce the capacitance by increasing the number of layers which is similar to having a serial connection of capacitances. Second, we can shift the wires between each two adjacent layers so that the wire on the upper layer is not directly parallel to the one in the lower layer. This latter method reduces the interlayer capacitance. In this work, we tried to implement both

methods in order to reduce the overall capacitance. Comparison for the implementation of the second method is presented in the last section (see section 3.3.1).

3.1.2 Magnetic detection coils

The two main parameters of a pick-up coil are: sensitivity and noise. From these parameters, the physical limits in terms of minimum detectable magnetic moment and magnetic moment sensitivity will be deduced.

3.1.2.1 Sensitivity

The sensitivity of a coil with respect to detecting nanoparticles is defined here as the ratio of the induced voltage to the magnetic moment that causes it:

$$S_{sensor} = \frac{U_{ind}(Z)}{m_z}[\frac{V}{Am^2}] \quad 3\text{-}9$$

where $m_z = m_0 \times \sin(2\pi ft)$ is the total magnetic moment of all SPN. This approximation is valid because each SPN is a single domain particle and all the nanoparticles exhibit the same magnetization response in both amplitude and direction when subjected to the same magnetic excitation field.

The induced voltage caused by m_z, that is from a distance Z to a single loop of radius R, can be expressed as:

$$U_{(z,t)} = -\frac{d\Phi}{dt} = \frac{1}{2R}\frac{\mu_0}{(r^2+z^2)^{\frac{3}{2}}} \times \frac{dm_z}{dt}(V) \quad 3\text{-}10$$

where $r = \frac{R}{R_1}, z = \frac{Z}{R_1}$ are the dimensionless parameters relative to the internal radius of the spiral coil.

Integrating over the width of the spiral coil gives the result in the form of:

$$U_{\text{ind}} = \frac{N}{w}\int_1^{1+w} U(z,t)dw = m_z\mu_0 2\pi f \frac{N}{2R_1} \times G(z,w)\ (V) \quad 3\text{-}11$$

with $G(z,w)$, the geometrical function representing the effect of the pick-up coil dimensions:

$$G(z,w)=\frac{1}{w}\left[\frac{1}{\sqrt{1+z^2}}-\frac{1+w}{\sqrt{(1+w)^2+z^2}}+\ln\left(\frac{1+w+\sqrt{(1+w)^2+z^2}}{1+\sqrt{1+z^2}}\right)\right] \quad 3\text{-}12$$

From this, we can easily deduce the total sensitivity forN_l layers as:

$$S_{sensor}=\mu_0 2\pi f\frac{N}{2R_1}\times\sum_{i=1}^{N_l}G(z_i,w)\left(\frac{V}{Am^2}\right) \quad 3\text{-}13$$

Here, $z_i$denotes the distance of each spiral layer to the magnetic moment (sample location).

Finally,we deduce that the sensitivity is greater when the frequency is bigger. In fact, the maximum excitation frequency that we can use is limited by two factors: the relaxation time of the SPN and the complexity of generating relatively high currents for the resulting high frequency impedance.

3.1.2.2 Noise considerations

With regard to noise, the aim is to approach the minimum detectable magnetic moment that is defined by the moment that can be detected when noise and signal become equal ($SNR=1$). Since it takes into account the first preamplifier stage, this measurable value is used to compare the efficiency of various sensors with respect to detecting magnetic beads.

Generally, a detection system includes a preamplification stage, a damping resistance (R_p) and a parallel capacitance (C_p). A coil can be represented electrically by its lumped parameters: InductanceL_s, an AC resistance R_s and a parallel capacitanceC_S. As stated in [1], the total noise voltage can be estimated:

$$U_N=\sqrt{U_{thermN}^2+U_{VNoise}^2+U_{CurN}^2} \quad 3\text{-}14$$

The noise voltage is thus composed of three different terms:

1. Thermal noise: $U_{thermN}=\sqrt{4k_bTR_s}$.
2. Voltage noise: $U_{VNoise}=\frac{U_a}{|TF(f)|}$ with $TF(f)$ the transfer function of the circuit
   a. $TF(f)=\frac{1}{1-\frac{f^2}{f_R^2}+\frac{i2Df}{f_R}}$ with $D=\frac{R_S}{2}\sqrt{\frac{C_S}{L_S}}$ the damping factor and $f_R=\frac{1}{2\pi\sqrt{L_SC_S}}$ the resonance frequency.

3. Current noise: $U_{CurN} = |R_s + i2\pi f L_s| \cdot \sqrt{\left(\frac{4k_B T}{R_P} + I_a^2\right)} \cong I_a |R_s + i2\pi f L_s|$ (R_p is supposed very big so its contribution can be neglected, see [1] for more detail)

U_a and I_a are the voltage and current noise of the preamplifier, respectively. $TF(f)$ is the transfer function of the detection circuit.

We can express this noise magnetically by the corresponding magnetic flux noise densityB_N. It can be deduced by multiplying the total noise voltage by the overall coil sensitivity:

$$B_N \cong \frac{2}{\pi^2 N_l N \times (2R_1 + H)^2 f} U_N \ [T] \qquad 3\text{-}15$$

Magnetic noise is then proportional to the voltage noise. As an example and in order to visualize and assess the contribution effects of thermal, current and voltage noise components, we plotted these contributions in the case of our PCB coils with respect to frequency in Figure 3-2.

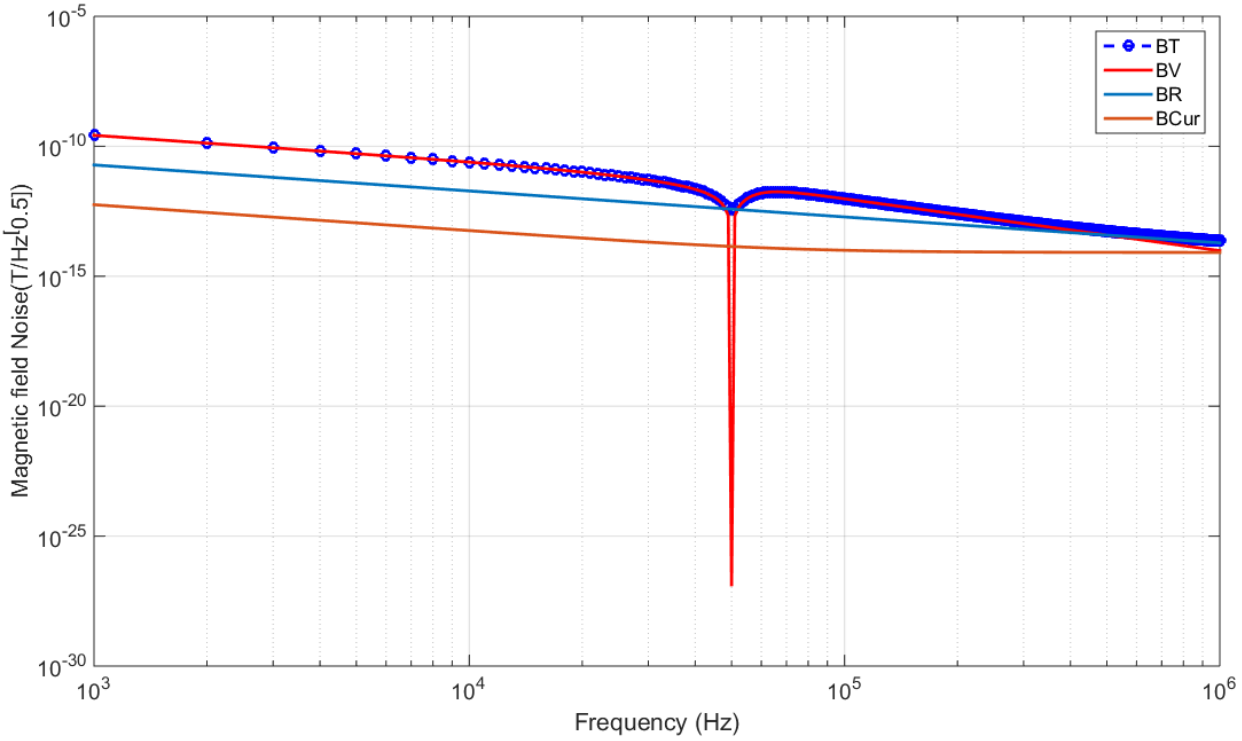

Figure 3-2: Magnetic field noise components effect with respect to frequency. Inner radius is fixed to 0.8 mm. BT: Total noise, BV: voltage noise, BR: resistance noise, BCur: current noise

These values were plotted by supposing a typical low noise preamplifier (AD745) and an approximated capacitance noise. Because of this latter approximation, the resonance effect

should not be taken into account.

We can see that the total magnetic field noise (B_T)exhibits a dependence that follows the voltage noise (for a given outer radius value). However, the minimum noise value is limited by the thermal noise, which is relative to the resistance of the coil.

All the electrical parameters should be optimized so that the Johnson noise (thermal) is dominant, so that only the sensor noise is left. Consequently, the sensor coil should be optimized to have maximum sensitivity with minimum resistance and inductance values. A high inductance value will result in a high current noise contribution. Also, since the resistance and frequency values are quite low, the choice of the preamplifier should be more on a device that has a very low voltage noise. The importance given on the voltage noise value is illustrated in the given example where the current noise is rather negligible comparing to other sources.

Two values of interest can be deduced from this; the signal to noise ratio (SNR) and the minimum detectable magnetic moment.

3.1.2.3 SNR and minimum detectable moment

In the case where the choice of readout electronics is correctly done, we can suppose that the SNR is the ratio of the detected signal versus the thermal noise: $U_N = \sqrt{4k_B T R_S}$. Consequently:

$$U_N = 4\sqrt{\frac{\rho\pi k_B T}{H_{wire}}} \times \frac{\sqrt{1+\frac{w}{2}}}{\sqrt{w}} \left[\frac{V}{\sqrt{Hz}}\right] \qquad 3\text{-}16$$

with ρ, k_B, T, H_{wire} denoting the resistivity, Boltzmann constant, absolute temperature and height of wire section, respectively. The SNR is then:

$$SNR = \frac{U_{ind}}{\sqrt{2}U_N} = m_z \frac{\mu_0\sqrt{\pi}}{4\sqrt{\rho k_B T}} f \times \left[\frac{\sqrt{H_{wire}}}{R_1} \times \frac{\sum_{i=1}^{N_l} G(z_i, w)}{N_l\sqrt{w}\sqrt{1+\frac{w}{2}}}\right] \qquad 3\text{-}17$$

Whereas SNR is directly observed and is related to the geometry of the coil, to the frequency and to the physical parameters, the minimum detectable moment gives a physical limit that

can be linked to the amount and concentration of a given amount of nanoparticles. A chosen indicative absolute limit of this value is when the SNR is equal to 1 (or 0 dB).

$$\frac{m_z}{\sqrt{\Delta f}} = \frac{4\sqrt{\rho k_B T}_0}{\mu_0\sqrt{\pi}} \frac{1}{f}\left[\frac{R_1}{\sqrt{H_{wire}}} \times \frac{N_l\sqrt{w}\sqrt{1+\frac{w}{2}}}{\sum_{i=1}^{N_l} G(z_i, w)}\right] (\frac{Am^2}{\sqrt{Hz}}) \quad 3\text{-}18$$

Consequently, smaller magnetic moments can be detected if higher frequencies and a smaller internal radius are used. Also, the coil should be put as close as possible to the sample reservoir in order to increase the sensitivity to smaller magnetic moments.

3.1.2.4 Optimization of detection coil dimensions: PCB coils design

The dimension of the pick-up coil is optimized by finding a compromise between sensitivity and minimum noise. For this optimization, the different limitations imposed by each fabrication procedure have to be taken into account. If we take as an example the printed circuit board technology, each manufacturer has a set of limitations concerning the cross section of the wire, the isolation between two adjacent wires and the total thickness of the board.

Next, we provide an example of one early realized prototype and how the choice was made between two manufacturers.

Table 3-2gives the technical limitations of each manufacturer.

Manufacturer	Smallest width of copper/Isolation(µm)	Thickness of copper (µm)	Total thickness of an 8-layer PCB (mm)
M1	100	35	1.55
M2	50	09	> 2

Table 3-2: Technical limitations of two chosen PCB manufacturers

Induced sensitivity and minimum detectable magnetic moments can be used jointly to assess the performance of any given coil. Figure 3-3shows the best sensing characteristics that we can get by applying PCB restrictions on copper section, interlayer distances and minimal practical internal radius. For this particular chosen manufacturer, copper section is equal to $35\mu m \times 100\mu m$ and inner radius is at a minimum of $0.8\,mm$. The calculation was done for a four-layer PCB coil.

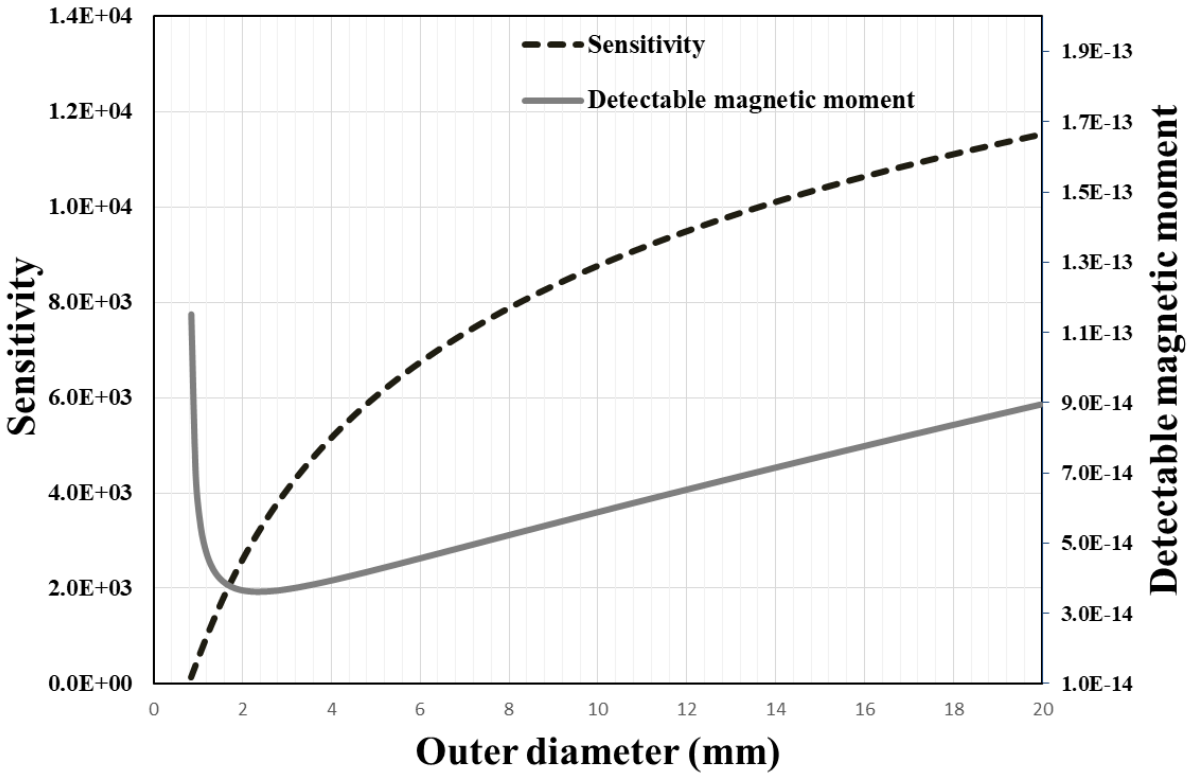

Figure 3-3:Pick-up coil optimization with sensitivity and minimum detectable moment versus coil outer radius. Internal radius fixed at 0.8 mm.

As we can see, for an outer radius ($R_{out} > 4\,mm$) there is an area where the added noise due to increasing number of turns becomes predominant with regard to the improvement of sensitivity.

In the following, we show an example of two possible detection coils fabricated using printed circuit board (PCB) technology. Each example is from a different PCB manufacturer.

Comparing the two graphs in Figure 3-4, we see that M1 yields the better compromise because it presents much less noise than M2 with similar results in sensitivity. For example, we can see that the best sensitivity in this case is about $10^4\ V/Am^2$, which is close to the aimed sensitivity of the previous macroscopic mixing frequency detection system. ($2.36\ 10^4\ V/Am^2$).

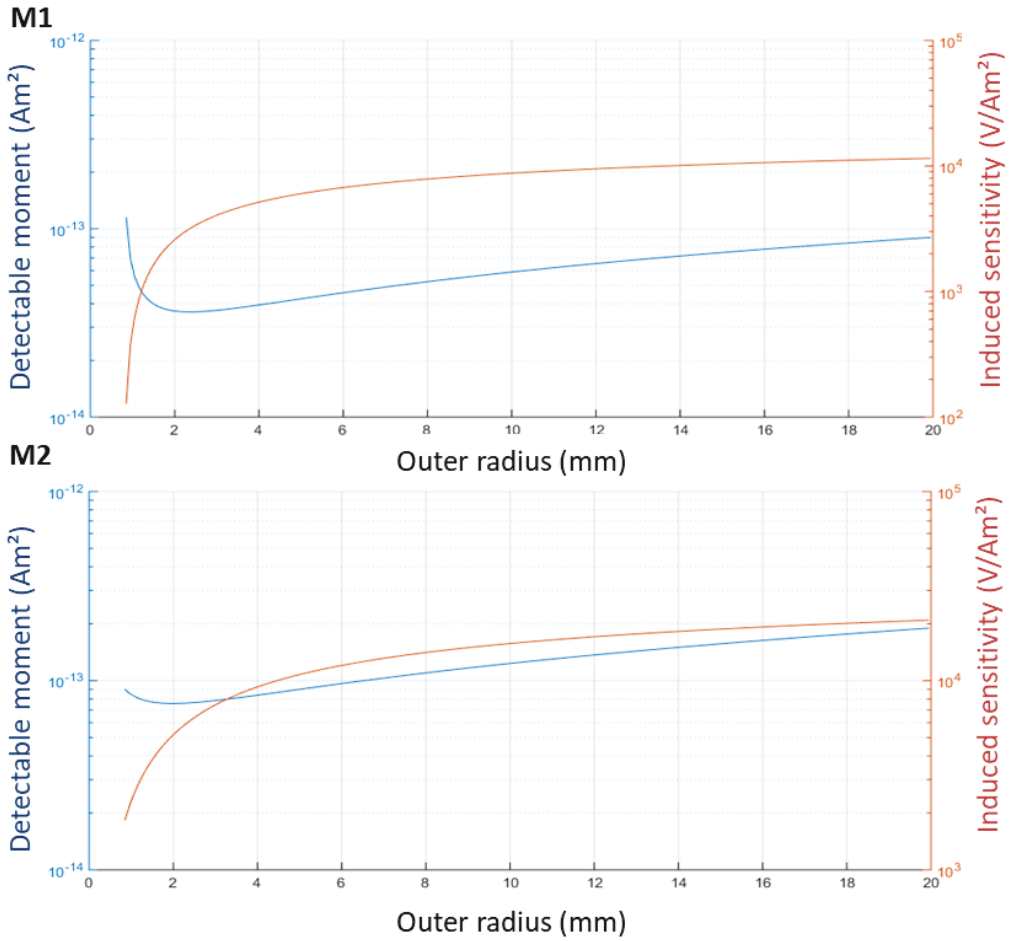

Figure 3-4: Sensitivity and detectable magnetic moment with respect to outer radius for two different manufacturers.

Moreover, the achievable value of the smallest detectable magnetic moment, is about $10^{-13}Am^2$ and if we suppose a single particle magnetic moment of about $10^{-18}Am^2$, we can estimate that 10^5 particles can be detected which correspond to about $10ng/mL$of detectable iron concentration which is 100 times better in theory than the previous macroscopic reader realized in Juelich.

Performance in terms of noise can further be assessed by evaluating the noise contribution of the different components with the two manufacturers' dimensional limitations. Thus, comparison between the two manufacturers in terms of the magnetic noise is given in figure 3-5. The manufacturer M2 gives slightly better results than M1.

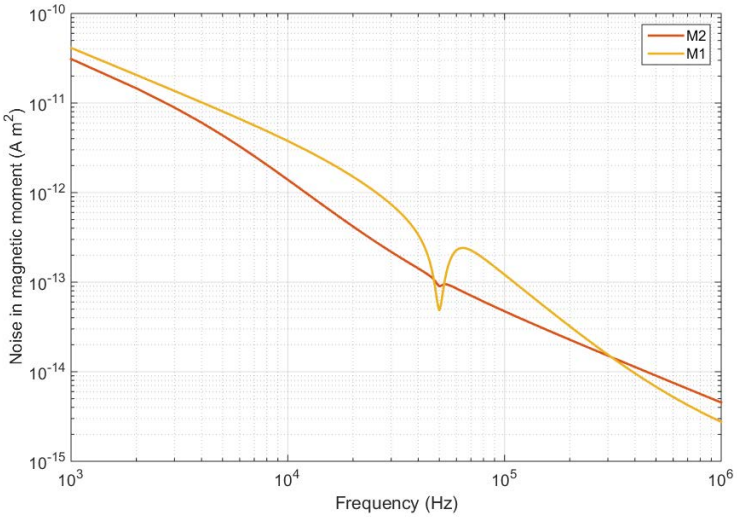

Figure 3-5: Smallest detectable magnetic moment versus frequency [155].

M1 and M2 are also compared with respect to outer radius (Figure 3-6).

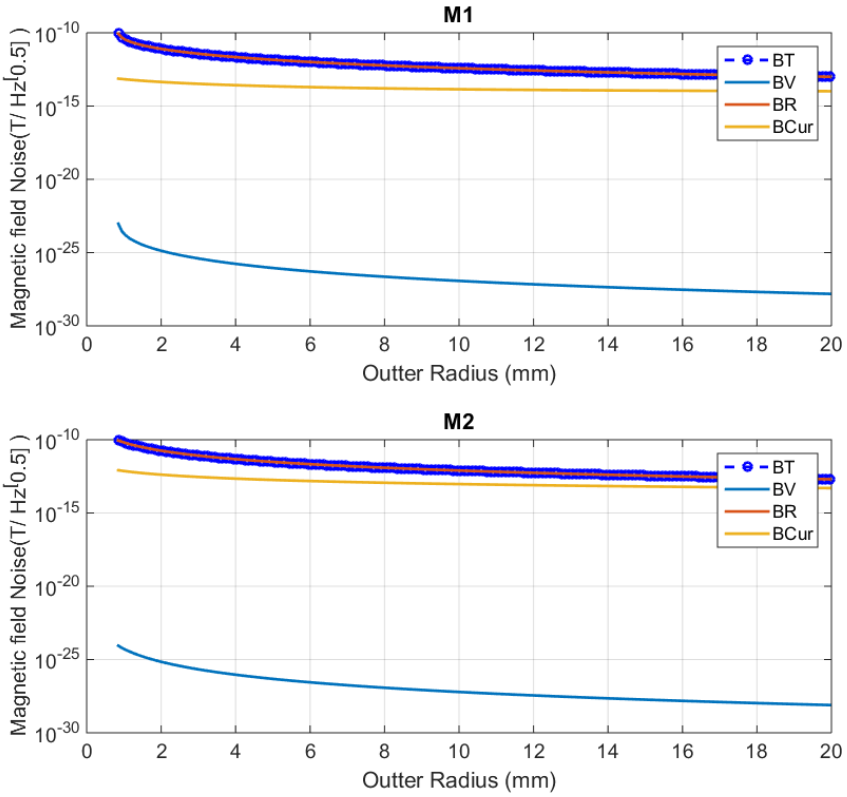

Figure 3-6: Magnetic noise with respect to outer radius for two manufacturers for a frequency of 50 kHz. Inner radius is fixed to 0.8 mm. BT: Total noise, BV: voltage noise, BR: resistance noise, BCur: current noise.

We see that for this given frequency of 50 kHz, the voltage noise is negligible and thus the main contributing factor is the resistance noise. In this case, M1 technology specifications

give better results and the curve of total noise field follows almost exactly the curve of the thermal noise field.

Finally, a compromise is made between the performance of detection coil and excitation coil along with the simulation aspect in order to select a good choice of dimensions. Table 3-3 gives one of the three choices of dimensions we made for PCB prototype made by manufacturer M1.

Type of coil	**Manufacturer**	**Inner radius (mm)**	**Outer radius (mm)**	**Number of turns**	**Number of layers**	**Calculated Sensitivity V/Am^2**
Pick-up coil	M1	0.8	10	59	4	10^4

Table 3-3: Example of chosen parameters for detection coil of the manufacturer M1.

These tools can be used to optimize the dimensions of pick up coils in the case of micro structure. Only the technological restrictions of the microfabrication technology in clean room must be taken into account before optimization. The choice of a fabrication method also leads to different limitations regarding the distance from the sample to the detection coil.

3.1.3 Magnetic excitation coils

Pick up coil optimization should be done in conjunction with excitation coils. Magnetic excitation of SPN is of high interest. In fact, the actual limit of detection in terms of number of SPN can be smaller than expected if the SPN are not properly magnetized.

Since the magnetic frequency mixing technique relies on the detection of the nonlinear response of SPN, the magnetic field amplitude should be adapted in consequence. As can be seen in Figure 3-7, a minimum magnetization point has to be reached so that the nonlinearity (represented in red) is sufficiently apparent, hence making the nonlinear response more significant. If the excitation field is too low, the response (in green) may just resemble a paramagnetic (linear) response and the mixed term amplitude would be too small.

As explained in [1], the low frequency field (f_2) is used as a drive field and the high

frequency field (f_1) is used as an excitation amplitude. For the case of relatively small magnetic fields, the amplitude of the mixed frequency term is proportional to the high frequency amplitude and to the square of the low frequency amplitude.

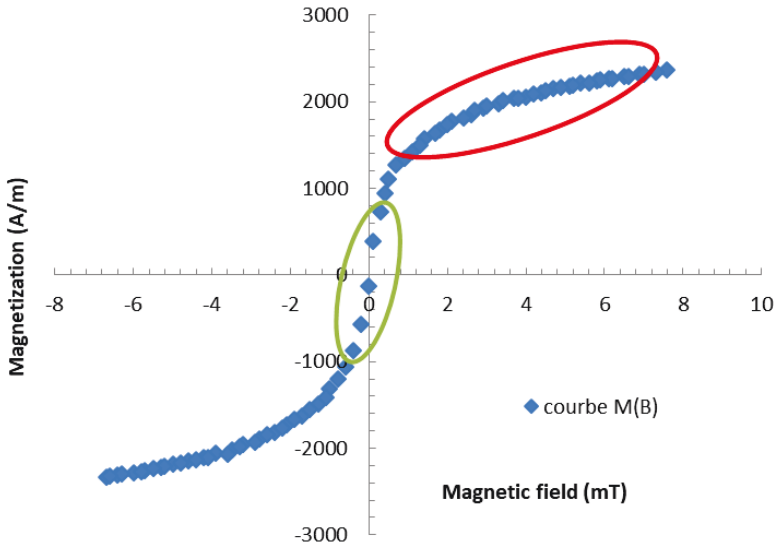

Figure 3-7: Representation on linear (green) and nonlinear (red) sections of the magnetization curve of SPN. Diameter is about 20 nm.

Because of this, emphasis on minimum required amplitude is directed to low frequency excitation, whereas for high frequency excitation, the frequency of use contributes more to the optimization of the system. For example, for 20 nm nanoparticles, we used 2 mT as drive amplitude and around half of it as excitation amplitude.

Also, if the low frequency magnetic field is not strong enough, we may be situated in the 'linear' part of the magnetization curve which would lead to poor nonlinear results.

3.1.3.1 Magnetic excitation field

Using the generated magnetic field from single turn circular coils, we sum the effect of the different radii to get the magnetic field density generated on the symmetry axis of the spiral coil:

$$B_z(z_i) = \frac{\mu_0 * N * I_{exc}}{2 * R_1} \times \sum_{i=1}^{i=N_l} G(z_i, h) \ [T] \qquad 3\text{-}19$$

where I_{exc} is the excitation current, N is the number of turns , R_I is the internal radius, G is the geometrical function and N_l is the number of layers. The formula is then used to find the minimum excitation current. The distribution of magnetic field should be rather homogeneous along the radial dimension of the reservoir in order to achieve a homogeneous sensitivity distribution. This assumption was confirmed by electrical simulations of the magnetic field generated by a spiral coil using COMSOL Multiphysics (see section 3.2.1). The homogeneity of the field depends on the inside and outside radius and on the distance of the reservoir from the center of the spiral coil. In order to get a proper magnetization of SPN for a fixed distance Z, we obtain the appropriate distance that a reservoir should be at and we deduce the maximum area that it can occupy.

The number of turns, N, helps to reduce the minimum required current, however, the added value of the external turns becomes negative after a certain threshold, where the number of turns increase the resistance and inductance in a linear and quadratic manner, respectively. This leads to a decrease in the resulting current because of their low contribution to the generated magnetic field.

In order to validate the analytical formula, 8-layer PCB coils of 16 and 20mm outer diameters were realized and their axial calculated and measured magnetic fields were compared. The measurements were done using a Gaussmeter (GM08) and a DC current and the comparion with calculated results is shown in Table 3-4.

8 mm PCB test coils	DC current $I_{exc}(A)$	Measured magnetic field $B_{meas}(mT)$	Calculated magnetic field $B_{theory}(mT)$	Error
$R_{out} = 16mm$	0.4	2.60	2.61	0.3%
$R_{out} = 20mm$	0.4	3.95	3.80	5%
2 stacked 20 mm sensors	0.2	3.00	3.07	2.3%

Table 3-4: Validation of the axial magnetic field formula at a distance from sampel of Z=3.3mm.

The measured magnetic field corresponds to the analytical calculations and thus the calculations are validated and can be used for the optimization of the excitation coils.

3.1.3.2 Optimization methodology of excitation coils dimensions

Excitation coils should be optimized in order to get the required magnetic field intensity in the

sample area. For this optimization, the different limitations imposed by each fabrication procedure have to be taken into account. If we take as an example printed circuit board technology, each manufacturer has a set of limitations concerning the thickness and cross section of the trace, isolation between two adjacent traces and total thickness of the board.

As with detection coils, we will provide an example of one early realized prototype and how the choice was made between two manufacturers.

While considering the technical limitation of each manufacturer (Table 3-2), the final choice is based on the calculations of the magnetic field, the total resistance and the heating power consumption.

Next, we plot the axial magnetic field intensity with respect to the vertical distance from the excitation coil center (Figure 3-8). This distance represents the prospective sample location.

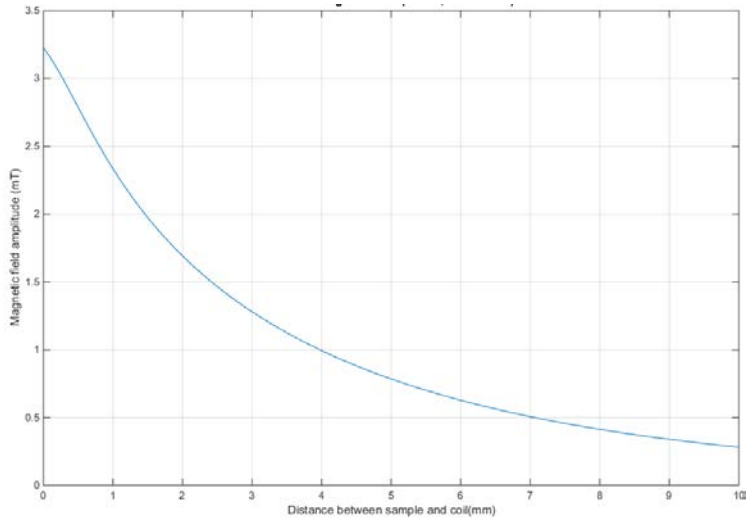

Figure 3-8: Axial excitation magnetic field with respect to the distance from the coil.

As can be shown, the magnetic field drops quickly with the distance from the coil to the sample which is an important parameter for having a good detection structure. For example, if the sample is put at $1mm$ instead of direct contact, a different excitation magnetic field of about $0.9mT$is obtained which is a huge difference because a magnetic field of about $3mT$ for a good non-linear response of the nanoparticles is required. This constitutes one of the main drawbacks of M2 manufacturer since it already puts the outer coil layers 0.6 mm away from the sample, as compared to M1.

After analyzing the behavior of the magnetic field, its intensity, the total impedance and the generated heating power in the case of the two coils are compared in Figure 3-9 by considering the technological limitations. The desired magnetic field as well as a minimum threshold of the heating power are also indicated in this figure.

As we can see, the second manufacturer M2 gives a bigger magnetic excitation field for smaller values of external radiuses. This is because for manufacturer M2 the Isolation/copper width is $50\mu m$, two times less than that for M1.

However, the total impedance of the coil is 10 times bigger for M2 than for M1, which leads to a rapid increase in the heating effect and a more difficult electronic excitation circuit, because the impedance values of M2 are not adapted to common amplifier circuits.

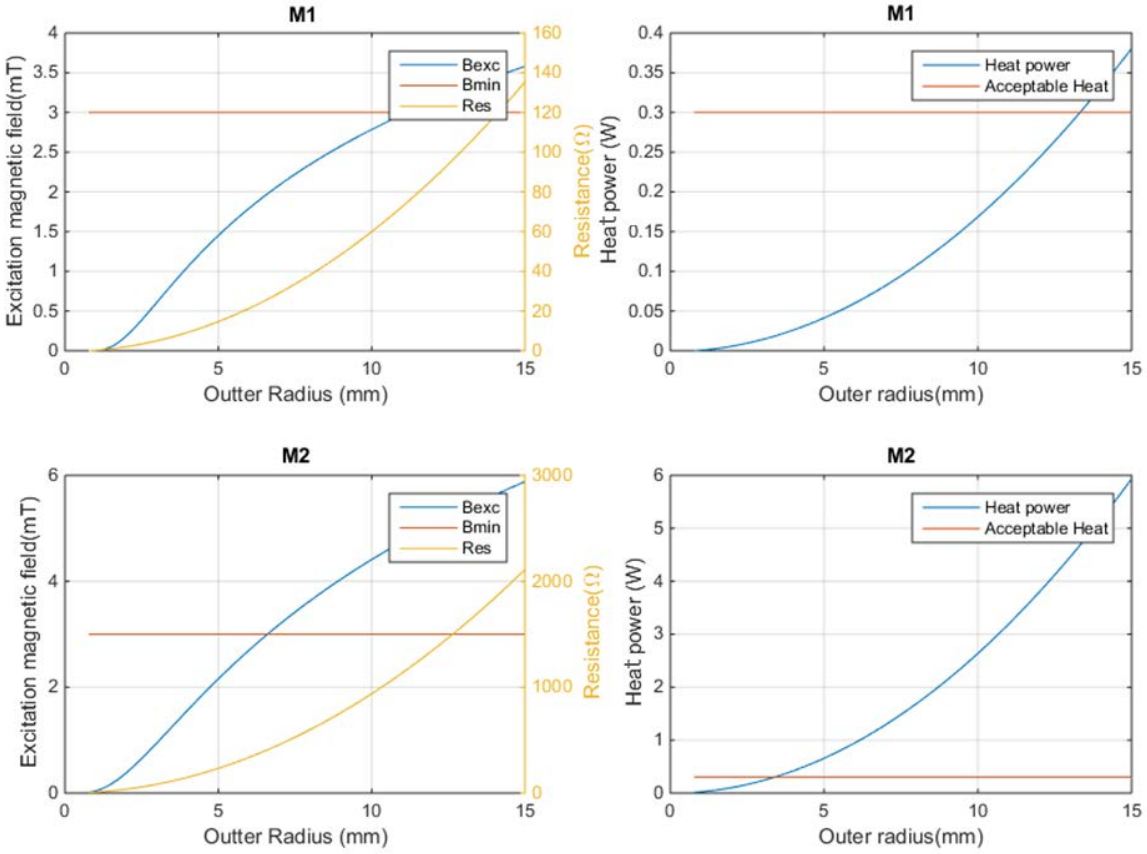

Figure 3-9: Excitation coil properties for two different manufacturers M1 and M2.

Since the low frequency magnetic field amplitude is very important for the magnetization response of the nanoparticles, the magnetic field in the case of using two low frequency excitation coils is calculated and shown in Figure 3-10.

Using two coils, the minimum required outer radius and the applied current in the sensor could be reduced, leading to lower power consumption, lower heating power and thus no heating problem in the reservoir.

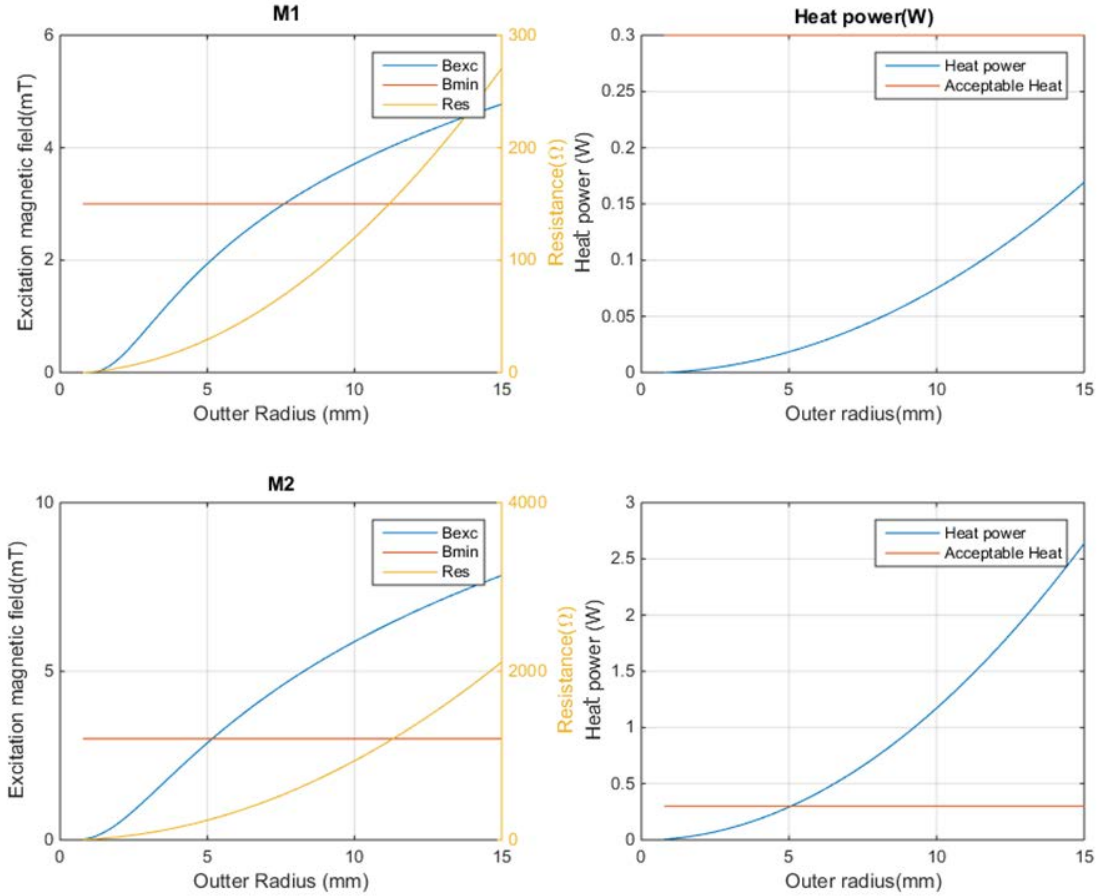

Figure 3-10: Effect of using two excitation coils for the two manufacturer.

Finally, after using the same methodology for the high frequency excitation and comparing the different performances of each manufacturer, the first manufacturer is chosen with the dimensions in Table 3-5:

Type of coil	**Manufacturer**	**Inner radius(mm)**	**Outer radius(mm)**	**Number of turns**	**Number of layers**
Low frequency coil	M1	0.8	12.6	59	4
High frequency coil	M1	0.8	13.25	62	4

Table 3-5: Chosen dimensions of the excitation coils for one optimized prototype with M1 manufacturer.

3.2 Multiphysics simulations

In order to conceive and realize a Lab on Chip (LoC) microstructure we have developed a set of multiphysics simulation using COMSOL software. These simulations allow us to optimize the microstructure and take into account proper magnetization of the nanoparticles, detection sensitivity, diffusion in the microfluidic channel and heat transfer effects and thus the viability of the biological samples. Multiphysics simulations allow reaching a good compromise between the various important parameters without the cost and the time of real fabrication. This is especially important for prospective clean room fabricated structures where the first prototype can take up from several weeks to few months to be realized.

In the next sections, we give information on the various simulation tools:

1) **Electromagnetic simulations**: This tool was used to study proper magnetization and detection of the ferrofluid response by modeling the excitation and detection coils as well as the sample reservoir.
2) **Heat transfer simulations:** We consider here the influence of the excitation current on theheating of the sample.
3) **Microfluidic simulations:** These simulations help to optimize the microfluidic channel.

We try to validate each simulation with realized structures (PCB coils, microfluidic channels). The primary goal here is to have a set of simulations that can be used later on for a completely miniaturized structure.

In all the COMSOL simulations, the workflow is:

1. **Choice of Space representation:** a complete simulation uses a 3D model but for many cases a 2D axisymmetric or a 2D model are sufficient for the purpose and are much less time and resource consuming.
2. **Choice of Physics interface:** This choice depends on the physics and on the size of the structure to be simulated. It is very important to choose the right physics interface, because each one relies on a set of assumptions and can only be used for a set of applications.
3. **Definitions**: Defining component parameters and variables.

4. **Define the geometry**: Drawing or importing the component geometry.
5. **Choosing the materials**: Assigning material properties to the geometry.
6. **Parametrization of the physics interface:** Setting up the model equations and boundary conditions.
7. **Setting the mesh:**a compromise should be found for the mesh sizes. Indeed, a high-resolution meshing produces a good precision while it makes the simulation more time consuming and in some cases, the elements are too small for the simulation to converge.
8. **Setting up the study parameters:** This node allows to define appropriate solvers and their corresponding parameters as well as setting the time steps, frequencies of operation...etc.
9. **Visualizing the results:** In this section we can visualize results in 1D, 2D or 3D format. It also allows to calculate variables by applying mathematical operators to the resulting variables.

Since we gave the basic workflow here, in each simulation, we will give directly the chosen space representation, physics interface and important chosen models.

3.2.1 Electromagnetic simulation of the system

Because the operating frequency is between 100 kHz and few Hz, the chosen physics interface is the 'AC/DC module'. It can model electric, magnetic, and electromagnetic fields in statics and low-frequency applications. The latter means that it covers the modeling of devices that are up to about 0.1 electromagnetic wavelengths in size, which constitute our case. Since our models do not exceed 20 cm in size, we can model up to frequencies around 100 MHz.

Regarding the space representations, we chose to develop two models: one 2D axisymmetric that allows rapid prototyping of the excitation coils and one complete 3D model representing the different coils and sample reservoir filled with a ferrofluid. The former allows to rapidly reduce the number of parameters to optimize in the 3D structure.

3.2.1.1 Simplified model of excitation coils (2D axisymmetric)

A 2D axisymmetric electromagnetic simulation was conducted in order to determine the coil dimensions that have to be used to obtain a homogeneous excitation magnetic field all over

the reservoir and to eventually simulate the nanoparticles reaction. This approximate model allows to better optimize the excitation coil dimensions in a rapid manner. In fact, simulating a spiral coil in 3D is very difficult and the computational time outweighs the benefits in term of precision of the excitation fields amplitudes. Consequently, for finding the best parameters for excitation coils, 2D axisymmetric configuration can be used as a first step.

Figure 3-11 shows the 2D axisymmetric model of a spiral coil.

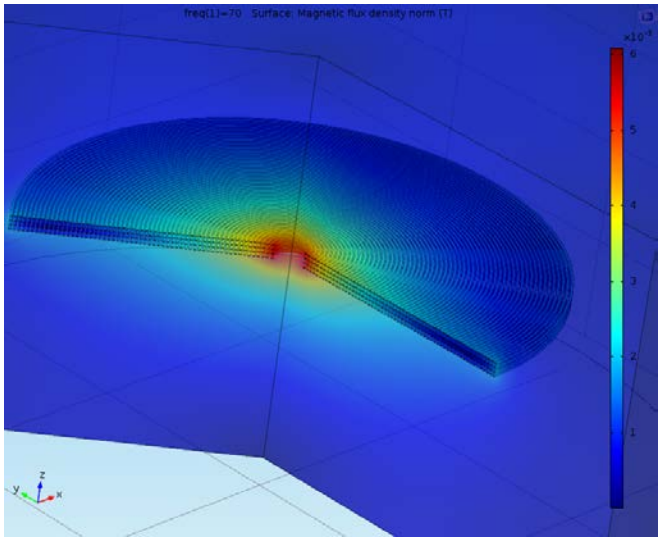

Figure 3-11: Example of magnetic simulation using AC/DC COMSOL Module. The figure represents results in term of total magnetic field amplitude of a 2D axisymmetrical magnetic simulation with a frequency of 70 Hz and an excitation current of 0.15 A. The color gradient is from shades of red (6mT) to shades of blue (0mT)

In order to model the magnetic field distribution of the spiral coil, we approximated the spiral coil by a set of circular coils with the same section and position. This given example (Figure 3-11) shows the simulated PCB coil. The air was modeled by a cylinder of a radius and height equal to 20mm and is sufficiently big to get a good approximation of the distribution of the magnetic field.

For the current distribution, the assumption was that the current had a homogeneous distribution over the coil section:

$$J_{coil} = \frac{I_{coil}}{Section_{coil}} = \frac{I_{coil}}{w * h} \qquad 3\text{-}20$$

We compared the simulation and the analytical calculation (Matlab) to evaluate the

approximated simulation error (Figure 3-12). We plotted the change of the magnetic field in the symmetry axe of the coil, from 1mm distance to 5 mm distance that is supposed to represent the probable position of the sample reservoir (PCB design).For this comparison we used a 4 layer spiral coil of 59 turns/layer with 0.8mm as the inside radius and a current of 0.12A.

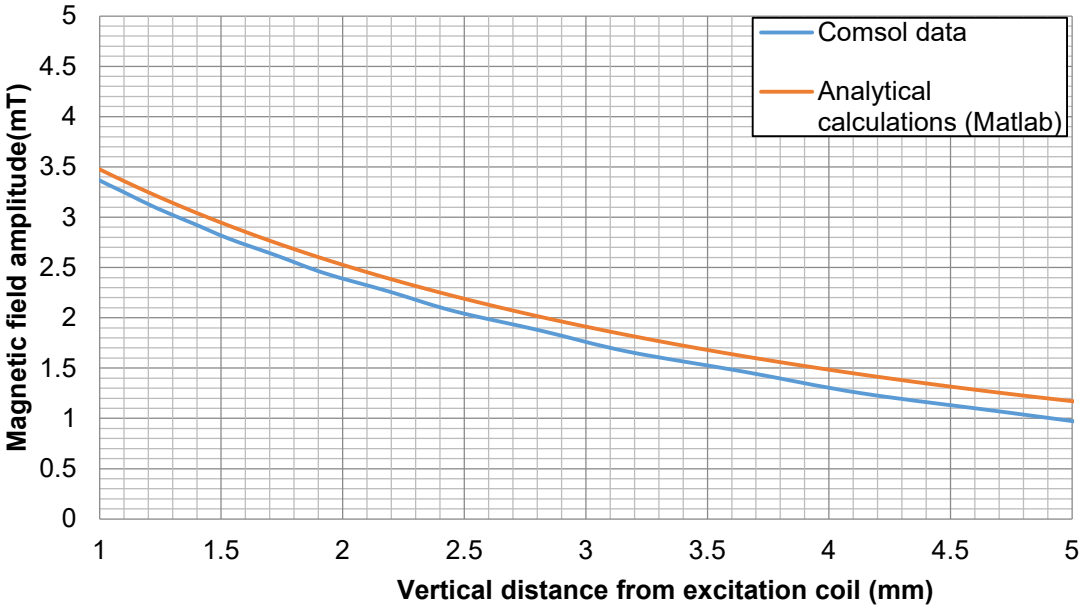

Figure 3-12: Comparison between 2D axisymmetric simulation and analytical calculations of the magnetic field.

From the figure 3-12, we can see that there is a small difference between the simulation and the analytical calculation. This could be because of the approximation of the geometry as well as in the calculations.

Following this evaluation, we plotted the magnetic field with respect to the number of turns. In this case, the number of turns were added by increasing the external radius. Thus, the added turns have increasing radii. This way of adding the turns is motivated by the practical limitation of fabrication techniques (here PCB).

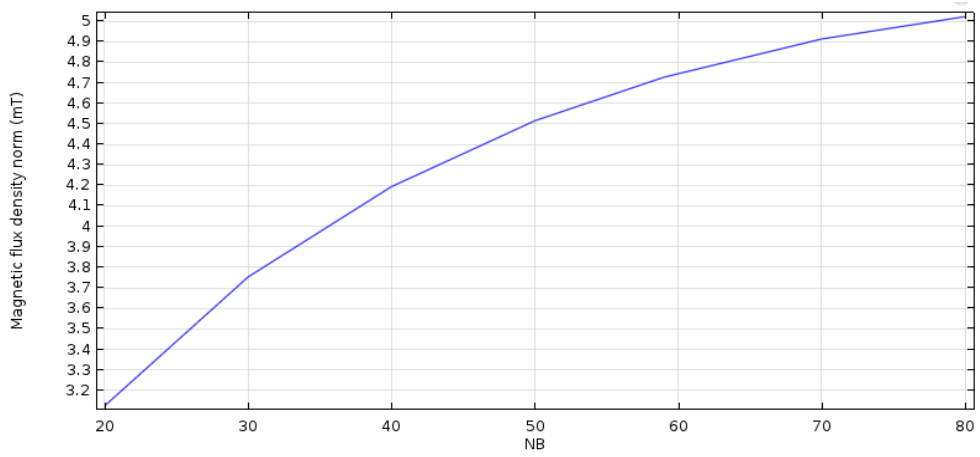

Figure 3-13: Effect of the number of turns on the magnetic field for a PCB modeled coil.

The magnetic field has a linear dependency to the applied current, which concords with theory. Regarding the effect of the number of turns, we see that the magnetic field approaches a limit and saturates. This is because the more external turns we add, the less contribution they have on the magnetic field.

Another concern for the magnetic field is its homogeneous distribution over the sample area. As an example, we draw the surface distribution of the magnetic field amplitude in the area of 1mm above the sensor ($Z = 1\ mm$).

From these two figures, we observe a fast decrease of the magnitude of the magnetic field of the spiral coil with respect to the distance from the center position of the coil on the coil axis. From various simulations of these cylindrically shaped coils, we also observe that this homogeneity is maintained especially at positions below the inner radius ($x < R_{in}$).This means that the sample reservoir diameter should not exceed a certain value, of which the nanoparticles near the outer radius will not be sufficiently driven by the magnetic excitation field.

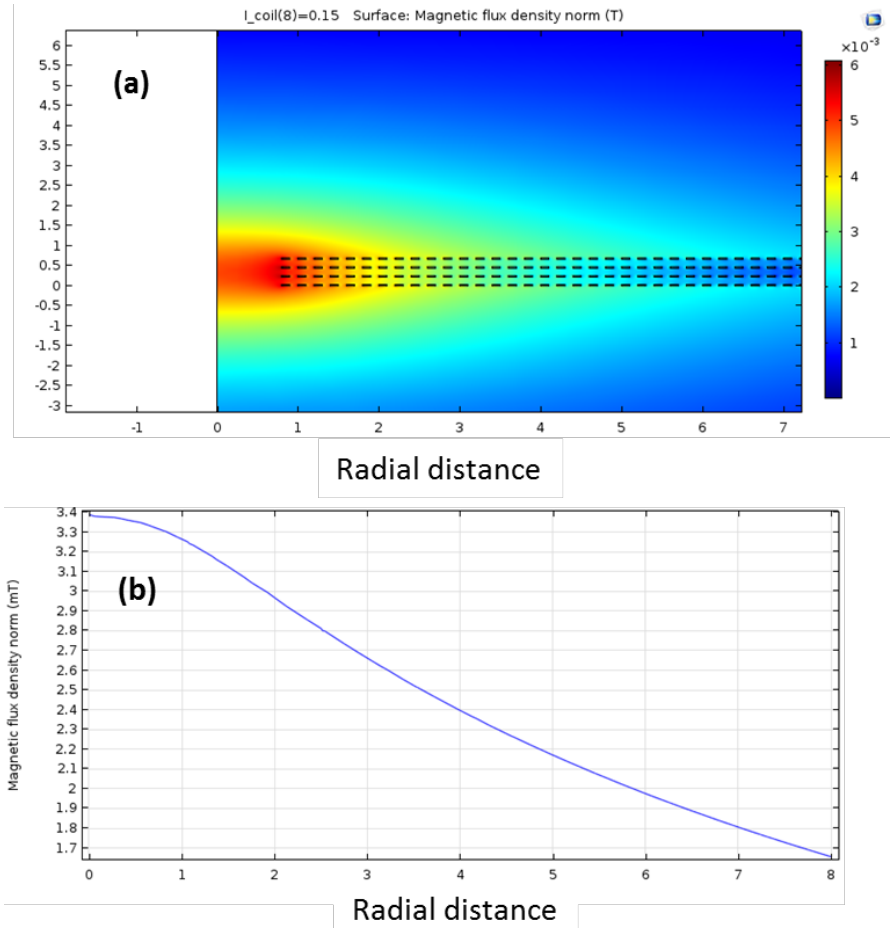

Figure 3-14: Total magnetic field distribution: a) over the whole cross section surface. Here, the blacklines represent the cross section of the coil traces. b) Function of radial distance from center position.

We conclude that we should think more about reducing the isolation thickness and increasing the filling factor so that we can get as many spiral windings as possible close to the sample reservoir. Also, the fast decrease in the magnetic field relatively to the vertical distance from sample suggests that this distance is very important for the detection system.

The simplicity of implementation constitutes the main advantage of this axisymmetrical model. One of the main drawbacks is that COMSOL does not recognize this coil model as a 'coil'. Thus, we cannot calculate the electrical parameters and the induced voltage (in the case of a pick-up coil).

3.2.1.2 Complete model of the structure (3D)

For complete simulation of the electromagnetic aspects of excitation and detection coils as well as the sample magnetic response, we simulate the whole structure in a 3D model.

In all the following, we chose to use the magnetic fields node in the AC/DC physics interface. Furthermore, for the sake of simplification, we used the available 'multi turn coil' domain feature. This feature allows to model the spiral coils using a cylinder of the same dimension. An example of the geometry is given in Figure 3-15.

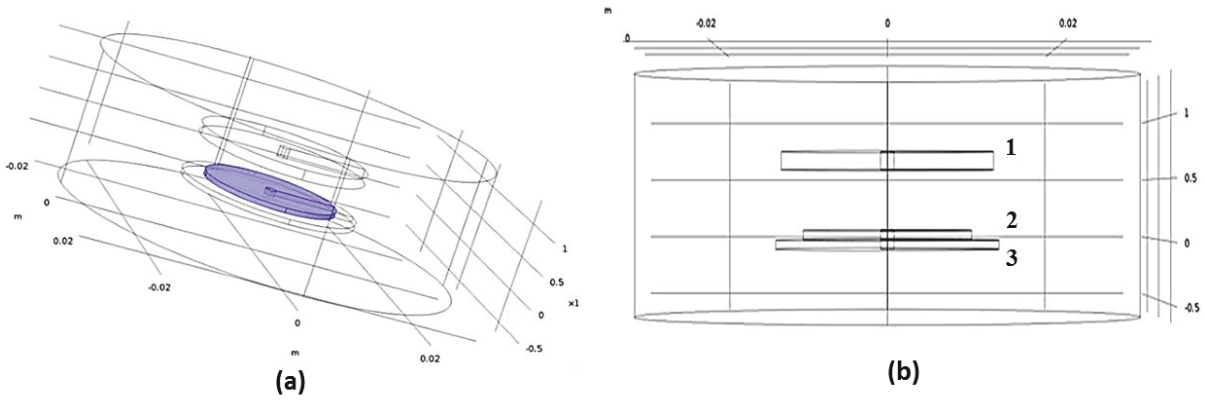

Figure 3-15: Geometry of coils. (1) Low frequency (LF) coil. (2) Sensor (Detection) coil. (3) High frequency (HF) coil.

Additionally, the coils can be electrically connected to voltage/current sources as well as impedances through the use of the 'electrical circuit' node. Finally, the sample is modeled using the 'Ampère's Law' node. It adds Ampère's law for the magnetic field and provides an interface for defining the constitutive relation and its associated properties as well as electric properties. We use this node to describe the macroscopic properties of the medium (relating the magnetic flux density *B* and the magnetic field *H*) and/or the applicable material properties, such as the relative permeability. In the final case of modeling superparamagnetic nanoparticles, we implemented the HB curve of our real nanoparticles samples using this later node. For these 3D simulations, we need to assess the accuracy of the chosen coil representation.

Assessment of the coil model accuracy

In the first step, to confirm simulation results, we consider one 4-layer coil with R_{in}=2mm. The distance between coil and measurement point is 1.467 mm. Wire width and space between them is 100 mm. The height of each layer is 35 mm. Total coil thickness is 0.775 mm. The coil is fed with 15 V. Figure 3-16 illustrates simulated model and results of analytical calculations.

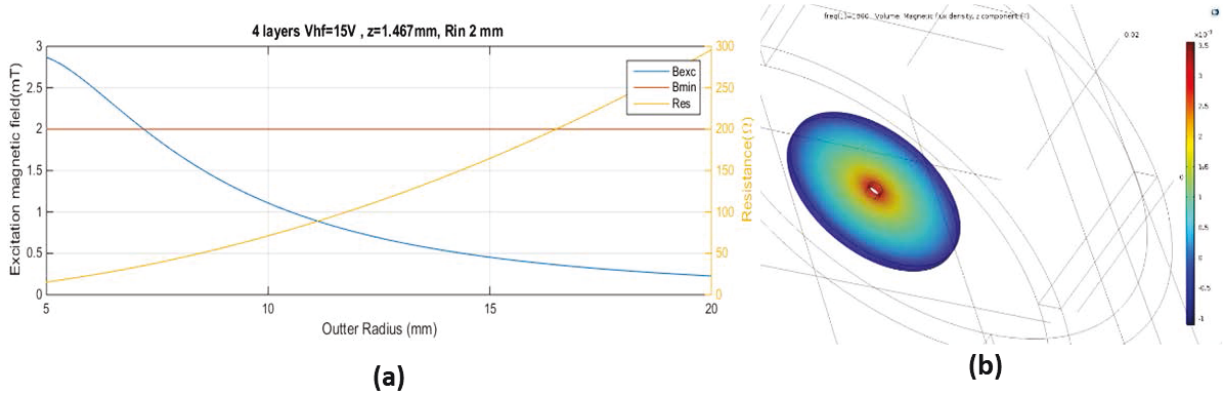

Figure 3-16: Calculation results for a 4-layer coil. (a) the analytical results of the magnetic excitation field as well as the calculated resistance with respect to the outer radius of the coil. Bexc: the excitation magnetic field. Bmin: minimum desired field amplitude. Res: resistance. (b) Magnetic field distribution over the volume. Gradient from red to blue depicts the highest (3.5 mT) and lowest value (0mT) of the magnetic field.

The results of simulation and calculation are in the same order but different in value. The magnetic field value for R_{out}= 10 mm is 1.1 mT and 1.5 mT in calculation and simulation, respectively.

We further compare simulation results with measurements results. The impedance of coils and magnetic field on the surface of detection and sensor coils were measured with an impedance analyzer and a Gaussmeter, respectively. The magnetic field was measured while the coils were biased with DC voltage (3, 4, 6 V). The parameters of the used coils are gathered in table 3-6:

	layer	R_{in} (mm)	R_{out}(mm)	Turns/layer
LF[1]	4	0.8	10	46
	4	3	10	35
HF[2]	4	2.5	9	35
sensor	4	0.8	10	46
(1)Excitation coil with lower frequency bias (Low frequency (LF) coil) (2)Excitation coil with higher frequency bias (High frequency (HF) coil)				

Table 3-6: Dimensions of tested PCB coil.

The comparison results in terms of electrical parameters and magnetic field are given in Table 3-7:

		Resistance	Inductance (mH)	V=3 V	V=4V	V=6 V
HF	**Measurements**	35 Ω	176	697 mT	890 mT	1.3 mT
	Simulation	24 Ω	192	727 mT	969 mT	1.45 mT
Detection	**Measurements**	44 Ω	265	708 mT	1.01 mT	1.45 mT
	Simulation	29.7 Ω	245	984 mT	1.31 mT	1.97 mT
LF	**Measurements**	90 Ω	950	581 mT	715 mT	1.11 mT
				600 mT	807 mT	1.39 mT
	Simulations	58 Ω	891	604 mT	806 mT	1.2 mT
				706 mT	941 mT	1.4 mT

Table 3-7: Comparison table of simulated and measured electromagnetic parameters. Magnetic field is given for different input voltages.

The simulations are in good agreement with measurements, with an acceptable error.

Next, the 3D simulations can be decomposed into frequency domain and time domain simulations.

Frequency domain simulation

Frequency domain simulations are used to compute the response of a linear or linearized model subjected to harmonic excitation**.** Here, the goal is to find the optimum frequency of excitation coils with maximizing magnetic flux at the sample area as well as theoutput voltage of the sensor coil. As a result, higher sensitivity can be obtained. The next figure shows the magnetic field distribution over the different coils and the effect of the frequency on the sensor coil output. The dimensions of the modeled coil represent the dimension of one of the chosen PCB prototypes (dimensions can be found in Table 3-9).

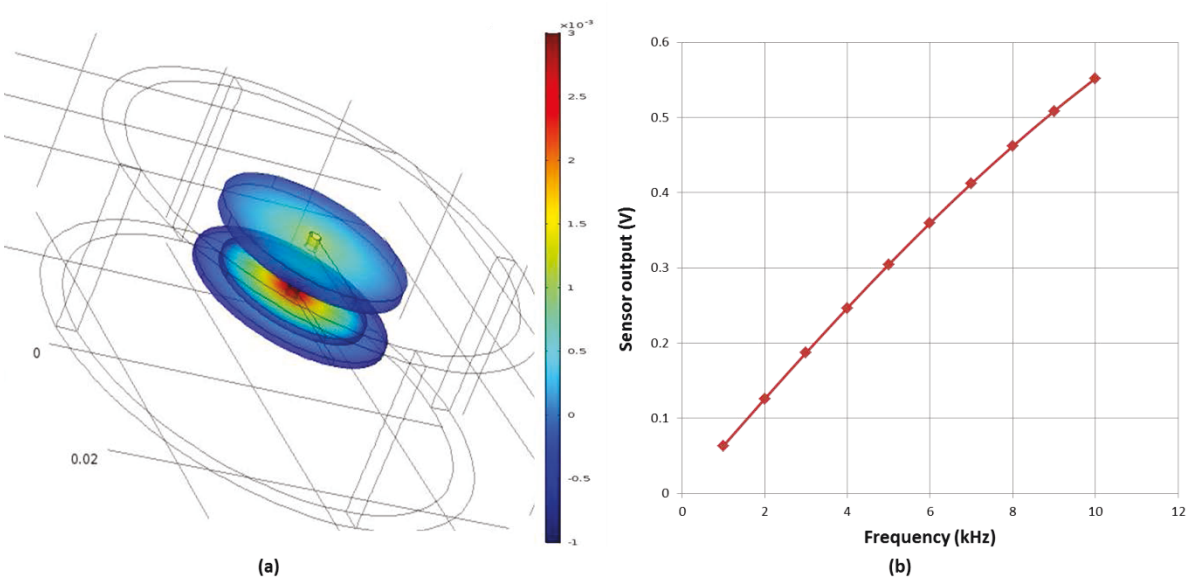

Figure 3-17: Frequency domain simulation. (a) Magnetic field distribution (range of values between -1 and 3 mT). (b) Sensor coil simulated output with respect to frequency. Simulation parameters: LF coils: 100 turns, 0 Vpp, 12 mm external radius. HF coils: 150 turns, 10Vpp, 12 mm external radius. Sensor coil: 100 turns, 10 mm external radius. Internal radius for all coils is 0.8 mm. Height of coils: 0.7mm and vertical distance between LF and sensor coils is 5 mm.

As it can be seen in figure 3-17, with the frequency we can optimize the output voltage response. The frequency domain simulation is faster than the time domain simulation but cannot simulate nonlinear responses of nanoparticles.

Time domain simulation

The time domain simulation was used for the general case when the field changes over time in an arbitrary manner. This more complete simulation allows optimization of the structure parameters such as shape, position, dimension and number of turns of coils, with maximizing the output voltage of the sensor coil in time domain simulations. Also, a miniaturized structure without loss of sensitivity can be realized.

In the next figure, the magnetic field distribution in a typical case of PCB coils (see prototype 2 in section 3.3.1) with microfluidic reservoir is represented.

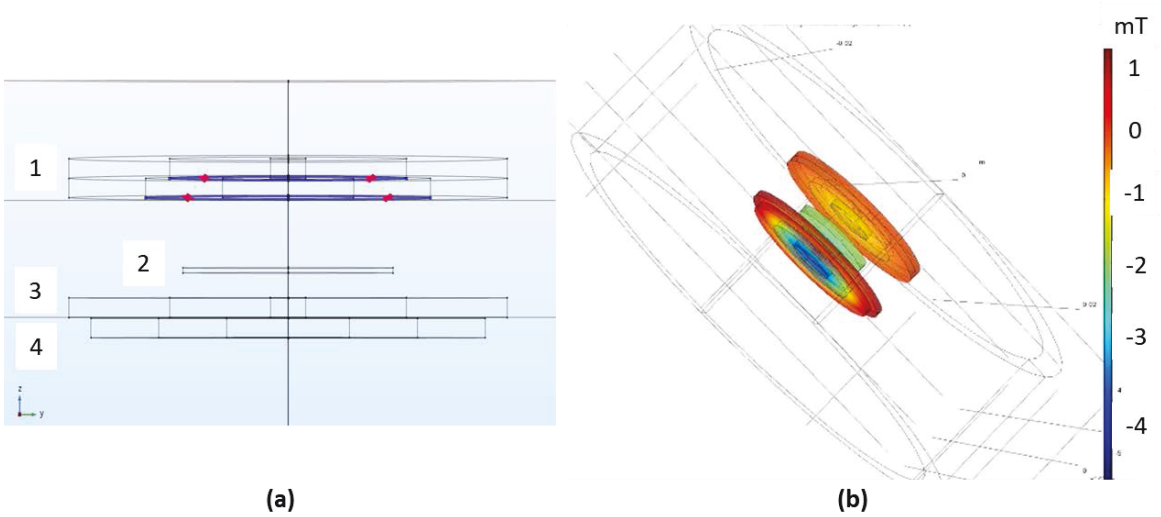

Figure 3-18: Coil geometry (a) and magnetic field distribution (b). 1: LF coil, 2: sample reservpor, 3: sensor coil, 4: HF coil.

In the next figure, we can see the resulting time variation of each coil current. Results are in accordance with the expected response. We can clearly see that the sensor coil current is composed of both high frequency and low frequency components.

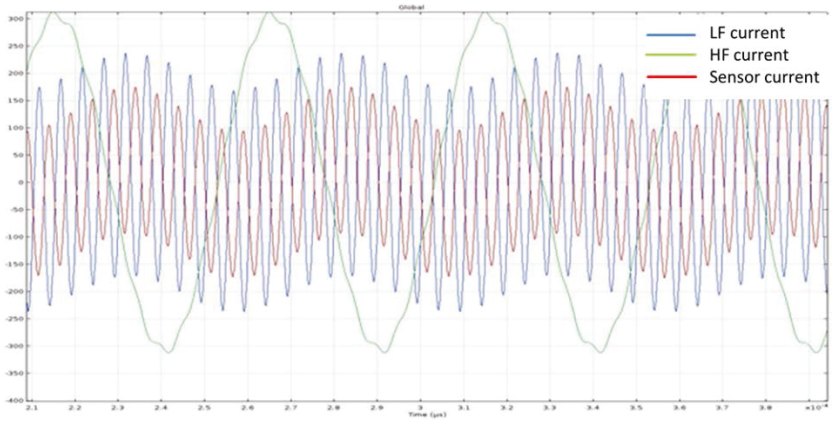

Figure 3-19: Time evolution of the current in the different LF, HF and sensor coils.

We also validated the nonlinear response by looking at the frequency components of the induced voltage. In this case, we used soft iron as a nonlinear material. Since the material is not superparamagnetic, the magnetic field excitation was increased. We can see the comparative results of with and without iron in Figure 3-20.

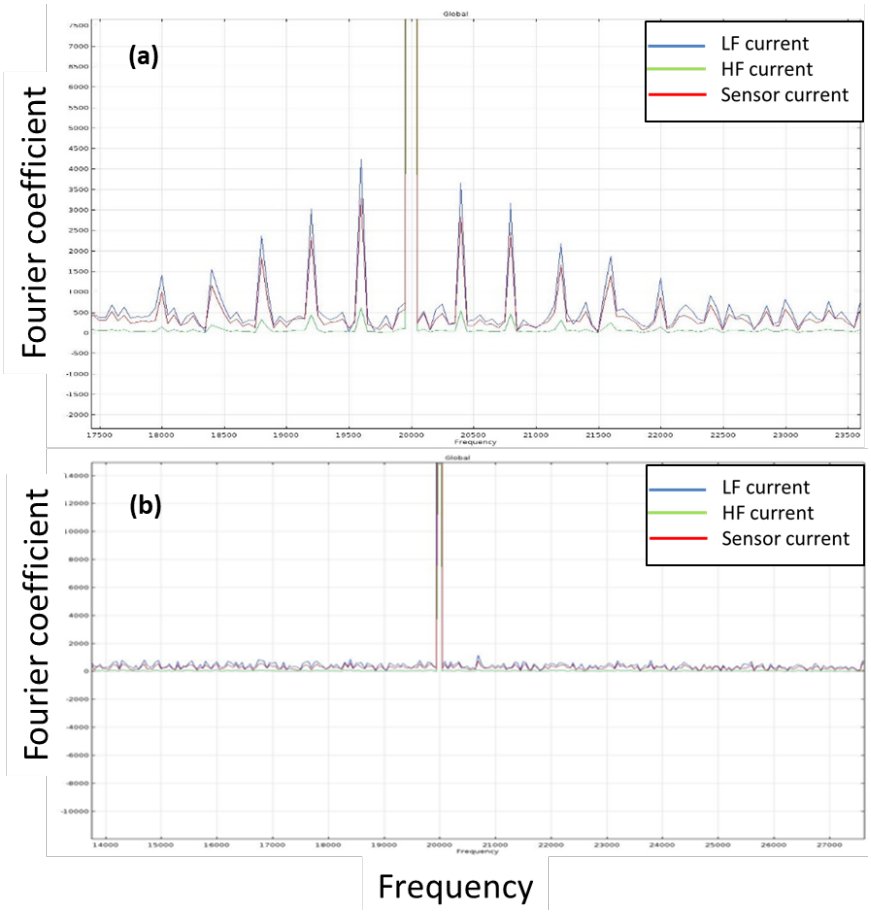

Figure 3-20: Frequency components of the sensor current in the presence (a) and absence (b) of the iron.

We can clearly see that in the case of the presence of a nonlinear magnetic component, the sensor's response is composed of mixing frequencies' signals as well as original frequency signals.

Study of the effect of the shape of the reservoir

In order to study the effect of the shape of the microfluidic reservoir on the magnetic response, we simulated a serpentine-like (meander) and a cylindrical reservoir of the same height. Their corresponding volumes were 7.8 and 6.6 10^{-8} m^3, respectively.

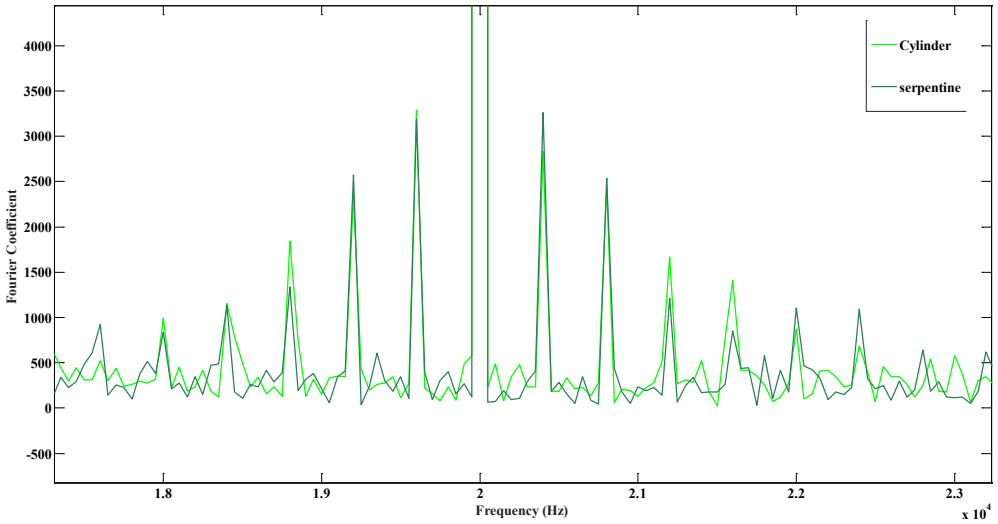

Figure 3-21: Magnetic response of serpentine and cylindrical microfluidic reservoirs.

We conclude from the figure 3-21 that the difference between the response of the serpentine and the cylinder is insignificant. This allows us to use the simpler representation form of the reservoir with an equivalent volume for further study of optimum dimensions and electrical parameters.

3.2.2 Heat transfer simulations

Because the structure is intended for immunoassays with biological samples, the electrical simulation is coupled with a heat transfer simulation (COMSOL Multiphysics). The coupled physics allow to take into account both electromagnetic and heat aspects. We can therefore predict the period of test time that we can allow ourselves, according to the maximum allowed temperature in the reservoir (37°C).

Since the tested sample will be biological samples, the temperature in the reservoir volume should not exceed a critical value. In order to model all the microstructures, we used the 2D axisymmetric model in COMSOL because of the symmetry of the phenomenon. Similarly to the magnetic simulations of excitation coils (section 3.2.1.1), each coil is represented by 4 layers of spiral copper, see Figure 3-22. Moreover, the materials modeled in this simulation are copper (coil windings), FR4 (PCB substrate), water (microfluidic reservoir) and SU8 or PDMS for the substrate of the microfluidic layer.

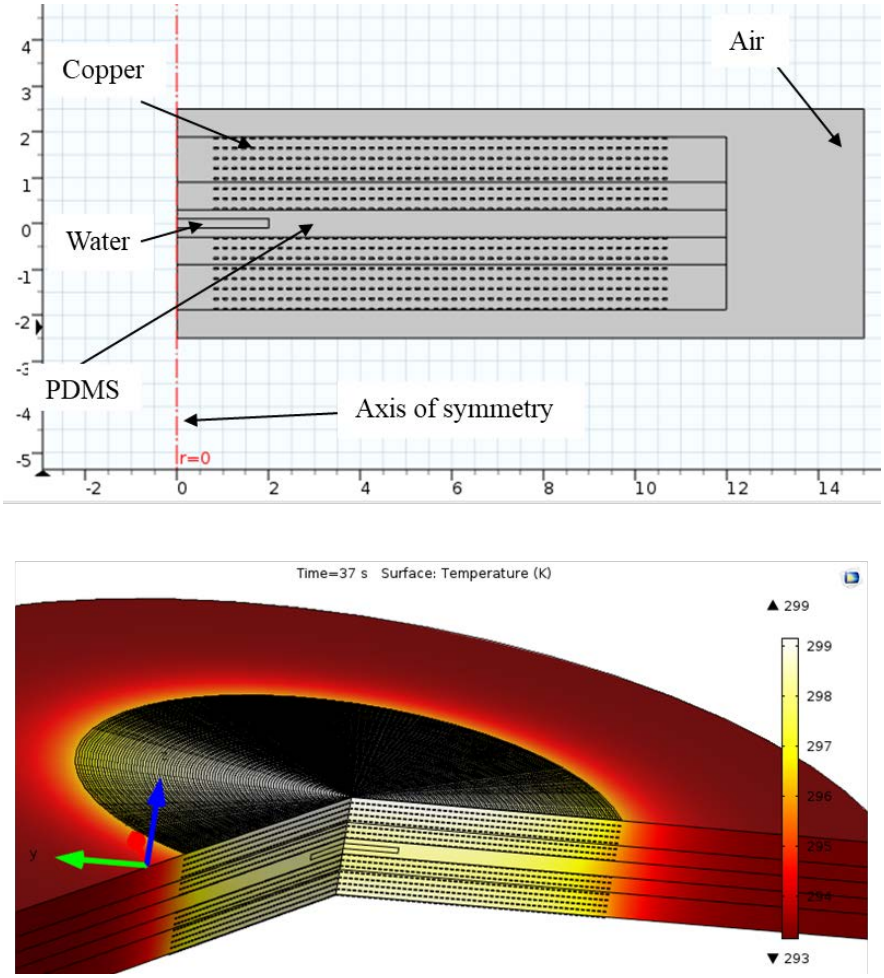

Figure 3-22: 2D axisymmetric model for PCB integrated structure. (Top) geometry and materials. (Bottom) example of heating effects.

In this simulation, for simplicity and for representing the worst case, we only consider heating through conduction. In this case, there is no reduction of heating through convection. The heat source is deduced from the equivalent current of the excitation coils.

$$P = R \cdot I_{\text{excitation}}^2 \qquad 3\text{-}21$$

To simplify the simulation, the heat source is supposed to be continuous and the power corresponds to the RMS value of the current.

The resulting change in temperature in the border of the reservoir can be seen in Figure 3-23.

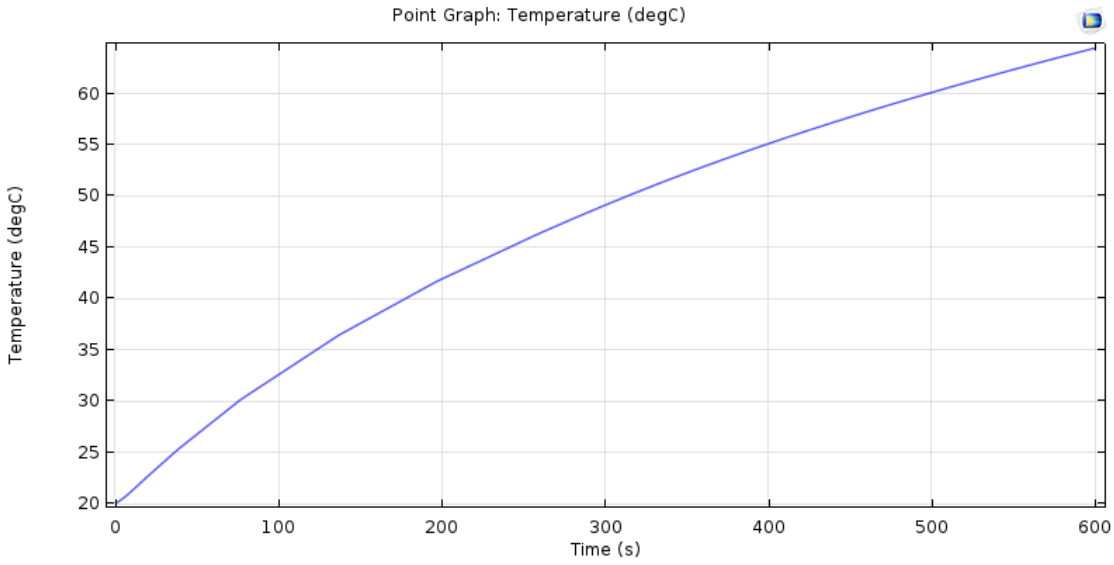

Figure 3-23: Temperature of the reservoir relative to the experimental time.

If we suppose an initial value of 20°, we see that the temperature increases rapidly and goes above 40° after an experimental time of about 180 seconds. However, since the measurement can be done within a few seconds, this should not be a problem. We should nonetheless consider this factor when reducing the size of structures and thus the distances between coils and sample reservoir. This constitutes the second main reason to optimize the excitation coils so that we do not use a high current.

3.2.3 Microfluidic simulations

Following the initial phase of testing disc shape reservoirs, we noticed a heterogeneous dispersion of the fluid in the reservoir (Figure 3-24), which leads to have some reservoir area that are not correctly filled with sample. We then performed a set of COMSOL simulations of the distribution of the fluid in our microfluidic reservoir to ensure a better filling of channels and thus greater measurement accuracy.

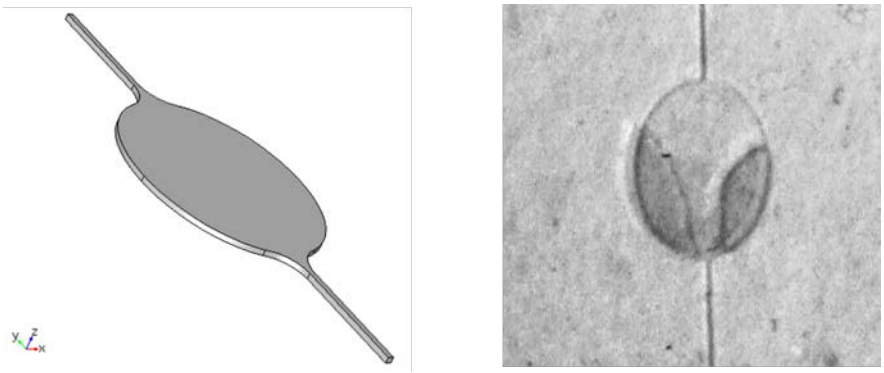

Figure 3-24: Geometrical model of the disc shape microfluidic reservoir (left). Nonhomogeneous filling due to high gradient between inlet and reservoir shape.

For this microfluidic simulation, we used the laminar flow physics node included in the microfluidic module. This node is suitable because we are in the case of low Reynolds numbers (in our case Re< 100).

The microfluidic reservoir can be either simulated in 2D or 3D. Figure 3-25 shows an example of 2D simulation results. The shape is composed of an ellipse representing the reservoir and two $100\ \mu m$ width channels that work as Inlet/Outlet. We use an average velocity of 0.1 mm/s and we change the shape of the ellipse (small and big radius).

Figure 3-25 shows the velocity field distribution for each case. We see that if we use a circular disc shape reservoir, there are some areas which the fluid will not reach; these are on the extreme left and right sides. This is because there is a significant width change between the inlet/outlet microchannel and the reservoir. We first deduce that we must use a more oval shape with input / output and less abrupt changes in dimensions.

We chose to reduce this gradient by using an elliptic shape along with a smooth fillet in the Inlet/reservoir and reservoir/outlet areas. The resulting velocity distribution is shown in Figure 3-25.c. The flow is thus more homogeneous.

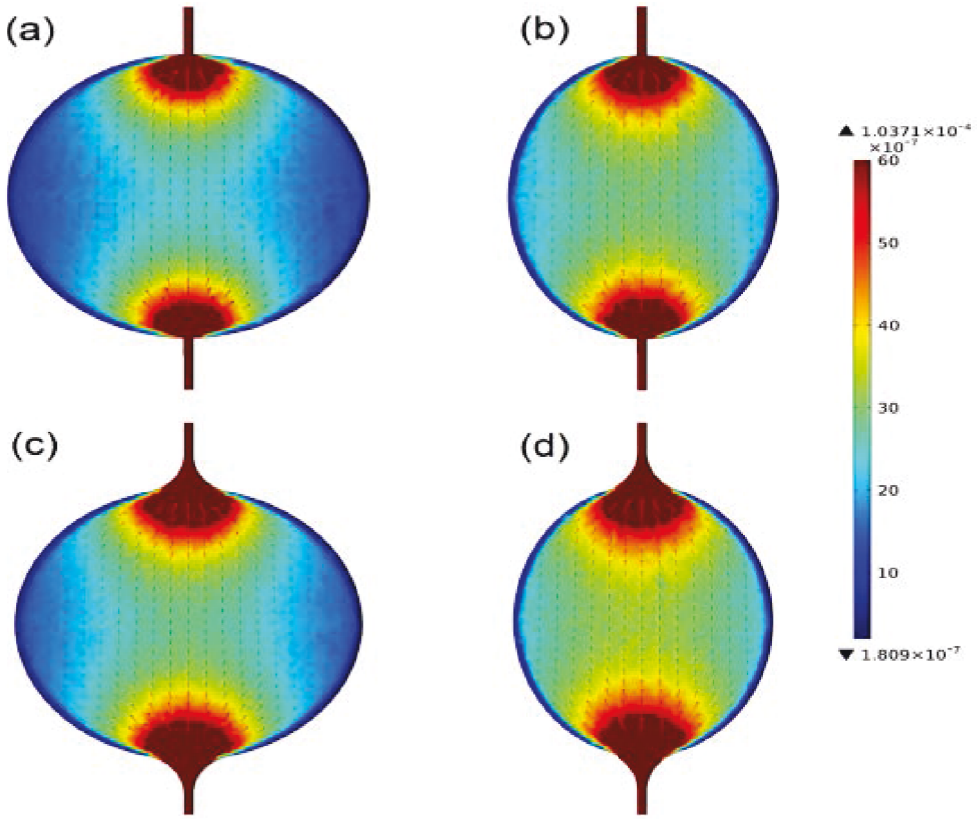

Figure 3-25: Simulations of the fluidic distribution depending on the shape of the reservoir.

In order to further improve the diffusion and to have a more complete simulation, a 3D simulation using a level set method for simulating a multiphase flow has been used. Figure 3-26 shows the dynamic filling of serpentine reservoir with water.

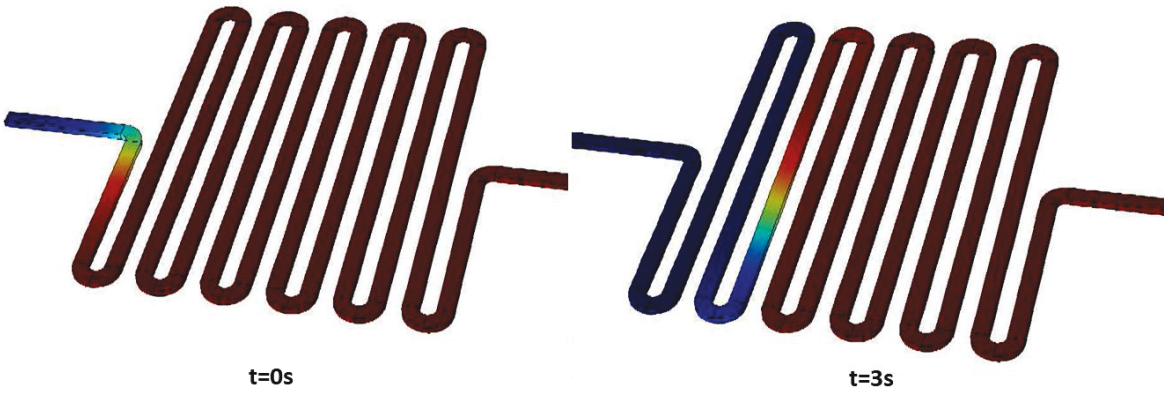

Figure 3-26: Diffusion of fluid in serpentine like reservoir.

The simulation allows to show two phases and their interaction through a level set approximation of the interface boundary. This simulation can later be enhanced by

considering the air bubbles effects on the microfluidic system and process. Finally, it can serve as a basis to find microfluidic reservoirs with higher surface to volume ratios in order to accommodate a higher density of functionalized primary antibodies.

3.3 Design and realization of PCB coils associated with microfluidic reservoir

Following the first experiments, simulations and calculations, we chose to embed all the coils at once. In this work, two fabrication methods are explored: (i) using PCB technology with a separate microfluidic reservoir or (ii) using clean room technology for both the coils and microfluidic reservoir. Table 3-8 depicts the advantages and drawbacks of these two methods.

Design technology	Advantages	Drawbacks
Printed circuit board+ Microfluidic structure	Fast realization process (within days after dimension optimization)	Lower limit of isolation not sufficient ($100\mu m$)
	Robust realization (external manufacturer)	No bonding possible between microfluidic structure and PCB: sample to coil distance is limited.
Clean room technology	High resolution, control of dimensions and possibility of microcoil realization and very low sample to coil distance	Higher probability of failure due to multiple realization steps that involve various parameters
	Fully embedded structure possible (coils + sample reservoir)	Difficult multilayer coil fabrication

Table 3-8: Comparison of PCB and clean room realization process solutions.

For the validation of the optimization tools and for a rapid prototyping, the PCB solution has been chosen. This choice will allow to rapidly design and optimize separately the microfluidic and coil parts for a relatively low price per prototype.

3.3.1 PCB coils

3.3.1.1 Design and realization

In order to assess the PCB technological choice, we designed and realized three prototypes from which two were retained for further testing. We also chose M1 PCB manufacturer for the fact that the company allows multilayer manufacturing of up to 32 layers with thick

copper sections (35 µm thickness). This latter property helps to have less resistance noise in pick-up coil and a smaller total thickness of the board, hence, a better proximity of external layers to the sample. We ultimately chose to use 8-layer PCB with a total thickness of 1.55 mm for all three prototypes. Table 3-9 summarizes the dimensions of the designed and realized PCB coils for each prototype. The copper width/isolation is the same for all prototypes and is equal to 100 µm (minimum limitation of the M1 manufacturer).

Prototype	**Coil function**	**Inside radius R_{In} [mm]**	**N_{turns} per layer**	**N layers**	**Total N_{turns}**
1	LF	0.8	59	4	236
	HF	0.8	62	4	248
	Sensor	0.8	46	4	184
2	LF	0.8	46	4	342
		3	35	4	
	HF	2.5	35	4	140
	Sensor	0.8	46	4	184
3 (symmetrical)	LF	1	45	2×2	340
		2	40	2×2	
	HF	2.15	40	2×2	160
	Sensor	0.8	41	2×2	164

Table 3-9: Dimensions of LF, HF and sensor coils for the different designed and realized prototypes.

The first two prototypes were made in an “asymmetrical” configuration. Prototype 1 presents excitation coils in one PCB and detection coils with optional second low frequency excitation coil in the second PCB. In prototype 2, the low frequency coil (LF) is fabricated in one separate PCB, the high frequency coil (HF) and the sensor coils are fabricated in another PCB part (Figure 3-27, prototypes 1 and 2). Concerning the third prototype, two identical PCB parts were fabricated and are arranged in a “symmetrical” configuration above and below the microfluidic part (Figure 3-27, prototype 3).

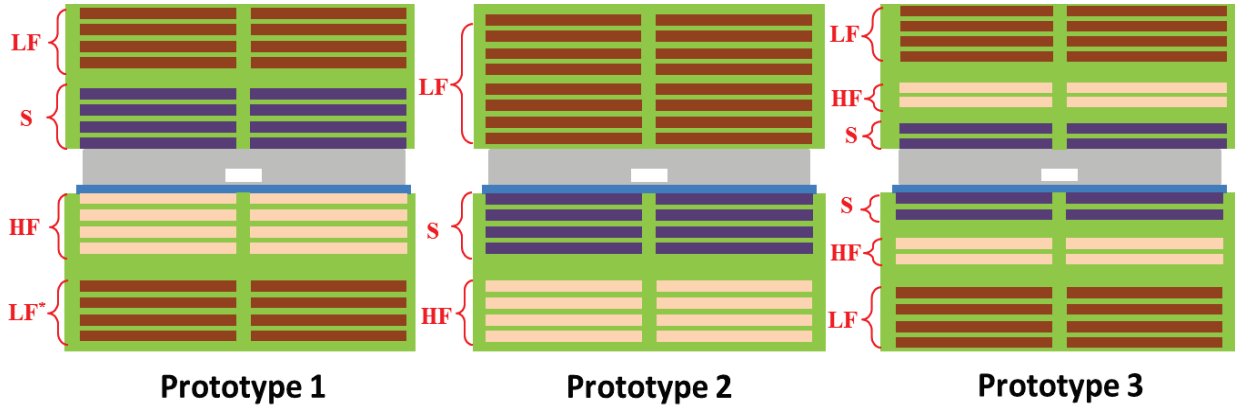

Figure 3-27: Different designed and fabricated configurations of PCB coils with the first two being the asymmetrical configurations and the third one the symmetrical configuration. The images are only representative to clarify the design. LF: low frequency, HF: high frequency and S: sensor or pick-up coil. LF*: is an additional 4 layer coil that can be used to make the LF magnetic field stronger. The grey part in the middle is the microfluidic structure, designed and realized separately and then assembled with the PCBs coils.

These different configurations and dimensions allow to test various effects such as the effect of the inside radius on the homogeneity of the field, the heating effects, the interference between coils as well as the validation of simulations tools.

Concerning the design of these configurations, we have used Pulsonix software because it allows both multilayer design and automatic drawing of spiral tracks. An example of the design is given in Figure 3-28.

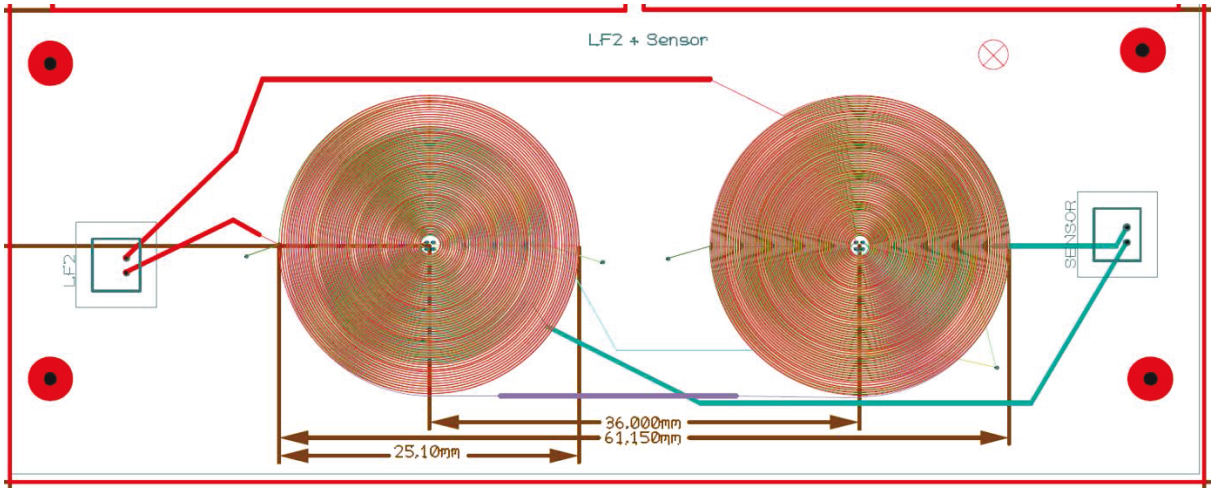

Figure 3-28: Example of the design of integrated coils using Pulsonix Software: here low frequency coil and pick-up coils are shown (four layers for each).

In this first prototype, the right set of coils will be used for detection and the left side for reference. Both sides are electrically connected internally in series. For each coil, all the

layers are connected using via holes. A two pin connection was then designed for external connections with the signal source (frequency generator) and the receiver device (Lock-in amplifier). Additionally, all excitation coils were wound in the same direction. However, the detection and reference pick-up coils were wound in opposite direction to have a differential (gradiometric) setup to reduce interference.

Finally, in order to improve the performance, prototype 2 and 3 are different from 1 in two aspects. First, they have different via holes protection: On one hand, prototype one has very efficient coating with nickel/gold but it has some nonlinear magnetic effects because of nickel. On the other hand, in prototypes 2 and 3 via holes have standard tin (Sn) protection that enables less magnetic noise but has the issue of longevity of the via to oxidation.

Second, prototype 2 and 3 have an improved winding feature. Each additional layer winding is shifted so that the upper copper section is almost parallel to the isolation space (Figure 3-29). The purpose is to reduce the parasitic capacitance due to interlayers.

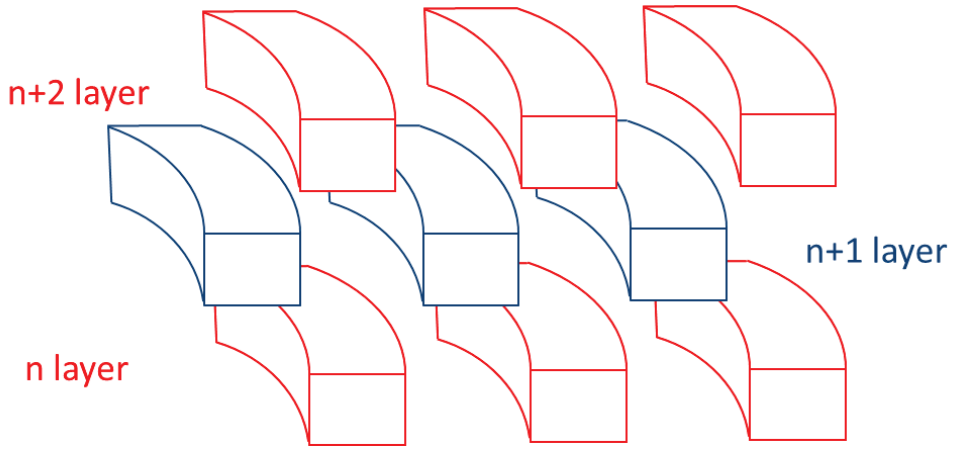

Figure 3-29: Strategy for reducing interlayer capacitance.

After the design of the coils, connections and mounting holes, the PCB prototypes were fabricated by the chosen M1 manufacturer. Figure 3-30gives an illustration of these realized PCB coils. It has to be noted that interlayer distances are not constant and that it has been considered for optimizing (Figure 3-30, left).

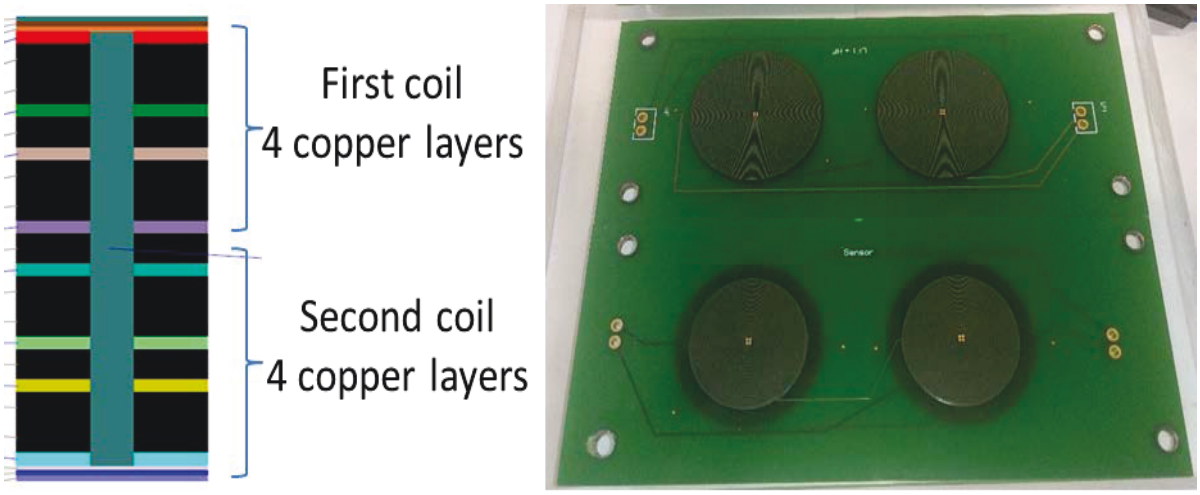

Figure 3-30: Realization of PCB coils: (left) stacked view of the 8 layers with representative different spacing, (right) example of realized structure (prototype 1).

3.3.1.2 Characterization of the PCB prototypes

The fabricated PCB coils were characterized using an impedance analyzer (HP 4194). The impedance and the phase changes of the different coils were characterized over a spectrum between a 4-5 kHz and 1MHz, respectively. Figure 3-31 shows the comparison between the sensor coils of prototype 1 and 2, respectively that have the same dimensions.

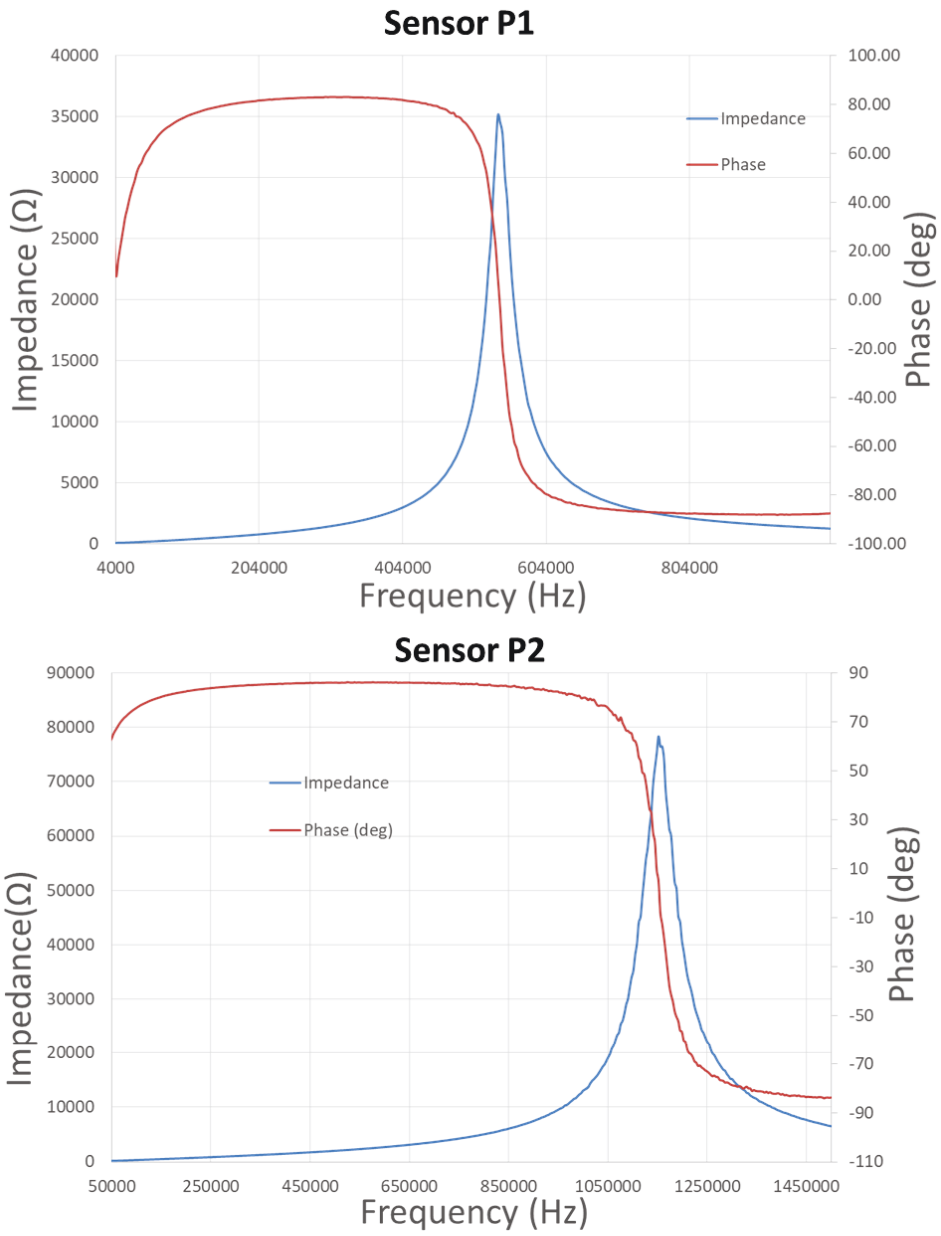

Figure 3-31: Sensor coils spectrum of impedance and phase for prototype 1 (P1) and 2 (P2).

From these two curves, we can observe that the improvement mentioned in the previous section helped to reduce the parasitic capacitance value. Also, for very low frequencies, the resistance effect is dominant over the inductance effect which shows that the optimization of low frequency excitation coil should not depend on the inductance value but only on the resistance value. Based on this observation and the fact that the magnetic excitation field of prototype 2is better, prototypes 2 and 3 are used for the next experiments.

We can also deduce that the AC effects of the resistance value do not have any impact. This can be verified by plotting the evolution of the measured real part of the impedance and the

calculated real part considering that R is constant throughout the entire spectrum (see Figure 3-32). Here the real part was deduced from the electrical equivalent model presented in section 3.1.1 and is equal to:

$$Z_{Sensor}(real) = \frac{R}{(1 - w^2LC)^2 + (wRC)^2} \quad (3\text{-}22)$$

where w represents the angular frequency.

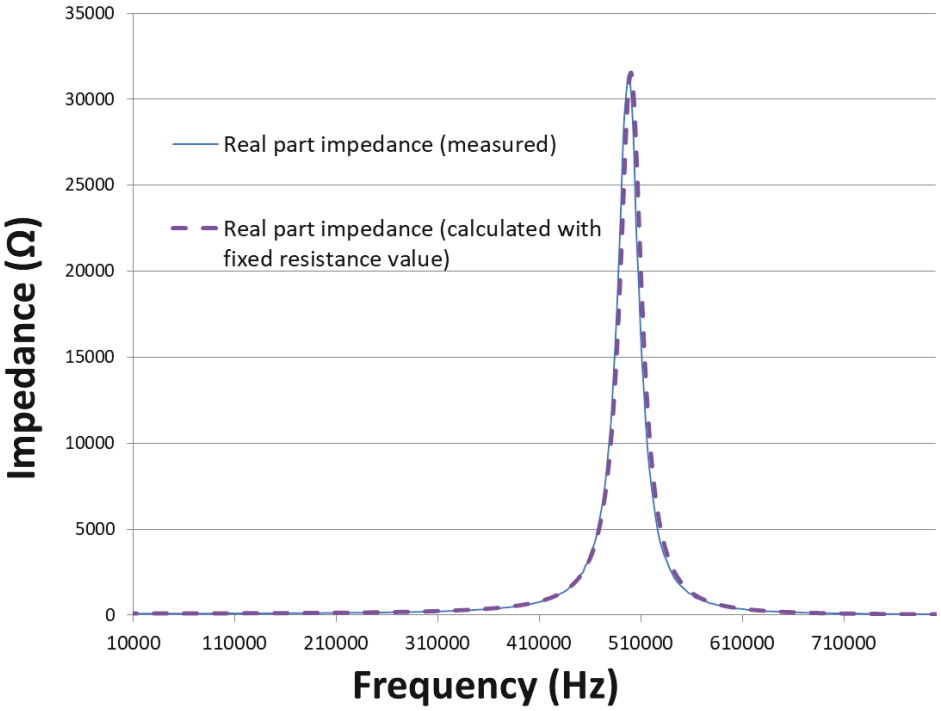

Figure 3-32: Effect of the operating frequency on the AC resistance.

We can see that the difference is insignificant and we can thus safely confirm that the resistance value did not change significantly for frequencies below 710 kHz.

The Figure 3-33presents the electrical behavior of the different coils in the case of prototype 2 (asymmetrical) and prototype 3 (symmetrical).

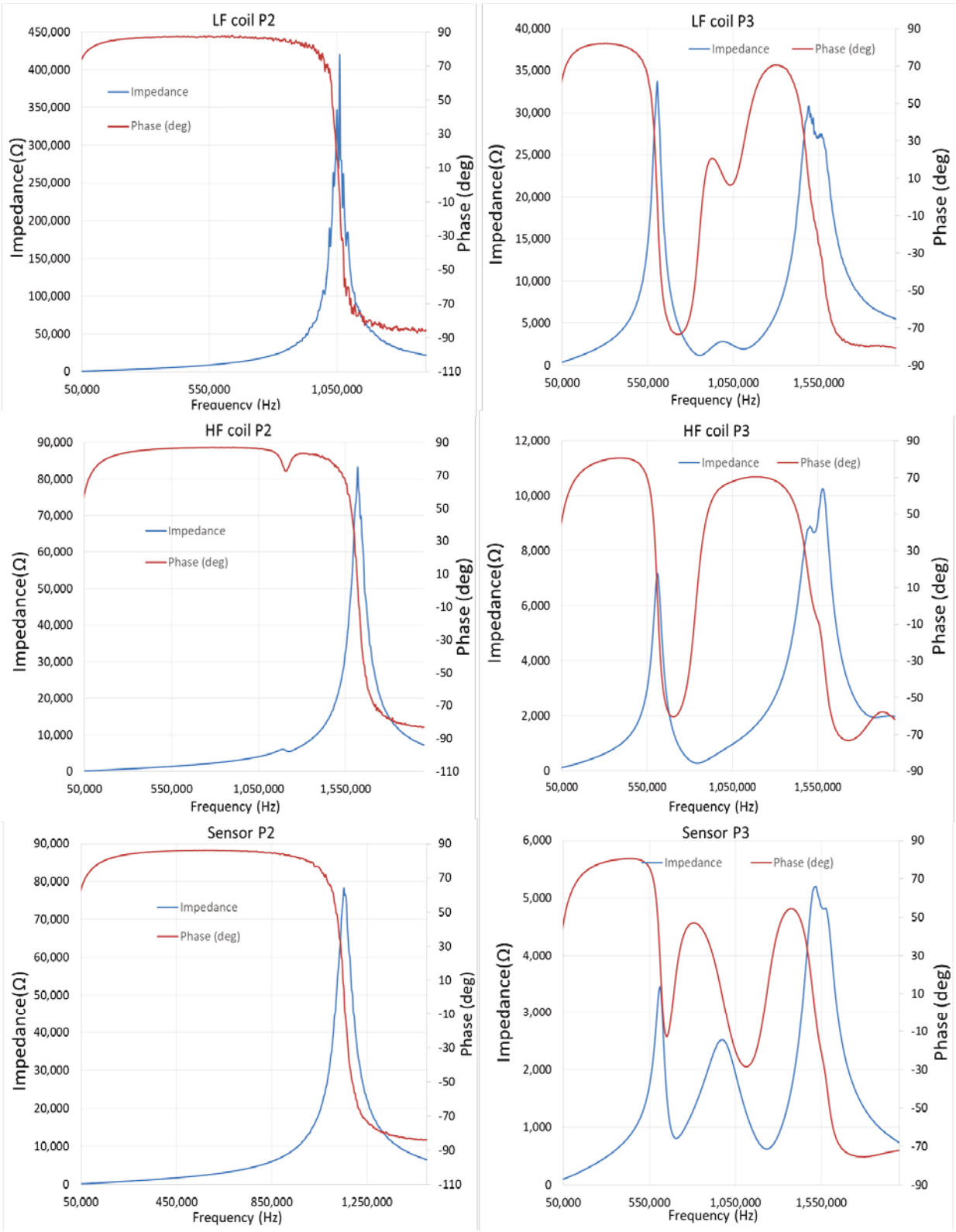

Figure 3-33: Coil characteristics for the asymmetrical (P2) and symmetrical (P3) PCB coils prototypes.

From these curves, we can clearly see that the asymmetrical configuration coils exhibits only one resonance whereas the symmetrical coils are affected by the fact that the 3 coils are all embedded in one PCB and therefore couple strongly. Consequently, in terms of resonance frequency and impedance stability, the asymmetrical configuration is better.

Concerning the symmetrical configuration (P3), the LF coil exhibits three resonance frequencies. These resonance peaks are likely attributed to the mutual inductance effect of the other two coils (HF and sensor coils). Also, the LF coil exhibits the biggest capacitance value of 68 pF because it has more layers per coil that the other (4 rather than 2). However, this is not an issue since the LF coil is only used with signals that have low operating frequencies (less than 200 Hz). Since the sensor coil is, by design, the farthest away from the LF coil, the sensor coil has lower impedance peaks due to mutual effects. Because it has two layers, it has lower inductance and higher capacitance (more interlayer potential gradient). Lastly, the HF coil is between the LF and sensor coils and thus suffers the effect of both coils. However, the effect of the LF coil is more important. We deduce that the HF excitation frequency should not exceed 120 kHz ($f_{Resonance}/5$) so that the capacitance effects does not interfere with the performance.

Concerning the asymmetrical configuration, the LF coil has the lowest resonance frequency since it is composed of 8 layers. Consequently, it has a higher inductance value, but it is not an issue since it is operated at low frequencies. The HF and sensor coils have higher resonance frequencies and less inductance. Also, the mutual effects are insignificant.
Finally, we sum up the electrical characteristics of P2 and P3 in Table 3-10.

Prototype	**Coil function**	**Resistance (total)[Ω]**	**Inductance [mH]**	**Capacitance (calculated) [pF]**	$f_{Resonance}$ **MHz**
2 (asymmetrical)	LF	160	1.8	12	1.06
	HF	68	0.4	33	1.62
	Sensor	80	0.52	39	1.16
3 (symmetrical)	LF	160	1	68	0.605
	HF	82	0.3	31	1.61
	Sensor	63	0.25	10	0.9

Table 3-10: Electrical components value for P2 and P3. The capacitance here is deduced from the self-resonance.

3.3.2 Microfluidic reservoir

3.3.2.1 Choice of fabrication procedure

The microfluidic reservoir is fabricated using the molding technique that consists in fabricating a master mold and then replicating the mold in a polymer. In this work, the PDMS was chosen because of its biocompatibility. Moreover, its use is well documented and it allows rapid prototyping and testing of the detection system.

The whole fabrication procedure is shown in Figure 3-34. The master mold can be fabricated either by photolithography with SU-8 as a photosensitive material deposited on a glass wafer by spin coating or by using a 3D printer.

The photolithography approach allows to have very precise channels that can be as small as micrometers or less. However, the master molds only lasts for a few replications due to the adherence between the resist and the substrate (especially for SU-8) and all the processing must be done in cleanroom., On the other hand, 3D printing constitutes a cheaper and faster alternative with the drawback of having less resolution in terms of channel dimensions.

Following the master fabrication, the PDMS along with its curing agent (ratio 10:1) are poured into the master mold to replicate the microfluidic channel. The result is an open PDMS microchannel that can be closed either by another flat PDMS layer or by glass using Oxygen (0_2) plasma bonding procedure.

Various prototypes were designed to assess the two approaches. Due to the mentioned benefits, we mainly focused our dimensioning on the 3D printing approach. The Table 3-11 presents the most successful prototypes dimensions:

Microfluidic prototype	Shape	Height of reservoir [µm]	Channel width[µm]	Total width /minor radius [mm]	Total length (meander)/major radius [mm]
Structure 1	Elliptic cylinder	200	500	3.5	13
Structure 2	Elliptic cylinder	200	500	4	13
Structure 3	Serpentine	200	500	12	12
Structure 4	Serpentine	100	500	12	12

Table 3-11: Microfluidic channel different shapes and dimensions for selected 3D molds.

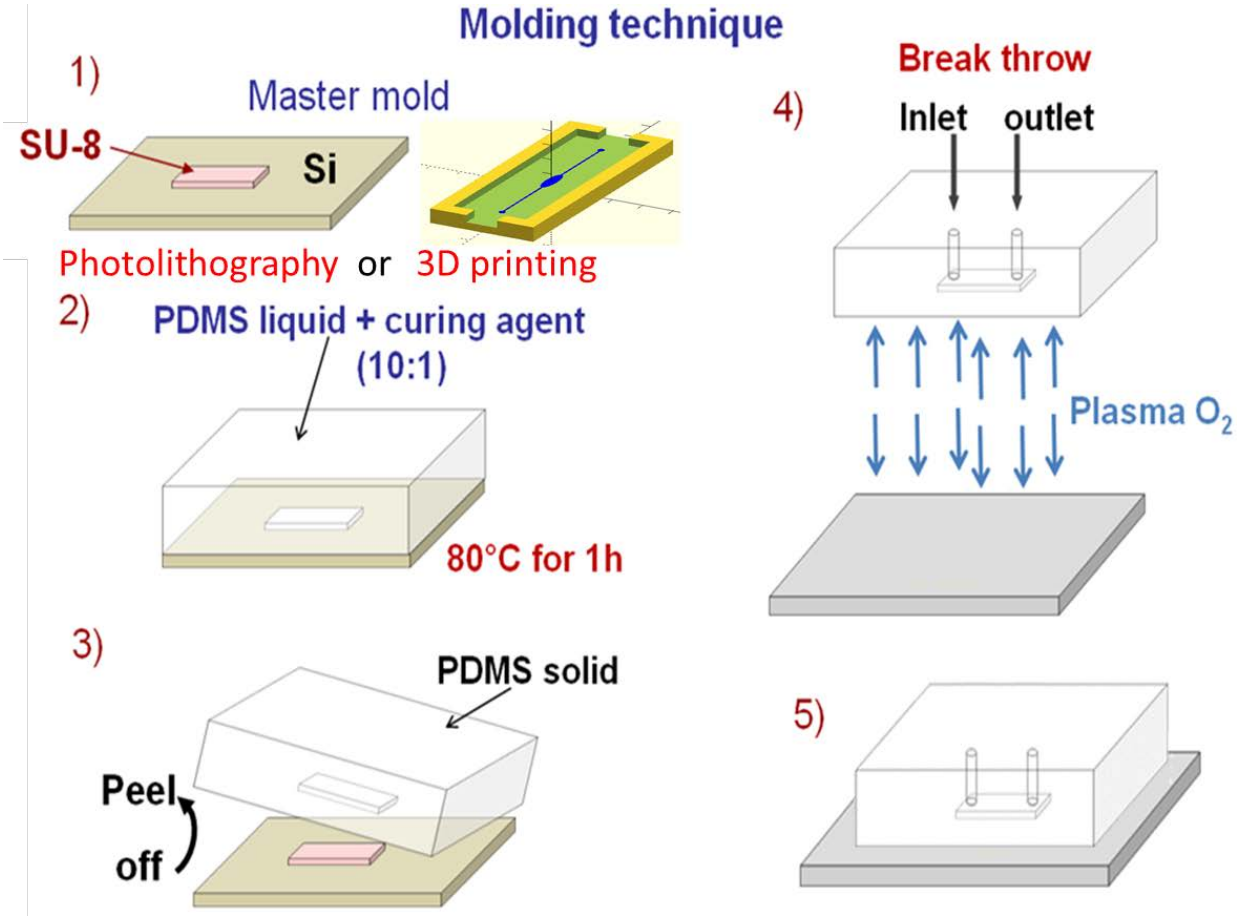

Figure 3-34: Illustration of the molding technique process using PDMS polymer.

3.3.2.2 Design and fabrication

The design of the chosen microfluidic structure is done either by using Clewin (photolithography) or Openscad (3D printing). Clewin allows to draw 2D shapes onto a wafer so that it can be used to fabricate the master mold using SU-8 photoresist. On the other hand, Openscad allows to draw 3D shapes representing the mold that will be directly printed using laser based high resolution printer (Formlabs II). Figure 3-35 shows the two designs. In designing both structures, we took care of providing a way so that the reservoir area is as thin as possible, thus bringing the reservoir closer to the excitation and detection coils and making the detection more sensitive.

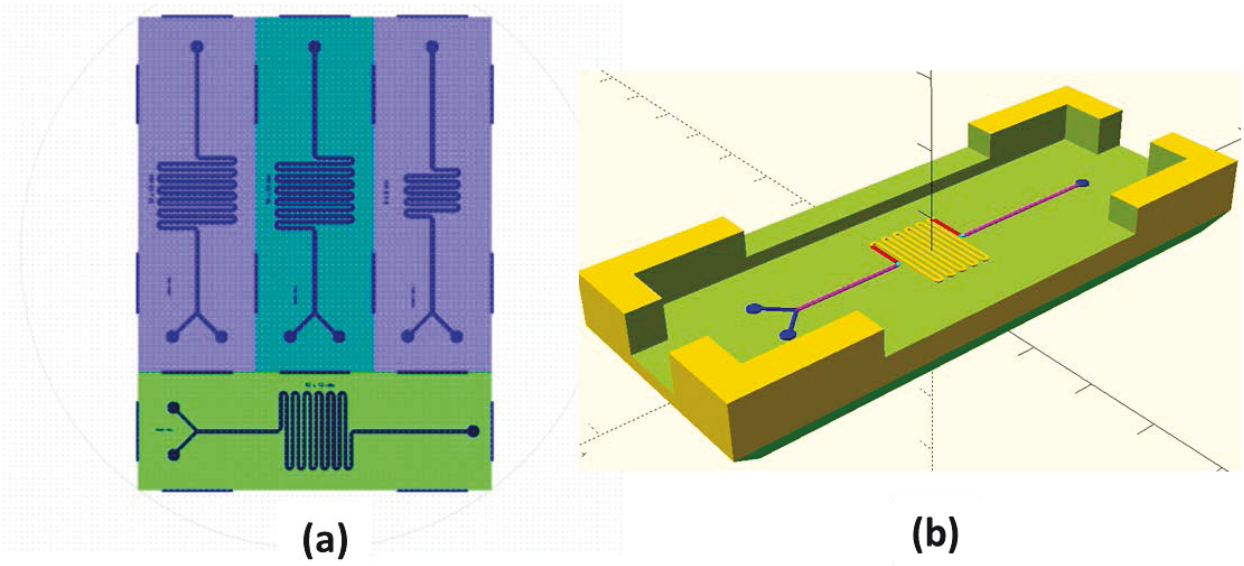

Figure 3-35: Design of the master mold using 2D (a) and 3D (b) design software for photolithography and 3D molding techniques respectively.

The performance of clean room photolithography is well known. We thus focused our attention on the assessment of the performance of the 3D printing procedure. In order to do that, various molds were printed using a *Formlab* printer and the corresponding microfluidic reservoirs were realized. Figure 3-36 gives some illustrative pictures of the printed 3D molds and of one of the realized microfluidic reservoir.

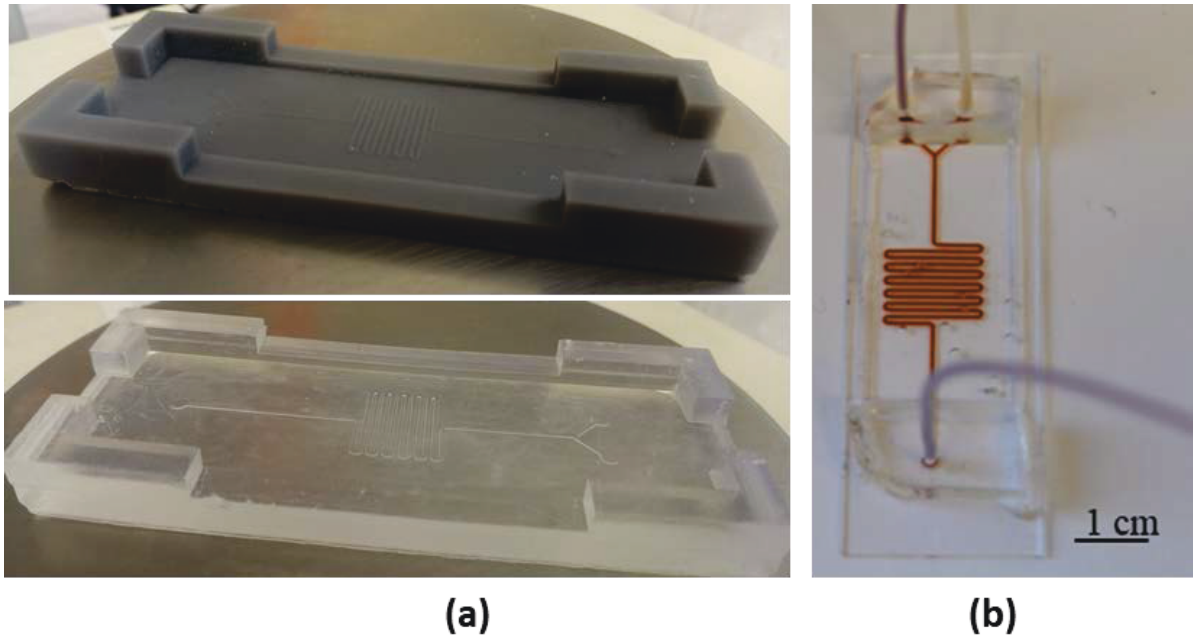

Figure 3-36: Example of 3D printed molds (a) and realized microfluidic serpentine reservoir (b)

Some of the 3D printed molds were not successful. In the serpentine like reservoir, we can

clearly see, using a profile projector (Nikon profile projector v-12), that in the case of small separation between channels, there is an overlap and thus the fluid thus flows directly without reaching the end of each meander segment. More than 100 µm spacing is needed in order to have a good printed channel (Figure 3-37). The 3D printer also has some limitations on the minimum height of the channel (must be >50µm) that should be taken into consideration.

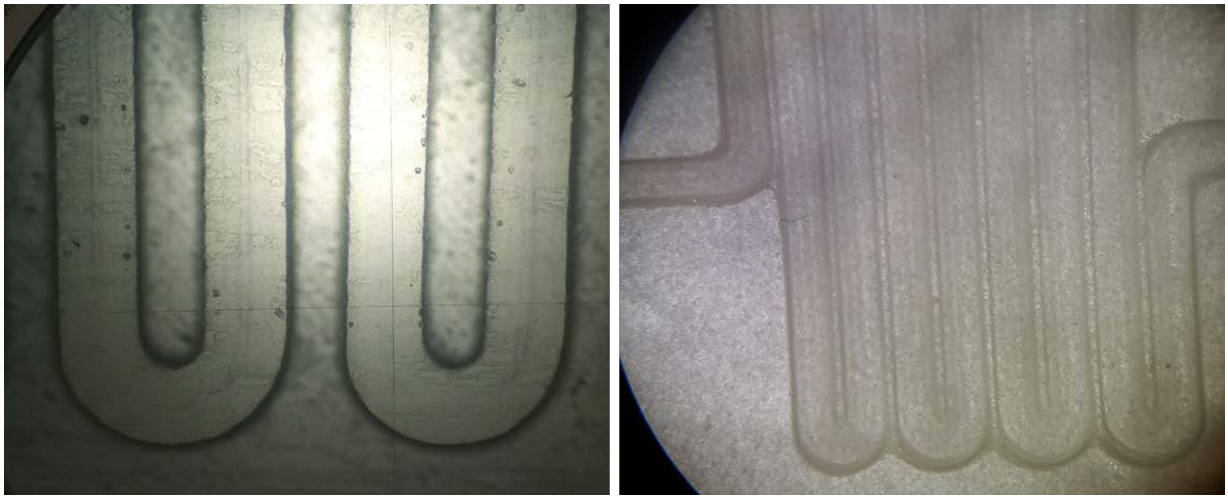

Figure 3-37: Photos of successful (left) and unsuccessful (right) printing strategies. The spacing between channels is 500 µm (left) and 100 µm (right). We can clearly see that there is some residues left during in the spacing between channels.

Finally, after different testing of the serpentine and cylindrically shaped reservoirs, we settled on the use of the serpentine-like (meander) reservoir. This choice is driven by the better fluid diffusion and better mixing possibilities. The constant channel section in this case allows to monitor the fluid velocity more accurately and to later find the best conditions for washing and incubation steps. A high enough fluid velocity allows to remove the unspecific bindings and a low enough velocity allows to have better incubation by increasing the allowed diffusion time.

3.3.3 Sandwich structure

The resulting whole prototype structure can be found in the given illustration (Figure 3-38). It is composed of two PCB coils and the microfluidic channel between them. In order to adjust the balancing, mechanical fixations are added. Similar as in case of the coils, we add a reference microfluidic reservoir in order to have also a reference fluid.

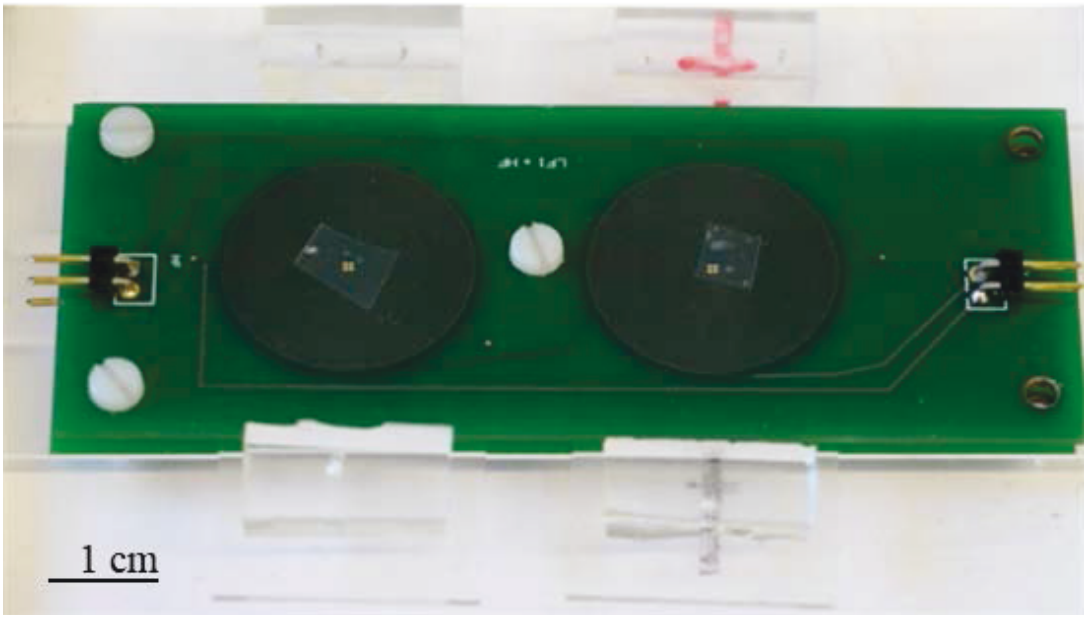

Figure 3-38: Detection structure composed of two PCB coils and the microfluidic sample and reference reservoirs between them.

3.4 Chapter summary

The goal of the work described in this chapter is to design and realize a first prototype structure.

For choosing the various dimensions, we reported analytical and multiphysics simulation tools that have been developed in order to optimize the dimensions of the detection structure. For choosing the dimensions of the coils, considered the proper magnetic excitation field while minimizing the heating effects. The detection coils must be designed as sensitive as possible with low self-generated noise.

Regarding the microfluidic channel dimensioning, the proper fluid diffusion has first been ensured. For this, a microfluidic simulation has been developed that may also allow later to simulate bubble generation and its effect on the fluid handling process.

After choosing a first set of dimensions, we realized both the coils and microfluidic channels. Benefiting from the rapid, robust and cost effective prototyping, we chosed to use PCB technology for the realization of the coils. Using the same strategy, we also focused the

development of microfluidic channels on the use of soft lithography of PDMS with 3D printed molds.

These developed prototypes have allowed to validate the various optimization tools. These tools can later be used for the development of a completely integrated and miniaturized LoC device.

In the next chapter, we evaluate the performance of these prototypes regarding the magnetic detection.

Chapter 4. Experiments and preliminary work on biosensing

In this chapter, the experimental set up and preliminary results are given. At first, we will describe the test setup with its various electronic components. The test bench is controlled by means of a LABVIEW developed software that allows studying the effect of various parameters on the magnetic response. Then, we present the tests of the performance of the realized prototypes. The PCB coils will be assessed in terms of gradiometric efficiency and sensitivity. After that, preliminary magnetic characterizations of various nanoparticles are performed. Finally, we will talk about the biosensing and corresponding important aspects. These results serve as a ground basis for further optimization of a fully integrated portable LoC.

4.1 Experimental setup

4.1.1 Test bench

A block diagram as well as representative pictures representing the test bench are given in Figure 4-1 and Figure 4-2. The experimental setup allows finding the best compromise of structure dimensions and electrical parameters before miniaturization of the electronics. Electronically, the test bench can be divided into the excitation and detection parts.

In the excitation part, the aim is to provide the excitation coils with sinusoidal signals. These signals are provided using two frequency generators for both LF and HF signals. The LF signal frequency range from few Hz to hundreds of Hz while the HF frequencies are between 10 kHz and 100 kHz. The high frequency is limited by the demodulating capacity of the Lock-in amplifiers and the response time of the nanoparticles. Furthermore, in the case of the low frequency signal, an amplifier must be added in order to have high enough driving magnetic fields.

Concerning the detection part, the detection coils transduce the change in magnetic field to a change in electrical signal. This signal must then be demodulated to the aimed mixing term ($f = f_1 + nf_2$). In order to do that, two Lock-in amplifiers are used for the sequential demodulation in f_1 and $n \cdot f_2$ respectively. The synchronization of the demodulation

frequency is performed by connecting the synchronization output of the frequency generators with the reference input of each lock-in amplifier.

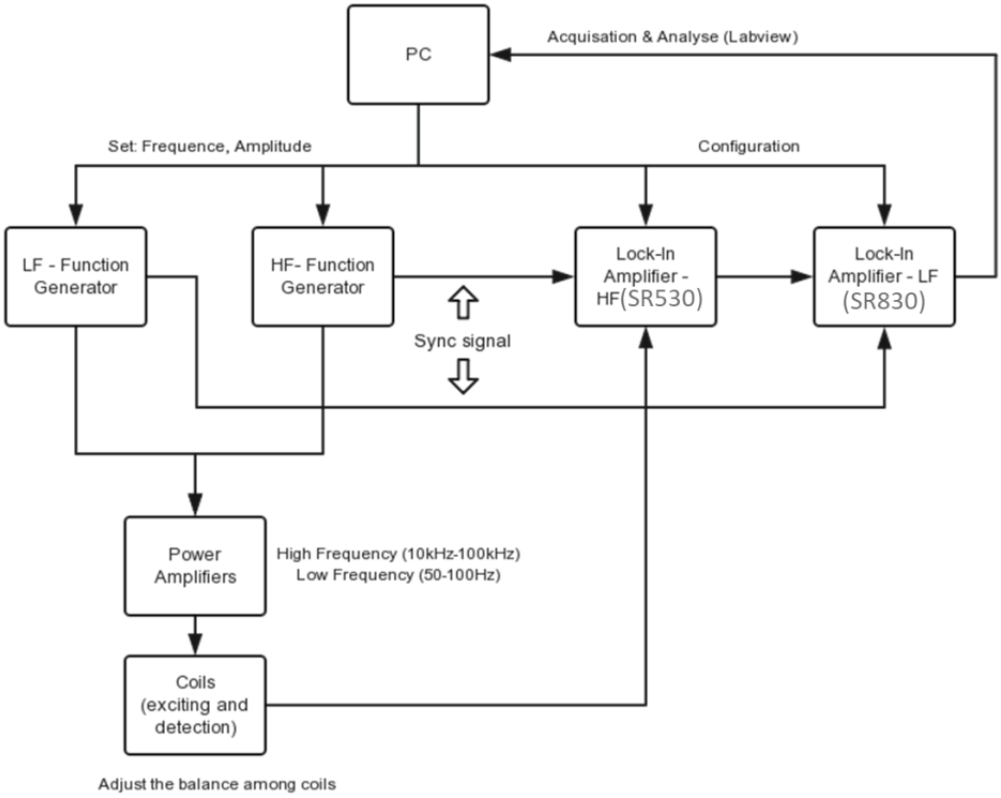

Figure 4-1: Block diagram of the experimental setup.

Finally, the microfluidic handling is performed using syringe pump (RAZEL R99-E) with varying velocity (Figure 4-2). That will allow optimizing the detection protocol in term of the velocity needed for proper binding and removing of unspecific adherence to the surface.

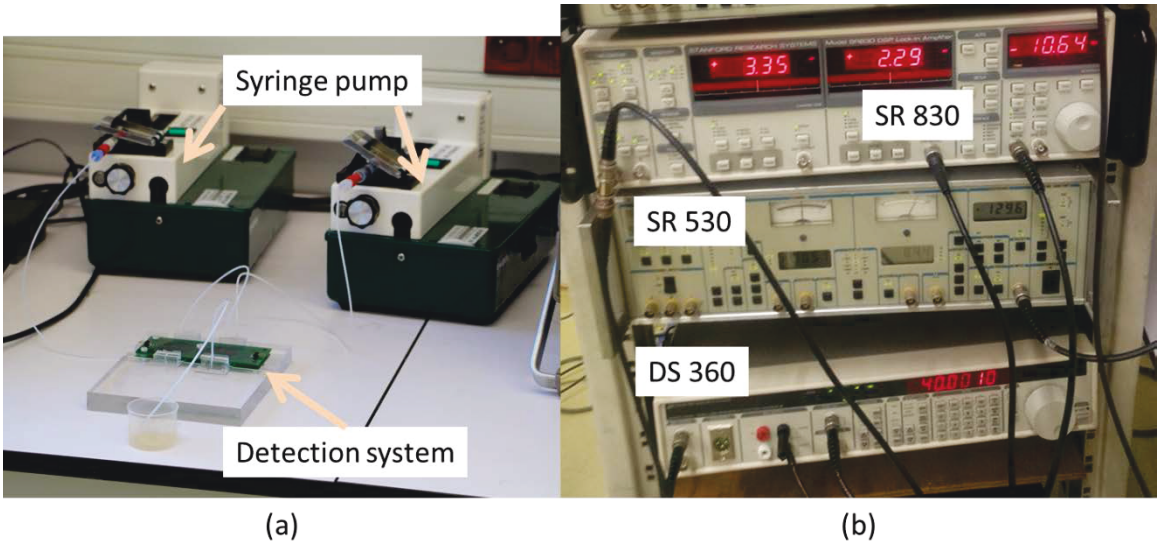

Figure 4-2: Detection system with PCB coils and microfluidic reservoirs connected to microfluidic handling with syringe pumps (a) and electronic equipments (b) of the test bench. SR 830 and SR530 are lock in amplifiers. DS 360 is a low noise frequency generator.

4.1.2 Demodulation and detection method using lock-in amplifiers

The locks in amplifiers are the principal components of the system. They allow sensitive detection of the mixing terms and analysis of the amplitude and phase of each term. The diagram of operation of one of the lock-in amplifiers (SR830) is described in Figure 4-3.

The basic functioning of the Lock-in, is that for demodulation, the signal is multiplied with the reference sinusoidal signal with two phases (θ and $\theta + 90°$deg). That gives X and Y components of the demodulation:

$$X = V_{Sensor} \sin(2\pi f_1 t + \theta) \ \ and \ Y = V_{Sensor} \cos(2\pi f_1 t + \theta)$$

Apart from demodulation, the lock-in amplifier also allows very low noise amplification ($6nV/\sqrt{Hz}$) and various filtering stages. Most of the filters can be set on/off except the low pass filter which is a simple RC filter and that is parameterized through a time constant.

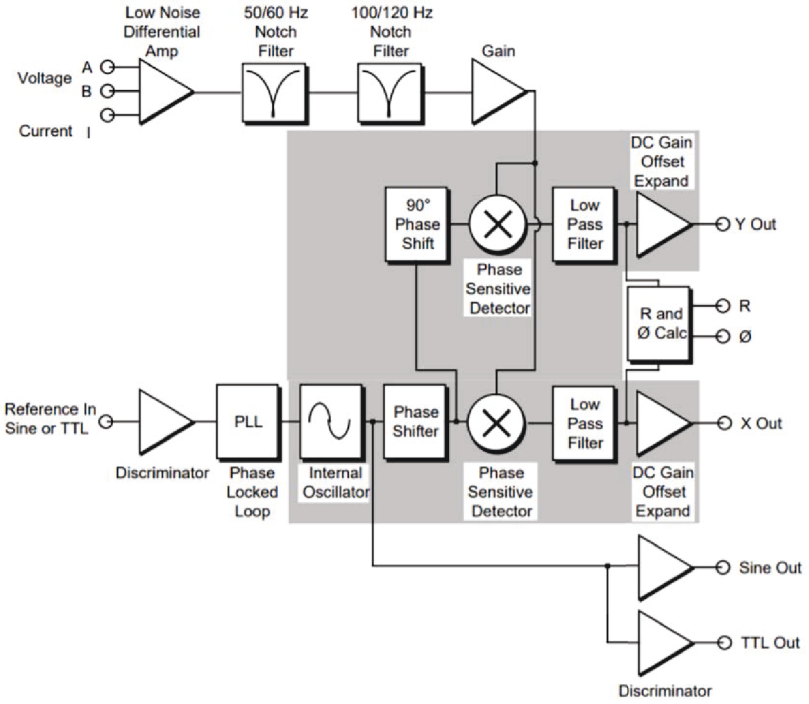

Figure 4-3: SR830 functional block diagram [156].

The demodulation of the mixing terms $(f_1 + n \cdot f_2)$ relies on a double demodulation that is illustrated via the spectral composition of the signal in each step (Figure 4-4).

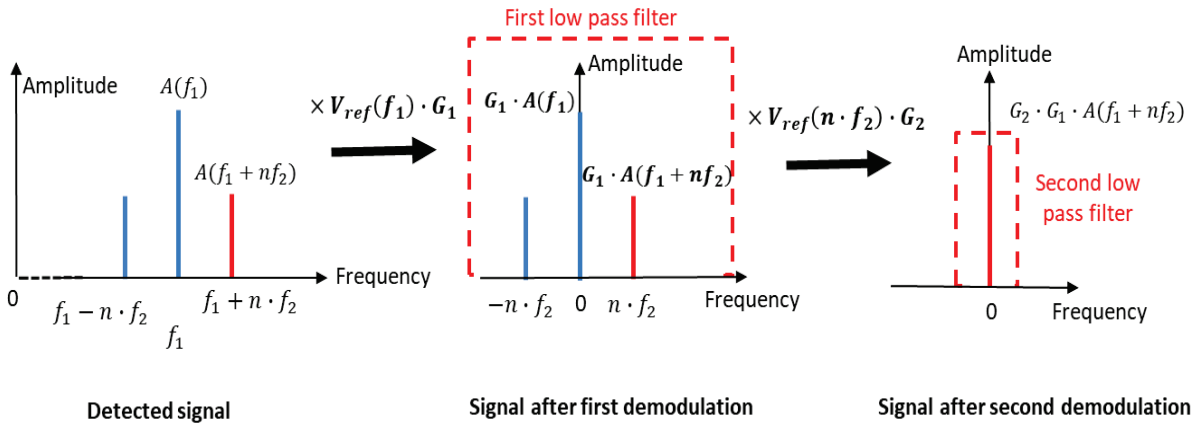

Figure 4-4: Double demodulation scheme using two lock-in amplifiers. The red peak represents the mixing term to be demodulated

For the first stage of demodulation (f_1), the signal is pre-amplified with a very low noise amplifier. The amplification is practically limited by the level of the f_1 peak signal. This is one of the reasons we must ensure optimal gradiometry by making the coils as symmetrical as possible in the design. We can also improve the gradiometry by balancing mechanically the

height of each side of the upper PCB coil (the one without sensor coil). After this first demodulation, the spectrum of the original detected signal is shifted by f_1 (Figure 4-4.b). We are left with a DC component relative to the high frequency and other AC components. Among the later there is the amplified mixing term.

For the second stage demodulation (Figure 4-4.c), the signal is demodulated at the frequency '$n \cdot f_2$'. It is further amplified by a factor G_2 and filtered. Here, we can assess the phase and amplitude change of each harmonic signal through the X and Y components of the first demodulated signal. This second lock-in thus scans the mixing terms and helps evaluate the nonlinear behavior of the magnetic response of each nanoparticle.

4.1.3 Developed LABVIEW control program

All the parameterization of the electronic devices is performed through a homemade instrumentation software based on LABVIEW programming software. This includes the function generators and the lock-in amplifiers. The basic functioning algorithm is depicted in the following algorithm of operation (Figure 4-5). The software performs a frequency sweep over the high frequency signal and a harmonic sweep to get the spectral information of each mixing term. This information is in the form of amplitude and phase responses.

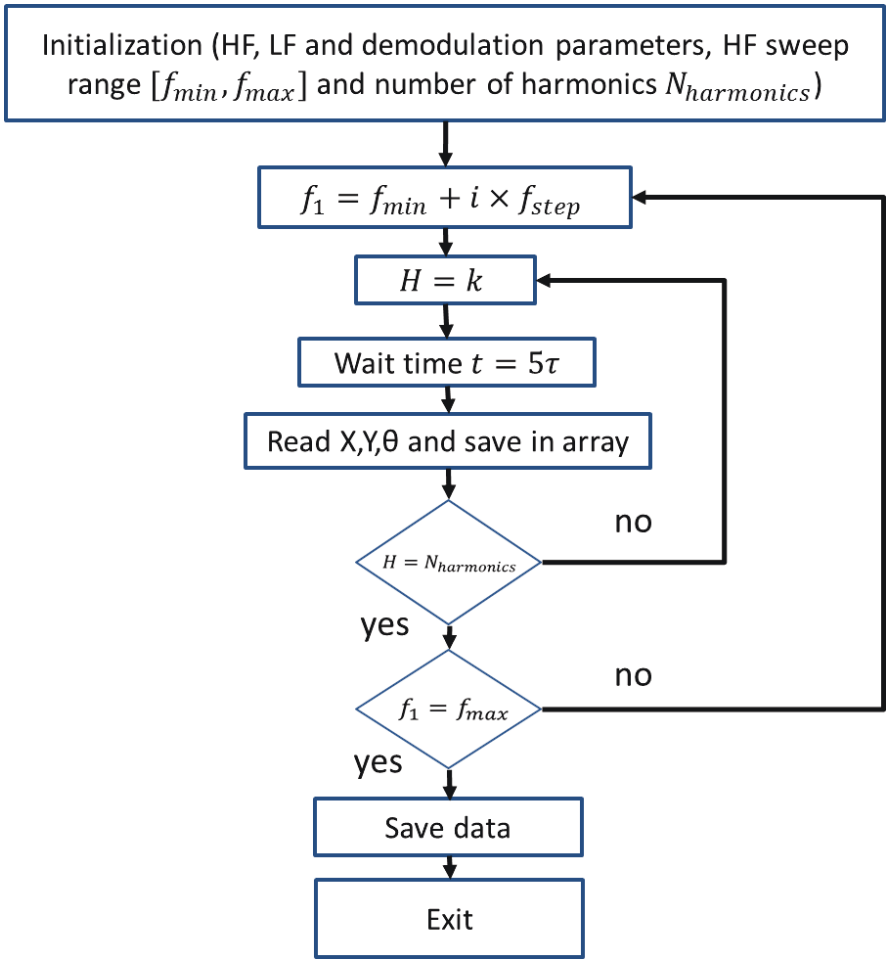

Figure 4-5: Algorithm of the control software, τ represents the time constant of the second lock-in amplifier.

4.2 Magnetic sensing

4.2.1 Characterization of the detection systems

In this section, we characterize the different detection systems that have been developed. These characterizations include the testing of the sensitivity of the symmetrical and unsymmetrical configuration regarding the influence of different general and specific parameters. General parameters include microfluidic reservoirs dimensions and the distance between upper and lower PCB whereas coils specific parameters include the effect of frequency and the efficiency of balancing.

4.2.1.1 Effect of the whole system parameters

Table 4-1 gives the detected signal in each case. For these tests we used a HF signal of 40

kHz with 28Vpp and LF signal of 65 Hz with an amplitude of 48Vpp. The output was amplified 200 times.

Prototype	Microfluidic reservoir		Height between PCBs [mm]	Detected signal [mV]
	Dimension reservoir [mm*mm]	Height channel [µm]		
Asymmetrical (P2)	12*12	200	2.4	5.60
	12*12	200	3.2	3.88
	12*12	100	2.4	2.77
	6*6	200	2.4	3.21
Symmetrical (P3)	12	200	2.4	3.02
	12	200	3.2	2.36
	12	100	2.4	1.56
	6	200	2.4	1.78

Table 4-1: Summary of characterization measures.

When we first compare both P1 and P2 prototypes, we can clearly observe that for these sets of dimensions, the asymmetrical configuration yields better performance overall. The sensitivity is better by a factor of almost 2. This is mainly due to the fact that the 2 PCBs are not very close to each other in the symmetrical configuration. Indeed, the symmetrical configuration is configured so that the PCBs are as close as possible then the upper sensor has the same sensitivity as the lower one. Unfortunately, that is not currently the case but this can be improved through the use of microfluidic reservoir with less overall height (more than 2mm currently).

Second, if we compare the effect of the reservoir dimensions we notice two things. First, the high of the channel is linearly related to the detected signal (for 100 and 200 µm). This confirms both the linearity of the measurements as well as the negligible effect of the heights of this order (100 µm) on the magnetic excitation fields. Second, when we reduce the total big dimensions of the reservoirs from 12*12 mm to 6*6 mm corresponding to a volume reduction

of 1/4; we notice that the detected signal ratio for the two PCBs is about 1.8 and 1.7 for the P2 and P3 prototypes respectively. This should have been a ratio of about 4 in a linear case. That could be explained by the decreasing excitation field magnitude corresponding to the nanoparticles that are far from the center of the coil. That is confirmed by simulations where we found that the best homogeneity is about the zone of the order of the internal radius of the excitation coils (about a few mms).

Third, if we consider the effect of the gap distance between PCBs, we see that the bigger this distance is, the worse is the sensitivity in both prototypes. This is more important in the asymmetrical configuration where the sensitivity ratio is about 1.5 between the distances 2.4 and 3.2 mm. This is explained by the weaker low frequency driving field which amplitude is quadratically related to the mixing term signal ($A(f_1 + 2f_2) \propto A(f_2)^2$).

4.2.1.2 Balancing efficiency, sensitivity and detection range

As the balancing is very important for noise reduction, we tried to approximate the balancing ratio of the two prototypes. For this, we tested put the PCBs in both aligned and orthogonal positioning for the same separating distance. In the aligned case, we get the remaining HF and LF peak signals relative to the error in balancing, while in the orthogonal case, we get the approximate detection of HF and LF peaks in the detection coil alone (without reference balancing).

Reported balancing ratios were about between 500 and 1000 for both symmetrical and unsymmetrical prototypes. This good balancing ratio allows the system to be more sensitive to the mixing term signals. The balancing ratio could be further improved by more mechanical balancing of one of the PCB (upper one) horizontal angle with respect to the other constituting PCB (lower one).

Moreover, if we study the effect of the frequency change in the case of fixed input voltage (case of a well-designed amplifier), we see that the increase in frequency contributes to the improvement of the detected signal only to a certain degree. The increased signal at higher frequency is partially or fully compensated by the decrease of the excitation current (due to inductance effect on impedance).

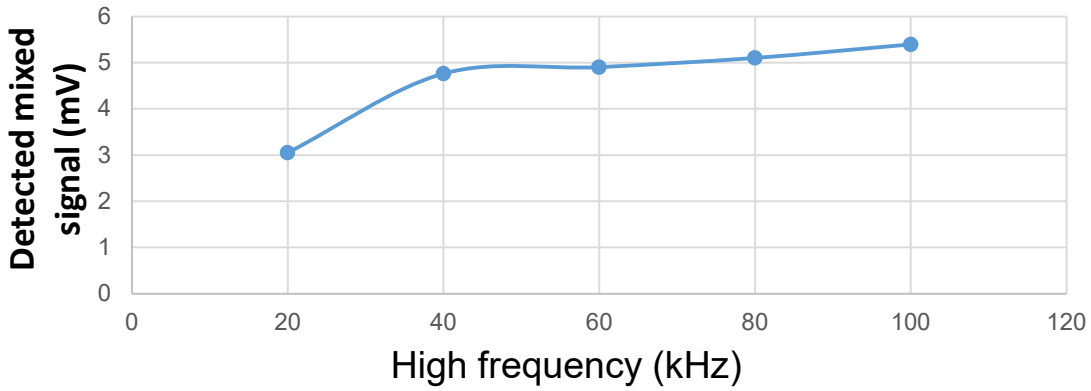

Figure 4-6: Frequency effect on the sensitivity of the detected signal for P2 with a fixed concentration of S540 NP.

Finally, we test the detection range and typical limit of detection of the PCB system with the 20nm core size iron oxide particles fabricated in the partner PHENIX laboratory (S540). Their flower-like structure offers stability at such large diameters, thus a higher magnetic moment response [157]. During our experiments to test the magnetic detection we chose a low frequency excitation of 80 Hz with a coil voltage of 14 Vpp and a high frequency of 40 kHz with a voltage of 30 Vpp. The response electronic signal which comes out of the detection coil is amplified by a factor of 500 using the lock-in amplifier. We put this SPN in the microfluidic channel composed of PDMS/glass structure of dimension 12 mm×12 mm and stopped the flow before performing the measurements.

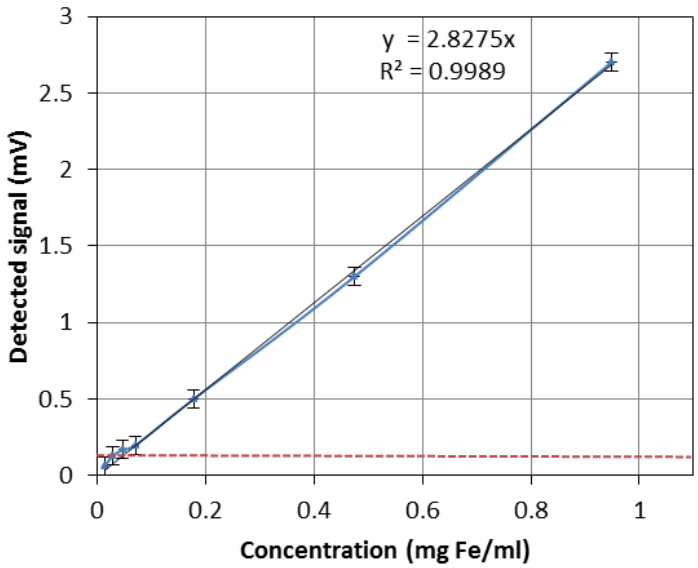

Figure 4-7:Magnetic response in function of the mass concentration of iron nanoparticles. The red dotted line indicate the limit of detection.

We obtained a curve of the magnetic response for different concentrations of iron nanoparticles in the microfluidic channel. We clearly observe a very good linearity with a coefficient of determination of $R^2 = 0.999$ for a linear range of 3 orders of magnitude.Furthermore, the test were repeated at day's intervals and proved to be very reproducible. With an accepted error of less than 20 %, our limit of detection is at about 15 ng/µL. If we consider the limit of detection in terms of iron quantity, it is roughly equivalent to 0.2 µg for a volume of 14 µL. This limit can be theoretically reduced to about 0.1 µg for a volume of 3.5 µL using the 6mm×6 mm microfluidic reservoir.

These preliminary results are very promising and validate the magnetic detection of nanoparticles in the conditions presented above. We expect further improvement with respect to decreasing of the limit of detection, especially with the miniaturized device.

Additional noise sources, both internal and external, increase the difference between theoretical and experimental LOD. The internal noise sources include: electrical noise from excitation circuit that results in crosstalk, white magnetic field noise, and small but contributing temperature gradient that changes slightly the magnetization. Diffusion heterogeneity of ferrofluids is also a contributing factor for the error bars shown in the above mentioned performance curve (Figure 4-7). External interfering signal can be in the form of magnetic field disturbance from adjacent power sources and electronic instruments.

4.2.2 Magnetic detection of SPN using the frequency mixing technique

After evaluation of the system performance, we assessed the applicability of laboratory and commercial nanoparticles in magnetic sensing applications. In fact, the optimization of the magnetic sensing system is also performed by a wise compromise of NP characteristics. As has been discussed in Chapter 2 (section 2.2.3), many factors influence the performance of magnetic nanoparticles with respect to magnetic detection. From these factors we can cite the chemical composition, composing matrix (for multicore big NP above 50 nm), and hydrodynamic as well as magnetic core sizes of the particles.

Our partnership with PHENIX laboratory allowed us to test the detection of 4 types of nanoparticles that are different in size, chemical composition, or synthesis method. In addition to these nanoparticles, we tested the performance of commercial streptavidin-coated superparamagnetic nanoparticles. Table 4-2 gives the different characteristics.

Nanoparticles references	S540	S499E	S505	S494P	Fluid-mag streptavidin
Composition	Fe2O3	CoFe2O4	CoFe2O4	CoFe2O4	Fe304/ strep-tavidin coated
Size (core)	20 nm	50 nm	10 nm	19 nm	200nm (hydrodynamic)
Magnetic compound concentra-tion (iron/cobalt) [mg/ml]	14.8	11.19	187.4	27.34	NA
Initial concentration (C0) whole molecule [mg/ml]	21.16	14.66	262.55	31.66	10
Initial molar concentration (whole molecule) [mol/l]	0.13	0.062	1.12	0.14	NA
Saturation magnetization (C0)[A/m]	1630	1012	20780	2790	590
Normalized Ms (saturation magnetization) (to reference 10mg/ml)	770.36	690.46	791.47	881.14	590

Table 4-2: Characteristics of the different tested magnetic nanoparticles. NA: not available values.

Saturation magnetization of these different nanoparticles is also given in the table. In order to compare the saturation magnetization, we normalized the magnetization by factoring all the concentrations to a reference concentration of 10 mg/ml. This allows a more proper comparison of this parameter. We can see that the commercial streptavidin coated magnetic nanoparticles have less saturation magnetization compared to the other *brut* magnetic nanoparticles (not coated). We assume that it is due to the dead volume caused by both the matrix that binds the various magnetic cores and to the streptavidin coating.

We tested the performances of these nanoparticles with our second asymmetrical P2 prototype. The next figure gives the sensitivity of these nanoparticles with respect to magnetic content, molar quantity and mass of the whole compound.

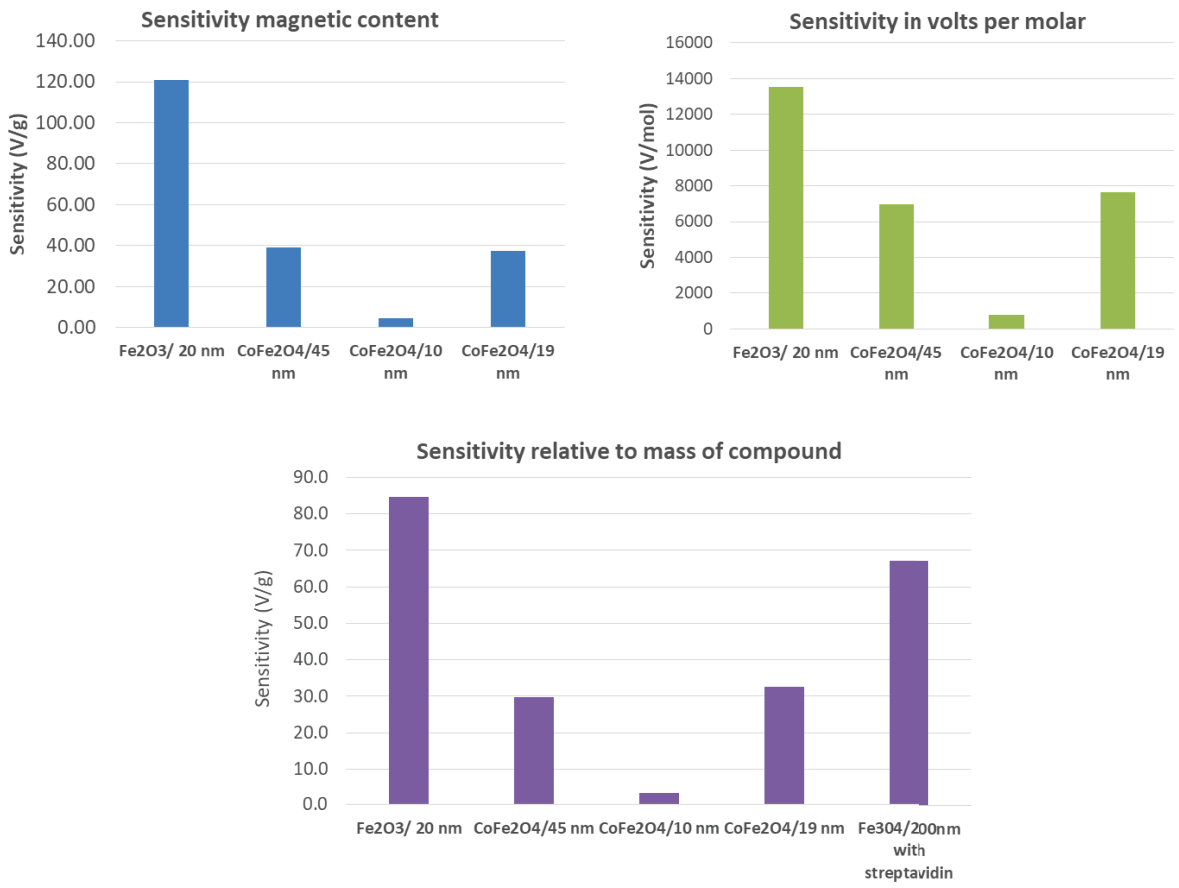

Figure 4-8: Sensitivity measurements of various laboratory and commercial nanoparticles.

From these curves we can firstly deduce that the performance of the smallest nanoparticle is the poorest, even with normalization to the magnetic mass. This might be due to the poor surface magnetization effects discussed earlier (section 2.2.3 spin-canting effects). Also, if we compare the second and fourth compounds with 45nm and 19nm respectively, we observe that the additional size of the particle has no effects on improving the magnetization. That might be due to the difference in synthesis procedure (Figure 4-9). This aspect ought to be investigated in more detail in the future.

Furthermore, if we compare the first and fourth compound, we see that they have the same size but they exhibit a notable difference in sensitivity. We assume that this is due to a better nonlinear performance of maghemite (Fe_2O_3).

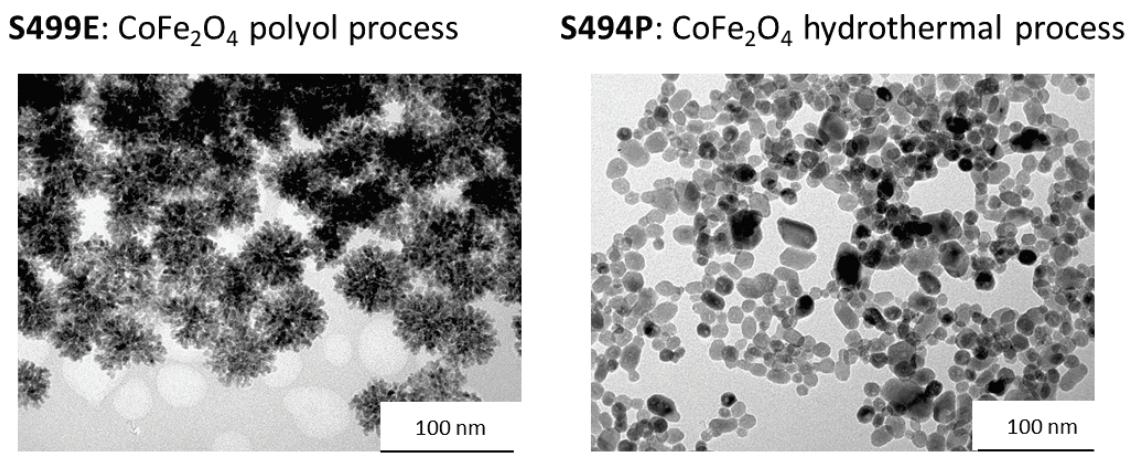

Figure 4-9: Transmission electron microscopy (TEM) pictures of the 50 and 19 nm nanoparticles realized through polyol and hydrothermal processes respectively.

To sum up, magnetic nanoparticles should be characterized for their usage in the mixing frequency technique. We deduce from these results and the magnetization curves that the mixing term signal ($V(f_1 + 2f_2)$) is dependent on the nonlinearity of the nanoparticles. Stronger saturation magnetization does not yield stronger performance because the operating magnetization fields are below the saturation zone. We also noted that some of the Cobalt based nanoparticles exhibit some hysteresis effects (especially for 50 nm particles). This effect has been already explained in chapter 2 (section 2.1.5).

Consequently, we deduce that the S540 constitutes a good compromise for magnetic sensing. It has strong superparamagnetic behavior (Figure 4-10) and good saturation magnetization as well as a good size. This particle should be tested in the context of biosensing after coating with streptavidin or other affinity binding molecules.

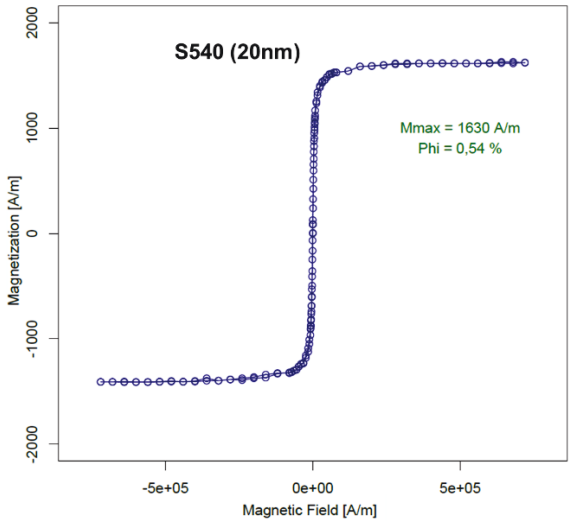

Figure 4-10: Magnetization curve of 20 nm maghemite (Fe_2O_3) nanoparticles.

4.3 Biosensing aspect

After assessment and validation of the detection structure with respect to magnetic sensing of SPN, we prepared the next step consisting of the biosensing detection. In order to achieve the best biosensing performance while considering cost and rapidity of implementation, we discuss the biofunctionalization of the PDMS surface with specific antibodies. Unfortunately, a final biosensing validation measurement of CRP protein could not be performed in the time scope of this thesis. More advanced equipment like XPS and AFM analyzing tools need to be used for quantitative measurement of the density of functionalized antibodies.

We have, however, studied the biofunctionalization aspects and present the state of the art and important criteria as well as a first choice of biofunctionalization protocol with preliminary validation steps. As discussed in chapter 1, the development of an efficient biofunctionalization protocol is very important for the development of a sensitive transducer.

4.3.1 State of the art of biofunctionalization techniques

As a reminder, Figure 4-11 shows the immunoassay sandwich principle in the case of the use of magnetic labels (SPN coated with streptavidin). The first step of this assay in to bind the specific primary antibodies of the target antigen to the microfluidic reservoir surface. Basically, the more antibodies are bound to the surface, the more antigens can bind to them. Hence, the amount of bound SPN will increase the yield and thus lead to a better sensitivity

performance.

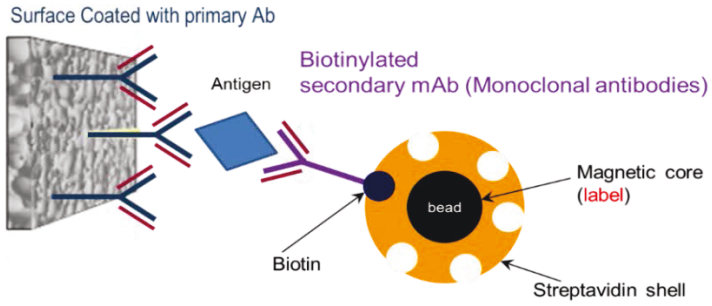

Figure 4-11: Principle of sandwich immunoassay using magnetic beads as labels.

From the literature, we find that efficient immobilization process on the surface of microchannel can be subjected to four different criteria:

1. **Amount of immobilized antibodies**: Indeed, the more functionalized antibodies we have, the more analyte can be bound to it, usually leading toa higher signal and lower detection limit.
2. **Amount of non-specific binding**: The second set of antibodies should not adsorb to the surface of the reservoir, this will lead to false positive results due to the fixation of the label to this non-specifically bound antibodies.
3. **Robustness of the process**: for the detection results to be meaningful and in the scope of making different tests for a long period, the immobilization process and the subsequent surface modification should last for a relatively long term.
4. **Reproducibility of process**: The process should yield similar results when applied to two reservoir chambers.

In addition to these criteria, we seek in the scope of this project, a cost effective solution, and for future work, a non-reversible immobilization process.

4.3.1.1 Immobilization techniques

Various immobilization techniques are employed to attach proteins to the detection surface (Figure 4-12). These techniques can be divided into three major categories: physisorption, covalent immobilization and affinity based immobilization [158]. In the context of this project, we focus on literature relevant to the immobilization of antibodies to a solid surface.

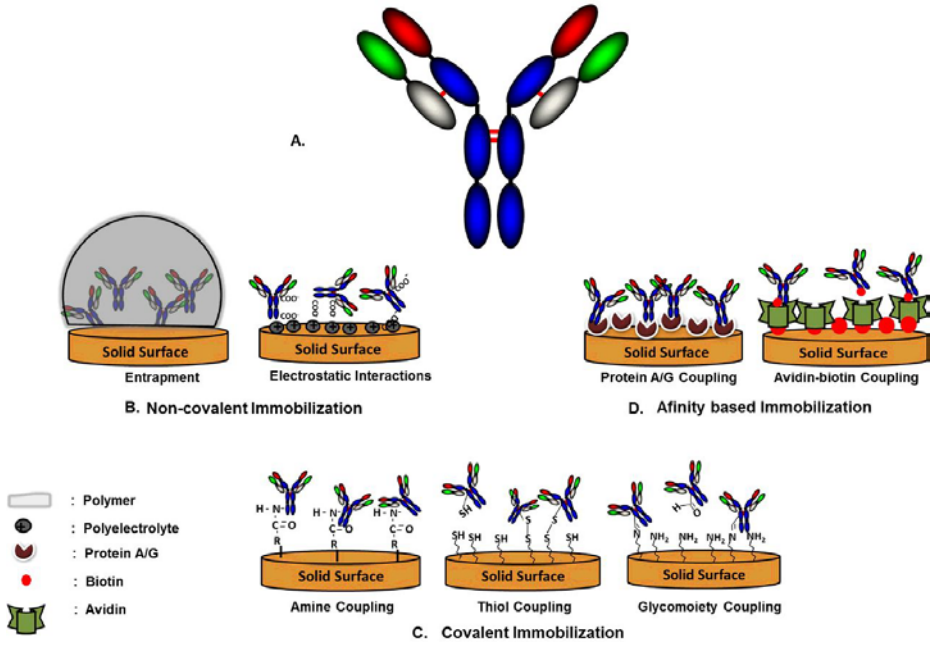

Figure 4-12: Common surface immobilization methods for heterogeneous assays. (a) Representation of an antibody. Schematic of immobilization mechanisms: (b) physisorption, (c) covalent bond and (d) bioaffinity interaction [159].

Physisorption

Physical adsorption is the easiest and simplest approach to attach proteins on a surface (Figure 4-12.b). In this case, proteins bind to the surface using intermolecular forces (hydrophobic, Van der Waals, electrostatic…etc.). These intermolecular forces are highly dependent on environmental parameters like temperature, surface condition and pH value.

The advantages of such techniques are:

a. Simple implementation without sophisticated chemical protocol
b. No toxic reagents
c. Rapidity

On the other hand, the main disadvantages can be summarized as follows:

a. Lack of stability due to high dependence on environmental factors.
b. Reduction of protein activity due to possible multiple binding sites.
c. Weak binding force to the surface.

Consequently, classical physisorption alone cannot yield stable efficient immobilization of proteins. In major literature, the use of spacers or intermediate molecules is used in order to

avoid blocking of active sites or to make stronger attachments. These intermediate molecules bind to the surface by covalent linkage on one end and provide hydrophobic or charged functional groups on the other end for protein physisorption.

Bioaffinity immobilization

While physisorption is the process of physical adsoption, bioaffinity is the biospecific adsorption between natural components. It exploits the already existing phenomena in nature. Major used interactions involve biotin-avidin, protein A/G-antibody, DNA hybridization and recently aptamers (Figure 4-12.d).

The advantages include:

a. Strong binding and stable process.
b. Precise orientation of proteins on the immobilization surface.
c. Specific interactions that prevent nonspecific bindings.
d. Possibility of reversible binding using post chemical treatments.

The disadvantages of such techniques consist in:

a. High cost.
b. Lower proteins coverage density.

The use of bioaffinity techniques is usually in conjunction with other techniques of immobilization like covalent bonding. This allows the efficient use of these affinity molecules only on the binding sites. In the case of common magnetic sandwich immunoassays, biotin-streptavidin interaction is used to bind biotinylated antibodies to streptavidin coated magnetic beads.

Covalent bond

This constitutes the most frequently used and most often reported technique used for microfluidic immunoassays. Active reagents are used to activate the surface. This activated surface reacts with amino-acid residues on the protein exterior (bonding sites). This latter step allows the antibodies to bind covalently to the surface (Figure 4-13). Finally, the remaining activation sites are blocked using common blocking agents like lysine, BSA …etc. The blocking agents should not interact with the bioentities of interest.

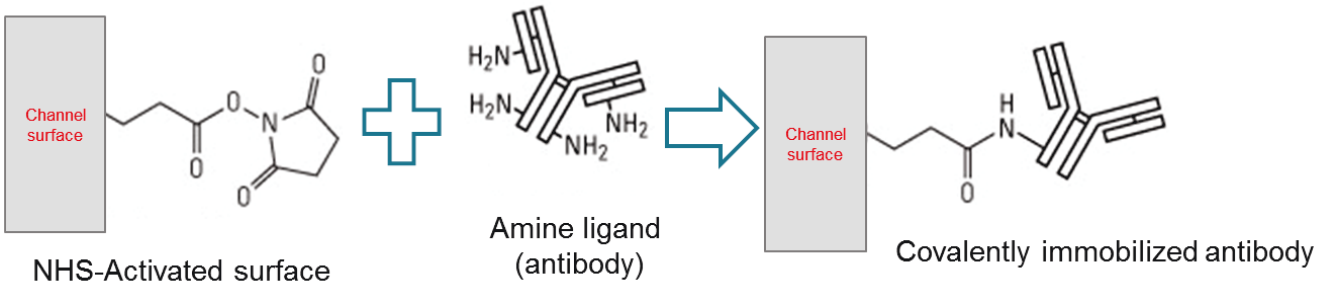

Figure 4-13: Example of Covalent bond immobilization of an Antibody.

The advantages of such techniques are:

a. High-density protein coverage compared to other methods.
b. Stable strong bonding to the surface.
c. Well-known surface modification procedures.
d. Cost effective, due to the wide availability of reagents.

The main drawbacks can be summarized in:

a. Risk of reduced activity of protein (by forming linkage on active sites)
b. Use of toxic reagents.
c. In many cases, the chemical process can be complicated.
d. Long preparation time: reservoir should be prepared in advance.
e. Mostly irreversible unless using strong oxidizers to refresh.

In order to find a method that takes into account all the above-mentioned criteria, one should aim at using a conjugated method that uses the advantages of covalent bonding and bioaffinity interactions.

4.3.1.2 PDMS as a functionalized surface

As discussed in chapter 1, poly(dimethylsiloxane) (PDMS) is a well-known polymer that is in general extensively used in microfluidic chips and LoC systems. The wide use of PDMS is due to its biocompatibility, low cost, small achievable structure sizes down to 0.1 μm and rapid prototyping possibilities. This material is transparent, which makes it suitable for optical detection methods. It is also permeable to gases and non-permeable to solutions like water. Its chemical structure is shown in Figure 4-14:

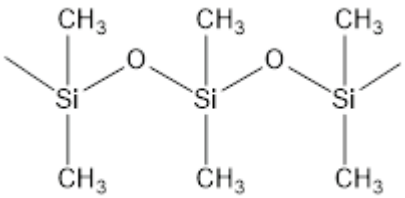

Figure 4-14: PDMS Chemical structure

However, if this elastomer is left without treatment, biomolecules can easily adsorb non-specifically to its surface due to its strong hydrophobic properties, thus encouraging false positive results. This is why, in common literature, PDMS microchannel are usually sealed with a glass or silica substrate. The substrate is then used as an immobilization surface instead of PDMS. The use of glass or silica substrates allows us to use robust immobilization techniques that exist since decades. Nevertheless, this process should be carried out carefully and it suffers from a main drawback: only one surface of the reservoir can be used for the immunoassay.

In order to use both reservoir surfaces (up and down), we can apply one of various surface modification techniques to transform the surface into a hydrophilic one. The process is called oxidation. The subsequent processes for biofunctionalization become similar with usual processes in glass and silica.

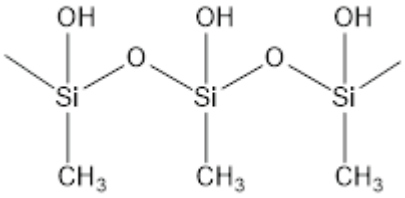

Figure 4-15: Oxidized PDMS presenting silanol groups.

A typical PDMS surface biofunctionalization procedure is explained in the next figure. After oxidation of the PDMS surface, an organosilane is added so that the PDMS surface will have functional groups (such as aldehyde) that can bind to the antibody functional groups (like amine groups). Antibodies are then added so that they bind to the silane, hence to the PDMS surface. Finally, the blocking agent is added (like BSA) which prevents non-specific binding.

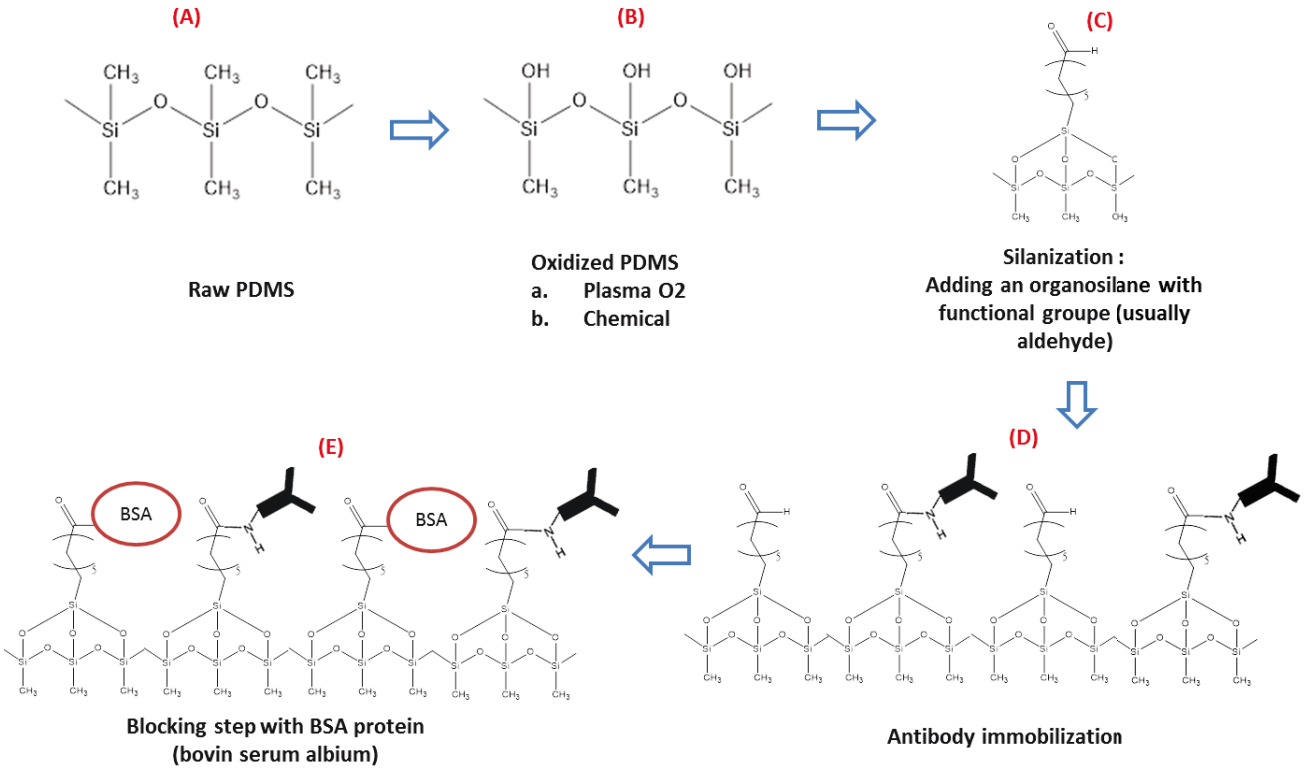

Figure 4-16: Typical covalent bond biofunctionalization of PDMS surface with antibodies.

4.3.2 Choice of biofunctionalization procedure

Priority will be given to covalent bonding techniques since the immobilization process is well known and the different reagents are widely available at an affordable price. Bioaffinity linkage will also be used in the sandwich immunoassay process in order to bind magnetic beads to a secondary set of antibodies.

A practical analysis of three different covalent bonding techniques is described in [160]. Our first chosen priority parameters are cost effectiveness, density of functionalized antibodies as well as robustness and repeatability of the procedure over time. For cost effectiveness and stability of the protocol, we chose to use a covalent binding procedure (Figure 4-16). This covalent binding procedure can be coupled with the deposition of an interface layer instead of changing the chemistry of the surface of PDMS. The interface layer of choice is PVA (polyvinyl alcohol). This procedure is compared with chemical and plasma oxidation of PDMS surface (Figure 4-17). The remaining biofunctionalization protocol is as described in Figure 4-16.

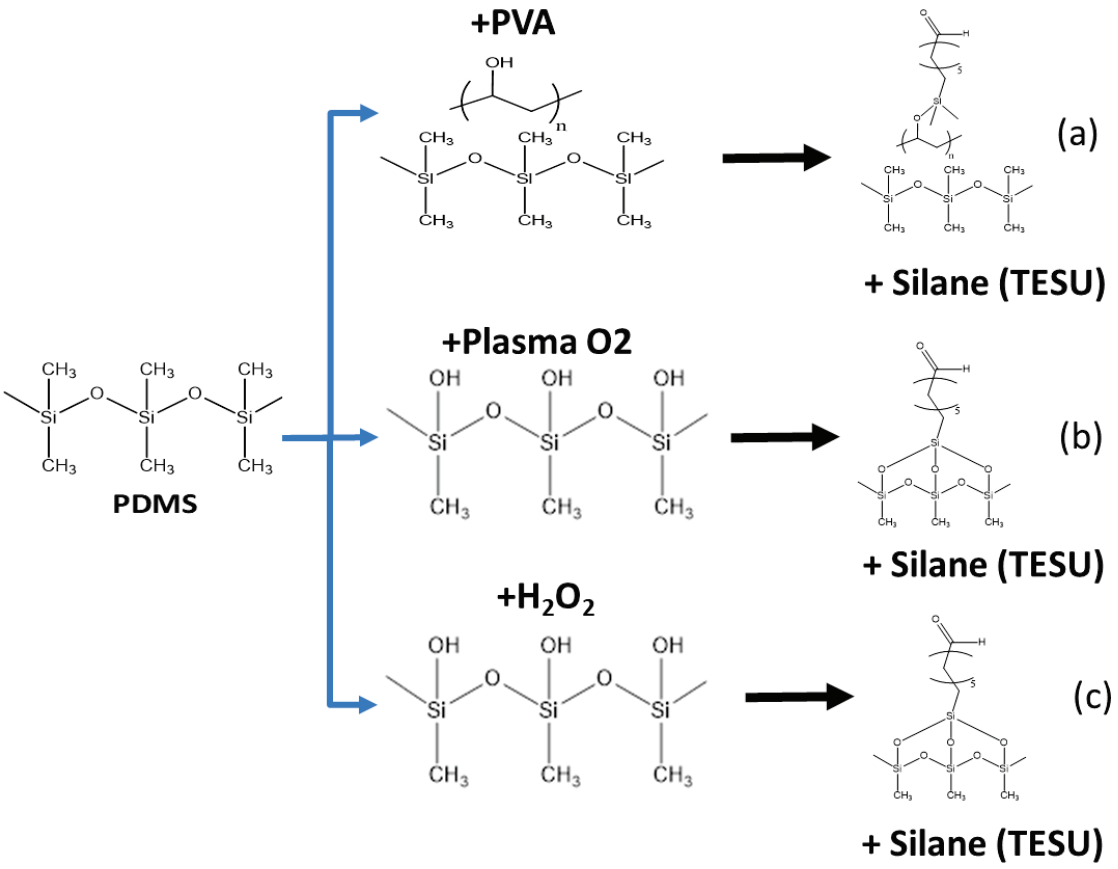

Figure 4-17: Scheme of the different modification approaches tested for the biofunctionalization of PDMS [160].

4.3.3 Preliminary validation of the biofunctionalization process

Preliminary validation of these oxidation alternatives (PVA, Plasma and H_20_2) was performed using contact angle measurements. A contact angle is the angle that the edges of a drop of water form with the substrate when deposited on top of its surface. Typically, contact angles of hydrophobic surfaces like non-treated PDMS are well above 90º whereas contact angles of hydrophilic surfaces like oxidized PDMS surface are 90º or less (Figure 4-18). We can thus assess the efficiency of the surface oxidation in a semi quantitative way.

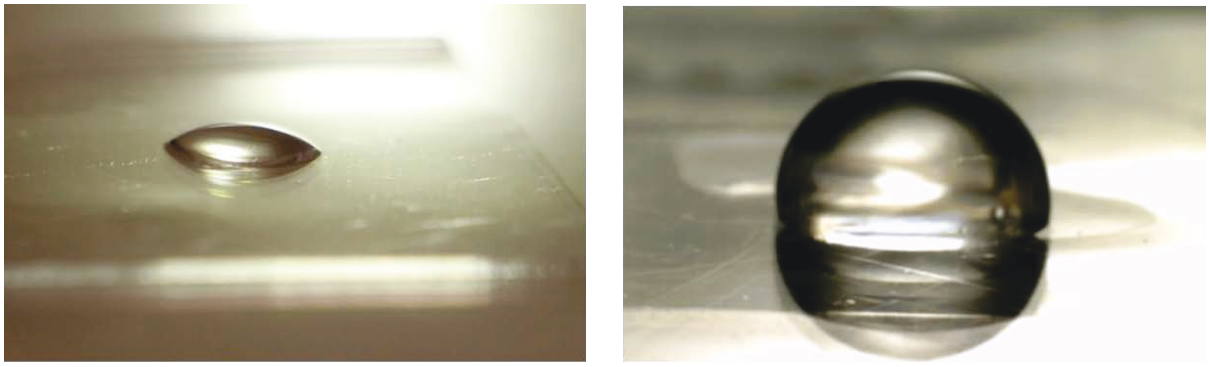

Figure 4-18: Example of oxidized (a) and raw PDMS(b) reaction to a drop of water (20µl).

For first validation and ease of characterization, measurements were performed using an open PDMS flat surface. Results are given in the following figure.

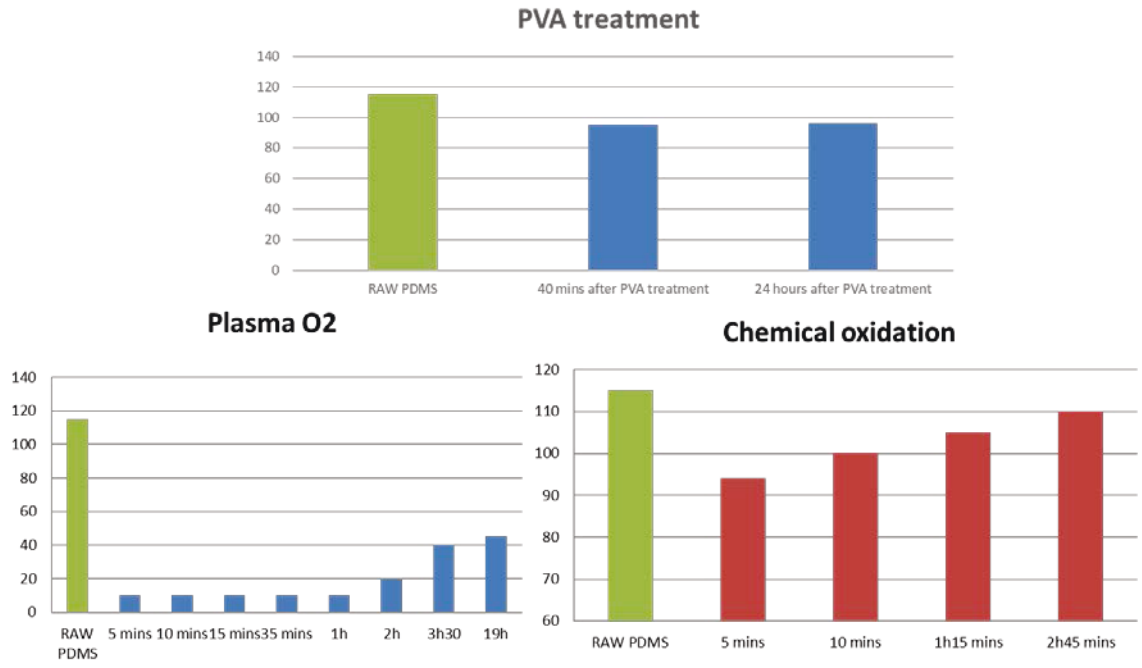

Figure 4-19: Preliminary results for contact angle measurements.

We can see from these tests that the plasma O_2 oxidizing procedure has the best performance overall. Contact angles are well below 90º and remain so for more than 19h. Chemical oxidation on the other hand gives the worst performance while PVA treatment gives a good compromise for an easy to use stable oxidation method. We consequently retain the PVA and plasma O_2 procedures.

As a next step, the addition of organosilanes must be validated through the use of XPS or AFM characterizations. In this thesis scope, such advanced equipments were not available. Direct detection of CRP protein as a validating substance could be performed but the measurements cannot be assessed due to the lack of this biofunctionalization validation step.

Finally, in the appendix A, we propose a protocol for the biofunctionalization of the PDMS surface based on these last results. If better performance is needed, we can combine this method and test the addition of a spacer (cross-linker) like Glutaldehyde (GA) in order to improve the SNR as it is reported in [161], [162] and [163] where GA improved substantially the immunoassays results.

4.4 Chapter summary

In this chapter, we presented the different experimental and preliminary work toward biosensing. A test bench was developed for the detection of magnetic nanoparticles through the use of frequency mixing technique. In this respect, an instrumentation and also LABVIEW acquisition and control program have been realized for the study and optimization of the magnetic sensing structure. The magnetic and microfluidic test bench has allowed optimizing the electrical parameters before the complete integration of the system. It has also allowed finding the best biosensing protocol by optimizing the flow rate so that proper binding can take place while unspecifically bound particles are removed by the drag force of the flow.

After that, experimental characterization of both the detection system as well as the magnetic nanoparticles was performed. Both symmetrical and unsymmetrical configurations of planar multilayer PCB coils were tested in terms of sensitivity and balancing efficiency. We concluded that the distance between the two PCBs above and under the microfluidic structure is of prime interest for enhancing the sensitivity. We also found that with the available developed prototypes, the size of the detection microfluidic reservoir could be reduced to 3.5 µl without compromising the sensitivity. Apart from the system, the magnetic nanoparticles were also tested for their prospective use in magnetic biosensing. We confirmed the assumptions of size effects and found that an intermediate size between small poor magnetic nanoparticles and large particles comprising some hysteresis must be found. The

20 nm maghemite particles constitute a best fit for magnetic testing. They should therefore be tested for biosening by coating them with affinity surface (like streptavidin).

Finally, we presented the biosensing aspects. Preliminary work for the biofunctionalization of the PDMS surface with primary antibodies has been described. A state of the art review followed by a choice of appropriate protocol was given andvalidations of the first phases of biofunctionalization were presented.

Future work consists of the complete validation of the protocol through the use of more advanced methodologies such as AFM and XPS that could not be made within the scope of this thesis. After that, the performances of the fabricated prototypes will be tested with respect to the detection of C-reactive protein (CRP) and Procalcitonin (PCT) to acheivea more complete biosensing validation of the system

Conclusions and outlook

Conclusions

In this thesis, an electromagnetic microsystem for the detection of magnetic nanoparticles in a microfluidic structure for immunoassays is presented. Since the final aim is to develop a completely miniaturized LoC pathogen sensing system, we started by a rather comprehensive review on the major critical aspects of such systems. Pathogen sensing, LoC technology as well as the immunoassay concepts and characteristics were presented. Understanding the various factors that influence the conception of a miniaturized system is of prime importance. All mentioned LoC biosensing aspects must be planned accordingly. This includes the fluid handling, the composing materials, the biofunctionalization process as well as the detection scheme. An ideal prototype would be one that included sensitive detection of pathogens with only few steps of operation and with as little as possible amount of reagents. Finally, since the system is intended for public use, a compromise between these parameters must be found in accordance with the society and market needs. In fact, to ensure a successful invention, we must align research objectives and market trends. Ease of use, cost, portability, rapidity of the tests as well as multiassay capacity constitute the main priorities.

For the development of such a system, we use a magnetic sensing approach based on the mixing frequency technique. Consequently, we covered magnetic sensing in general and the mixing frequency technique in particular. Magnetic sensing is advantageous in that it is as it is contactless, sensitive and can be integrated with actuation methods without being affected by the biological noise. The superparamagntisque nanoparticles (SPN) have a high binding affinity and specificity and due to these advantages, they constitute the main component for many magnetic and nonmagnetic detection methods. Thus, we presented a set of general requirements that help choosing the appropriate SPN in the case of magnetic sensing. Afterwards, we covered theoretical concepts and previous experimental work on the mixing frequency technique that allows to detect the specific nonlinearity of SPN magnetization response. The collective advantages of this technique and immunoassays in general have been considered for the development of the envisioned LoC system.

Realizing such LoC systems requires multidisciplinary work. Thus, we decided to develop first a set of analytical and multiphysics simulations. They have allowed us to optimize and to miniaturize the detection system by taking into account as much parameters as possible. The system is composed of both an electromagnetic detection system and a microfluidic structure for sample handling. The electromagnetic system is comprised of planar coils intended for both generation and detection of changes in magnetic field. The analytical and simulation tools have thus ensured proper description of the magnetization and of sensitive detection of the SPN. In addition, the heating effects of excitation currents in the final LoC must be reduced to a minimum in order not to affect the viability of the biological medium. Regarding the microfluidic part, critical aspects are proper filling, diffusion and mixing properties. All these criteria can be assessed through the use of the developed microfluidic simulations. These tools allow to reduce both time and cost of the clean room prototyping of the coils and microfluidic structures.

In order to validate these tools, a first design and realization scheme has been developed. The prototype systems included a set of PCB printed coils and a PDMS microfluidic channel with the use of 3D printed molds. This approach allows cost effective and rapid prototyping that may allow the design and testing of many prototypes. The different prototypes were then characterized electromagnetically. Developed tools were assessed by comparing the theoretical and simulated results with the prototypes characteristics.

We assessed the performance of the prototype systems with respect to magnetic detection. Sensitivity, balancing efficiency as well as the effect of various electrical and dimensional parameters have been analyzed by developing a test bench with accompanying instrumentation and LABVIEW programs. The results can serve as a basis for further improvement of the optimization tools. Moreover, the prototype systems allowed us to test various magnetic particles in the framework of their usage with the frequency mixing technique. We concluded that strong nonlinearity of SPN is very important for the technique.

Finally, we presented the preliminary work on biofunctionalization that has been done during the scope of this thesis. In fact, the choice and development of an efficient biofunctionalization technique is as important as the development of a good transduction method. If the biofunctionalization is not thoroughly validated, the whole system may not yield any acceptable pathogen sensing results. Biofunctionalization affects the repeatability,

stability, cross-reactivity and sensitivity of the prospective system. Towards the choice of the biofunctionalization protocol, a state of the art along with proposed protocols have been described. The aim is to find a compromise between cost effective and robust biofunctionalization procedure. For this, we propose the use of a covalent binding technique combined with either robust modification of the PDMS surface or plasma treatment.

In the next section, we will present an outlook to future work with important comments concerning each aspect of the LoC system.

Outlook

The developed tools and the first experimental results are very promising and prove that a good LoC magnetic pathogen sensing system based on the mixing frequency technique could be achieved with the proposed dimensioning procedure. However, several aspects need to be considered for both final validations of the prototypes as well as the design of a completely integrated LoC pathogen sensing system.

Through the various experiments and multidisciplinary literature review, we identified key aspects to be considered. This include both the realized tools as well as the prospective completely miniaturized system. These aspects can be divided into four major categories: optimization tools, magnetic detection, microfluidics and biofunctionalization.

Improvement of the optimization tools can be done by:

- Optimizing the accuracy and ability of the analytical tools: In fact, the analytical calculations allow finding the best compromise for the characteristics of the multilayer spiral coils for both excitation and detection. However, the calculations can be improved by considering the mutual relation between the dimensions of the constituting coils as well as the homogeneity of the field. In fact, the positioning of one coil affects the possible position of the other (superposed). Optimization algorithms can be used in order to find the best set of dimensions. Furthermore, a more complete calculation considering the sensitivity of the system with direct relation to the mixing terms might be a more direct approach. In this respect, an optimal ratio between HF and LF magnetic field as well as minimal magnetic

excitation fields for proper mixing frequency detection is expected. When applied with chosen SPN, a substantial improvement in sensitivity is expected.

- Improving the versatility of multiphysics simulation tools: the first version of the simulation tools allows to validate some critical aspects of the system such as heating, magnetic nonlinear sensing and proper liquid diffusion. Nonetheless, these tools must be further developed by including more practical cases like the study of thermal cooling methods (like Peltier effect) and the convection effects on the sample temperature. Also, we can assess the detection of SPN with any concentration by testing its voltage or magnetic response in the simulations and comparing it to calculated and measured limit of detections. We can also find the best distance between the reference and detection coils. Finally, we could improve the microfluidic simulation by studying the mixing, fluid handling aspects and practical issues.

The magnetic detection can be optimized by:

- Studying the multiassay capability through the difference in mixing signal response (amplitude and phase) by using the test bench along with its developed software.
- Reducing the number of coils by adding a DC magnetization field in the form of a well-studied permanent magnet. That may allow to combine both excitation signals, DC and AC in this case, using one coil.
- Conceiving a shielding environment for the miniaturized detection structure.
- Proper noise reduction by means of better balancing of the reference and detection sides and good filtering of the excitation signals.

Concerning the biofunctionalization of the reservoir:

- Validation of the chosen procedure : The thoroughly validation can be done by evaluating the density of functionalized antibodies on the surface. It can also be done by assessing the unspecific adsorption or binding to the surface of either non-targeted biological compounds or SPN. Finally, a test of cross-reactivity with two target entities should be done.
- The functionalization can be improved by enhancing the surface to volume ratio. We can provide two possible solutions; the use of relatively big (several μm) silica beads in the microfluidic reservoir or the conception of reservoirs filled with functionalized

pillars.

As for the microfluidics, next work should include:

- Choice of the microfluidic circuit taking into account fluid handling and mixing possibilities: Both capillary and pressure driven actuation seem to be a good choice. The final goal is a one-step detection procedure. For this design, the complete biosensing protocol with washing and binding steps must be studied and designed.
- Choice of prototyping and industrialization of constituting material : As discussed in chapter 1, PDMS constitutes a very good choice for prototyping. However, it is not suited for mass production. Consequently, we must choose beforehand the well adapted material, as it will impact the biofunctionalization protocol and fluid handling design processes.

This PhD research work has constituted a ground basis for the long term goals. As it can be seen, many aspects need to be considered before having an efficient completely integrated pathogen sensing LoC system.

To conclude, this project has currently received the unanimous approval of the scientific and administration committees of the Technology Transfer Acceleration Company, “SATT Lutech” as a partner of UPMC for a prospective maturation program and a funding for 18 months from January 2018. The maturation program will allow the design and realization of a completely integrated and portable automated system relying on embedded electronics and microfluidic handling systems (Figure 4.20). This program allows also the biological validation of the system with detection of C-reactive protein and Procalcitonin (PCT).

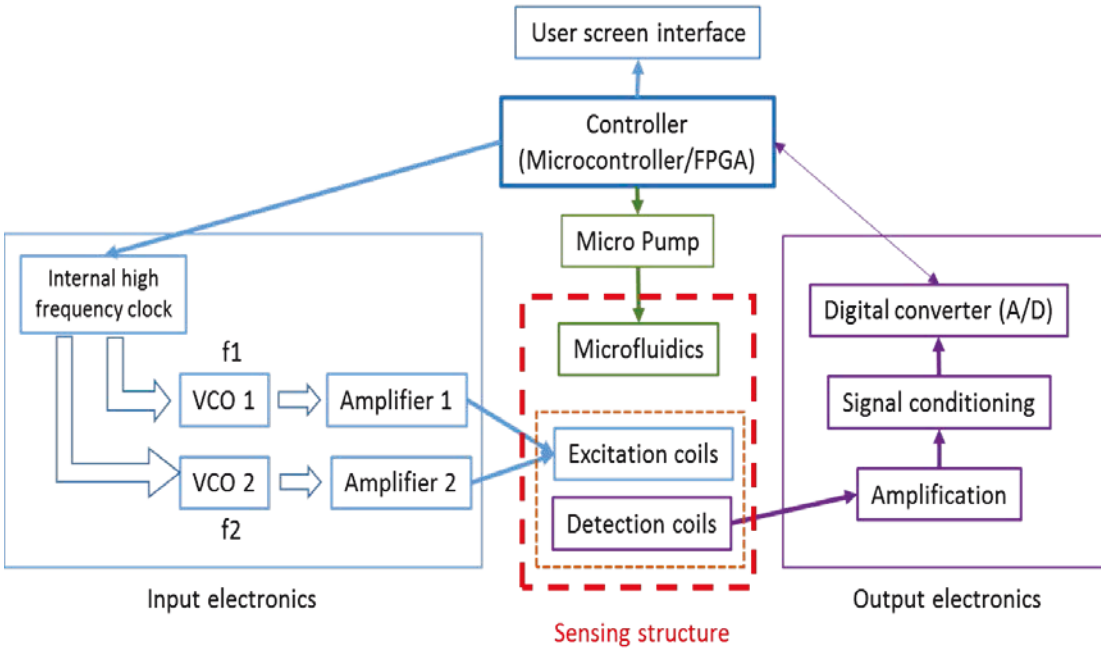

Figure 4-20: Schematic diagram of the prospective integrated and portable system for the maturation program.

Appendix A: Protocol for biofunctionalization of PDMS

Reagents

- Poly(dimethylsiloxane) (PDMS)
- Polyvinyl alcohol 99%
- Triethylamine 99% (TEA)
- 11-triethoxysilyl undecanal 90% (TESU)

Reagent setup

PVA solution: dissolve 25 mg in 25 mL DI H_2O. High temperature (60 ºC) and stirring is needed to dissolve it.

TESU solution: dilute 50 µL TESU and 50 µL TEA in 2.5 mL ethanol 99.5%.Caution:Avoid the vapors coming from TEA by preparing the solution mix in a fume hood.

Procedure for the biofunctionalization of the PDMS surfaces

1. **Clean flat PDMS surfaces**: first with ethanol 96% and then with DI H_2O.Flat PDMS surfaces are used for an easier characterization of the resulting modifications.
2. **Create hydroxyl groups on the PDMS surface:**
   A. Modification with PVA: immerse the PDMS in a 1 mg/ml PVA solution in DI H_2O. Leave to react for 1 hour. Then rinse with DI H_2O and dry with N_2.
   B. Use Plasma O_2
   C. Chemical oxidation: immerse the PDMS in an acidic solution containing DI H2O, 37% HCl and 30% H_2O_2 in a 5:1:1 (v/v/v) ratio18. Then rinse with DI H_2O and dry with N_2.
3. **Silanization step**:
   a. Create aldehyde groups on the PDMS surface by incubating them in a 99.5% ethanol solution containing 2% TESU and 2% TEA for 1 hour.
   b. Rinse with 99.5% ethanol and dry them at 80ºC for 2 hours. Avoid the vapors coming from TEA by preparing the solution mix in a fume hood**.** This step should be done in a closed container and using enough solvent to avoid the total evaporation of the liquid. It should also be carried out in an inert atmosphere like nitrogen or argon without humidity presence.

4. **Antibody immobilization**: After preparation, add an antibody solution in 0.1 M carbonate buffer with pH 9.6. According to experience, an antibody concentration of 20 µg/mL is recommended. Incubation time is still not certain, but a minimum of 1h at room temperature is advised.
5. **Blocking step**: Uncoated areas of the functionalized surface should be passivated with "biotin free" BSA or other blocking protein (Lysine…etc.). The recommended BSA concentration is 10 mg/mL. BSA could be incorporated in a PBS buffer. Subsequently, the column should be washed in a last step with PBS only buffer (pH 7.4).

Appendix B: List of publications

European patent:

H. KOKABI, H.-J. KRAUSE, K. NGO, **A. RABEHI**, "Electromagnetic sensinsg device for detecting magnetic nanoparticles", reference EP17306381.9, 28466/004EP1, submitted on 12 octobre 2017.

International conferences:

1. **A. RABEHI**, B. GARLAN, F. SHANEHSAZZADEH, H. KOKABI, K. NGO, H.-J. KRAUSE, "Magnetic detection structure for LOC immunoassays, multiphysics simulations and experimental results", *proceedings of EUROSENSORS 2017*, vol.1, no.4, pp.529, 2017, Paris.
2. **A. RABEHI**, H. KOKABI, K.A. NGO, H.-J. KRAUSE, "Simulation and optimization of a magnetic frequency mixing detection system of magnetic nanoparticles for immunoquantification in a microfluidic structure", *Comsol Conference 2016*, Munich, Allemagne, (Oct. 2016).
3. **A. RABEHI**, H. KOKABI, N. YAKDI, K.A. NGO, V. DUPUIS, S. NEVEU, S. GRAFF-DUBOIS, L. CHEN, H.-J. KRAUSE, "Study of a new microfluidic detection system of magnetic nanoparticles for the immunological tests", *SymiBio Workshop* (Synergy Microfluidics & Biology), Paris, (Mars 2016).
4. H. KOKABI, **A. RABEHI**, S. FATTOUM, N. YAKDI, K.A. NGO, V. DUPUIS, A. KRINGS, L. CHEN, H.-J. KRAUSE, "Magnetic frequency mixing detection of magnetic nanoparticles for immunoquantification in a microfluidic structure", *International Symposium on Biomaterials and Smart Systems*, Cergy-Pontoise, (Oct. 2014).

National conferences:

1. **A. RABEHI**, B. GARLAN, H. KOKABI, K. A. NGO, H.-J. KRAUSE, "Electromagnetic immunoassays using magnetic nanoparticles in a microfluidic structure", *jetsan (journées d'etude sur la telesante)*, bourges, (mai 2017).
2. **A. RABEHI**, H. KOKABI, K.A. NGO, V. DUPUIS, S. NEVEU, S. GRAFF-DUBOIS, H.-J. KRAUSE, "Electromagnetic Microsystem for the Detection of Magnetic Nanoparticles in a Microfluidic Structure for Immunoassays", *colloque UPMC/ISEP «Internet des objets pour les applications biomédicales »,* Paris (Nov 2016).
3. **A. RABEHI**, H. KOKABI, N. YAKDI, K.A. NGO, V. DUPUIS, S. NEVEU, S. GRAFF-DUBOIS, L. CHEN, H.-J. KRAUSE, "Microsystème électromagnétique de détection des nanoparticules magnétiques dans une structure microfluidique pour les tests immunologiques", *Assemblée générale du GDR Ondes*, Lyon, (Oct. 2015).
4. **A. RABEHI**, H. KOKABI, N. YAKDI, K.A. NGO, V. DUPUIS, S. NEVEU, S. GRAFF-DUBOIS, L. CHEN, H.-J. KRAUSE, "Etude d'un microsystème électromagnétique de détection des nanoparticules magnétiques pour les tests immunologiques", *Journées Scientifiques des facultés de Biologie et de médecine de l'UPMC*, Paris, (Sept. 2015).
5. **A. RABEHI**, H. KOKABI, N. YAKDI, K.A. NGO, V. DUPUIS, S. GRAFF-DUBOIS, L. CHEN, H.-J. KRAUSE, "Microsystème électromagnétique de détection des nanoparticules magnétiques dans une structure microfluidique pour les analyses

immunologiques", *Journée Nationale du Réseau Doctoral en Microélectronique*, Bordeaux, (Mai 2015).

Abbreviations

Abbreviation	Description
Abs	Antibodies
AFM	Atomic Force Microscopy
Ags	Antigens
AP	alkaline phosphatase
AuNP	Gold nanoparticles
BSA	Bovin Serum Albumin
CCD Camera	Charged coupled device Camera
CFU	Colony Forming Unit
CNT	carbon nanotubes
CV	Coefficient of Variation
DNA	Deoxyribonucleic acid
E.Coli	Escherichia coli
ELISA	Enzyme-Linked Immunosorbent Assay
FEDC	ferrocenedicarboxylic acid
FM	ferromagnetic
GMR	giant magnetoresistor effect sensors
GOx	Glucose Oxidaze
HER2	human epidermal growth factor receptor-2
HRP	Horseradish peroxidase
ICs	Integrated Circuits
IME	interdigitated microelectrodes
LFA	Lateral Flow Assay
LOB	Limit of Blank
LoC	Lab on Chip
LOD	Limit of Detection
LOQ	Limit of Quantification
Magnetic nanoparticles	MNP
MEMS	Microelectromechanical systems
MR	magnetoresistive
MRsws	magnetic relaxation switches
MTJ	magnetic tunnel junction
MWCNT	multi-wall carbon nanotube
NEMS	nano-electro mechanical system
NMR	nuclear magnetic resonance
PAPP	p-aminophenyl phosphate
PCR	Polymerase Chain Reaction

PFU	plaque forming unit
POC	Point Of Care
QCM	Quartz Crystal Microbalance
RNA	Ribonucleic acid
SAMs	Self-Assembled Monolayers
SAW	Surface Acoustic Wave
SD	Standard Deviation
SNR	Signal to noise ratio
SPR	Surface Plasmon Resonance
SQUID	Superconducting Quantum Interference Device
ssDNA	single-stranded deoxyribonucleic acid
SV	spin valve
TMR	tunneling magnetoresistance effect sensors

List of tables

List of figures

Bibliography

[1] H.-J. Krause, N. Wolters, Y. Zhang, A. Offenhausser, P. Miethe, M. H. Meyer, M. Hartmann and M. Keusgen, "Magnetic particle detection by frequency mixing for immunoassay applications," *Journal of Magnetism and Magnetic Materials,* vol. 311, no. 1, pp. 436-444, 2007.

[2] M. H. Meyer, H.-J. Krause, M. Hartmann, P. Miethe, J. Oster and M. Keusgen, "Francisella tularensis detection using magnetic labels and a magnetic biosensor based on frequency mixing," *Journal of magnetism and magnetic materials,* vol. 311, no. 1, 2007.

[3] Meyer, M. H. a. Hartmann, M. a. Krause, G. a. M.-C. Hans-Joachim and Blankenstein, B. a. Oster, J. a. Miethe, P. a. Keusgen and Michael, "CRP determination based on a novel magnetic biosensor," *Biosensors and bioelectronics,* vol. 22, no. 6, 2007.

[4] M. H. Meyer, M. Stehr, S. Bhuju, H.-J. Krause, M. Hartmann, P. Miethe, M. Singh and M. Keusgen, "Magnetic biosensor for the detection of Yersinia pestis," *Journal of microbiological methods,* vol. 68, no. 2, 2007.

[5] H.-B. Hong, H.-J. Krause, K.-B. Song, C.-J. Choi, M.-A. Chung, S.-w. Son and A. Offenhausser, "Detection of two different influenza A viruses using a nitrocellulose membrane and a magnetic biosensor," *Journal of immunological methods,* vol. 365, no. 1, pp. 95-100, 2011.

[6] S. Vigneshvar, C. Sudhakumari, B. Senthilkumaran and H. Prakash, "Recent Advances in Biosensor Technology for Potential Applications--An Overview," *Frontiers in bioengineering and biotechnology,* vol. 4, 2016.

[7] R. Vargas-Bernal, E. Rodriguez-Miranda and G. Herrera-Perez, "Evolution and expectations of enzymatic biosensors for pesticides," in *Pesticides-Advances in Chemical and Botanical Pesticides*, InTech, 2012.

[8] P. Mehrotra, "Biosensors and their applications--A review," *Journal of oral biology and craniofacial research,* vol. 6, no. 2, pp. 153-159, 2016.

[9] W.-C. Tian and E. Finehout, "Microfluidic diagnostic systems for the rapid detection and quantification of pathogens," in *Microfluidics for Biological Applications*, Springer, 2008, pp. 271-322.

[10] R. Stanier, J. Ingraham, M. Wheelis and P. Painter, The Microbial World, 5th edit, Prentice-Hall, Englewood Cliffs, NJ, 1986.

[11] A. Mulchandani, "Principles of enzyme biosensors," *Enzyme and Microbial Biosensors: Techniques and Protocols,* pp. 3-14, 1998.

[12] A. Bange, H. B. Halsall and W. R. Heineman, "Microfluidic immunosensor systems," *Biosensors and Bioelectronics,* vol. 20, no. 12, pp. 2488-2503, 2005.

[13] R. L. Caygill, G. E. Blair and P. A. Millner, "A review on viral biosensors to detect human pathogens," *Analytica Chimica Acta,* vol. 681, no. 1, pp. 8-15, 2010.

[14] G. Shruthi, C. Amitha and B. B. Mathew, "Biosensors: A modern day achievement," *Journal of Instrumentation Technology,* vol. 2, no. 1, pp. 26-39, 2014.

[15] G. Rocchitta, A. Spanu, S. Babudieri, G. Latte, G. Madeddu, G. Galleri, S. Nuvoli, P. Bagella, M. Demartis and V. Fiore, "Analytical Problems in Exposing Amperometric Enzyme Biosensors to Biological Fluids," *Sensors,* vol. 16, no. 6, 2016.

[16] G. Rocchitta, A. Spanu, S. Babudieri, G. Latte, G. Madeddu, G. Galleri, S. Nuvoli, P. Bagella, M. I. Demartis, V. Fiore and others, "Enzyme biosensors for biomedical applications: Strategies for safeguarding analytical performances in biological fluids," *Sensors,* vol. 16, no. 6, p. 780, 2016.

[17] A. P. Turner, "Biosensors: sense and sensibility," *Chemical Society Reviews,* vol. 42, no. 8, pp. 3184--3196, 2013.

[18] J. Wu and M. Gu, "Microfluidic sensing: state of the art fabrication and detection techniques," *Journal of biomedical optics,* vol. 16, no. 8, pp. 080901-080901, 2011.

[19] S. M. Yoo and S. Y. Lee, "Optical biosensors for the detection of pathogenic microorganisms," *Trends in biotechnology,* vol. 34, no. 1, pp. 7-25, 2016.

[20] J.-Y. Yoon and B. Kim, "Lab-on-a-chip pathogen sensors for food safety," *Sensors,* vol. 23, no. 8, pp. 10713-10741, 2012.

[21] G. A. Posthuma-Trumpie, J. Korf and A. van Amerongen, "Lateral flow (immuno) assay: its strengths, weaknesses, opportunities and threats. A literature survey," *Analytical and bioanalytical chemistry,* vol. 393, no. 2, pp. 569-582, 2009.

[22] M. P. Laitinen and M. Vuento, "Affinity immunosensor for milk progesterone: identification of critical parameters," *Biosensors and Bioelectronics,* vol. 11, no. 12, pp. 1207-1214, 1996.

[23] G. C. Gussenhoven, M. Van der Hoorn, M. Goris, W. J. Terpstra, R. A. Hartskeerl, B. W. Mol, C. Van Ingen and H. L. Smits, "LEPTO dipstick, a dipstick assay for detection of Leptospira-specific immunoglobulin M antibodies in human sera.," *Journal of clinical Microbiology,* vol. 35, no. 1, pp. 92-97, 1997.

[24] K. Snowden and M. Hommel, "Antigen detection immunoassay using dipsticks and colloidal dyes," *Journal of immunological methods,* vol. 140, no. 1, pp. 57-65, 1991.

[25] R. D. Molony, J. M. Rice, J. S. Yuk, V. Shetty, D. Dey, D. A. Lawrence and M. A. Lynes, "Mining the Salivary Proteome with Grating-Coupled Surface Plasmon Resonance Imaging and Surface Plasmon Coupled Emission Microarrays," *Current protocols in toxicology,* pp. 16-18, 2012.

[26] P. S. Dittrich and A. Manz, "Single-molecule fluorescence detection in microfluidic channels—the Holy Grail in µTAS?," *Analytical and bioanalytical chemistry,* vol. 382, no. 8, pp. 1771-1782, 2005.

[27] L. Riegger, M. Grumann, T. Nann, J. Riegler, O. a. B. W. Ehlert, K. Mittenbuehler, G. Urban, L. Pastewka and T. a. o. Brenner, "Read-out concepts for multiplexed bead-based fluorescence immunoassays on centrifugal microfluidic platforms," *Sensors and Actuators A: Physical,* vol. 126, no. 2, pp. 455-462, 2006.

[28] H. Mukundan, J. Z. Kubicek, A. Holt, J. E. Shively, J. S. Martinez, K. Grace, W. K. Grace and B. I. Swanson, "Planar optical waveguide-based biosensor for the quantitative detection of tumor markers," *Sensors and Actuators B: Chemical,* vol. 138, no. 2, pp. 453-460, 2009.

[29] L. Su, W. Jia, C. Hou and Y. Lei, "Microbial biosensors: a review," *Biosensors and Bioelectronics,* vol. 26, no. 5, pp. 1788-1799, 2011.

[30] J. H. Niazi, B. C. Kim, J.-M. Ahn and M. B. Gu, "A novel bioluminescent bacterial biosensor using the highly specific oxidative stress-inducible pgi gene," *Biosensors and Bioelectronics,* vol. 24, no. 4, pp. 670-675, 2008.

[31] Sigmaaldrich, "Introduction to the Methods Used to Detect Proteins and Nucleic Acids Bound to Membranes," [Online]. Available: http://www.sigmaaldrich.com/technical-documents/articles/biology/detection-methods.html. [Accessed 03 08 2017].

[32] M. Varshney, Y. Li, B. Srinivasan, S. Tung, G. Erf, M. Slavik, Y. Ying and W. Fang, "A microfluidic filter biochip-based chemiluminescence biosensing method for detection of Escherichia coli O157: H7," *Transactions of the Asabe,* vol. 49, no. 6, pp. 2061-2068, 2006.

[33] J. Zhu, Z. Zhu, Z. Lai, R. Wang, X. Guo, X. Wu, G. Zhang, Z. Zhang, Y. Wang and Z. Chen, "Planar amperometric glucose sensor based on glucose oxidase immobilized by chitosan film on Prussian blue layer," *Sensors,* vol. 2, no. 4, pp. 127-136, 2002.

[34] X. Cai, N. Klauke, A. Glidle, P. Cobbold, G. L. Smith and J. M. Cooper, "Ultra-low-volume, real-time measurements of lactate from the single heart cell using microsystems technology," *Analytical chemistry,* vol. 74, no. 4, pp. 908-914, 2002.

[35] N. Ohgami, S. Upadhyay, A. Kabata, K. Morimoto, H. Kusakabe and H. Suzuki, "Determination of the activities of glutamic oxaloacetic transaminase and glutamic pyruvic transaminase in a microfluidic system," *Biosensors and Bioelectronics,* vol. 22, no. 7, pp. 1330-1336, 2007.

[36] R. H. Liu, J. Yang, R. Lenigk, J. Bonanno and P. Grodzinski, "Self-contained, fully integrated biochip for sample preparation, polymerase chain reaction amplification, and DNA microarray detection," *Analytical chemistry,* vol. 76, no. 7, pp. 1824-1831, 2004.

[37] Z.-Y. Wu, F. Fang, J. Josserand and H. H. Girault, "On-column conductivity detection in capillary-chip electrophoresis," *Electrophoresis,* vol. 28, no. 24, pp. 4612-4619, 2007.

[38] S. B. Adeloju, S. J. Shaw and G. G. Wallace, "Polypyrrole-based amperometric flow injection biosensor for urea," *Analytica Chimica Acta,* vol. 323, no. 1, pp. 107-113, 1996.

[39] J. Albers, T. Grunwald, E. Nebling, G. Piechotta and R. Hintsche, "Electrical biochip technology—a tool for microarrays and continuous monitoring," *Analytical and Bioanalytical Chemistry,* vol. 377, no. 3, pp. 521-527, 2003.

[40] K. J. Cash and H. A. Clark, "Nanosensors and nanomaterials for monitoring glucose in diabetes," *Trends in molecular medicine,* vol. 16, no. 12, pp. 584-593, 2010.

[41] M. Billah, H. C. Hays and P. A. Millner, "Development of a myoglobin impedimetric immunosensor based on mixed self-assembled monolayer onto gold," *Microchimica Acta,* vol. 160, no. 4, pp. 447-454, 2008.

[42] H. C. Hays, P. A. Millner and M. I. Prodromidis, "Development of capacitance based immunosensors on mixed self-assembled monolayers," *Sensors and Actuators B: Chemical,* vol. 114, no. 2, pp. 1064-1070, 2006.

[43] A. C. Barton, S. D. Collyer, F. Davis, G.-Z. a. T. G. a. T. E. a. O. R. Garifallou, T. Gibson, P. A. Millner and S. P. Higson, "Labeless AC impedimetric antibody-based sensors with pgml- 1 sensitivities for point-of-care biomedical applications," *Biosensors and Bioelectronics,* vol. 24, no. 5, pp. 1090-1095, 2009.

[44] B. Wang, S. Takahashi, X. Du and J.-i. Anzai, "Electrochemical biosensors based on ferroceneboronic acid and its derivatives: a review," *Biosensors,* vol. 4, no. 3, pp. 243-256, 2014.

[45] F. Ricci, G. Adornetto and G. Palleschi, "A review of experimental aspects of electrochemical immunosensors," *Electrochimica Acta,* vol. 84, pp. 74-83, 2012.

[46] D. Prashar, "Self assembled monolayers-a review," *Int. J. ChemTech Res,* vol. 4, no. 1, pp. 258-265, 2012.

[47] A. M. A. Melo, D. L. Alexandre, R. F. Furtado, M. F. Borges, E. A. T. Figueiredo, A. Biswas, H. N. Cheng and C. R. Alves, "Electrochemical immunosensors for Salmonella detection in food," *Applied microbiology and biotechnology,* vol. 100, no. 12, pp. 5301-5312, 2016.

[48] P. Leonard, S. Hearty, J. Brennan, L. Dunne, J. Quinn, T. Chakraborty and R. O'Kennedy, "Advances in biosensors for detection of pathogens in food and water," *Enzyme and Microbial Technology,* vol. 32, no. 1, pp. 3-13, 2003.

[49] S. Liebana, A. Lermo, S. Campoy, M. P. Cortes, S. Alegret and M. I. Pividori, "Rapid detection of Salmonella in milk by electrochemical magneto-immunosensing," *Biosensors and Bioelectronics,* vol. 25, no. 2, pp. 510-513, 2009.

[50] R. Wang, Y. Wang, K. Lassiter, Y. Li, B. Hargis, S. Tung, L. Berghman and W. Bottje, "Interdigitated array microelectrode based impedance immunosensor for detection of avian influenza virus H5N1,"

Talanta, vol. 2009, no. 2, pp. 159-164, 2009.

[51] M. Hnaien, M. F. Diouani, S. Helali, I. Hafaid, W. M. Hassen, N. J. Renault, A. Ghram and A. Abdelghani, "Immobilization of specific antibody on SAM functionalized gold electrode for rabies virus detection by electrochemical impedance spectroscopy," *Biochemical Engineering Journal,* vol. 39, no. 3, pp. 443-449, 2008.

[52] X. Fang, O. K. Tan, M. S. Tse and E. E. Ooi, "A label-free immunosensor for diagnosis of dengue infection with simple electrical measurements," *Biosensors and Bioelectronics,* vol. 25, no. 5, pp. 1137-1142, 2010.

[53] X. Jiang and M. G. Spencer, "Electrochemical impedance biosensor with electrode pixels for precise counting of CD4+ cells: A microchip for quantitative diagnosis of HIV infection status of AIDS patients," *Biosensors and Bioelectronics,* vol. 25, no. 7, pp. 1622-1628, 2010.

[54] R. Wang, Y. Wang, K. Lassiter, Y. Li, B. Hargis, S. Tung, L. Berghman and W. Bottje, "Interdigitated array microelectrode based impedance immunosensor for detection of avian influenza virus H5N1," *Talanta,* vol. 164, no. 2, p. 159, 2009.

[55] S. Farrell, N. J. Ronkainen-Matsuno, H. B. Halsall and W. R. Heineman, "Bead-based immunoassays with microelectrode detection," *Analytical and bioanalytical chemistry,* vol. 379, no. 3, pp. 358-367, 2004.

[56] B. Byrne, E. Stack, N. Gilmartin and R. O'Kennedy, "Antibody-based sensors: principles, problems and potential for detection of pathogens and associated toxins," *Sensors,* vol. 9, no. 6, pp. 4407-445, 2009.

[57] Z. Muhammad-Tahir and E. C. Alocilja, "A conductometric biosensor for biosecurity," *Biosensors and Bioelectronics,* vol. 18, no. 5, pp. 813-819, 2003.

[58] M. Hnaiein, W. Hassen, A. Abdelghani, C. Fournier-Wirth, J. Coste, F. Bessueille, D. Leonard and N. Jaffrezic-Renault, "A conductometric immunosensor based on functionalized magnetite nanoparticles for E. coli detection," *Electrochemistry Communications,* vol. 10, no. 8, pp. 1152-1154, 2008.

[59] M. Li, R. Li, C. Li and N. Wu, "Electrochemical and optical biosensors based on nanomaterials and nanostructures: a review," *Frontiers in bioscience (Scholar edition),* vol. 3, pp. 1308-1331, 2010.

[60] P. Chumyim, P. Rijiravanich, M. Somasundrum and W. Surareungchai, "Detection of Salmonella enterica serovar Typhimurium in milk sample using electrochemical immunoassay and enzyme amplified labeling," *Int Conf Agric Environ Biol Sci,* pp. 24-25, 2014.

[61] C. Lui, N. C. Cady and C. A. Batt, "Nucleic acid-based detection of bacterial pathogens using integrated microfluidic platform systems," *Sensors,* vol. 9, no. 5, pp. 3713-3744, 2009.

[62] J. Arlett, E. Myers and M. Roukes, "Comparative advantages of mechanical biosensors," *Nature nanotechnology,* vol. 6, no. 4, pp. 203-215, 2011.

[63] N. Backmann, C. Zahnd, F. Huber, A. Bietsch, A. Pluckthun, H.-P. Lang, H.-J. Guntherodt, M. Hegner and C. Gerber, "A label-free immunosensor array using single-chain antibody fragments," *Proceedings of the National Academy of Sciences of the United States of America,* vol. 102, no. 41, pp. 14587-14592, 2005.

[64] G. Wu, R. H. Datar, K. M. Hansen, T. Thundat, R. J. Cote and A. Majumdar, "Bioassay of prostate-specific antigen (PSA) using microcantilevers," *Nature biotechnology,* vol. 19, no. 9, pp. 856-860, 2001.

[65] T. Naik, E. K. Longmire and S. C. Mantell, "Dynamic response of a cantilever in liquid near a solid wall," *Sensors and Actuators A: physical,* vol. 102, no. 3, pp. 240-254, 2003.

[66] G. Sauerbrey, "Use of a quartz vibrator from weighing thin films on a microbalance," *Z. Phys.,* vol. 155, p. 206, 1959.

[67] S.-H. Chen, V. C. Wu, Y.-C. Chuang and C.-S. Lin, "Using oligonucleotide-functionalized Au

nanoparticles to rapidly detect foodborne pathogens on a piezoelectric biosensor," *Journal of Microbiological Methods,* vol. 73, no. 1, pp. 7-17, 2008.

[68] S.-H. Chen, Y.-C. Chuang, Y.-C. Lu, H.-C. Lin, Y.-L. Yang and C.-S. Lin, "A method of layer-by-layer gold nanoparticle hybridization in a quartz crystal microbalance DNA sensing system used to detect dengue virus," *Nanotechnology,* vol. 20, no. 21, p. 215501, 2009.

[69] S. Pan and L. Rothberg, "Chemical control of electrode functionalization for detection of DNA hybridization by electrochemical impedance spectroscopy," *Langmuir,* vol. 21, no. 3, pp. 1022-1027, 2005.

[70] V. S. A. Jayanthi, A. B. Das and U. Saxena, "Recent advances in biosensor development for the detection of cancer biomarkers," *Biosensors and Bioelectronics,* 2016.

[71] C. Zuniga, M. Rinaldi and G. Piazza, "High frequency Piezoelectric Resonant Nanochannel for bio-sensing applications in liquid environment," in *Sensors, IEEE*, 2010.

[72] T. Braun, V. Barwich, M. K. Ghatkesar, A. H. Bredekamp, C. Gerber, M. Hegner and H. P. Lang, "Micromechanical mass sensors for biomolecular detection in a physiological environment," *Physical Review E,* vol. 72, no. 3, p. 031907, 2005.

[73] K. Lange, F. J. Gruhl and M. Rapp, "Surface Acoustic Wave (SAW) biosensors: coupling of sensing layers and measurement," in *Microfluidic Diagnostics: Methods and Protocols*, Springer, 2013, pp. 491-505.

[74] F. J. Gruhl and K. Lange, "Surface modification of an acoustic biosensor allowing the detection of low concentrations of cancer markers," *Analytical biochemistry,* vol. 420, no. 2, pp. 188-190, 2012.

[75] H. Lee, T.-H. Shin, J. Cheon and R. Weissleder, "Recent developments in magnetic diagnostic systems," *Chemical reviews,* vol. 115, no. 19, pp. 10690-10724, 2015.

[76] I. Giouroudi and F. Keplinger, "Microfluidic biosensing systems using magnetic nanoparticles," *International journal of molecular sciences,* vol. 14, no. 9, pp. 18535-18556, 2013.

[77] M. Muluneh and D. Issadore, "Microchip-based detection of magnetically labeled cancer biomarkers," *Advanced drug delivery reviews,* vol. 66, pp. 101-109, 2014.

[78] C. Tamanaha, S. Mulvaney, J. Rife and L. Whitman, "Magnetic labeling, detection, and system integration," *Biosensors and Bioelectronics,* vol. 24, no. 1, pp. 1-13, 2008.

[79] I. Giouroudi and G. Kokkinis, "Recent Advances in Magnetic Microfluidic Biosensors," *Nanomaterials,* vol. 7, no. 7, p. 171, 2017.

[80] C. B. Kriz, K. Radevik and D. Kriz, "Magnetic permeability measurements in bioanalysis and biosensors," *Analytical Chemistry,* vol. 68, no. 11, pp. 1966-1970, 1996.

[81] J. Kiely, P. Hawkins, P. Wraith and R. Luxton, "Paramagnetic particle detection for use with an immunoassay based biosensor," *IET science, measurement & technology,* vol. 1, no. 5, pp. 270-275, 2007.

[82] D. Issadore, Y. Park, H. Shao, C. Min, K. Lee, M. Liong, R. Weissleder and H. Lee, "Magnetic sensing technology for molecular analyses," *Lab on a Chip,* vol. 14, no. 14, pp. 2385-2397, 2014.

[83] K. Park, T. Harrah, E. B. Goldberg, R. P. Guertin and S. Sonkusale, "Multiplexed sensing based on Brownian relaxation of magnetic nanoparticles using a compact AC susceptometer," *Nanotechnology,* vol. 22, no. 8, p. 085501, 2011.

[84] I. Koh and L. Josephson, "Magnetic nanoparticle sensors," *Sensors,* vol. 9, no. 10, pp. 8130-8145, 2009.

[85] H. Grossman, W. Myers, V. Vreeland, R. Bruehl, M. Alper, C. Bertozzi and J. Clarke, "Detection of bacteria in suspension by using a superconducting quantum interference device," *Proceedings of the*

National Academy of Sciences, vol. 101, no. 1, pp. 129-134, 2004.

[86] D. Issadore, J. Chung, H. Shao, M. Liong, A. A. Ghazani, C. M. Castro, R. Weissleder and H. Lee, "Ultrasensitive clinical enumeration of rare cells ex vivo using a micro-hall detector," *Science translational medicine,* vol. 4, no. 141, pp. 141ra92-141ra92, 2012.

[87] W. Thomson, "On the electro-dynamic qualities of metals:--effects of magnetization on the electric conductivity of nickel and of iron," *Proceedings of the Royal Society of London,* vol. 8, pp. 546-550, 1856.

[88] R. Hunt, "A magnetoresistive readout transducer," *IEEE Transactions on Magnetics,* vol. 7, no. 1, pp. 150-154, 1971.

[89] P. Freitas, R. Ferreira, S. Cardoso and F. Cardoso, "Magnetoresistive sensors," *Journal of Physics: Condensed Matter,* vol. 19, no. 16, p. 165221, 2007.

[90] D. A. Hall, R. S. Gaster, K. A. Makinwa, S. X. Wang and B. Murmann, "A 256 pixel magnetoresistive biosensor microarray in 0.18 μm CMOS," *IEEE journal of solid-state circuits,* vol. 48, no. 5, pp. 1290-1301, 2013.

[91] J. Slaughter, E. Chen, R. Whig, B. Engel, J. Janesky and S. Tehrani, "Magnetic tunnel junction materials for electronic applications," *JOM(USA),* vol. 52, no. 6, p. 11, 2000.

[92] S. S. Parkin, C. Kaiser, A. Panchula, P. M. Rice, B. Hughes, M. Samant and S.-H. Yang, "Giant tunnelling magnetoresistance at room temperature with MgO (100) tunnel barriers," *Nature materials,* vol. 3, no. 12, p. 862, 2004.

[93] J. B. Haun, T.-J. Yoon, H. Lee and R. Weissleder, "Magnetic nanoparticle biosensors," *Wiley Interdisciplinary Reviews: Nanomedicine and Nanobiotechnology,* vol. 2, no. 3, pp. 291-304, 2010.

[94] H. Lee, E. Sun, D. Ham and R. Weissleder, "Chip-NMR biosensor for detection and molecular analysis of cells," *Nature medicine,* vol. 14, no. 8, pp. 869-874, 2008.

[95] J. Grimm, J. M. Perez, L. Josephson and R. Weissleder, "Novel nanosensors for rapid analysis of telomerase activity," *Cancer Research,* vol. 64, no. 2, pp. 639-643, 2004.

[96] C.-C. Lin, J.-H. Wang, H.-W. Wu and G.-B. Lee, "Microfluidic immunoassays," *JALA: Journal of the Association for Laboratory Automation,* vol. 15, no. 3, pp. 253-274, 2010.

[97] D. Wild, The immunoassay handbook, Elsevier, 2013.

[98] I. A. Darwish, "Immunoassay methods and their applications in pharmaceutical analysis: basic methodology and recent advances," *Int J Biomed Sci,* vol. 2, no. 3, pp. 217-235, 2006.

[99] Gringer, wikipedia. [Online]. Available: https://commons.wikimedia.org/w/index.php?curid=31253976.

[100] A. H. Ng, U. Uddayasankar and A. R. Wheeler, "Immunoassays in microfluidic systems," *Analytical and bioanalytical chemistry,* vol. 397, no. 3, pp. 991-1007, 2010.

[101] N. Chiem and D. J. Harrison, "Microchip-based capillary electrophoresis for immunoassays: analysis of monoclonal antibodies and theophylline," *Analytical chemistry},* vol. 69, no. 3., pp. 373-378, 1997.

[102] A. Hatch, A. E. Kamholz, K. R. Hawkins, M. S. Munson, E. A. Schilling, B. H. Weigl and P. Yager, "A rapid diffusion immunoassay in a T-sensor," *Nature biotechnology,* vol. 19, no. 5, p. 461, 2001.

[103] V. K. Yadavalli and M. V. Pishko, "Biosensing in microfluidic channels using fluorescence polarization," *Analytica chimica acta,* vol. 507, no. 1, pp. 123-128, 2004.

[104] X. Guan, H.-j. Zhang, Y.-n. Bi, L. Zhang and D.-l. Hao, "Rapid detection of pathogens using antibody-coated microbeads with bioluminescence in microfluidic chips," *Biomedical microdevices,* vol. 12, no. 4, pp. 683-691, 2010.

[105] D. R. Reyes, D. Iossifidis, P.-A. Auroux, A. Manz and others, "Micro total analysis systems. 1. Introduction, theory, and technology," *ANALYTICAL CHEMISTRY-WASHINGTON DC-,* vol. 74, no. 12, pp. 2623-2636, 2002.

[106] P.-A. Auroux, D. Iossifidis, D. R. Reyes and A. Manz, "Micro total analysis systems. 2. Analytical standard operations and applications," *Analytical chemistry,* vol. 74, no. 12, pp. 2637-2653, 2002.

[107] D. Kim and A. E. Herr, "Protein immobilization techniques for microfluidic assays," *Biomicrofluidics,* vol. 7, no. 4, p. 041501, 2013.

[108] H. Becker and L. E. Locascio, "Polymer microfluidic devices," *Talanta,* vol. 56, no. 2, pp. 267-287, 2002.

[109] D. J. Guckenberger, T. E. de Groot, A. M. Wan, D. J. Beebe and E. W. Young, "Micromilling: a method for ultra-rapid prototyping of plastic microfluidic devices," *Lab on a Chip,* vol. 15, no. 11, pp. 2364-2378, 2015.

[110] M. W. Toepke and D. J. Beebe, "PDMS absorption of small molecules and consequences in microfluidic applications," *Lab on a Chip,* vol. 6, no. 12, pp. 1484-1486, 2006.

[111] J. R. Anderson, D. T. Chiu, H. Wu, O. Schueller and G. M. Whitesides, "Fabrication of microfluidic systems in poly (dimethylsiloxane)," *Electrophoresis,* vol. 21, no. 1, pp. 17-40, 2000.

[112] S. Qi, X. Liu, S. Ford, J. Barrows, G. Thomas, K. Kelly, A. McCandless, K. Lian, J. Goettert and S. A. Soper, "Microfluidic devices fabricated in poly (methyl methacrylate) using hot-embossing with integrated sampling capillary and fiber optics for fluorescence detection," *Lab on a Chip,* vol. 2, no. 2, pp. 88-95, 2002.

[113] U. M. Attia, S. Marson and J. R. Alcock, "Micro-injection moulding of polymer microfluidic devices," *Microfluidics and nanofluidics,* vol. 7, no. 1, p. 1, 2009.

[114] H. Cao, J. O. Tegenfeldt, R. H. Austin and S. Y. Chou, "Gradient nanostructures for interfacing microfluidics and nanofluidics," *Applied Physics Letters,* vol. 81, no. 16, pp. 3058-3060, 2002.

[115] T. Mappes, S. Achenbach and J. Mohr, "X-ray lithography for devices with high aspect ratio polymer submicron structures," *Microelectronic engineering,* vol. 84, no. 5, pp. 1235-1239, 2007.

[116] J. Rossier, F. Reymond and P. E. Michel, "Polymer microfluidic chips for electrochemical and biochemical analyses," *Electrophoresis,* vol. 23, no. 6, pp. 858-867, 2002.

[117] H. Kim, D. Park, B. Ryu and K. Lim, "Design and modeling of piezoelectric pump for microfluid devices," *Ferroelectrics,* vol. 378, no. 1, pp. 92-100, 2009.

[118] S.-M. Ha, W. Cho and Y. Ahn, "Disposable thermo-pneumatic micropump for bio lab-on-a-chip application," *Microelectronic engineering,* vol. 86, no. 4, pp. 1337-1339, 2009.

[119] M. A. Hayes, I. Kheterpal and A. G. Ewing, "Effects of buffer pH on electroosmotic flow control by an applied radial voltage for capillary zone electrophoresis," *Analytical chemistry,* vol. 65, no. 1, pp. 27-31, 1993.

[120] E. M. Miller and A. R. Wheeler, "Digital bioanalysis," *Analytical and bioanalytical chemistry,* vol. 393, no. 2, pp. 419-426, 2009.

[121] J. Moorthy, G. A. Mensing, D. Kim, S. Mohanty, D. T. Eddington, W. H. Tepp, E. A. Johnson and D. J. Beebe, "Microfluidic tectonics platform: A colorimetric, disposable botulinum toxin enzyme-linked immunosorbent assay system," *Electrophoresis,* vol. 25, no. 10, pp. 1705-1713, 2004.

[122] L. Qin, O. Vermesh, Q. Shi and J. R. Heath, "Self-powered microfluidic chips for multiplexed protein assays from whole blood," *Lab on a Chip,* vol. 9, no. 14, pp. 2016-2020, 2009.

[123] J. Kong, L. Jiang, X. Su, J. Qin, Y. Du and B. Lin, "Integrated microfluidic immunoassay for the rapid

determination of clenbuterol," *Lab on a Chip,* vol. 9, no. 11, pp. 1541-1547, 2009.

[124] M. Madou, J. Zoval, G. Jia, H. Kido, J. Kim and N. Kim, "Lab on a CD," *Annu. Rev. Biomed. Eng.,* vol. 8, pp. 601-628, 2006.

[125] V. Linder, "Microfluidics at the crossroad with point-of-care diagnostics," *Analyst,* vol. 132, no. 12, pp. 1186-1192, 2007.

[126] B. D. Iverson and S. V. Garimella, "Recent advances in microscale pumping technologies: a review and evaluation," *Microfluidics and Nanofluidics,* vol. 5, no. 2, pp. 145-174, 2008.

[127] T. Li, L. Zhang, K. M. Leung and J. Yang, "Out-of-plane microvalves for whole blood separation on lab-on-a-CD," *Journal of Micromechanics and Microengineering,* vol. 20, no. 10, p. 105024, 2010.

[128] L. Gervais and E. Delamarche, "Toward one-step point-of-care immunodiagnostics using capillary-driven microfluidics and PDMS substrates," *Lab on a Chip,* vol. 9, no. 23, pp. 3330-3337, 2009.

[129] M. Zimmermann, H. Schmid, P. Hunziker and E. Delamarche, "Capillary pumps for autonomous capillary systems," *Lab on a Chip,* vol. 7, no. 1, pp. 119-125, 2007.

[130] V. Studer, G. Hang, A. Pandolfi, M. Ortiz, W. French Anderson and S. R. Quake, "Scaling properties of a low-actuation pressure microfluidic valve," *Journal of applied physics,* vol. 95, no. 1, pp. 393-398, 2004.

[131] Y. Gao, G. Hu, F. Y. Lin, P. M. Sherman and D. Li, "An electrokinetically-controlled immunoassay for simultaneous detection of multiple microbial antigens," *Biomedical microdevices,* vol. 7, no. 4, pp. 301-3012, 2005.

[132] R. Sista, Z. Hua, P. Thwar, A. a. S. V. Sudarsan, A. Eckhardt, M. Pollack and V. Pamula, "Development of a digital microfluidic platform for point of care testing," *Lab on a Chip,* vol. 8, no. 12, pp. 2091-2104, 2008.

[133] C.-H. Wang and G.-B. Lee, "Pneumatically driven peristaltic micropumps utilizing serpentine-shape channels," *Journal of Micromechanics and Microengineering,* vol. 16, no. 2, p. 341, 2006.

[134] K. Hosokawa, M. Omata, K. Sato and M. Maeda, "Power-free sequential injection for microchip immunoassay toward point-of-care testing," *Lab on a Chip,* vol. 6, no. 2, pp. 236-241, 2006.

[135] Y. Wang, W. Knoll and J. Dostalek, "Bacterial pathogen surface plasmon resonance biosensor advanced by long range surface plasmons and magnetic nanoparticle assays," *Analytical chemistry,* vol. 84, no. 19, pp. 8345-8350, 2012.

[136] E. T. Silva, D. E. Souto, J. T. Barragan, J. F. Giarola, A. C. Moraes and L. T. Kubota, "Electrochemical biosensors in point-of-care devices: recent advances and future trends," *ChemElectroChem,* 2017.

[137] B. M. Moskowitz, "Hitchhiker's guide to magnetism.," *Environmental Magnetism Workshop (IRM),* vol. 279, p. 48, 1991.

[138] A. D. Elster, "Magnetic dipole moment," 2017. [Online]. Available: http://mri-q.com/magnetic-dipole-moment.html. [Accessed 01 09 2017].

[139] J. Coey, "Basic Concepts in Magnetism," [Online]. Available: http://magnetism.eu/esm/2009/slides/coey-slides-2.pdf. [Accessed 08 2017].

[140] Q. A. Pankhurst, J. Connolly, S. Jones and J. Dobson, "Applications of magnetic nanoparticles in biomedicine," *Journal of physics D: Applied physics,* vol. 36, no. 13, p. R167, 2003.

[141] "Domain theory of Ferromagnetism," GITAM University, [Online]. Available: http://eresources.gitam.edu/Engg_Phys/semester_2/magnetic/domain.htm. [Accessed 01 08 2017].

[142] W. D. Callister and D. G. Rethwisch, Materials science and engineering, John Wiley , 2011.

[143] U. Jeong, X. Teng, Y. Wang, H. Yang and Y. Xia, "Superparamagnetic colloids: controlled synthesis and niche applications," *Advanced Materials,* vol. 19, no. 1, pp. 33-60, 2007.

[144] K. M. Krishnan, "Biomedical nanomagnetics: a spin through possibilities in imaging, diagnostics, and therapy," *IEEE transactions on magnetics,* vol. 46, no. 7, pp. 2523-2558, 2010.

[145] S.-h. Noh, W. Na, J.-t. Jang, J.-H. Lee, E. J. Lee, S. H. Moon, Y. Lim, J.-S. Shin and J. Cheon, "Nanoscale magnetism control via surface and exchange anisotropy for optimized ferrimagnetic hysteresis," *Nano letters,* vol. 12, no. 7, pp. 3716-3721, 2012.

[146] B. H. Kim, N. Lee, H. Kim, K. An, Y. I. Park, Y. Choi, K. Shin, Y. Lee, S. G. Kwon, H. B. Na and others, "Large-scale synthesis of uniform and extremely small-sized iron oxide nanoparticles for high-resolution T 1 magnetic resonance imaging contrast agents," *Journal of the American Chemical Society,* vol. 133, no. 32, pp. 12624-12631, 2011.

[147] G. Vasilescu, "Chapter 12: Methods of Increasing Immunity to interfering signals," in *Electronic noise and interfering signals: principles and applications*, Springer Science & Business Media, 2006, pp. 389-392.

[148] Rettcher, S. a. Jungk, F. a. Kuhn, C. a. Krause, G. a. C. Hans-Joachim and Nolke, U. a. Fischer, R. a. Schillberg, S. a. Schroper and Florian, "Simple and Portable Magnetic Immunoassay for Rapid Detection and Sensitive Quantification of Plant Viruses," *Applied and environmental microbiology,* vol. 81, no. 9, 2015.

[149] H. Kokabi, A. Rabehi, S. Fattoum, N. Yakdi, K. Ngo, V. Depuis, A. Krings, L. Chen and H.-J. Krause, "Magnetic frequency mixing detection of magnetic nanoparticles for immunoquantification in a microfluidic structure", International Symposium on Biomaterials and Smart Systems," in *International symposium on Biomat*, Cergy-Pontoise, France, 2014.

[150] R. Boll, K. Overshott, W. Gopel, J. Hesse and J. Zemel, "Sensor a Comprehensive Survey Volume 5 Magnetic Sensor," *VCH, Weinhein,* 1989.

[151] J.-R. Riba, "Calculation of the ac to dc resistance ratio of conductive nonmagnetic straight conductors by applying FEM simulations," *European Journal of Physics,* vol. 36, no. 5, p. 55019, 2015.

[152] A. Reatti and M. K. Kazimierczuk, "Comparison of various methods for calculating the AC resistance of inductors," *IEEE Transactions on Magnetics,* vol. 38, no. 3, pp. 1512-1518, 2002.

[153] J. Zhao, "A new calculation for designing multilayer planar spiral inductors," *EDN (Electrical Design News),* vol. 55, no. 14, p. 37, 2010.

[154] G. Dehmel, "Magnetic field sensors: induction coil (search coil) sensors," in *Sensors Set: A Comprehensive Survey*, Wiley Online Library, 1989, pp. 205-253.

[155] A. Rabehi, Kokabi.H, Yakdi, Ngo.K, Dupuis.V, Neveu.S, Graff-Dubois.S, Chen.L and KrauseH.-J., "Etude d'un microsystème électromagnétique de détection des nanoparticules magnétiques pour les tests immunologiques," in *Journées Scientifiques des facultés de Biologie et de médecine de l'UPMC*, Paris, 2015.

[156] S. R. Systems, "MODEL SR830 DSP Lock-In Amplifier," Sunnyvale, USA, 2011.

[157] P. Hugounenq, M. Levy, D. Alloyeau, L. Lartigue, E. Dubois, V. Cabuil, C. Ricolleau, S. Roux, C. Wilhelm, F. Gazeau and others, "Iron oxide monocrystalline nanoflowers for highly efficient magnetic hyperthermia," *The Journal of Physical Chemistry C,* vol. 116, no. 29, pp. 15702-15712, 20112.

[158] D. Kim and A. E. Herr, "Protein immobilization techniques for microfluidic assays," *Biomicrofluidics,* vol. 7, no. 4, p. 041501, 2013.

[159] S. Sharma, H. Byrne and R. J. O'Kennedy, "Antibodies and antibody-derived analytical biosensors," *Essays in biochemistry,* vol. 60, no. 1, pp. 9-18, 2016.

[160] B. Ibarlucea, C. Fernandez-Sanchez, S. Demming, S. Buttgenbach and A. Llobera, "Biofunctionalization of PDMS-based microfluidic systems," 2011.

[161] J. Yakovleva, R. Davidsson, A. Lobanova, M. Bengtsson, S. Eremin, T. Laurell and J. Emneus, "Microfluidic enzyme immunoassay using silicon microchip with immobilized antibodies and chemiluminescence detection," *Analytical chemistry,* vol. 74, no. 13, pp. 2994-3004, 2002.

[162] D. Belder, A. Deege, H. Husmann, F. Kohler and M. Ludwig, "Cross-linked poly (vinyl alcohol) as permanent hydrophilic column coating for capillary electrophoresis," *Electrophoresis,* vol. 22, no. 17, pp. 3813-3818, 2001.

[163] M. S. Thomsen, P. Polt and B. Nidetzky, "Development of a microfluidic immobilised enzyme reactor," *Chemical Communications,* no. 24, pp. 2527-2529, 2007.

Résumé :

La détection et quantification d'agent biologique occupe une place prépondérante dans la prévention et la détection des dangers possibles pour la santé publique (épidémie ou pandémie), l'environnement ainsi que d'autres risques contextuelles (bioterrorisme, armes biologique ou chimiques…etc.). Par conséquent, le développement d'un système portable et à moindre coût permettant de détecter ces dangers constitue l'axe de recherche pluridisciplinaire de la collaboration entre différents laboratoires de l'UPMC (Paris 6) et « RWTH university » à Aachen en Allemagne.

Dans ce projet, nous avons étudié les aspects pluridisciplinaires d'un microsystème (LoC) électromagnétique de détection immunologique basé sur l'utilisation de nanoparticules magnétiques (MNP). En raison de leur extractibilité et de leur triabilité, les MNP sont adaptées à l'examen d'échantillons biologiques, servant de marqueurs pour des réactions biochimiques. La plupart des techniques classiques de détection existantes sont basées sur des méthodes colorimétrique, fluorescence ou électrochimique qui souffrent en majorité de problème de temps d'analyse et de sensibilité. A cet égard, Les méthodes d'immunodétection magnétiques constituent une alternative prometteuse. Cette détection est effectuée à l'aide des MNP qui sont spécifiquement bio-fonctionnalisés en surface afin d'être liée à la cible (virus, anticorps…etc).

La nouvelle méthode magnétique de mélange de fréquence permet la détection et la quantification de ces MNP avec une grande dynamique. Dans cette thèse, l'effort est dirigé vers la miniaturisation de ce système. Pour ce faire, nous avons développé un ensemble d'outils analytiques et de simulations multiphuysqies afin d'optimiser les dimensions des parties électromagnétique (bobines planaires) et microfluidiques. Par la suite, des prototypes de cette structure de détection à partir de bobines en circuits imprimés et de réservoirs microfluidiques en PDMS sont dimensionnés et réalisés. Les performances de ces prototypes ont été évaluées en termes de limite de détection de MNP, linéarité et plage dynamique. En outre, ces prototypes ont permis de valider les outils de dimensionnement réalisés. Une limite de détection de nanoparticles magnetiques de 15ng/mL a été mesurée avec un volume d'échantillon de 14 µL correspondant à une goutte de sang. Finalement, la validation du système quant à l'immuno-détection est abordée avec un état de l'art et le développement d'une procédure de fonctionnalisation biochimique de surface ainsi que des premiers tests pour sa validation.

Mots-Clé : detéction de pathogènes, Lab-on-Chip, détection magnétique, technique de mélange de fréquences.

Abstract:

The detection and quantification of a biological agent or entity has become paramount to anticipate a possible health threat (epidemic or pandemic), environmental threat or to combat other contextual threats (bioterrorism, chemical and biological weapons, drugs). Consequently, developing a portable cost effective device that could detect and quantify such threats is the research focus of the joint multidisciplinary project between UPMC (Paris 6) laboratories and RWTH university in Aachen, Germany.

In the framework of this project, we have studied the multidisciplinary aspects of an electromagnetic microsystem for immunologic detection based on magnetic nanoparticles (MNP) in a microfluidic lab-on-chip (LoC). Because of their extractability and sortability, magnetic nanoparticles are adapted for examination of biological samples, serving as markers for biochemical reactions. So far, the final detection step is mostly achieved by well-known immunochemical or fluorescence-based techniques which are time consuming and have limited sensitivity. Therefore, magnetic immunoassays detecting the analyte by means of magnetic markers constitute a promising alternative. MNP covered with biocompatible surface coating can be specifically bound to analytes, cells, viruses or bacteria. They can also be used for separation and concentration enhancement.

The novel frequency mixing magnetic detection method allows quantifying magnetic nanoparticles with a very large dynamic measurement range. In this thesis, emphasis is put on the miniaturized implementation of this detection scheme. Following the development of analytical and multiphysics simulations tools for optimization of both excitation frequencies and detection planar coils, first multilayered printed circuit board prototypes integrating all three different coils along with an adapted microfluidic chip has been designed and realized. These prototypes have been tested and characterized with respect to their performance for limit of detection (LOD) of MNP, linear response and validation of theoretical concepts. Using the frequency mixing magnetic detection technique, a LOD of 15ng/mL for 20 nm core sized MNP has been achieved with a sample volume of 14 µL corresponding to a drop of blood. Preliminary works for biosensing have also been achieved with a state of the art of surface functionalization and a developed proposed biochemical immobilization procedure and preliminary tests of its validation.

Keywords: pathogen sensing, Lab-on-Chip, magnetic detection, frequency mixing technique.